**THE EUROPEAN
PHYSICAL JOURNAL
SPECIAL TOPICS**

Review

Active Brownian Particles

From Individual to Collective Stochastic Dynamics

P. Romanczuk[1,a], M. Bär[2], W. Ebeling[3], B. Lindner[3],
and L. Schimansky-Geier[3]

[1]Max-Planck-Institute for the Physics of Complex Systems Dresden, Nöthnitzer Str. 38,
01187 Dresden, Germany
[2]Physikalisch-Technische Bundesanstalt, Abbestr. 2-12, 10587 Berlin, Germany
[3]Institute of Physics, Humboldt Universität zu Berlin, Newtonstr. 15, 12489 Berlin, Germany

Abstract. We review theoretical models of individual motility as well as collective dynamics and pattern formation of active particles. We focus on simple models of active dynamics with a particular emphasis on nonlinear and stochastic dynamics of such self-propelled entities in the framework of statistical mechanics. Examples of such active units in complex physico-chemical and biological systems are chemically powered nano-rods, localized patterns in reaction-diffusion system, motile cells or macroscopic animals. Based on the description of individual motion of point-like active particles by stochastic differential equations, we discuss different velocity-dependent friction functions, the impact of various types of fluctuations and calculate characteristic observables such as stationary velocity distributions or diffusion coefficients. Finally, we consider not only the free and confined individual active dynamics but also different types of interaction between active particles. The resulting collective dynamical behavior of large assemblies and aggregates of active units is discussed and an overview over some recent results on spatiotemporal pattern formation in such systems is given.

1 Introduction

In recent years there has been a strong growth of research activities regarding the statistical description of systems far from equilibrium. A whole class of biological and physical systems which may be referred to as *active matter* have been studied theoretically and experimentally. The term "active" refers here to the ability of individual units to move actively by gaining kinetic energy from the environment. Examples of such systems range from the dynamical behavior of individual units such as Brownian motors [285], motile cells [42,128,318], macroscopic animals [187,200] or artificial self-propelled particles [169,265] to large ensembles of interacting active particles and

---

[a] e-mail: prom@pks.mpg.de

their large scale collective dynamics [23,61,361]. A major driving force of the *active matter* research are the continuously improving experimental techniques such as automated digital tracking [17,318,326] or the realization of active granular and colloidal systems (see e.g. [12,82,207,265,346]).

This review is devoted to the analysis of simple dynamical models of active systems. In particular we will focus on stochastic models of individual active particles or agents as well as on large scale collective phenomena arising in systems of such interacting active particles. We define active motion as motion of particles or agents due to an internal driving, which may have different causes such as biological activity or non-equilibrium dynamics in artificial driven systems. It is fundamentally different from standard purely passive dynamical behavior of particles in gases, liquids or solid states at thermal equilibrium. In contrast, active particles or agents are assumed to have an internal propulsion mechanism ("motor"), which may use energy from an external source and transform it under non-equilibrium conditions into directed motion.

The great number of publications on active particle systems makes a complete review, describing all the different approaches across the different scientific disciplines, impossible. Thus, we will focus here on the review and analysis of generic models of individual active particles as well as their large scale collective dynamics, which may be considered as an extension of concepts well known in physics, such as ordinary Brownian motion, ferromagnetic or nematic media. In particular, we will focus on the mathematical description and analysis of such systems from a (statistical) physicist's point of view.

There are many fascinating research areas, which we will not discuss in this review, such as the dynamics of microswimmers at low Reynolds numbers (see e.g. [7,87, 90,277,281], or a recent review in [211]), or the biological implications of collective behavior of organisms and animals, for example, flocks of birds or schools of fish [71,150,202,336].

An important feature of most *active matter* systems, are the non-negligible random fluctuations in the motion of individual active units. This apparent randomness may have different origins, for example, environmental factors or internal fluctuations due to the intrinsic stochasticity of the processes driving individual motion. In animals, they may be also associated with abstract decision processes which govern the direction and/or the speed of individual motion and which may appear as random to an external observer. A simple way to account for such fluctuations without being able to resolve the underlying mechanisms is to introduce stochastic forces into the equations of motion of individual units. Thus our general modelling approach will be based on the concept of stochastic differential equations (Langevin equation, SDE) and the corresponding Fokker-Planck equations for the evolution of the probability densities of the involved (stochastic) variables [136,292,357].

A large part of this review evolves around the concept of "Active Brownian Particles" introduced more than a decade ago. The term was first introduced by [308], referring to Brownian particles with the ability to generate a field, which in turn can influence their motion. In the following Ebeling, Schweitzer and others used this term in the context of self-propelled particles far from equilibrium (see e.g. [106,116,297,311,312]). In general we will refer to "Active Brownian Particles" in the latter context as Brownian particles performing active motion, which may be accounted for by an internal energy depot and/or a (nonlinear) velocity-dependent friction function.

Throughout this review, we will focus on topics and research questions, which we have been actively working on over the past years. Hereby, an emphasis is put on presentation of the mathematical framework together with the discussion of its application to various problems.

1.1 Individual dynamics

When the botanist Robert Brown observed the erratic motion of small pollen grain particles immersed in a liquid in 1827 [48], he considered them first as living entities. However Brown, being also the discoverer of the cellular nucleus, was a thorough scientist. He repeated the experiments with granular and glassy material, and discovered its purely physical nature. Although his name is associated with the physical phenomenon of Brownian motion, he was certainly not the first one to observe it. The phenomenon of irregular motion of coal dust particles immersed in a fluid had already been reported by Jan Ingen-Housz in 1784 [177].

Later on, in 1863, the origin of the never-vanishing motion was experimentally traced back to the motion of the molecules of the surrounding liquid by C. Wiener [370], who was familiar with Maxwell's kinetic theory. Afterwards M. Gouy [145] found that the motion is amplified if viscosity of the liquid is lowered. After the turn of the century, A. Einstein [108, 109], M. Smoluchowski [364], P. Langevin [209], and others showed theoretically that the behavior of Brownian particles are due to the permanent molecular agitation of the solution on the immersed particle. Eventually, J. Perrin [269] was awarded the Nobel Prize in 1926 for the experimental observation of Brownian motion, which confirmed the theoretical findings and permitted the first realistic determination of Avogadro's number as indicator of the molecular structure of matter.

Without doubt, the theory of Brownian motion not only assumed a central role in the foundation of thermodynamics and statistical physics, but is still a major interdisciplinary research topic. Although Brownian motion is purely physical in origin, many models of bacterial and small animal motion have employed the framework of Brownian motion or its discrete counterparts, which are random walks. In parallel to Einsteins work, K. Pearson [266–268] in 1905 invented the term "random walks" and used the concept for a statistical description of insects migration.

Probably the first experiments on random motion of (living) microorganisms – which consitute clearly a system far from equilibrium – influenced by the theory of Brownian motion were performed by Przimbram in the second decade of the 20th century [278, 279]. Przibram has shown that the mean squared displacement of the protozoa in water increases linearly in time in analogy to Brownian motion but with a larger diffusion coefficient then predicted by the equilibrium kinetic theory of Brownian motion. Przimbrams work is the first experimental evidence of active Brownian motion. In fact, in his second paper Przimbram reported increasing diffusion coefficients of rotifiers with their increasing concentration, which appears to be the first report on hydrodynamically interacting active Brownian particles [279].

Przimbram's work was followed up by Fürth [131], who based on his own experimental findings, introduced the notion of persistent random walk in the description of the motion of biological agents. Fürth arrived independently at the same result as Ornstein [256] who considered inertial Brownian motion in thermal equilibrium.

The mathematical description of the apparently random motion of biological agents and the corresponding diffusion processes are fundamental to understanding the ability of individuals to explore their environment and to describe the large scale dispersal of populations [252]. Since the first pioneering works of Przimbram and Fürth there have been a great number of publications on the theory of random walks and their application to biology and ecology. A prominent example is the work of Howard C. Berg [32], who made random walk theory an intrinsic part of modeling; new concepts along these lines are developed even nowadays [107, 234]. From the huge literature, we would like to highlight here few examples, such as the work by H. Gruler and M. Schienbein [305], by H. Othmer and coworkers [165, 257]

or the recent integrated theoretical and experimental approach by H. Flyvberg and collaborators [318,319].

Because of the strong connections between the theory of Brownian motion and random walk theory to models of self-propelled or active Brownian particles, we will start this review with a summary of general findings of the classical theory and some important mathematical concepts.

In the following sections, we will focus on the concept of self-propulsion in the framework of active Brownian particles. We will discuss various models of active motion not only differing in their deterministic equations of motion but also subject to different types of fluctuations: e.g. internal and external Gaussian fluctuations, (energetic) shot noise or dichotomous Markov noise. We will analyze the characteristics observables of individual active motion such as speed and velocity probability distributions or the mean squared displacement. In addition, we will discuss the behavior of active particles under external constraints, such as e.g. external potentials.

Despite the intense interdisciplinary research on active Brownian motion, there is still a lack of theoretical foundations. For example, one issue that has been neglected is the distinction between passive fluctuations (e.g. thermal fluctuations) and stochastic forces which have their origin in the active nature of the system and their different impact on the experimentally accessible observables such as stationary velocity and speed distributions. Only recently it was shown how internal (or active) fluctuations may lead to a complex behavior of the mean squared displacement of active particles with multiple crossovers or to characteristic deviations of stationary velocity and speed distributions in comparison to ordinary Brownian motion [273,298].

1.2 Collective dynamics

In the last two sections of this review, we will extend our scope to self-organization phenomena in systems of interacting active particles and the resulting modes of collective motion. In this context we introduce the term "swarms" of active particles. We use it here to refer to a confined systems of particles (animals in two dimensions and more general objects) performing collective motions under far from equilibrium conditions. The dynamics of swarms of animals is a traditional object of biological and ecological investigations [252] but still a rather young field of physical studies (see e.g. Refs. [159,235,311,360]). Here we will develop rather simple models which are based on the idea that swarm motion possesses some kind of universality [252]. The existence of universal features makes it possible to study swarm motion using simple models which are in the same universality class. Assuming that this hypothesis is true, we have the choice between different models of swarm motion which are in the universality class preferring the simplest ones. The idea which we will follow here is: Swarms may be modelled as active particles using the concepts of active Brownian motion [9,107].

Over the past decades, collective dynamics of swarms of driven particles has captured the growing interest of various theoretical groups. Many interesting effects of the self-organization of swarms have been revealed and in part already explained. We mention here the comprehensive survey of Okubo and Levin [252] on swarm dynamics in biophysical and ecological context. Studies of Helbing [159] relate to traffic phenomena and related self-driven many-particle systems. Broad context of swarming dynamics in natural science is also brought up in the comprehensive books and reviews by T. Vicsek [360,362], A.S. Mikhailov and V. Calenbuhr [235], F. Schweitzer [311], I.D. Couzin [69], D.J.T. Sumpter [335] and Toner et al. [350].

A major shortcoming of the research in collective motion was the lack of empirical data on the structure and dynamics of real swarms. However, the situation

is improving, due to technological advances in digital tracking and data processing, the empirical study of large scale collective motion in the field has become possible [17,55,225]. Furthermore, an increasing number of controlled laboratory experiments is being performed on collective motion of such different organisms as fish [1], insects [27,51], bacteria [326,327] or keratocytes (active tissue cells) [340]. The resulting data provide the foundation to address the question on actual properties of social interactions in real world swarms and flocks.

Beyond the dynamics of cohesive swarms, we will discuss systems of active particles with a alignment interaction, which may lead to large scale collective motion.

The most prominent (minimal) model of collective motion of this type was introduced by Vicsek and collaborators in 1995 [361]. Vicsek et al. have shown how an initially disordered state without collective motion at large noise intensities becomes unstable if the noise is decreased below a critical value and how large scale collective motion emerges via a spontaneous symmetry breaking.

We establish a link to publications on mesoscopic equation of motion for density and velocity fields of self-propelled particles [239,322,323,348,349], where the mesoscopic equations of motion for the density and velocity fields were constructed using symmetry and conservation laws. Recently, a corresponding kinetic description was derived by a Boltzmann approach [36]. Here, we derive the field equations in a systematic way from the microscopic Langevin equations of active Brownian motion without a restriction to constant speeds. In addition to the density and velocity fields, we consider explicitly the effective temperature field of the active Brownian particle gas. We consider also the important special case of self-propelled particles with constant speed and discuss in this context local alignment with different interaction symmetries.

In the end of Sect. 6, we mention briefly other swarming mechanisms, such as chemotactic coupling or selective attraction/repulsion interactions (escape & pursuit).

We will then turn our attention to pattern formation of self-propelled particles with alignment and discuss clustering, phase separation, and emergence of large-scale coherent structures in such systems.

Finally, we will conclude this review with a summary of the contents together with a more detailed discussion of related expermental results as well as other modelling approaches and their relation to the theoretial framework presented in the paper.

2 Brownian motion and beyond

2.1 Brownian motion revisited

The behavior of ordinary Brownian particles is determined by the (passive) stochastic collisions, the particles suffer from the surrounding medium. There is no active transfer of energy to the particles. The energetic equilibrium between particles and surrounding medium, which balances dissipation and fluctuations, is expressed by the fluctuation–dissipation theorem.

In the most common way (at first glance, also the simplest way), Brownian motion is described by Newtonian dynamics including friction and stochastic forces [209]. The motion of a Brownian particle subject to Stokes friction with coefficient γ in a space-dependent potential $U(\mathbf{r})$ can be described by the Langevin equation

$$\frac{\mathrm{d}\mathbf{r}}{\mathrm{d}t} = \mathbf{v}; \quad m\frac{\mathrm{d}\mathbf{v}}{\mathrm{d}t} = -\gamma\mathbf{v} - \nabla U(\mathbf{r}) + \mathcal{F}(t) \tag{1}$$

with $\nabla U = 0$ in the original publication by Langevin. He assumed temporally short correlated random forces $\mathcal{F}(t)$, independence between coordinate $\mathbf{r}(t)$ and velocity

$\mathbf{v}(t)$, and the equipartition theorem $\langle \mathbf{v}^2 \rangle = 3k_{\mathrm{B}}T/m$ where k_{B} is Boltzmann's constant. Ornstein and Uhlenbeck [355] pointed out that the stochastic force should be Gaussian distributed with independent components and δ-correlated time dependence

$$\langle \mathcal{F}(t) \rangle = 0; \quad \langle \mathcal{F}_i(t)\mathcal{F}_j(t') \rangle = 2D_p \delta_{i,j}\, \delta(t - t'), \quad i,j = x,y,z. \tag{2}$$

The components $\mathcal{F}_i(t)$ are referred to as Gaussian white noise with intensity D_p. Integrated over small time intervals dt, a stationary Wiener process is obtained. In the Newtonian equation, these forces yield an increment of momentum in dt with Gaussian distribution

$$\mathrm{d}W_{\mathrm{d}t,i} = \int_t^{t+\mathrm{d}t} \mathrm{d}s\, \mathcal{F}_i(s), \quad i = x,y,z, \tag{3}$$

the average of which vanishes and second moment of which grows linear in dt with slope $2D_p$. Increments at different times are independent [136,292].

The noise strength D_p for the momentum is connected with the noise strength for the velocities D by the simple relation $D_p = m^2 D$. In thermal equilibrium, according to Langevin's assumption, the loss of energy due to friction compensates on average the gain of energy resulting from the stochastic force. In this case, the fluctuation-dissipation theorem states:

$$D_p = D\, m^2 = k_{\mathrm{B}}\, T\, \gamma, \tag{4}$$

where T is the absolute temperature.

We may rewrite the Langevin equation for the velocities as follows

$$\frac{d\mathbf{r}}{dt} = \mathbf{v}; \quad \frac{d\mathbf{v}}{dt} = -\frac{\gamma}{m}\,\mathbf{v} - \frac{\nabla U(\mathbf{r}))}{m} + \sqrt{2D}\xi(t), \tag{5}$$

where the stochastic source term obeys

$$\langle \xi(t) \rangle = 0, \quad \langle \xi_i(t)\xi_j(t') \rangle = \delta(t - t'), \quad i,j = x,y,z. \tag{6}$$

For $\nabla U(\mathbf{r}) = 0$, the integration of Eq. (5) to obtain the mean squared displacement $\langle \mathbf{r}^2(t) \rangle$ starting at $t = 0$ at the origin gives in equilibrium using (4):

$$\langle \mathbf{r}(t)^2 \rangle = 6\,\frac{k_{\mathrm{B}}T}{\gamma}\left[t - \frac{1}{\gamma}\left(1 - \exp\left(-\frac{\gamma}{m}t\right)\right) \right]. \tag{7}$$

This expression yields a ballistic growth for times smaller than $t \leq 1/\gamma$ and a linear growth for larger times

$$\langle \mathbf{r}(t)^2 \rangle = 2dD_{\mathrm{eff}}\, t, \tag{8}$$

with d is the dimension of the Brownian motion. The diffusion coefficient obeys the Einstein-Sutherland relation [108,338]

$$D_{\mathrm{eff}} = \frac{k_{\mathrm{B}}T}{\gamma}. \tag{9}$$

The linear regime in t is valid at length scales exceeding the brake path $l \propto \sqrt{k_{\mathrm{B}}Tm}/\gamma$.

In the following we will always use dimensionless units and set the mass to $m = 1$, resulting in $D_p = D$. Further on, we use D for noise intensity of purely additive Gaussian white noise in the velocity coordinate.

We are interested in the general statistical descriptions of self-moving objects. In the Markovian description, full information is provided by the transition probability $P(\mathbf{r}, \mathbf{v}, t | \mathbf{r_0}, \mathbf{v_0}, t_0)$ to find the particle at location $\mathbf{r}$ with velocity $\mathbf{v}$ at time t if started

at $\mathbf{r_0}$ with $\mathbf{v_0}$ at initial time t_0. As well known [28, 292], the distribution function density which corresponds to the Langevin equation (5), is the solution of a Fokker-Planck equation of the form:

$$\frac{\partial P(\mathbf{r}, \mathbf{v}, t | \mathbf{r_0}, \mathbf{v_0}, t_0)}{\partial t} + \mathbf{v} \frac{\partial P}{\partial \mathbf{r}} + \nabla U(\mathbf{r}) \frac{\partial P}{\partial \mathbf{v}} = \frac{\partial}{\partial \mathbf{v}} \left[\gamma \mathbf{v} P + D \frac{\partial P}{\partial \mathbf{v}} \right]. \tag{10}$$

For harmonic potentials $U(\mathbf{r})$, the solutions is a multi-modal Gaussian distribution [58] with time-dependent moments. In the long-time limit, the stationary solution of Eq. (10) becomes independent of the initial distribution $P_0(\mathbf{r}, \mathbf{v})$ and with Eq. (4) the ensemble of Brownian particles obeys in equilibrium the Maxwell-Boltzmann distribution:

$$P_0(\mathbf{r}, \mathbf{v}) = \mathcal{N} \exp \left\{ -\frac{1}{k_B T} \left[\frac{1}{2} \mathbf{v}^2 + U(\mathbf{r}) \right] \right\}. \tag{11}$$

An important limiting case of Eq. (5) is the so-called overdamped Brownian motion. As pointed out by Purcell [280] and Berg [32], this limit should be considered in the motion of bacteria and other small micro-swimmers due to the low Reynolds number governing their dynamics. Overdamped Brownian motion can be obtained from the Langevin equation under the assumption of large friction where inertial effects can be neglected, resulting in

$$\frac{d\mathbf{r}}{dt} = \mathbf{v} = -\frac{\nabla U(\mathbf{r})}{\gamma} + \sqrt{2D_r} \xi(t) \tag{12}$$

with intensity $D_r = D/\gamma^2$.

The corresponding Fokker-Planck equation for the overdamped dynamics reads

$$\frac{\partial P(\mathbf{r}, t | \mathbf{r_0}, t_0)}{\partial t} = \frac{\partial}{\partial \mathbf{r}} \left[\frac{\nabla U(\mathbf{r})}{\gamma} P \right] + D_r \frac{\partial^2 P}{\partial \mathbf{r}^2} \tag{13}$$

with the stationary solution

$$P_0(\mathbf{r}) = \mathcal{N} \exp \left[-\frac{U(\mathbf{r})}{\gamma D_r} \right]. \tag{14}$$

In thermal equilibrium, this becomes equal to the Boltzmann distribution by virtue of $D_r = k_B T / \gamma$, which holds true according to the relation Eq. (4).

We note that the Langevin Eq. (5) has been generalized in many ways. First of all, the description applies not only to mechanical degrees of freedom but also to voltage fluctuations in electric circuits ('Johnson noise') and to fluctuations in the number of molecules undergoing chemical reactions ('Chemical Langevin equation'), to name only two prominent examples. Finite correlations in equilibrium fluctuations and dissipation ('memory damping') have been taken into account in the generalized Langevin equation [157, 205, 244, 383]. The consequences of nonlinear dissipation in equilibrium systems were studied as well [197]. More recently, also formulations of Langevin and Fokker-Planck equations that are consistent with special relativity have drawn much attention (for a comprehensive review on relativistic Brownian motion, see [93]). As for the many other generalizations and applications in nonequilibrium systems, we just can refer the interested reader to recent collections of articles on these topics [146, 154, 156, 222] and the references given therein.

2.2 Polar representation of Brownian dynamics

Let us now consider the dynamics in two spatial dimensions and without external forces. A very useful representation is obtained in polar coordinates of the velocities [306]. The Cartesian components of the velocity v_x, v_y may be written in terms of polar coordinates as

$$v_x = s(t) \cos \varphi(t), \quad v_y = s(t) \sin \varphi(t) \tag{15}$$

with $s(t) = |\mathbf{v}(t)| \geq 0$ being the speed of the particle and $\varphi(t)$ the polar angle defining the direction of motion, i.e. the angle between the velocity vector and the x-axis.

The two spatial components for the position follow the dynamics

$$\frac{\mathrm{d}}{\mathrm{d}t}\mathbf{r}(t) = \mathbf{v}(t) = s(t)\mathbf{e}_v(t), \tag{16}$$

were $\mathbf{e}_v(t) = \{\cos \varphi(t), \sin \varphi(t)\}$ is the unit vector in the velocity direction at time t. The corresponding stochastic equations for $s(t)$ and $\varphi(t)$ contain multiplicative noise

$$\frac{\mathrm{d}}{\mathrm{d}t}s = -\gamma s + \sqrt{2D}\,\xi_s(t), \quad \frac{\mathrm{d}}{\mathrm{d}t}\varphi = \frac{1}{s}\sqrt{2D}\,\xi_\varphi(t) \tag{17}$$

and have to be interpreted in the sense of Stratonovich. The noise terms $\xi_v(t), \xi_\varphi(t)$ read

$$\xi_s(t) = \left(\xi_x(t) \cos \varphi + \xi_y(t) \sin \varphi\right), \quad \xi_\varphi(t) = \left(-\xi_x(t) \sin \varphi + \xi_y(t) \cos \varphi\right) \tag{18}$$

and are statistically independent. However, in contrast to the angle noise $\xi_\varphi(t)$ the mean of the speed noise $\langle \xi_s(t) \rangle$ does not vanish. The corresponding Fokker-Planck equation for the transition probability in the new variables $\tilde{P}(s, \varphi, t|s_0.\varphi_0, t_0)$ reads

$$\frac{\partial \tilde{P}(s, \varphi, t|s_0.\varphi_0, t_0)}{\partial t} = -\frac{\partial}{\partial s}\left\{\left(-\gamma s + \frac{D}{s}\right)\tilde{P}\right\} + D\frac{\partial^2 \tilde{P}}{\partial s^2} + \frac{D}{s^2}\frac{\partial^2 \tilde{P}}{\partial \varphi^2}, \tag{19}$$

which in the long time limit becomes independent of the angle and approaches the Rayleigh speed distribution

$$\tilde{P}_0(s, \varphi) = \mathcal{N}\,s\,\exp\left(-\frac{\gamma s^2}{2D}\right). \tag{20}$$

We note here that the probability to have zero speed vanishes in agreement with the Maxwellian velocity distribution. The stochastic force agitating the particle permanently hinders it to come to full rest. This is one particular reason why the concepts of the simple Brownian motion framework have to be critically reviewed when applied to self-propelled objects.

2.3 Internal coordinates frame for polar particles

Many active particles, such as for example biological agents, may have a distinct body axis defining their preferred direction of motion (head-tail axis). Whereas this asymmetry is obvious in higher organisms, it should be noted that the crawling motion of cells is also driven by a polar actin cytoskeleton [180,204,241,289]. Also, for artificial active particles, such as chemically-driven colloids, it might be natural to assume a preferred direction of motion based on their propulsion mechanism[1] [169,265,300].

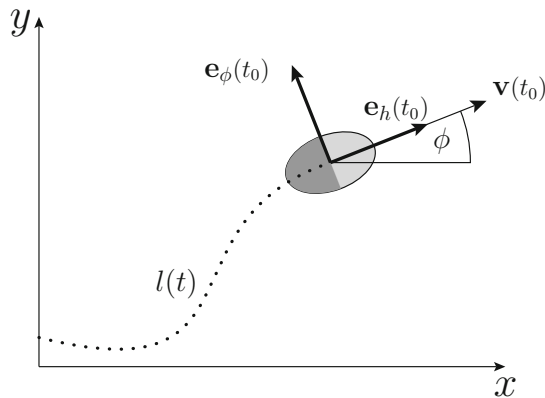[1] See also Sect. 3.4 for models where the velocity and propulsion are not in parallel.

Fig. 1. Schematic visualization of the motion of a polar particle with unit vectors of the internal coordinates $\mathbf{e}_h(t), \mathbf{e}_\phi(t)$ at a given point in time $t = t_0$. The dashed lines indicates the trajectory of the particle $l(t)$.

Without resolving the details of the origin of the asymmetry we simply assume that the polarity of particles introduces a distinct orientation, which we will refer to as *heading*. In general, we define the heading by a time dependent unit vector $\mathbf{e}_h$, which in two dimensions is entirely determined by a single angular variable ϕ:

$$\mathbf{e}_h(t) = (\cos\phi(t), \sin\phi(t)). \tag{21}$$

Thus the velocity of a point-like polar particle can be expressed by its velocity with respect to the heading and the corresponding heading vector $\mathbf{v} = v\mathbf{e}_h$. The velocity v can be positive or negative, which can be identified with "forward" and "backwards" motion with respect to the heading. In order to be able to span the two dimensional space we need a second unit vector, which can be associated with the angular direction perpendicular to the heading direction

$$\mathbf{e}_\phi(t) = (-\sin\phi(t), \cos\phi(t)). \tag{22}$$

Here, we should emphasize that, despite the apparent similarities, the (v,ϕ)-coordinates have to be distinguished from polar coordinates (s,φ). In polar coordinates the speed is always positive $s(t) = |\mathbf{v}|$ and the velocity unit vector $\mathbf{e}_v$ is defined by the direction of the velocity vector at time t. In (v,ϕ)-coordinates the velocity v of a polar particle can be also negative, corresponding to backwards motion of the particle with respect to its heading. Furthermore, the heading vector does not depend on the momentary velocity but is defined by the intrinsic polarity of the particle. In Fig. 1 a schematic visualization of a moving polar particle and the corresponding unit vectors is given.

In general the following relations hold between the two coordinate systems:

$$\mathbf{e}_h \cdot \mathbf{e}_v = \begin{cases} +1 & \text{for } v > 0 \\ -1 & \text{for } v < 0 \end{cases} \qquad \phi = \begin{cases} \varphi & \text{for } v > 0 \\ \varphi + \pi & \text{for } v < 0 \end{cases} \tag{23}$$

In cases, where the velocity v is restricted to positive values, or where the particle is apolar, in the sense that its velocity dynamics are indistinguishable for forward and backwards motion, the internal coordinate frame cannot be distinguished from the polar coordinates. In this cases we will use throughout the review the corresponding polar coordinate unit vectors $(\mathbf{e}_h \to \mathbf{e}_v, \mathbf{e}_\phi \to \mathbf{e}_\varphi)$.

2.4 Markovian dichotomous process and white shot noise

In this review, we will often make use of the dichotomous Markovian process (DMP), also called, the random telegraph noise. For this reason, we give here more details on this process and its white-noise limit case, called white shot noise or Schottky-noise [46, 136].

Because we are concerned with random motion, we illustrate the DMP by the example of dispersing particles immersed in a flow through a cylindrical tube with layers of different velocities. We follow here the work by van den Broeck [80] who revisited Taylor dispersion in 1990. The problem was first considered experimentally and theoretically by G.I. Taylor in 1921 [345] and in a series of papers in 1953/54 [342–344]. Similar theoretical problems have been formulated also by S. Goldstein and others [142, 185, 257]; comprehensive reviews about DMP in dynamical systems can be found in [16, 30, 167].

Taylor found that particles subject to layers of different flow velocities undergo additionally to the main stream flow a diffusion-like motion. To obtain this behavior, he considered scattering of the particles in the stream causing random jumps of the particle to other velocity layers. He even linked this behavior and his analysis to Pearson's problem of random insect migration.

Let us consider a flow in one dimension with two layers and with $x(t)$ denoting the position of the suspended particle in the frame co-moving with the mean flow. It is assumed that the particle changes randomly with a given constant rate λ between the two layers in which it moves with a constant relative velocity, either $+v_0$ or $-v_0$. The velocity is then a DMP $\xi_{DMP}(t)$, and the Langevin equation for the particle reads

$$\frac{\mathrm{d}}{\mathrm{d}t}x(t) = \xi_{DMP}(t). \tag{24}$$

For a temporally symmetric DMP, the life time of one of the velocities (before switching to the respective other one) is governed by an exponential distribution

$$w(\tau)\,\mathrm{d}\tau = \lambda\exp(-\lambda\tau)\mathrm{d}\tau. \tag{25}$$

The transition probability densities $P_\pm(x,t|x_0,\xi_0,t_0,)$ for the particle to be at r and the DMP to be at $\xi(t) = \pm v_0$ at time t given the particle was at r_0 and the DMP was at ξ_0 at time t_0 is governed by equations like

$$\frac{\partial P_+}{\partial t} = -v_0\frac{\partial P_+}{\partial x} - \lambda P_+ + \lambda P_-, \tag{26}$$

$$\frac{\partial P_-}{\partial t} = +v_0\frac{\partial P_-}{\partial x} + \lambda P_+ - \lambda P_-. \tag{27}$$

The conditions for t_0 enter by the initial conditions for $P_\pm$ at $t = t_0$. The probability averaged over the two velocity states and their initial states $P(x,t) = P_+(x,t) + P_-(x,t)$ is given by the known second-order telegraph equation [16, 30, 46, 167, 320]

$$\frac{\partial^2 P}{\partial t^2} + 2\lambda\frac{\partial P}{\partial t} - v_0^2\frac{\partial^2 P}{\partial x^2} = 0. \tag{28}$$

This equation can be solved in terms of modified Bessel functions but has been supplemented by initial conditions for $P_{\pm\xi_0}$ or, respectively, P and the flux $J = v_0(P_+ - P_-)$ at t_0. Multiplication by x^2 and integrating over x yields the same equation which Langevin earlier obtained for Brownian motion [209] with the respective

re-assignments. By starting exactly at $x_0 = 0$ at time $t_0 = 0$, one finds that the mean squared displacement evolves according to

$$\langle x^2(t) \rangle = \frac{v_0^2}{\lambda} \left[t - \frac{1}{2\lambda} \left(1 - \exp(-2\lambda t) \right) \right], \tag{29}$$

which should be compared to Eq. 7: 2λ corresponds to the relaxation rate (γ in Eq. 7) and $v_0^2/(2\lambda)$ is the spatial diffusion coefficient ($k_B T/\gamma$ in Eq. 7); an additional factor of three in Eq. 7 is due to the difference in spatial dimensions.

A generalization to an asymmetric two state process with different rates $\lambda_\pm$ and different values of the velocity $\xi_{DMP}(t) = v_\pm$ can be easily formulated. The transition probability is expressed by the equation

$$\frac{\partial^2 P}{\partial t^2} + (\lambda_+ + \lambda_-) \left(\frac{\partial P}{\partial t} + \langle v \rangle \frac{\partial P}{\partial x} \right) + v_+ v_- \frac{\partial^2 P}{\partial x^2} + (v_+ + v_-) \frac{\partial^2 P}{\partial t \partial x} = 0. \tag{30}$$

Here the mean velocity $\langle v \rangle = (\lambda_- v_+ + \lambda_+ v_-)/(\lambda_+ + \lambda_-)$ was used. The diffusion coefficient in the asymmetric case can be calculated as

$$D_{\text{eff}} = \frac{\lambda_+ \lambda_- (v_+ - v_-)^2}{(\lambda_+ + \lambda_-)^3}. \tag{31}$$

We now outline the DMP's limit case of white shot noise [46]. The asymmetric DMP, as discussed so far, acts like a colored noise. Its inverse correlation time is given by the sum of the switching rates $\tau_c^{-1} = \lambda_- + \lambda_+$. The noise strength is determined by $D_{DMP} = (v_+ - v_-)^2 \tau_c/4$. The limit to white noise can be taken if shifting one of the possible velocity values to infinity combined with a simultaneous vanishing of its live time. Specifically, we let the upper level $v_+ \to \infty$ and its live time $\tau_+ = 1/\lambda_+ \to 0$ while keeping the mean area $v_+ \tau_+ = h$ constant. In this way, the DMP $\xi_{DMP}(t)$ collapses to shot noise $\xi_{SN}(t)$. It consists of a sequence of δ peaks with weights h_i:

$$\xi_{SN}(t) = \sum_i^{n(t)} h_i \, \delta(t - t_i). \tag{32}$$

The number of events $n(t)$ in the interval $(0, t)$ follows from a Poisson distribution [53, 73, 111, 195, 229, 259, 384].

$$P(n(t)) \equiv Prob[n(t) = n] = \frac{(\lambda T)^n}{n!} \exp(-\lambda t). \tag{33}$$

Here λ is the rate of generating spikes, which equals the inverse living time of the lower state v_- of the DMP, i.e. $\lambda = \lambda_- = 1/\tau_-$.

The weights h_i are exponentially distributed, which is a property inherited from the statistics of the stochastic duration of the DMP's upper state [46] - the latter remains exponentially distributed even in the limit case of a vanishing mean live time. Its mean value approaches the fixed area in the limit $\langle h_i \rangle = h = \lim_{\tau_+ \to 0} v_+ \tau_+$.

How similar is shot noise to the more commonly used Gaussian white noise? Like the latter, shot noise is a white noise, i.e. these fluctuations are δ correlated. This can be also seen by means of the correlation time $\tau_c = (\lambda_+ + \lambda_-)^{-1}$, which vanishes if one of the live times (λ_+^{-1} or λ_-^{-1}) goes to zero. Remarkably, τ_c is dominated by the smaller of the two mean live times (i.e. by the higher rate).

While temporal correlations of shot noise and Gaussian white noise are similar, the distribution of shot noise is obviously not that of a mean-zero Gaussian distribution. First of all, shot noise has a mean value $\langle \xi_{SN}(t) \rangle = v_- + h/\tau_-$ which is

in general different from zero. Secondly, there is a strong asymmetry between the positive spikes and the negative base line v_-, which stands in marked contrast to the reflexion symmetry of any Gaussian distribution. This asymmetry affects also severely the statistics of dynamical systems driven by shot noise (see, for instance, studies by Richardson and Gerstner [287,288]).

The difference from a Gaussian process can be quantified by the parameter [46]

$$G = |v_+ - v_-|\, \tau_c. \tag{34}$$

This value will vanish if simultaneously both lower and upper levels diverge according to $v_\pm \to \pm\infty$ and the respective mean live times vanish $\lambda_\pm^{-1} \to 0$ while the two mean areas $v_+\tau_+$ and $v_-\tau_-$ are kept constant and equal to each other. Obviously, this limit restores the symmetry of the process. Furthermore, it can be shown that third- and higher-order cumulants of the increments of this symmetric shot noise become negligible and that its effect on any dynamical system is completely equal to that of Gaussian white noise. In this sense, the DMP approaches Gaussian white noise in the above limit, although it still attains only two discrete values in this limit.

3 Basic concepts of self-propulsion

3.1 Dynamics of active Brownian particles

3.1.1 Nonequilibrium, nonlinear friction and external forcing

So far energy was supplied to the particle by molecular agitation which has led to stochastic forces. In this Section, we want to generalize the idea of Brownian particles by including an additional energy input. In this way we will be able to derive a simplified model of biological motion which we call Active Brownian motion.

The major question we will address now is how this known picture changes if we add an internal "activity" of particles. Our main assumption is the additional inflow of energy leading to active motion can be described effectively by negative dissipation in the direction of motion. Hence, it will be modeled by negative friction instead of a constant friction coefficient γ. We introduce a nonlinear friction $\gamma(\mathbf{r}, \mathbf{v})$ which is a function of the position and velocity and, what is most important, has regions in the phase space $(\mathbf{r}, \mathbf{v})$, where it assumes negative values. In addition, fluctuation-dissipation relation becomes invalid for the non-equilibrium case of self-propulsion [181].

Simple models of such active Brownian particles were studied already in several earlier works (see e.g. [196,235,291,305,308,311,330]). Here we will review and analyze in a more systematic way models of active Brownian particles with negative friction as well as the depot model of particles which are able to store the inflow of energy in an internal depot and to convert internal energy to perform different activities [106,312]. Other versions of active Brownian particle models [291,308] consider more specific activities, such as environmental changes and signal–response behavior. In these models, the active Brownian particles (or active walkers, within a discrete approximation) are able to generate a self-consistent field, which in turn influences their further movement and physical or chemical behavior. This non-linear feedback between the particles and the field generated by themselves results in an interactive structure formation process on the macroscopic level. Hence, these models have been used to simulate a broad variety of pattern formations in complex systems, ranging from physical to biological and social systems [161,235,308,311,314,315].

Most of the time we will consider problems homogeneous in space with $\gamma(\mathbf{r}, \mathbf{v}) = \gamma(\mathbf{v})$. The situation of spatially localized energy sources (food centers) generates more

complicated dynamics and was discussed in [106]. For such energetic pumps, the basic ideas about nonlinear friction have been formulated by Helmholtz and Rayleigh, whose aim was to model the complex energy input in musical instruments. These models applied to walkers will be the starting point, followed by a model of particles with an internal energy depot. It will be assumed that the Brownian particles have the ability to take up energy from the environment, to store it in an internal depot and to convert internal energy into kinetic energy. Further on, we will discuss some specific models of active Brownian particles with a particular focus on the role of active fluctuations. We will conclude this section with a brief discussion of a generalized model of active particles, where the direction of propulsion (motor direction) is considered as an additional degree of freedom.

In other words we use Langevin equations which include acceleration terms resulting from the energy inflow. We will show, that in comparison with simple Brownian particles, the dynamics of active particles becomes much more complex, which result in new dynamical features as e.g.:

- new diffusive properties with large mean squared displacements,
- unusual velocity distributions with crater like shape,
- formation of limit cycles under confinement corresponding to motion on circles in space.

Some of these features may resemble active biological motion. Hence, the basic idea can be formulated as follows: how much physics is needed to achieve a degree of complexity which gives us the impression of motion phenomena found in biological systems?

In order to avoid misunderstandings we would like to stress again, that we do not intend here to model any particular biological or social object but instead to analyze general physical systems far from equilibrium, which exhibit active motion and new types of dynamics.

3.1.2 Active Brownian particles with velocity-dependent friction

The motion of Brownian particles with general velocity- and space-dependent friction in a space-dependent potential $U(\mathbf{r})$ can be described again by the Langevin equation (see Eq. (1):

$$\frac{d\mathbf{r}}{dt} = \mathbf{v}; \quad \frac{d\mathbf{v}}{dt} = \mathbf{F}_{diss} - \nabla U(\mathbf{r}) + \mathcal{F}(t). \tag{35}$$

The new feature is the dissipative force which is now given with a position and velocity dependent coefficient

$$\mathbf{F}_{diss} = -\gamma(\mathbf{r}, \mathbf{v})\mathbf{v}. \tag{36}$$

The force acts in direction of the motion and the friction $\gamma(\mathbf{r}, \mathbf{v})$ may depend on space, velocity and time. The term $\mathcal{F}(t)$ is a stochastic force with strength D and a δ-correlated time dependence, see Eq. (2). But now, due to nonequilibrium, this noise strength is independent of the parameters in the dissipative force and the Einstein relation is considered invalid.

We consider, without loss of generality, $m = 1$ and D_p becomes D, which gives us the following Langevin equation with unscaled Gaussian white noise $\xi(t)$ as defined in Eq. (6).

$$\frac{d\mathbf{r}}{dt} = \mathbf{v}; \quad \frac{d\mathbf{v}}{dt} = -\gamma(\mathbf{r}, \mathbf{v}) - \nabla U(\mathbf{r}) + \sqrt{2D}\xi(t). \tag{37}$$

It gives the basis for the derivation of an energetic balance. From the time derivative of the full mechanical energy one obtains

$$\frac{\mathrm{d}}{\mathrm{d}t} E = \mathbf{v}\,\frac{\mathrm{d}\mathbf{v}}{\mathrm{d}t} \,+\, \nabla U(\mathbf{r})\frac{\mathrm{d}\mathbf{r}}{\mathrm{d}t} \tag{38}$$

which averaged over the noise yields

$$\frac{\mathrm{d}}{\mathrm{d}t} \langle E \rangle = -\gamma(\mathbf{v}, \mathbf{r})\,\mathbf{v}^2 + D. \tag{39}$$

One sees that negative values of the friction coefficient lead to an increase of the mechanical energy.

Since the fluctuating source is Gaussian white noise the transition distribution density $P(\mathbf{r}, \mathbf{v}, t | \mathbf{r}_0, \mathbf{v}_0, t_0)$ obeys a Fokker-Planck equation

$$\frac{\partial P(\mathbf{r}, \mathbf{v}, t | \mathbf{r}_0, \mathbf{v}_0, t_0)}{\partial t} + \mathbf{v}\,\frac{\partial P}{\partial \mathbf{r}} + \nabla U(\mathbf{r})\,\frac{\partial P}{\partial \mathbf{v}} = \frac{\partial}{\partial \mathbf{v}}\Big[\gamma(\mathbf{r}, \mathbf{v})\,\mathbf{v}\,P + D\,\frac{\partial P}{\partial \mathbf{v}}\Big]. \tag{40}$$

In the important case that the friction coefficient is only velocity dependent and external forces are absent ($\nabla U(\mathbf{r}) = 0$) the velocity distribution becomes stationary and it holds

$$P_0(\mathbf{v}) = \mathcal{N}\,\exp\Big\{-\frac{1}{D}\int^{\mathbf{v}}\mathrm{d}\mathbf{v}'\,\gamma(\mathbf{v}')\,\mathbf{v}'\Big\} = \mathcal{N}\,\exp\Big\{-\frac{\Phi(\mathbf{v})}{D}\Big\}, \tag{41}$$

where $\Phi(\mathbf{v})$ is the effective velocity potential. Let us consider now several models of the self–propelling mechanism. Velocity-dependent friction plays an important role e.g. in certain models of the theory of sound developed by Rayleigh and Helmholtz. Following them we assume a parabolic behavior of the friction coefficient

$$\gamma(\mathbf{r}, v) = -\,\alpha\,+\,\beta\mathbf{v}^2 = \alpha\left(\frac{v^2}{v_0^2}\,-\,1\right) = \beta\,(v^2\,-\,v_0^2). \tag{42}$$

This Rayleigh-Helmholtz- model is a standard model studied in earlier papers on Brownian dynamics [121,196]. We note that $v_0^2 = \alpha/\beta$ defines a special value of the velocities where the friction is zero. At low velocities ($v^2 < v_0^2$) the friction is negative. Hence, the particle gains kinetic energy from the pump. Alternatively motion with greater velocities will be damped.

Without noise the direction of motion is defined by the initial condition. With noise the particle moves in the long time limit in all directions. This is seen from the shape of the stationary velocity distribution

$$P_0(\mathbf{v}) = \mathcal{N}\,\exp\Big\{\frac{1}{D}\left(\alpha\frac{\mathbf{v}^2}{2}\,-\,\beta\,\frac{\mathbf{v}^4}{4}\right)\Big\}. \tag{43}$$

Dependent on the sign of α, the particle is passive ($\alpha < 0$) or active ($\alpha > 0$) extracting or pumping energy, out of or into the kinetic energy of the particle, respectively. The corresponding single peaked and crater-like distributions are presented in Fig. 2.

The second standard model for active friction with a stationary velocity v_0 was derived from experiments with moving cells and analyzed by Schienbein and Gruler in 1993 [121,305].

It was originally formulated for the speed as a variable and may be seen as a linear simplification of the Rayleigh-Helmholtz friction. The dissipative friction force can be written in terms of speed $s = |\mathbf{v}|$ and the corresponding unit vector $\mathbf{e}_v = \mathbf{v}/s$ as

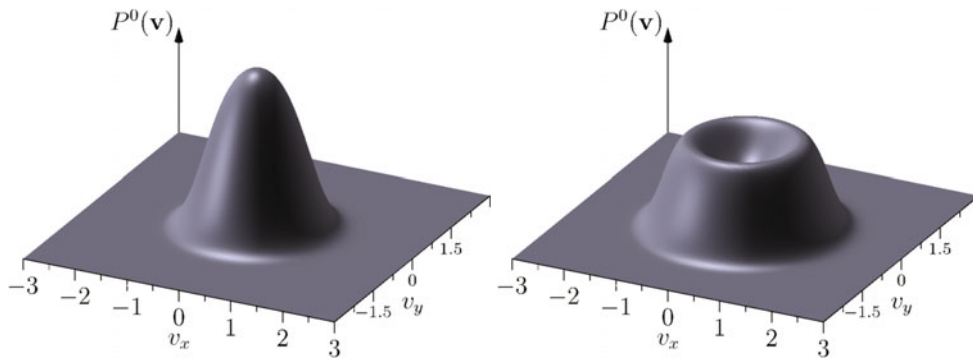$$-\gamma(\mathbf{v})\mathbf{v} = -\gamma_0\,(s - v_0)\,\mathbf{e}_v. \tag{44}$$

Fig. 2. Stationary Cartesian velocity distribution in case of Rayleigh-Helmholtz friction. Left panel: passives regime with $\alpha = -0.1$; right panel: active regime with $\alpha = 1.0$; other parameter values: $\beta = 1.0$, $D = 0.5$.

It was shown by the mentioned authors that this model allows to describe the active motion of several cell types as e.g. granulocytes. A disadvantage of this model is the discontinuity of the friction term at $\mathbf{v} = 0$. An advantage is the convergence of the friction for large speeds s to linear (Stokes) friction. The stationary velocity distribution for the friction function in Eq. (44) in Cartesian coordinates reads [121]

$$P_0(\mathbf{v}) = \mathcal{N} \exp\left\{-\frac{\gamma_0}{2D} \left(|\mathbf{v}| - v_0\right)^2\right\}. \tag{45}$$

An alternative formulation of the Schienbein-Gruler friction takes into account the polarity of an active particle (see Sect. 2.3), which may be motivated by the distinct body axis of many organisms, defining their preferred direction of motion (head-tail axis). Also, for artificial active particles it is often natural to assume a preferred direction of motion based on their propulsion mechanism. The preferred direction of motion (heading) is given by the unit vector $\mathbf{e}_h$ ($|\mathbf{e}_h| = 1$) and the Schienbein-Gruler friction can be written as (see Sect. 2.3):

$$-\gamma(\mathbf{v})\mathbf{v} = -\gamma_0 \left(v - v_0\right) \mathbf{e}_h. \tag{46}$$

Please note that the two different Schienbein-Gruler variants are only equivalent if we define the heading vector as the velocity unit vector $\mathbf{e}_h = \mathbf{e}_v = \mathbf{v}/|\mathbf{v}|$. In the general case, the second (polar) variant of the Schienbein-Gruler friction (46) is not symmetric with respect to $v = 0$. It accounts also for the possibility of backwards motion with respect the heading direction, which Schienbein and Gruler neglected in their original work [305]. As a consequence the first variant of the friction function is symmetric with respect to $v = 0$ (apolar): there is no front or back for an active particle - the particle moves always to the "front". Related equations of motion with constant propulsion and linear friction have been used for example in the description of bacterial motion [67,74].

In the following we will use, if not otherwise stated, the polar variant of the Schienbein-Gruler friction [298].

With velocities in polar representation (see Sect. 3.2) the stationary distribution can be derived. It will be reached at times large compared with $1/\gamma_0$ and is independent on the direction of motion and reads for the polar Schienbein-Gruler friction:

$$P_0(\mathbf{v}) = \mathcal{N} \exp\left\{-\frac{1}{2D} \gamma_0 \left(|\mathbf{v}| - v_0\right)^2\right\} \left[1 + \exp\left\{-\frac{2}{D} v_0 |\mathbf{v}|\right\}\right]. \tag{47}$$

Again a crater-like distribution is established if $v_0 > 0$ [298].

3.1.3 Depot model

Now we will consider a friction function which is well behaved in the full velocity range. This friction function is based on the idea of particles with an energy depot [106,311,312], and has been recently used in the context of bacterial motion [68,134]. We assume that the Brownian particle itself should be capable of taking up external energy storing some of this additional energy into an internal energy depot, $e(t)$. This energy depot as an internal property of the considered objects may be altered by three different processes:

1. take-up of energy from the environment; where $q(\mathbf{r})$ is a space-dependent pump rate of energy
2. internal dissipation, which is assumed to be proportional to the internal energy. Here, the rate of energy loss, c, is assumed to be constant.
3. conversion of internal energy into motion, where $h(\mathbf{v})$ is the rate of conversion of internal to kinetic degrees of freedom. This means that the depot energy may be used to accelerate motion on the plane.

The extension of the model is motivated by investigations of active biological motion, which relies on the supply of energy, which is dissipated by metabolic processes, but can be also converted into kinetic energy. The resulting balance equation for the internal energy depot, e, of a pumped Brownian particle is then given by:

$$\frac{\mathrm{d}}{\mathrm{d}t}e(t) = q(\mathbf{r}) - c\,e(t) - h(\mathbf{v})\,e(t). \tag{48}$$

A simple ansatz for $q(\mathbf{r})$ and $d(\mathbf{v})$ reads:

$$q(\mathbf{r}) \equiv q_0 \qquad h(\mathbf{v}) = d\mathbf{v}^2 \tag{49}$$

where $d > 0$ is the conversion rate of internal into kinetic energy. Under the condition of stationary depots we get

$$e_0 = \frac{q_0}{c + d\mathbf{v}^2}. \tag{50}$$

The energy conversion may result in an additional acceleration of the Brownian particle in the direction of movement. This way we get for the dissipative force including the usual passive friction and the acceleration on the cost of the depot

$$\mathbf{F}_{diss} = -\gamma_0\mathbf{v} + de(t)\mathbf{v}. \tag{51}$$

Correspondingly, we find a Langevin equation which contains an additional driving force, $de(t)\mathbf{v}$:

$$\frac{\mathrm{d}}{\mathrm{d}t}\mathbf{v} + \gamma_0\mathbf{v} + \nabla U(\mathbf{r}) = de(t)\mathbf{v} + \mathcal{F}(t). \tag{52}$$

Hence, the Langevin Eq. (52) is now coupled with the equation for the energy depot, Eq. (48).

The energy loss of the depot is fully converted into kinetic energy of motion of the Brownian particle. This is confirmed by the balance of the kinetic energy:

$$\dot{E}_{kin} = v_x\dot{v}_x + v_y\dot{v}_y = (de - \gamma_0)\mathbf{v}^2 + \sqrt{2D}\,\mathbf{v}\cdot\boldsymbol{\xi} \tag{53}$$

where the first term on the r.h.s., the input of kinetic energy, is equal to the negative of the last term in Eq. (48).
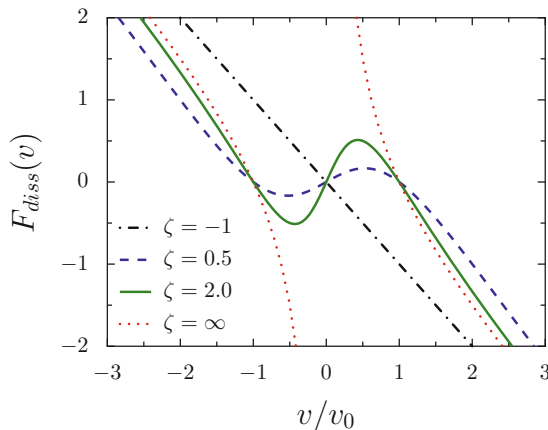
Fig. 3. Friction force driving active particles corresponding to the depot model (SET-model): (i) passive friction force $q = 0, \zeta = -1$ (dash-dotted straight line crossing the center). (ii) Depot model for positive values of the strength of driving: $\zeta = 0.5$ (dashed line); $\zeta = 2$ full line; $\zeta = \infty$ (dash-dotted line with a step at zero).

In most cases we will assume in the following that the energy depot is stationary $\dot{e}(t) = 0$. This allows the adiabatic elimination of the energy and leads to an effective dissipative force (see Fig. 3):

$$\mathbf{F}_{diss}(\mathbf{v}) = -\left[\gamma_0 - \frac{dq}{c + d\mathbf{v}^2}\right]\mathbf{v}. \tag{54}$$

The corresponding friction function is

$$\gamma(\mathbf{v}) = \gamma_0 - \frac{dq}{c + d\mathbf{v}^2} \ . \tag{55}$$

The behavior of the force and the friction changes qualitatively in dependence on the bifurcation parameter [121]

$$\zeta = \frac{dq}{c\gamma_0} - 1. \tag{56}$$

For positive ζ–values we observe that the force disappears for three values of the velocity, corresponding to an unstable velocity fixed point for vanishing velocity $v = 0$ and two stable fixed points at a finite speed $v^2 = v_0^2 > 0$.

Let us now consider several special cases in more detail: In the case that the velocities are small $(\mathbf{v}^2 \ll c/d)$ we get for the friction law

$$\gamma(\mathbf{v}) = \left(\gamma_0 - \frac{dq}{c}\right) - \frac{q\,d}{c^2}\mathbf{v}^2 + \mathcal{O}\left(\mathbf{v}^4\right), \tag{57}$$

which corresponds with

$$\alpha = \frac{dq}{\gamma_0} - \gamma_0; \qquad \beta = \frac{qd}{c^2} \tag{58}$$

to the Rayleigh-Helmholtz model discussed above (42).

The dissipative force for different values of ζ is shown in Fig. 3. For positive ζ, due to the pumping with free energy, slow particles are accelerated and fast particles are
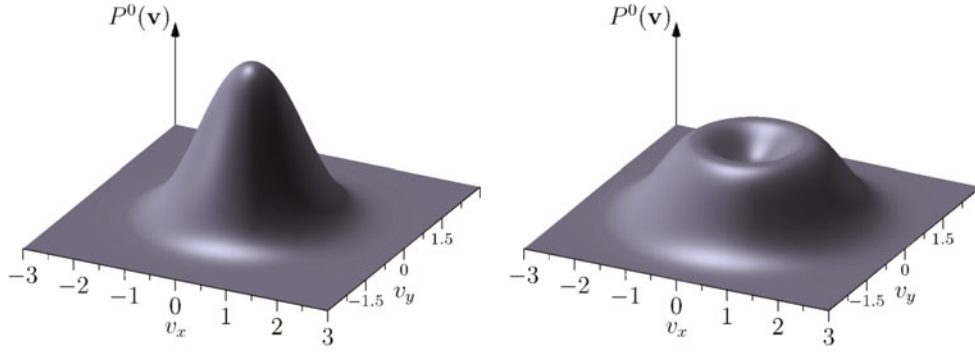
Fig. 4. Stationary Cartesian velocity distribution function of active Brownian particles for the depot model with under-critical values of the parameters (left panel; passive regime, $q_0 = 0.5$) and with over-critical parameter values (right panel; active regime, $q_0 = 2.0$). Other parameter values: $d = c = \gamma_0 = 1.0$, $D = 0.5$.

damped. At certain conditions our active friction functions have a zero corresponding to stationary velocities v_0, where the friction function and the friction force disappear. The deterministic trajectory of our system moving on a plane is in both cases attracted by a cylinder in the 4d-space given by

$$v_1^2 + v_2^2 = v_0^2 \tag{59}$$

where v_0 is the value of the stationary velocity. For the Rayleigh-Helmholtz model (RH) and the depot model (DM) the stationary velocities read:

$$v_0^2 = \frac{\alpha}{\beta} \text{ (RH)}; \qquad v_0^2 = \frac{q_0}{\gamma_0} - \frac{c}{d} \text{ (DM)}. \tag{60}$$

We insert the effective force of the depot-model (54) into the Fokker-Planck equation. The stationary solution of the latter reads approximately

$$P_0(\mathbf{v}) = \mathcal{N} \left(1 + \frac{d}{c} \mathbf{v}^2 \right)^{\frac{q_0}{2D}} \exp\left[-\frac{\gamma_0}{2D} \mathbf{v}^2 \right]. \tag{61}$$

The Fig. 4 shows a cross section of the probability distribution for Rayleigh-Helmholtz and Schienbein-Gruler-Helbing friction function. In case of strong noise and low pumping the particles approach high velocities and broad distributions. Except in the close vicinity of vanishing velocities the pre-factor in equation (61) can be neglected.

3.1.4 The limiting case of constant speed

The velocity distributions, Eqs. (43), (45), (47) and (61), collapse to a δ-peaked distribution at v_0 in the limit of vanishing noise with respect to the pumping term. The limit has to be taken such that β/D or $\gamma_0/D \to \infty$, respectively, and with $v_0 = const. \neq 0$ one gets

$$P_0(|\mathbf{v}|) \propto \delta(|\mathbf{v}| - v_0). \tag{62}$$

It yields the case of constant speed in which the dynamics of the particles can be described by the angular direction $\varphi(t)$ and spatial coordinates. The dynamics is

given by Eq. (16) and the corresponding Langevin equation for the angle, i.e. the velocity dynamics Eq. (17) reduces to

$$s(t) = v_0 = \ const., \quad \frac{\mathrm{d}}{\mathrm{d}t}\varphi = \frac{1}{v_0}\sqrt{2D}\,\xi(t). \tag{63}$$

A more detailed discussion of specific aspects of these models will be given throughout the next two sections. Here we point out that the important class of models with constant speed emerge from the Active Brownian particles framework in the discussed limit. Thus, we emphasize, that the concept of Active Brownian particles goes beyond this restriction and accounts naturally for fluctuations of the speed.

Assuming constant speed $s(t) = v_0 = const.$ $(v_0 > 0)$ the Fokker-Planck-Eq. (19) describes transitions in the angle dynamics by $P(\varphi, t|\varphi_0, t_0)$ and reduces to

$$\frac{\partial P(\varphi, t|\varphi_0, t_0)}{\partial t} = \frac{D}{v_0^2}\frac{\partial^2 P}{\partial \varphi^2}. \tag{64}$$

With the initial condition $P(\varphi, t_0|\varphi_0, t_0) = \delta(\varphi - \varphi_0)$, this equation is solved by a Gaussian with phase diffusion coefficients

$$D_\varphi = D/v_0^2. \tag{65}$$

Taking into account the periodicity of the heading $P(-\pi, t) = P(\pi, t)$, the time dependent solution of (64) reads

$$P(\varphi, t|\varphi_0, t_0) = \frac{1}{\pi}\left(\frac{1}{2} + \sum_{n=1}^{\infty}\cos n(\varphi - \varphi_0)\,\exp\left(-n\frac{D}{v_0^2}(t - t_0)\right)\right). \tag{66}$$

For large times $(t - t_0 \to \infty)$, the distribution $P(\varphi, t|\varphi_0, t_0)$ converges towards the homogeneous distribution $1/(2\pi)$, which corresponds to a complete loss of information of the initial direction. The relaxation rate of the angular function in Eq. (64) is given by the relaxation rate of the first Fourier mode $(n = 1)$, i.e. $\tau_r = v_0^2/D$.

It might be of interest to inspect the full dynamics of Eq. (63) in Cartesian velocity components. The Fokker-Planck equation for the probability distribution of positions and velocities assumes the form

$$\frac{\partial P(\mathbf{r}, \mathbf{v}, t|\mathbf{r_0}, \mathbf{v_0}, t_0)}{\partial t} = -v_x\frac{\partial P}{\partial x} - v_y\frac{\partial P}{\partial y} + \frac{D}{\mathbf{v}^2}\left[\frac{\partial}{\partial v_x}v_y - \frac{\partial}{\partial v_y}v_x\right]^2 P, \tag{67}$$

where we have used the Stratonovich interpretation of the stochastic integral. This equation is the starting point for the derivation of equations for the moments of the probability distribution. Later, we will use them to formulate hydrodynamic equations for the density, velocity, and temperature of an ensemble of active particles. Here, it is instructive to look at the dynamics of the mean velocity $\mathbf{u}(t)$. To obtain the dynamics for $\mathbf{u}$, Eq. (67) is multiplied by $\mathbf{v}$ and integrated over possible velocity values. This expression is normalized by the local density. Further, for simplicity we assume a homogeneous situations and put all spatial derivatives to zero. This yields

$$\frac{\mathrm{d}}{\mathrm{d}t}\mathbf{u}(t) = -\frac{D}{v_0^2}\mathbf{u}. \tag{68}$$

The mean velocity relaxes to zero and the mean relaxation time $\tau_r = v_0^2/D$ is inverse to the intensity D of the noise which acts on the angle leading to a loss of directed motion.

3.1.5 Angular dynamics of Active Brownian particles

Some of recent measurements [255] indicate that during short time intervals the hops leading to the overall random motion of Daphnia may follow with some preferred angle to the left or right with respect to their previous direction of motion. In the following we will consider generic models which describes such kind of motion. We will present some details within a model of active Brownian motion and formulate also random walk model for a hopping dynamics.

The aim is to develop powerful techniques for the determination of the diffusion coefficient. This diffusion coefficient if of central interest [252] in certain problems e.g. in ecology and has received renewed attention recently [200,219,220,236,273,307]. It was proposed to be the central interest since an optimally selected diffusion coefficient might give an advantage in the search for food [77,78,133]. Food consumption in a fixed time and in bounded geometries depend significantly on the value of the spatial diffusion and can be maximized by optimal selection of its value [307].

Here we look first at active Brownian particles performing the motion with a preferred rotation direction, quantified by the angular velocity Ω. Motivated by the example of Daphnia mostly performing an in-plane motion, we confine ourselves to a two-dimensional situation. In what follows, we first consider the properties of the angular motion of such active particles. In the next chapter, we will discuss how they affect their spatial diffusion. Here, we concentrate on the quite realistic case when the speed (absolute value of the velocity) can be taken as a constant but fluctuations in the direction of motion cannot be neglected.

The inclusion of turning angles is best represented in a polar coordinates description. Simply requiring that the angle will change per unit time by a fixed amount is described as

$$\frac{\mathrm{d}}{\mathrm{dt}}\,\varphi(t) = \Omega(t)g(s) + \frac{\sqrt{2D}}{s}\xi(t), \tag{69}$$

where $\Omega(t)$ is the instantaneous angular velocity. The function $g(s)$ shall describe a principal variation of the angular velocity in dependence on the speed $s = |\mathbf{v}|$. It is obvious that this function can be also a function of φ if the problem is not isotropic, say in case of applied external forces.

The second term on the r.h.s. of Eq. (69) stands for the fluctuating force with intensity D. An important case is that Ω is constant or switches between two different constant values, which represent two possible turning behaviors of the particle (dichotomous switching). As a transition rule for the switching between the two turning velocities one might assume that the dynamics follows a dichotomous Markov process, or as shown in the next section, the problem can be formulated as a renewal process with arbitrary waiting times densities in both states. Last but not least, Ω can be also a second Gaussian random process, which we will introduce later on as active internal noise. It has a component perpendicular to the direction of motion with $g(s) = 1/s$ (see Eq. 86) and stands for a random variation of the angular velocity.

In case of active Brownian particles we formulate the problem as a Newtonian dynamics with specific forces. The arising question what forces correspond to the introduced angular velocity can be easily answered via a transformation back to Cartesian velocities. In the two dimensional case we find in addition to the active pump and the noise term a force with

$$\frac{\mathrm{d}}{\mathrm{dt}}\mathbf{v}(t) \propto \mathbf{F}_{turning} = g(|\mathbf{v}|) \begin{pmatrix} \Omega(t)v_y \\ -\Omega(t)v_x \end{pmatrix}. \tag{70}$$

It resembles a Lorentz or Coriolis force with a vector $\Omega = (0, 0, \Omega)$ pointing in the z-direction perpendicular to the plane of motion. For the Lorentz-force, if the vector

is the magnetic field and $g(|\mathbf{v}|) = 1$, a charged particle performs a Larmor precision motion on a circle with radius depending on the initial conditions. Choosing $g(|\mathbf{v}|) = 1/|\mathbf{v}|$ the turning force becomes independent on the speed, which has been verified in experiments on artificial active particles [265]. We point out that the consideration of white noise (shot or Gaussian) will lead to a Stratonovich term, which will be discussed later on.

We proceed with the assumption that the velocity approaches quickly a stationary speed ($s \to v_0$, Eq. 62). From (69) one obtains the Fokker-Planck-equation (for the case that the angular velocity is not a white noise)

$$\frac{\partial}{\partial t} P(\varphi, t) = -\Omega(t) \frac{\partial P}{\partial \varphi} + D_\varphi \frac{\partial^2 P}{\partial \varphi^2} \tag{71}$$

with D_φ defined in Eq. (65). We note that D_φ is not necessarily small: For the Rayleigh-Helmholtz model (42) with $\alpha^2/\beta \gg D$ the value of v_0 is of the order $\sqrt{\alpha/\beta}$ and $D_\varphi \simeq D\beta/\alpha$ can be rather large for moderate values of α.

For a constant value of the angular velocity Ω this motion can be described by the following unwrapped transition probability density ($t \geq 0$):

$$P(\varphi, t | \varphi_0, 0) = \frac{1}{\sqrt{2\pi D_\varphi t}} \cdot \exp\left(-\frac{(\varphi - \varphi_0 - \Omega t)^2}{4 D_\varphi t}\right). \tag{72}$$

3.1.6 Active Brownian dynamics resulting from coupling of molecular motors

An example for active Brownian motion arising as a collective effect is the intracellular transport by coupled molecular motors. Motor proteins like myosin or kinesin run along filaments (actin, microtubules) within the cell, transport vesicles, or provide active forces [168, 181]. Single motors have a preferred direction of motion along a given filament, a motion that is powered by ATPase. In many situations motors are coupled, for instance, when pulling collectively at a large vesicle [149]. Collective effects in motor assemblies can be studied *in vitro* in motility assays in which the roles of transporter and track are reversed: on a glass surface covered with motors fixed in their position, a filament is transported involving typically a large number of motors (up to a few hundreds). A genuine collective effect which has been found in such experiments, is the occurrence of bidirectional motion. A filament running for a while in one direction suffers apparently spontaneously a reversal of the direction of motion and runs "backwards" [114]. This and other features of coupled molecular motors have been studied in the model by Jülicher and Prost, that we briefly discuss and for which we review the relation to an active Brownian particle's dynamics in the following.

The interaction between motor proteins and filament can be captured by different free energy landscapes between which the system switches by binding and release of ATP/ADP. Essential features of the motor's dynamics can be already captured in a model system switching between only two potentials where one of them is flat while the other one possesses a periodic structure with broken spatial symmetry (ratchet potential). Typically, the unbinding of the motor depends on its position along the backbone while the binding of ATP can be assumed to be independent of the motor position. The motion of the motor is affected by two kinds of noise: the thermal motion and the switching between the two states which is likewise stochastic. In a simple approach to the dynamics of motor assemblies, the coupling of motors can be regarded as rigid leading to only one spatial degree of freedom: the position of the backbone (e.g. its center of mass). In this approximation, the force acting on each
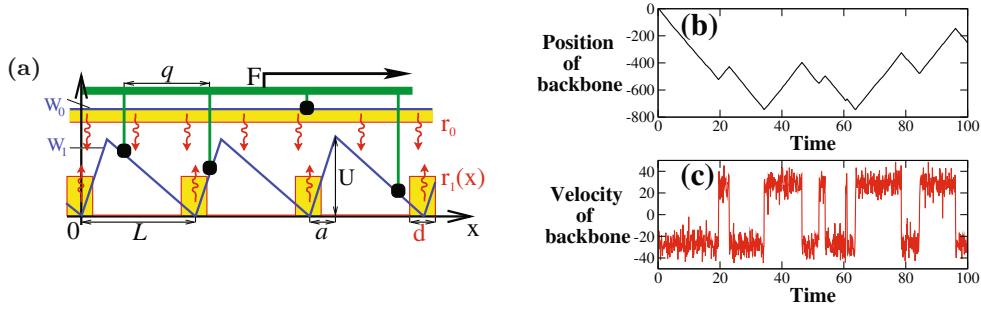
Fig. 5. Model of coupled molecular motors (CMM) (a), a typical trajectory of the backbone (b), and the corresponding velocity (c) for $N = 300$ and $a = L/2$. For large N, the dynamics of the CMM model can be approximated by the dynamics of an active Brownian particle. Panel (a) modified from [223].

motor contributes to the total force on the filamentous backbone and, in turn, the velocity of the single motor is given by that of the backbone. The equations for the overdamped dynamics of the backbone read

$$\Lambda\dot{x} = F_{ext} - \frac{1}{N}\sum_{j=1}^{N}\sigma_j(t)W'(x + j\cdot q) + \sqrt{\frac{k_B T\lambda}{N}}\eta(t),$$

$$\sigma_j = 0 \underset{r_1(x+j\cdot q)}{\overset{r_0}{\rightleftharpoons}} \sigma_j = 1. \tag{73}$$

Here, x is the central coordinate of the backbone, λ is a an effective friction coefficient per motor, F_{ext} an external force applied to the backbone, and $W(x)$ is the piecewise linear ratchet potential shown in Fig. 5a, the asymmetry of which determined by the parameter a (see Fig. 5a; for $a = L/2$ the potential is symmetric). The state of a given motor j at time t is determined by the variable $\sigma_j(t)$ which takes the values 0 or 1. The switching rate r_0 for the transition $0 \rightarrow 1$ does not depend on the spatial position. The rate for the transition $1 \rightarrow 0$ attains the value $\hat{r}_1$ only if the motor is within the neighborhood of size d centered around the potential minimum and is zero otherwise. Parameters in the following are $L = 1$, $d = 0.2L$, $\hat{W} = 1$, $\lambda = 0.01$, $r_0 = 40$, and $\hat{r}_1 = 500$. For simplicity, thermal fluctuations are neglected.

Simulations of the model for a large number of motors reveal a bidirectional motion of the assembly (cf. Fig. 5b) corresponding to a bistable velocity dynamics (Fig. 5c). It has been suggested [14, 223, 351] that the velocity of a large motor assembly ($N \gg 1$) can be well described by

$$\dot{x} = v, \qquad \dot{v} = f(v) + g(v)\xi(t), \tag{74}$$

i.e. by an active Brownian particle (ABP) model, in which we also allow for a speed-dependent noise intensity. This means essentially that for large N (i) the space dependence of the problem vanishes and (ii) the many dichotomous degrees of freedom together with the interaction of motors and potential results in one continuous degree of freedom (the velocity). The original problem does not possess any inertia, the new time scale introduced in Eq. (74) comes from the switching times of the motor and the relaxation of the probability density of motors in the spatial ratchet potential.

We can write down a rather lengthy Master equation with one spatial degree and N dichotomous degrees of freedom for the system Eq. (73) and try to approximate
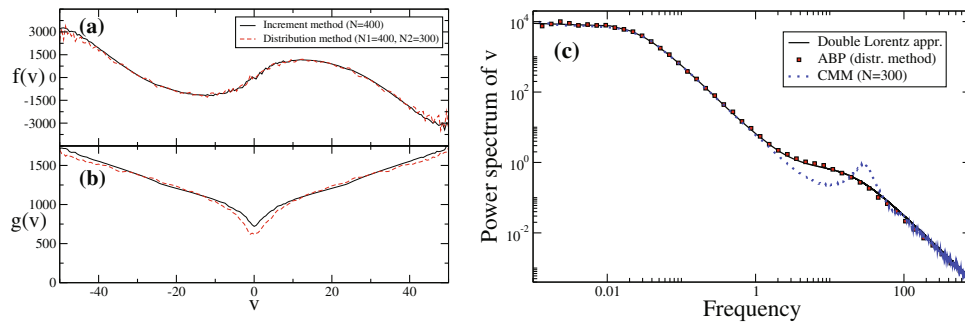
Fig. 6. Drift (a) and noise amplitude (b) of the CMM model estimated by the increment (solid) and distribution (dashed lines) methods for the symmetric system with $a = L/2$. In (c) the velocity power spectrum of the CMM model (dashed line) is compared to that of the approximating ABP model; for the latter, $f(v)$ and $g(v)$ were estimated via the distribution method. Also shown in (c) is the analytical approximation Eq. (75) (solid line) to the ABP's power spectrum consisting of two Lorentzian spectra. Modified from [351].

this equation by a Fokker-Planck equation with one spatial and one velocity degree of freedom corresponding to Eq. (74). Whether this is possible and if so how this mapping can be carried out analytically is still an open problem. In the following, we present some numerical evidence that a mapping from CMM to ABP model is a meaningful approximation.

Assume, that Eq. (74) is a reasonable approximation of the CMM model and suppose, a long time series of the assembly's velocity is given, how could we determine the functions $f(v)$ and $g(v)$? There are two methods to determine these functions [351,377]. First, we could measure how the velocity changes on a short time-scale. Mean and variance of the instantaneous velocity changes should be proportional to $f(v)$ and $g(v)$, respectively. Put differently, one measures the Kramers-Moyal coefficients of $v(t)$ [292]. Secondly, we could also measure the stationary distribution $P(v)$ (long-time statistics), which is uniquely determined by the two functions we are seeking. Together with one additional piece of information involving the time scale of the system (e.g. the rate of velocity reversals or the spatial diffusion coefficient), one can determine both functions $f(v)$ and $g(v)$.

The two methods have been applied to the CMM model in Ref. [351], and the resulting drift and diffusion functions in the symmetric case are shown in Fig. 6. The agreement between the functions determined by the independent increment and distribution methods is remarkable and thus shows that the ABP model is a reasonable approximation of the CMM model. The function $f(v)$ displays the shape of an inverted N, in particular, it possesses a negative slope for $v = 0$, i.e. a vanishing velocity is dynamically unstable. The noise in the approximate ABP dynamics is indeed multiplicative as the noise amplitude $g(v)$ increases for increasing speed. The latter feature is in marked contrast to the system studied by Yates et al. [377] in which the noise amplitude decreases with increasing speed.

However, despite the consistent nature of the ABP approximation at short and long time scales, there exists also a discrepancy between the CMM and ABP models on an intermediate time scale. The power spectra of both systems, shown in Fig. 6c display a good agreement at low to intermediate frequencies and at very high frequencies. In either limits the spectrum is well described by Lorentzian spectra, which correspond to those of a two state process of velocity reversals (range of low frequencies) and an approximate Ornstein-Uhlenbeck process for small-scale fluctuations around the two metastable velocities. For the ABP model, summing up these

two contributions [351]

$$S(f) \approx \frac{2D_{\text{eff}}}{1 + (\pi f/r)^2} + \frac{2g^2(v_{min})/N}{f'(v_{min})^2 + (2\pi f)^2} \qquad (75)$$

gives a reasonable approximation of the total spectrum (solid line in Fig. 6c). The CMM model, however, shows one additional feature, which is not captured by the ABP approximation: there is a pronounced peak around $f = 25$. This corresponds to a small-scale damped oscillation in the velocity around its metastable states, which cannot be captured by a first-order velocity dynamics as in Eq. (74). In summary, the velocity process of the CMM model in all its details is more complicated than the simple ABP dynamics even in the limit of a very large number of motors. Nevertheless, with respect to the statistics of the velocity and its reversals, to the spatial diffusion coefficient, and to the high-frequency fluctuations, the ABP model is an excellent approximation.

3.1.7 Depot model for internal motors and broken friction symmetry

So far, we have considered active motion induced by negative dissipation either through an internal energy depot or an effective velocity-dependent friction. In principle, such active Brownian particle models can always be considered as an effective, or "coarse grained", theoretical description of more complex microscopic dynamics leading to self-propelled motion as discussed in the previous section (Sect. 3.1.6) in the context of cooperative motion of many coupled molecular motors.

The physics of active transport on the sub-cellular level by such molecular motors and of related ratchet systems is a fascinating field of research, which has been under intensive investigation for decades now. A detailed review of the field is far beyond the scope of this work and we refer the interested reader to other comprehensive reviews on the subject [155,182,285]. Nevertheless, it leads us to a fundamental question, which we would like to address here in the context active particles: How can directed, self-propelled motion emerge in simple mechanical systems? In the case of directed transport in a ratchet, the directionality is based on breaking of the spatial symmetry of the underlying effective potential and in the presence of symmetric periodic forces or non-equilibrium fluctuations.

However, as seen by examples in living systems and technical systems, directed motion is possible also without any imposed external spatial asymmetry. The world around us is full of creatures like insects, birds and fishes, which are capable to move in a uniform medium by using special mechanisms developed in the process of evolution. Most of these creatures use some kind of periodic motion in order to propel themselves using specialized "devices", such as wings or fins. The corresponding motion of individuals consists of interchanging intervals of acceleration and slowing down, and in a simplified picture we may think of an internal oscillating motor driving this periodic motion. Typically the various mechanisms are connected to the head-tail polarity of the animals and to periodic changes of the shape of the individual and the related changes in the friction with respect to the external medium (see e.g. Fig. 7). This leads to a symmetry breaking in the velocity space, leading to asymmetry with respect to forward and backward motion of a polar particle, which allows an effective directed motion even if the oscillatory dynamics of the motor are symmetric. Recently, several models for directed motion have been proposed which employ similar mechanisms of a broken symmetry with respect to an internal degree of freedom [18,63,81,208,251,295].

We consider now the situation where the energy depot is coupled to such an internal degree of freedom. Here, we assume that it drives the internal oscillatory
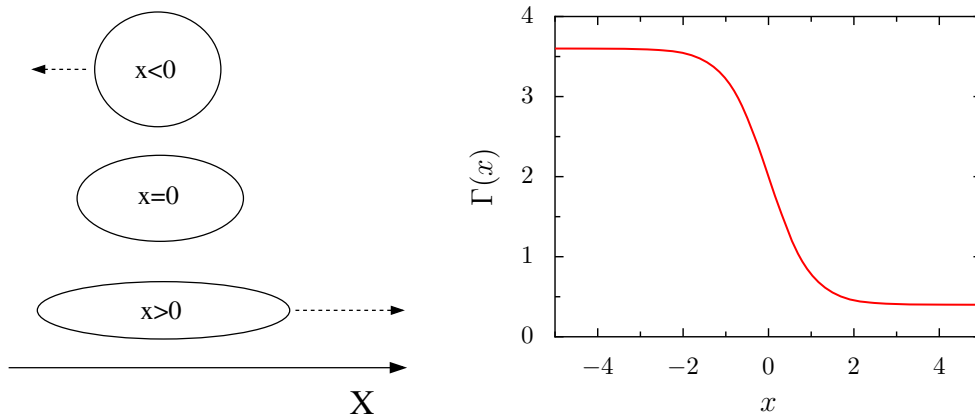
Fig. 7. Left panel: a possible scenario for the dependence of the friction coefficient along the direction of motion X on the internal coordinate x coupled to the propulsion force indicated by the dashed lines. Right panel: nonlinear friction depending on the internal distance of the dimer in dependence on the amplitude of oscillations according to the KRR model with $\Gamma_0 = 2$ and $C = 0.8$ or $\gamma_h = 3.6, \gamma_l = 0.4$.

dynamics in the inchworm model introduced by Kumar, Rao and Ramaswamy (KRR-model) [24, 208]. This new ansatz eliminates some shortcomings of the original depot model, such as, the absence of periodic accelerations observed in animal motion, or the difficulty to account for the case of large friction (overdamped limit) [295]. Let us explain the latter in more detail: Within the original depot model described in Sect. 3.1.3 the dynamics of the energy depot $e(t)$ depend on three constants: q - input rate, c - decay rate and d - rate of transmission to energy of motion, which determine the functioning of the motor mechanism. From the natural condition $v_0 > 0$, it follows that the depot model works only if

$$\gamma_0 < \frac{q_0 d}{c}. \tag{76}$$

This inequality means that the mechanism of the depot model breaks down at large friction values and, in particular, in the overdamped limit $\gamma_0 \to \infty$. However, in many biological examples, such as the motion of microorganism at low Reynolds numbers, this is the relevant limit. Here, we should mention the famous "Scallop theorem" formulated Purcell [280], which states that a net-displacement of swimmers at low Reynolds numbers is only possible if the symmetry of the motion is broken with respect to time-reversal, which shows the fundamental role of broken symmetries for directed motion [125].

Instead of considering particular swimming or propulsion mechanisms in the overdamped case, we discuss here a simple but generic variation of the depot model, which can be easily considered in the respective limit.

The basic idea of the model is the following:

1. The energy depot drives oscillations of an internal degree of freedom x (internal motor).
2. The internal oscillations are transformed into translational motion of the active object via a friction function dependent on the internal degree of freedom.

The varying friction can be realized for example in the following way: We consider a two-dimensional ellipse-like object with the axes a and b. We assume that the objects

moves on a line parallel to the larger axis ($b > a$). Let c be the equilibrium distance between the two focal points of the ellipse and the internal coordinate $x(t)$ describe the temporal deviations of the equilibrium distance. If $x(t) > 0$ than the ellipse is more stretched and for $x(t) < 0$ it assumes a more spherical shape. Thus a periodic change in $x(t)$ leads to a periodic change in the friction of the object. If further the force leading to a displacement of the center of mass of the object $X(t)$ is coupled to the internal variable x (simplest case: elastic coupling), than directed motion of the object can be observed despite symmetrical internal oscillations.

As a model of such a mechanism we consider an object with a large mass $M \gg 1$, located at position $X(t)$ which is elastically coupled to an internal degree of freedom $x(t)$ [295]:

$$\dot{X} = V, \qquad M\dot{V} = -M\Gamma(x)V + kx + Noise. \tag{77}$$

Further we assume the internal degree of freedom (the motor) to have the following dynamics driven by the energy depot (see Eq. 52)

$$\dot{x} = v, \qquad \dot{v} = (dev - \gamma_0)v - kx - \omega_0^2 x + noise. \tag{78}$$

The dynamics of the internal degree of freedom correspond to an active Brownian particle of unit mass in a confining harmonic potential $U(x) = (k + \omega_0^2)x^2/2$. The depot energy observes the standard balance equation

$$\dot{e} = q_0 - ce + dv^2 e. \tag{79}$$

We assume in our model, that the friction acting on the big mass M in the medium depends on the internal motor variable $x(t)$ as in the KRR-model [208] with

$$\Gamma(x) = \Gamma_0(1 - C\tanh(Bx)). \tag{80}$$

The friction is Γ_0 for $x = 0$ and decreases with increasing x up a minimal value $\Gamma_{\min} = \Gamma_0(1 - C)$ for $x \to \infty$. It increases with decreasing x with $\Gamma_{\max} = \Gamma_0(1 + C)$ for $x \to -\infty$. The internal degree of freedom x corresponds in the original KRR-model to the relative distance of the two masses constituting the dimer.

We see that the motor plays the role of an effective bridge between the energy depot and the dynamics of the mass M. The above mechanism of self-propulsion, only seemingly violates the principle of mechanics that internal forces do not affect the motion of the center of mass. However, internal forces may affect the external dissipation, and may therefore lead to directed motion [40,63,138,251].

In Fig. 8 we shows an example of the temporal dynamics of different model variables. A characteristic feature of the dynamics is the periodic structure of acceleration, velocities and trajectories. Similar structures of the trajectories are quite typical mode of translational motion of animals. For example, the motion of different organisms such as Daphnia [133], Chlamydomonas [89,132] consist of periodically repeating intervals. Each interval contains at the beginning a subinterval of strong displacement, corresponding to a large accelerating force and a second subinterval where the displacement is nearly zero. Correspondingly, the velocity is a periodic function which alternates between high and low values. In our model this time structure is based on the action of a periodically working internal motor which generates the periodic accelerations.

Please note that the above model is only valid if the feedback of the time-dependent external friction $\Gamma(x)$ on the motor dynamics can be neglected. This approximation may lead to problems with the energy balance for example at small k-values and big amplitudes of the friction which are neglected here.
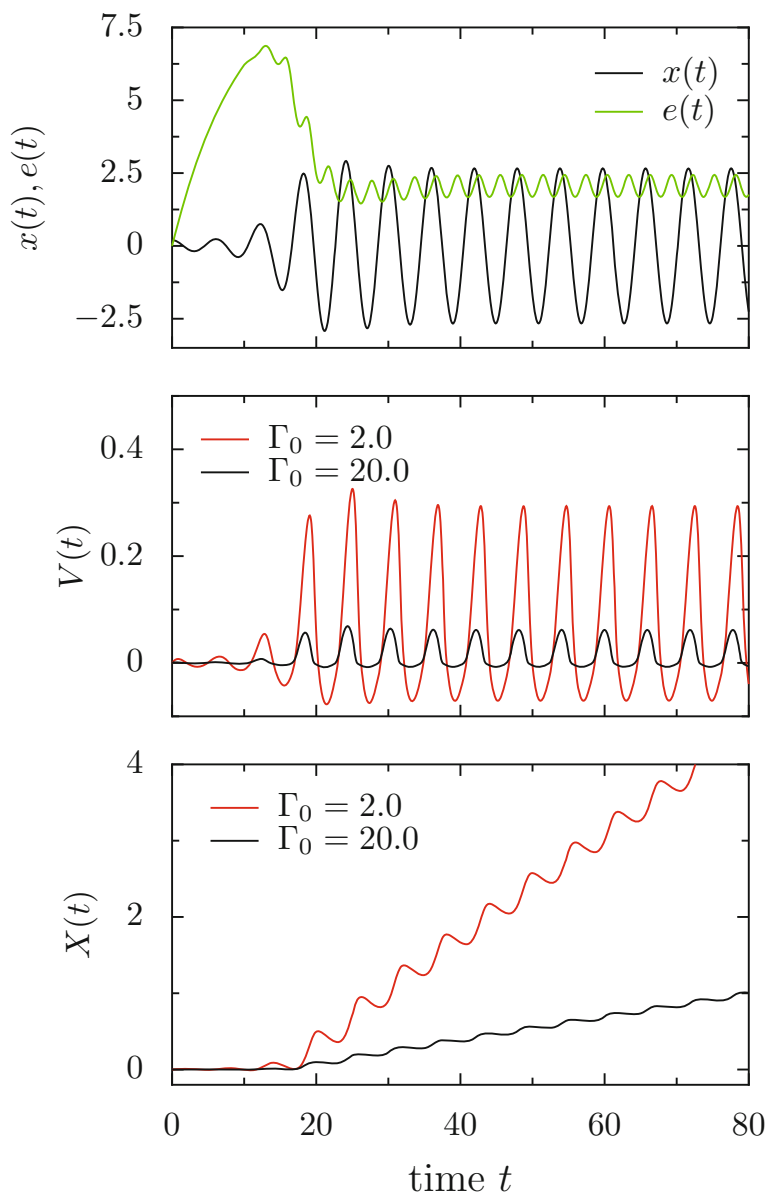
Fig. 8. Propulsion via an oscillating internal motor: internal coordinate $x(t)$ and energy depot $e(t)$ (top); external velocity $V(t)$ (center) and position $X(t)$ for two different friction coefficients $\Gamma_0 = 2$ and $\Gamma_0 = 20$. Other parameters: $\gamma_0 = 0.2$, $k = 1$, $\omega_0 = 0.1$, $M = 10$, $q = 1$, $d = c = 0.1$, $b = 1$, $C = 0.8$.

3.2 Particles driven by active fluctuations

Another important difference between ordinary Brownian motion and active moving objects consists in the possible directions of the fluctuations and their statistical properties. This will be the central point of this section and we will distinguish between passive noise terms from external sources acting as random (undirected) forces, e.g. the molecular agitation in Brownian motion and active from internal noise sources

connected with the active dynamics of the particle such as its propulsion mechanism. The latter is connected to the actual state of the particle including its direction of motion. In the next Sect. 3.2.4 we introduce a fluctuating energy supply which will affect the particle's motion in a similar manner.

We look again at two spatial dimensions and consider polar active particles with the heading unit vector $\mathbf{e}_h$ as defined in Sect. 2.3. The time derivative of the velocity vector yields

$$\dot{\mathbf{v}} = \dot{v}\mathbf{e}_h + v\dot{\phi}\mathbf{e}_\phi \tag{81}$$

which gives two Langevin equations for the evolution of the velocity v and the orientation ϕ^2:

$$\dot{v} = -\gamma(v)v + \mathcal{F}(t)\mathbf{e}_v \tag{82}$$

$$\dot{\phi} = \frac{1}{v}\,\mathcal{F}(t)\mathbf{e}_\phi. \tag{83}$$

Let us first concentrate on the random force $\mathcal{F}(t)$ in Eqs. (82). Further on, we will distinguish two different types of fluctuations, which we will refer to as *passive* (or *external*) and *active* (or *internal*) fluctuations, respectively. Passive fluctuations are assumed to have their origin in an fluctuating environment in which the particle moves. In a homogeneous environment the passive random force $\mathcal{F}_\mathrm{p}(t)$ has to be independent on the direction of motion. The prominent example of particles subjected to passive fluctuations is ordinary Brownian motion as presented in Sect. 2, where the random force is associated with the random collisions of the particle with the molecules of the surrounding fluid. Thus, we introduce the external fluctuations in the same way as we did for Brownian motion in two dimensions, i.e. as a random noise vector with the components of the vector given by two uncorrelated, Gaussian white noise terms with the same noise intensity D. The noise vector reads:

$$\mathcal{F}_\mathrm{p}(t) = \sqrt{2D}(\xi_x(t)\mathbf{e}_x + \xi_y(t)\mathbf{e}_y). \tag{84}$$

Here, $\xi_i(t)$ $(i = x, y)$ are δ-correlated, normally distributed random variables with zero mean (see Eq. 6, white Gaussian noise):

$$\langle\xi_i(t)\rangle = 0 \quad \langle\xi_i(t)\xi_j(t')\rangle = \delta_{ij}\delta(t - t'), \, i = x, y. \tag{85}$$

A second possible model of fluctuations is assumed to have its origin in the internal dynamics of active particles. This active fluctuations are a pure far-from equilibrium phenomenon and are relevant in the motion of an biological agents or artificial self-propelled particles. The origin of these fluctuations can be for example variations in the propulsion of chemically powered colloids [169, 265, 300], complex intra-cellular processes in cell motility [42, 318] or unresolved internal decision processes in animals [27, 200, 250]. For example, the motion of a macroscopic animal moving in a homogeneous environment, where the fluctuations due the environment can be assumed as negligible, may nevertheless appear random to an external observer. The apparent randomness of the motion stems from internal decisions of the biological agent to change its direction of motion ϕ and/or its velocity $v(t)$ (internal coordinates). On the other hand, for artificial active particles, fluctuations in a microscopic power engine might occur due to its smallness. They may be associated, for example, with fluctuations in the concentration of fuel molecules driving self-propelled colloids (see

---

² Note that the angular dynamics diverge for $v = 0$. This is due to the fact that we are considering point-like polar particles, which for vanishing velocity may turn infinitely fast. This divergence can be eliminated by considering finite sized particles.
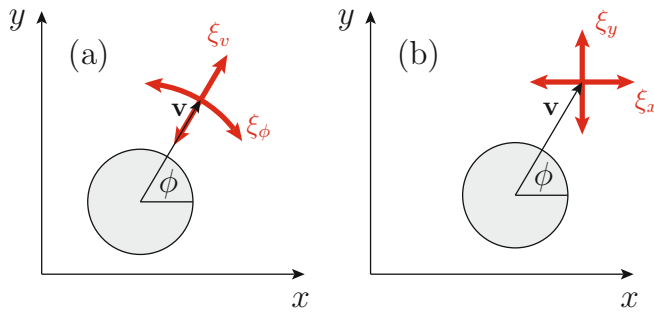
Fig. 9. Visualization of the difference of passive (external) and active (internal) fluctuations (thick red/gray arrows). (a) Passive fluctuations $\xi_x(t)$ and $\xi_y(t)$ uncorrelated to the direction of motion. (b) Active fluctuations $\xi_v(t)$ and $\xi_\phi(t)$ (thick red/gray arrows). Parallel and perpendicular to the direction of motion (heading).

e.g. [265, 300]). The important point is that the fluctuating forces are intrinsically connected with the internal propulsion mechanism of the active particle. Thus, the corresponding direction of the active fluctuating forces turn with the particles orientation.

We do not intend to resolve the internal processes, and assume for simplicity fluctuations in the direction of motion and in the velocity of the agent as independent stochastic processes, with possible different statistical properties (see also [273]).

Here, we make a simple ansatz for the active fluctuations, as independent Gaussian white noise in the direction of motion $\mathbf{e}_h$ and in the angular direction $\mathbf{e}_\phi$:

$$\mathcal{F}_a(t) = \sqrt{2D_v}\xi_v(t)\mathbf{e}_h + \sqrt{2D_\phi}\xi_\phi(t)\mathbf{e}_\phi \tag{86}$$

with $\xi_i(t)$ as defined in Eq. 85 ($i = v, \phi$). In the general case we have to assume different noise intensities of the active angular and velocity noise: $D_\phi \neq D_v$.

We mention that smaller objects will experience always molecular agitation or the stochastic character of the external forces. Therefore the general situation is the combination of the introduced passive (84) and active (86) fluctuations. A visualization of the different fluctuation types is shown in Fig. 9.

3.2.1 Quasi-Brownian particles with active fluctuations

Before we investigate (stochastically) pumped particles, we sketch shortly the difference between the two different fluctuating forces by considering a simple model with linear friction discussed in Sect. 2 in the context of ordinary Brownian motion.

Let us start with particles which are subject to Stokes friction and noise. The case of passive fluctuations (ordinary Brownian motion) was discussed in Sect. 2. The stationary velocity distribution according to Eq. 11 is a two dimensional Gaussian distribution centered at the origin with width D/γ. Please note that the simple Stokes friction is apolar by definition (symmetric with respect to $v = 0$). Thus, the heading vector is equivalent to the velocity unit vector $\mathbf{e}_h = \mathbf{e}_v = \mathbf{v}/|\mathbf{v}|$.

The dynamics for purely active noise read:

$$\frac{\mathrm{d}}{\mathrm{d}t}\mathbf{v} = -\gamma\mathbf{v}(t) + \sqrt{2D_v}\,\mathbf{e}_v(t)\xi_v(t) + \sqrt{2D_\phi}\,\mathbf{e}_\phi(t)\xi_\phi(t), \tag{87}$$
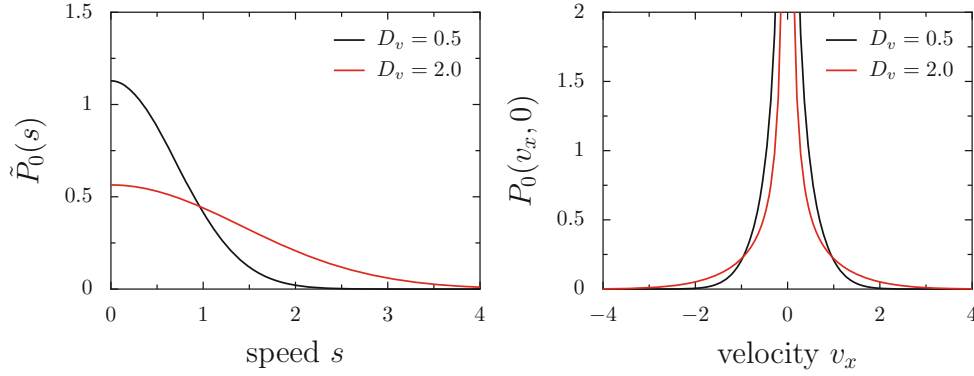
Fig. 10. Stationary distributions of a linearly damped particle with internal noise for two different noise intensities D_v. Left panel: stationary speed distribution $\tilde{p}_0(s)$; right panel: cross section of the corresponding Cartesian velocity distribution $P_0(v_x, v_y)$.

where the stochastic sources are defined in Eq. 86. In (v, ϕ)-coordinates, we obtain two decoupled differential equations for the velocity and the angle:

$$\frac{\mathrm{d}}{\mathrm{d}t}v = -\gamma v + \sqrt{2D_v}\,\xi_v(t) \qquad \frac{\mathrm{d}}{\mathrm{d}t}\phi = \frac{1}{v}\sqrt{2D_\phi}\,\xi_\phi(t). \tag{88}$$

As $t \to \infty$ the velocity distribution becomes stationary without any preferred direction. It is a Gaussian in the velocity v

$$P_0(v) = \mathcal{N}\,\exp\left(-\frac{\gamma\,v^2}{2D_v}\right), \qquad P_0(\phi) = \frac{1}{2\pi}. \tag{89}$$

For the speed $s = |v|$ we derive

$$\tilde{P}_0(s) = \frac{1}{2}\Big(P_0(v) + P_0(-v)\Big) = \mathcal{N}\,\exp\left(-\frac{\gamma\,s^2}{2D_v}\right), \tag{90}$$

which in contrast to the Rayleigh distribution (20) assigns maximal probability density to the state with zero speed. The reverse transformation to Cartesian velocities gives us the corresponding velocity distribution

$$P_0(v_x v_y) = \mathcal{N}\,\frac{1}{\sqrt{v_x^2 + v_y^2}}\,\exp\left(-\frac{\gamma\,(v_x^2 + v_x^2)}{2D_v}\right), \tag{91}$$

which exhibits a singularity at the coordinate origin ($x = 0, y = 0$). The distribution is clearly a nonequilibrium one. The peak at the origin is due to the many stochastic transitions created by $\xi_v(t)$ which pass through the state with vanishing velocities. In Fig. 10 two examples of the stationary velocity distribution are shown.

The most common situation is the presence of both, active and passive noise sources, with different intensities. Therefore we consider

$$\frac{\mathrm{d}}{\mathrm{d}t}\mathbf{v} = -\gamma\,\mathbf{v} + \mathcal{F}_a(t) + \mathcal{F}_p(t) \tag{92}$$

where the different noise terms are defined in Eqs. 84 and 86. Changing to internal coordinates, we obtain the Fokker-Planck equation for $P = P(v, \phi, t | v_0. \phi_0, t_0)$ with

the typical D/v term in analogy to polar representation, see (19),

$$\frac{\partial P}{\partial t} = -\frac{\partial}{\partial v}\left\{\left(-\gamma v + \frac{D}{v}\right)P\right\} + (D + D_v)\frac{\partial^2 P}{\partial v^2} + \frac{D + D_\phi}{v^2}\frac{\partial^2 P}{\partial \phi^2}. \qquad (93)$$

D, D_v and D_ϕ are intensities of the different noise sources: passive and active velocity and angular noise. One can solve for the stationary distribution which factorizes again. Without a preferred direction we get again the uniform distribution for the angular dependence which is due to increased noise intensity approached at a faster time scale. The velocity distribution is symmetrical with respect to $v = 0$ and reads

$$P_0(v) = \mathcal{N} |v|^{\frac{D}{D+D_v}} \exp\left\{-\frac{\gamma}{2(D + D_v)} v^2\right\}, \qquad (94)$$

which for the limiting cases $D \to 0$ and $D_v \to 0$ gives the known distributions (89) and (20). Due to the symmetry the speed distribution corresponds directly to the velocity distribution, with $v \to s = |\mathbf{v}|$ and an additional factor $1/2$ in the normalization constant $\mathcal{N}$. Finally we obtain the Cartesian velocity distribution to

$$P_0(v_x, v_y) = \mathcal{N} (v_x^2 + v_y^2)^{-\frac{D_v}{2(D+D_v)}} \exp\left\{-\frac{\gamma}{2(D + D_v)}(v_x^2 + v_y^2)\right\}. \qquad (95)$$

It reduces the Maxwellian velocity distribution for $D_v = 0$ and the case (91).

3.2.2 Active shot noise fluctuations

Active, or internal, noise as discussed is not restricted to Gaussian white noise. We assume that an active particle is subjected to white shot noise as introduced in [46] as a limit of a dichotomous Markov process. The random "force shots" occur at exponentially distributed times t_i with the mean interval τ or rate $\lambda = 1/\tau$ The weights h_i, which the delta spikes in the shot noise are multiplied, are due to the distribution with $\rho(h)$ with average $\langle h \rangle$.

$$\xi_{SN}(t) = \sum_i h_i \delta(t - t_i), \quad \langle t_{i+1} - t_i \rangle = \tau, \quad \langle h_i \rangle = h. \qquad (96)$$

As the shot noise is the limiting case of a dichotomous Markov process the weights are exponentially distributed. Subsequently the white shot noise has the properties:

$$\langle \xi_{SN}(t) \rangle = \frac{h}{\tau}, \quad \langle \xi_{SN}(t_1)\xi_1(t_2) \rangle - \langle \xi_{SN} \rangle^2 = \frac{h^2}{\tau} \delta(t_1 - t_2). \qquad (97)$$

The internal driving is assumed to act along the heading direction according to

$$\frac{\mathrm{d}}{\mathrm{d}t} \mathbf{v} = -\gamma \mathbf{v} + \mathbf{e}_h(t)\xi_{SN}(t) + \sqrt{2D_\phi}\,\mathbf{e}_\phi \xi_\phi(t). \qquad (98)$$

The dynamics are not overdamped, i.e. the shots do not affect the coordinate immediately but act as forces pulses on the velocity. The angular noise is assumed to be Gaussian and white as defined in (6).

Distributions of the velocities obtained from simulations are presented in Fig. 11. For fast appearance of subsequent shots with short mean interval τ the velocity distribution is approximately Gaussian around the mean value of the speed which is h/τ (note that the velocity scale at the abscissa starts at $v = 0$). It results in a crater-like distribution in the Cartesian frame. Otherwise, in case of rare shots the particles
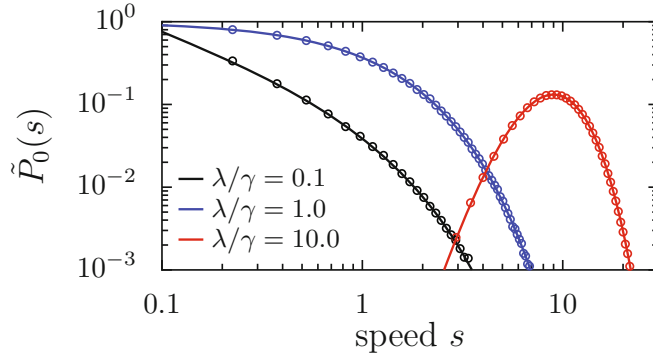
Fig. 11. Stationary speed distributions $\tilde{p}_0(s)$ for Stokes friction with active shot-noise fluctuations for different values of $\lambda/\gamma = 1/(\tau\gamma)$. Solid lines show the result obtained in Eq. (101), whereas symbols show numerical results [298].

spend much time at the origin leading to the peak in the Cartesian distribution. We do not show here the situation where instantaneously the crater and the peak at zero exist.

In polar representation with $v_x = v\cos(\phi)$ and $v_y = v\cos(\phi)$ the equations of motion become

$$\dot{v} = -\gamma v + \xi_1(t) \quad \dot{\phi} = \frac{1}{v}\sqrt{2D_2}\,\xi_2(t). \tag{99}$$

The equation for the velocity distribution is independent of the angle dynamics [73]

$$\frac{\partial}{\partial t}P(v.t|v_0,t_0) = \frac{\partial}{\partial v}\gamma v P - \lambda P(v,t|v_0,t_0) + \lambda \int_0^\infty dh\,\rho(h)P(v-h,t|v_0,t_0). \tag{100}$$

The velocity is strictly non-negative and the difference to the speed disappears. In Fig. 11 we present results of computer simulations for three different sets of parameters. Despite its simplicity the model features typical properties of active motion like directed motion with non-vanishing mean velocity.

In the stationary limit the ϕ-distribution becomes uniform again. The v-distribution can be calculated taking the shot-noise limit of the balance equation for the probability density function of a dichotomous Markov process. It reads

$$P^0(v) = \mathcal{N}\,v^{\left(\frac{\lambda}{\gamma}-1\right)}\,\exp\left(-\frac{v}{h}\right), \quad v \geq 0. \tag{101}$$

Please note that as $v \geq 0$ the above velocity distribution corresponds directly to the stationary speed distribution $P_0(v) = \tilde{P}_0(s)$.

In Cartesian coordinates the probability distribution becomes sharply peaked at the origin for $1/(\gamma\tau) < 2$:

$$P^0(v_x,v_y) = \mathcal{N}\,|\mathbf{v}|^{\left(\frac{1}{\gamma\tau}-2\right)}\,\exp\left(-\frac{|\mathbf{v}|}{h}\right), \quad |\mathbf{v}| = \sqrt{v_x^2+v_y^2}. \tag{102}$$

Examples of the distribution functions obtained from numerical simulations shown in Fig. 12 confirm our analytical findings. We point out that with constant weights the probability distribution functions obtained from simulations (not shown) differ strongly from the result obtained in Eq. (102).
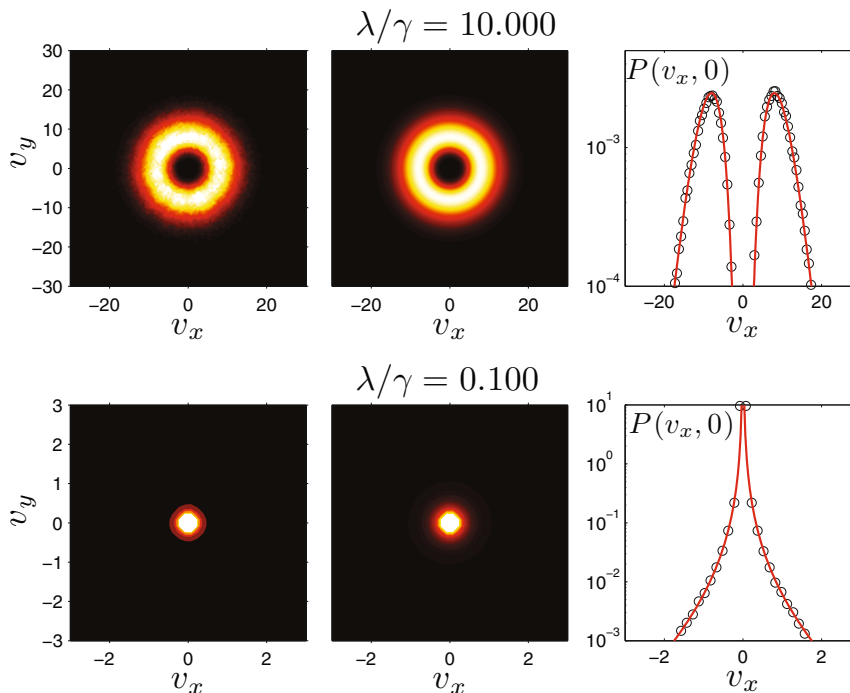
Fig. 12. $P_0(v_x, v_y)$ with internal shot noise, top: the case of fast occurrences of spikes $\lambda = 10$ and damping $\gamma = 1$, bottom: the case of rare generation of spikes $\lambda = 0.1$ and damping $\gamma = 1$, left: simulations; central: analytics; right: cross-sections $P_0(v_x, 0)$ analytics (solid) vs. numerics (symbols). Other parameter: $a = 1$.

3.2.3 Nonlinear friction and asymmetric driving

In absence of external forces, the shape of the velocity distribution does not depend on the angle dynamics, as $P(v, \phi, t) = P(v.t) P(\phi, t|v)$. On the other hand the angle dynamics depends on the velocity since the derivative of $\phi(t)$ scales with $1/v$. Therefore a full factorization becomes only possible in the case of constant velocities or as an approximations. Furthermore the distribution function is isotropic in the long time limit (independent on ϕ) only in the absence of external forces.

Therefore the consideration of two- and also three dimensional problems with internal noise acting on the scalar velocity $v(t)$ simplifies the stationary analysis and many different models become tractable. Our third example is motivated by vibrational dynamics and deals with nonlinear friction and an asymmetric driving with vanishing mean. Surprisingly this dynamics may lead to a directed motion of particles resulting in a non-vanishing mean velocity v.

As in vibrational dynamics we will assume nonlinear friction [40] and, in contrast to the shot-noise case, stochastic forces acting on the particle with a vanishing mean

$$\frac{\mathrm{d}}{\mathrm{d}t}\mathbf{v} = -\gamma|\mathbf{v}|^{n-1}\mathbf{v}(t) + \mathbf{e}_v(t)\xi_{DMP}(t) + \sqrt{2D_\phi}\,\mathbf{e}_\phi(t)\xi_2(t). \tag{103}$$

Here, the stochastic term acting on the velocity $\xi_{DMP}(t)$ is assumed to be stochastic force given by a dichotomous Markov process (see Sect. 2.4), whereas the angular noise is again white and Gaussian.

Prominent types of friction are Stokes friction ($n = 1$) or the "quadratic drag force" ($n = 2$) occurring for objects moving at large velocities through fluids, e.g.
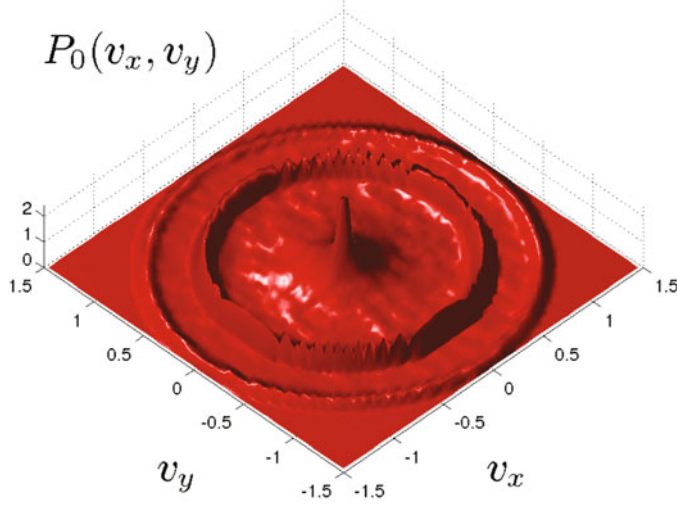
Fig. 13. Stationary velocity distributions (Cartesian frame) of particle driven by an internal DMP and Gaussian white noise in the angle-dynamics obtained from simulations. The "double-crater" arise due to the asymmetry of the forward and backward motion.

in aerodynamic engineering. Another prominent type of friction is the so called "dry friction" with $n = 0$.

It was shown by Cebiroglu et al. [57], that for a nonlinear friction the particle starts to move into the direction of $\mathbf{e}_h$ even if the time average of the stochastic force vanishes ($\langle \xi_{DMP}(t) \rangle = 0$) as long as $\xi_{DMP}(t)$ is asymmetric. This was considered by Blekhman [40] in an investigation of trajectories, whereas in [57] stochastic methods have been used to find the vanishing average. The dichotomous Markov process $\xi_{DMP}(t)$ can assume two values $A_\pm$ and $\lambda_\pm$ are the rates giving the probability per unit time to leave the corresponding states. The time average of the applied stochastic force vanishes if

$$\langle \xi_{DMP}(t) \rangle = \frac{A_+ \lambda_- + A_- \lambda_+}{\lambda_+ + \lambda_-} = 0. \tag{104}$$

The asymmetry of ξ_{DMP} is described by the ratio

$$p = |A_-/A_+|, \quad \text{with} \quad 0 \le p \le 1, \tag{105}$$

where we assume, without loss of generality, $|A_-| \le |A_+|$.

Here we present only the stationary velocity probability density function

$$P_{st}(v) = N|i_+(v)i_-(v)| \exp\left[-\kappa_+ \int^v i_+(v')dv' - \kappa_- \int^v i_-(v')dv'\right],$$

where the functions $i_\pm(v)$ are defined by the inverse of the acting forces

$$i_\pm(v) = \frac{1}{-\gamma|v|^n \text{sign}(v) + A_\pm}$$

which due to the applied angular noise is independent on ϕ.

The velocity distribution mapped back to Cartesian velocities is shown in Fig. 13 with a central peak at the origin and a "double-crater" like distribution. The ring-like maxima of the probability density function correspond to the preferred speed values in any direction. The peak at the origin stems from the finite probability of vanishing
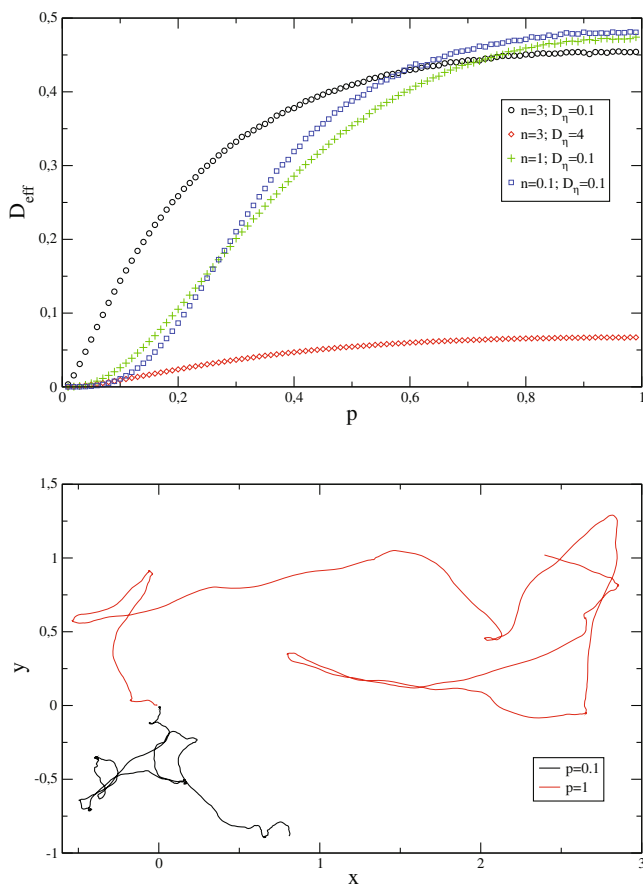
Fig. 14. Particles with nonlinear friction subject to DMP fluctuations with vanishing mean. Bottom: two paths of particles in two dimensions for different asymmetry of strokes. Top: diffusion coefficient for different exponents in the friction coefficient (103) as function of the asymmetry [57].

speed, as for particles with Stokes friction with active Gaussian velocity fluctuation (see Sect. 3.2.1).

We have simulated [57] the two dimensional situation

$$\frac{\mathrm{d}}{\mathrm{d}t}\mathbf{r}(t) = \mathbf{v}(t) \quad \text{while} \quad \mathbf{v}(t) = v(t) \cdot \mathbf{e}_h(t) \tag{106}$$

and two paths of realizations are shown in Fig. 14.

The particles have a nonzero average speed. The diffusive motion is becoming stronger if the asymmetry vanishes $p \to 1$, which is reflected in the diffusion coefficient shown in Fig. 11. This growth is caused mostly by the variance of the velocities which scales the diffusion coefficient and which increases if the strokes becomes more symmetric [57].

3.2.4 Fluctuating energy depots

Another example where noise depends on the orientation can be discussed within the depot model. We so far assumed a permanent food supply. Here we study the situation that the food supply occurs randomly and underlies stochastic influences. Doing so,

we extend the model with energy depot (see Sect. 3.1.3) to the case that the energy is provided at discrete times with packets of chemical energy which is subsequently converted into acceleration of motion [331]. In contrast to mechanical external noise which has not preferred direction, such energetic noise is directed likewise an internal noise and acts into the direction of motion. We assume, that alterations of the direction have a different origin than the energetic noise supply.

We propose here an oversimplified model [331] and assume that the food supply is a Poissonian shot noise process as it was introduced in Sect. 2.4. More precisely we assume that the particles are supplied at discrete times with packets of chemical energy which is subsequently converted into acceleration of motion. This should model the situation that animals, birds, insects or bacteria pick up nutrients at different, randomly distributed times. For simplicity we assume that the time intervals between the food-supplies follow the pattern of a Poisson point process [53, 73, 111, 195, 229, 259, 384]. Possible application to ratchet problems with energy supply modeled as shot noise imposed on Brownian motion have also been presented [101, 123, 124].

We relate a shot-noise driven energy depot with the Brownian dynamics of individual particles. We adapt the picture in which the energy depot accelerates the particle along the direction of motion with the strength d [101, 106, 123, 312, 331] as introduced in Section 3.1.3. The new assumption is that the carried energy in the depot $e(t)$ now obeys the stochastic balance equation

$$\frac{\mathrm{d}}{\mathrm{d}t} e = q(t) - (c + d\mathbf{v}^2)e. \tag{107}$$

Therein the function $q(t)$ corresponds to a shot noise consisting of energy packets h_i which are exponentially distributed with mean h and arriving at discrete times t_i with rate $\lambda = 1/\tau$. The time average of the shot noise process is denoted as $\langle q(t) \rangle = q_0 = h/\tau$.

In the case of vanishing mechanical noise, we obtain two stationary solutions for the velocities averaged over the stochastic food supply. The first is resting with $\langle \mathbf{v}_1 \rangle = 0, \langle e_1 \rangle = q_0/c$ and the second stands for running with $\langle \mathbf{v}_2^2 \rangle = q_0/\gamma_0 - c/d$, $\langle e_2 \rangle = \gamma_0/d$. Therefore dependently on the energy supply, the system exhibits two different regimes. When the energy input is high enough, the particle moves at a non-zero velocity. If the energy input is too small, the energy fluctuates but the velocity remains zero.

Further on, we can distinguish two limiting cases [331]: (i) The smooth regime: Here the shots are so dense that the mechanical system sees practically a continuous flow of energy. This is the case, when the mean time interval between two shots $\langle t_{shot} \rangle = \tau$ is much shorter than the timescale of the decay of the energy depot $t_e = 1/(c + d\mathbf{v}^2)$. Now we insert the stationary solution for the velocity, Eq. (60, DM). Then we speak of a smooth regime when the rate of the shots $1/\tau \gg dq_0/\gamma_0$. In this situation, the stochastic food supply can be well approximated by Gaussian noise. (ii) The shot regime: The shots arrive so seldom that every shot is a special event which accelerates the particle. This is the case when the mean time interval between two shots is much longer than the timescale of the decay of the energy depot, i.e. the rate $1/\tau \ll dq_0/\gamma_0$.

Typical trajectories and energy distributions of the smooth and the shot regime are shown in Fig. 15 and Fig. 16. Note that the mean energy input is equal for the two regimes. In the smooth regime, the energy shows a maximum at $e = \gamma_0/d$. In the shot regime we observe a maximum at very low energies and additional smaller maxima at multiples of h. The maximum at low energies occurs because the particle converts the available energy from the depot to kinetic energy much faster than the average
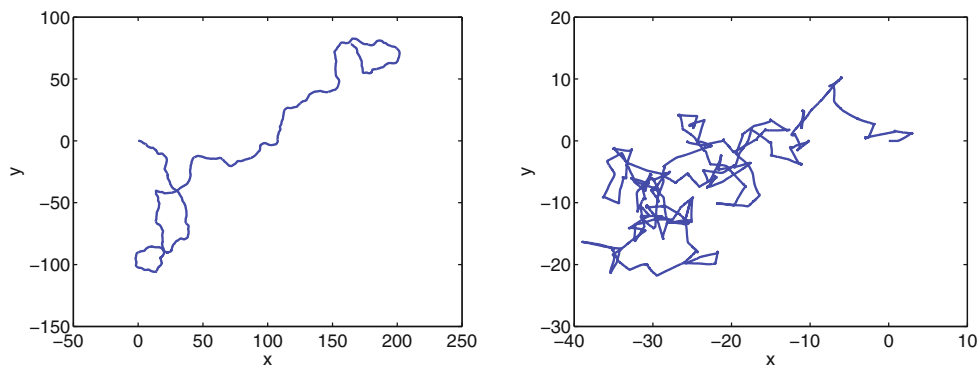
Fig. 15. Typical trajectories in the smooth regime (left, $\tau = 0.05$) and shot regime (right, $\tau = 5$). The simulation times are equal for both figures, however the length scales are different. Other parameter values: $q_0 = 1, D = 0.01, \gamma_0 = 10, c = 0.1, d = 10$ [331].
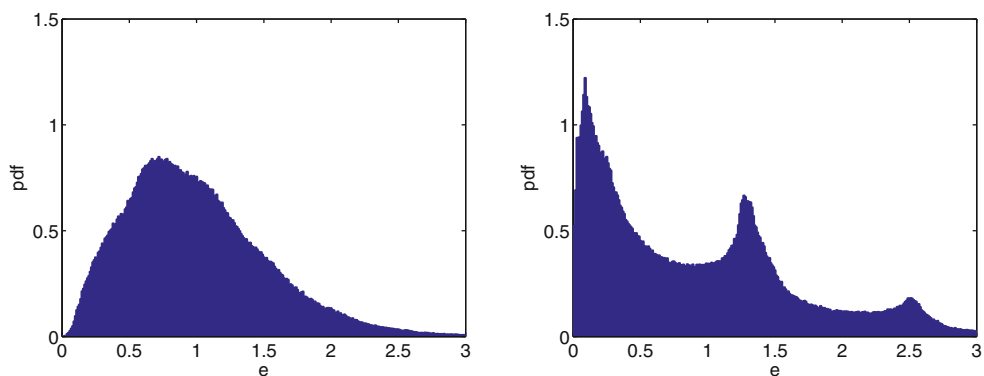

Fig. 16. Energy distributions for the smooth regime: (left $\tau = 0.05$) and shot regime (right, $\tau = 5q$). $q_0 = 10$, other parameter values as in Fig. 15 [331].

time between two shots. The maxima at multiples of h occur when multiple shots of energy arrived before the particle converted the energy of the depot to kinetic energy and accelerated its motion.

Now we will concentrate on the impact of the shot noise and set the external Gaussian white noise acting on the velocity D to zero. Like in Sect. 2.4 we will treat the white Poisson shot noise as a limit of the dichotomous Markovian process (DMP) [46,73,130,384]. This will allow us to derive an expression for the stationary probability distributions for velocities and energy.

Because of our shot noise source does not change the direction of the velocity it acts like an internal noise as introduced previously. Therefore we may restrict the consideration to the motion along the direction of motion. We change to the polar representation and get

$$\dot{s} = (de - \gamma_0)s, \quad \dot{e} = q(t) - e[c + ds^2]. \tag{108}$$

Please note that the polar representation is equivalent to the internal coordinates as the velocity can assume only positive values $s(t) = v(t) \geq 0$. In the following we will discuss two cases for which we can specify the stationary distributions.

(i) Adiabatic approximation: For $q_0 \gg \gamma_0^2/d$ we use the adiabatic approximation $\dot{e} \approx 0$ and insert $e(t) = q(t)/c + ds^2(t)$ into Eq. (108),

$$\dot{s} = -\gamma_0 s + \frac{dv}{c + ds^2} q(t) = f(s) + g(s) q(t). \tag{109}$$

Following the approach that $q(t)$ is a limit of a DMP we obtain

$$\tilde{P}_0(s) = \mathcal{N} \, s^{\left(\frac{q_0}{\gamma_0 h} - \frac{c}{dh} - 1\right)} \exp\left\{-\frac{s^2}{2h}\right\}. \tag{110}$$

(ii) Static regime: For $q_0 < c\gamma_0/d$ the system is in the static regime, so that $s = 0$. Therefore the dynamics reduces to

$$\dot{e} = q(t) - c\,e. \tag{111}$$

we obtain

$$P_0(e) = \mathcal{N} e^{\frac{1}{\tau c - 1}} \exp\left\{-\frac{e}{h}\right\}. \tag{112}$$

The second term of this expression yields a monotonous decreasing for all parameter values. The first term is monotonously increasing if $c\tau < 1$ and decreasing otherwise. Therefore the probability distribution of the internal energy shows a maximum in the static regime when $1/\tau > c$.

In another limit, we consider small mean time interval τ between the spikes and low mean amplitudes h. We assume that the energy input contains a constant and a fluctuating part,

$$q(t) = q_0 + \eta(t). \tag{113}$$

where q_0 is the mean value of the energy input. We approximate the fluctuating part as Gaussian white noise $\eta(t) = \sqrt{2D_q} \, \xi_q(t)$. According to [46], white shot noise with exponentially distributed weights h_i converges to Gaussian white noise in the limit $\tau \to 0, h \to 0$ with constant noise strength $D_q = h^2/\tau = q_0^2 \tau$. The parameter G of (34) than vanishes.

If the energy follows changes in the velocity very fast, we can assume that the energy takes quickly values such that $\dot{e} \approx 0$ in (107). We solve (107) for $e(t)$ and insert the expression into the equation for the speed. Afterwards, we obtain in Cartesian coordinates an additive external noise and a multiplicative internal noise caused by the fluctuating energy supply

In polar coordinates we obtain the following equations of motion:

$$\dot{s} = \left(\frac{dq_0}{c + ds^2} - \gamma_0\right) s + \sqrt{2D} \, \xi_s + \frac{ds}{c + ds^2} \sqrt{2D_q} \xi_q, \tag{114}$$

$$\dot{\varphi} = \frac{\sqrt{2D}}{s} \xi_\varphi(t). \tag{115}$$

Therein $\xi_s(t)$, $\xi_\varphi(t)$ are due to Eqs. (18).

The total noise in both equations consists of two terms, (1) the standard white mechanical noise, which has no preferred direction, and (2) the driver noise which is directed pointing to the direction of the velocity $\mathbf{e}_v = \mathbf{v}/s$. As a result, the shot-noise affects only the speed.

From the two equations we obtain the corresponding Fokker-Planck equation and look for the stationary solution. It reads

$$P_0(s) = \mathcal{N} s \left[D + D_q \left(\frac{ds}{c + ds^2}\right)^2\right]^{-\frac{1}{2}} \exp[-\Phi(s)] \tag{116}$$
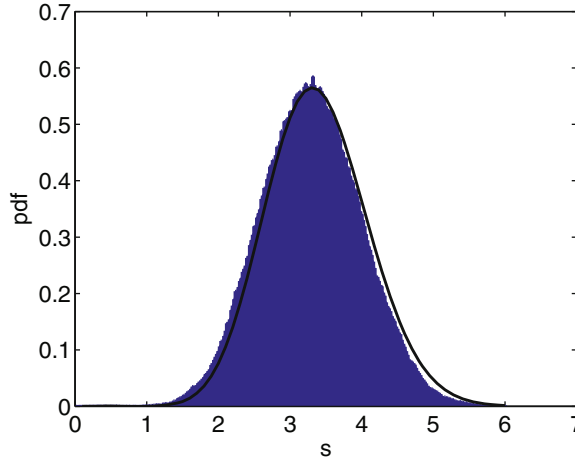
Fig. 17. Speed distribution and theoretical estimate (solid line, Eq. (116)). Parameter values: $\gamma_0 = 0.1$, $c = 0.01$, $d = 1$, $D = 0.1$, $q_0 = 1$, $\tau = 0.01$, $D_q = 0.01$ [331].

where the potential

$$\Phi(s) = - \int^s \mathrm{d}s' \frac{\left(\frac{dq_0}{c+ds'^2} - \gamma_0\right) s' - D_q \left(\frac{ds'}{c+ds'^2}\right)^2}{D + D_q \left(\frac{ds'}{c+ds'^2}\right)^2}. \tag{117}$$

In the limits of this approximation the analytical result fits well the numerical simulations as seen in Fig. 17.

3.3 Active Brownian particles: active versus passive fluctuations

Now we consider active Brownian particles with an intrinsic polarity defined by the heading vector $\mathbf{e}_h$ (see Sect. 2.3). In case of the Schienbein-Gruler friction (46), the equations of motion with both passive and active noise (Sect. 3.2.1, Eqs. 84, 86) in v, ϕ-coordinates read

$$\frac{\mathrm{d}}{\mathrm{d}t} v = \gamma_0 (v_0 - v) + \sqrt{2D}(\xi_x(t) \cos \phi + \xi_y(t) \sin \phi) + \sqrt{2D_v}\xi_v(t), \tag{118}$$

$$\frac{\mathrm{d}}{\mathrm{d}t} \phi = \frac{1}{v} \left(\sqrt{2D} \left(-\xi_x(t) \sin \phi + \xi_y(t) \cos \phi\right) \right) + \sqrt{2D_\phi}\xi_\phi(t). \tag{119}$$

The above Langevin equations equations have multiplicative noise terms and the corresponding Fokker-Planck equation for $P(v,\phi,t|v_0,\phi_0,t_0)$ again gets the Stratonovich shift and reads:

$$\frac{\partial P(v,\phi,t|v_0,\phi_0,t_0)}{\partial t} = -\frac{\partial}{\partial v} \left\{ \gamma_0 (v_0 - v) P + \frac{D}{v}P - (D + D_v)\frac{\partial P}{\partial v} \right\} + \frac{D + D_\phi}{v^2} \frac{\partial^2 P}{\partial \phi^2}. \tag{120}$$

Please note that the angular diffusion given by the last term of the above equation depends directly on $v(t)$. In the case of vanishing external forces ($\mathbf{F}_{\mathrm{ext}} = 0$) there is no distinguished angular direction. The stationary distribution with respect to ϕ is
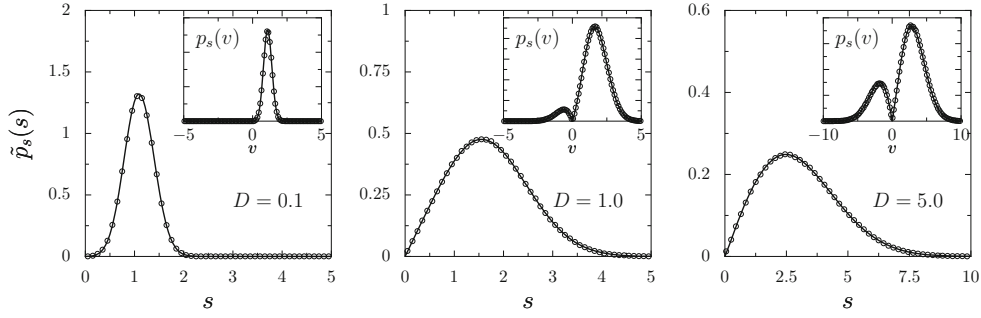
Fig. 18. Stationary speed distribution $\tilde{P}_0(s)$ of the Schienbein-Gruler model with external noise for different noise strengths: analytical solution obtained from (125) (solid line) and numerical results (symbols). The insets show the corresponding plots for the velocity distributions $P_0(v)$ (123). Other parameters $\gamma_0 = 1.0$, $v_0 = 1.0$ [298].

homogeneous and we may write $P_0(v,\phi) = P_0(v|\phi)/(2\pi)$ whereas $P_0(v|\phi)$ has to fulfill the following equation:

$$0 = -\frac{\partial}{\partial v}\left\{\left(-\gamma(v)v + \frac{D}{v}\right)P_0 - (D + D_v)\frac{\partial}{\partial v}P_0\right\}. \tag{121}$$

By inserting the Schienbein-Gruler friction (46) and solving the above equation we obtain the stationary velocity distribution for any given heading angle as

$$P_0(v|\phi) = \mathcal{N}|v|^{\frac{D}{D+D_v}}\exp\left\{-\frac{\gamma_0(v-v_0)^2}{2(D+D_v)}\right\}. \tag{122}$$

This is the general solution for the probability density function of the velocity with respect to the heading in the presence of both noise types. In the following we discuss the stationary distributions for the two limiting cases of only passive and only active fluctuations.

The stationary velocity density for only passive fluctuations can be directly obtained from (122) by setting $D_v = 0$ to

$$P_0(v|\phi) = \mathcal{N}_p|v|\exp\left\{-\frac{\gamma_0(v-v_0)^2}{2D}\right\}. \tag{123}$$

The inverse normalization constant in this case can be calculated using $\int_{-\infty}^{\infty} P(v|\phi)\mathrm{d}v = 1$ to:

$$\mathcal{N}_p^{-1} = \frac{2D}{\gamma_0}\exp\left(-\frac{\gamma_0 v_0^2}{2D}\right) + \frac{\sqrt{2\pi D}}{\gamma_0}v_0\,\mathrm{Erf}\left(\sqrt{\frac{\gamma_0 v_0^2}{2D}}\right). \tag{124}$$

This result is confirmed by the velocity distribution obtained from numerical simulations of the Schienbein-Gruler model in two dimensions (SG2d-model) with only external fluctuations as shown in Fig. 18. At vanishing noise intensities $D/\gamma_0 \to 0$ the distribution converges towards a δ-peak at v_0. With increasing noise intensity it is approximately given by a narrow Gaussian around v_0. With a further increase in D clear deviations from the Gaussian distribution become evident by the appearance of a second maximum of the probability density at negative velocities, caused by backwards motion of the particle with respect to its heading. The action of the external

fluctuation leads to a vanishing probability of $v = 0$. Finally, at D/γ_0 the distribution approaches a symmetric distribution which corresponds to the Rayleigh-distribution mirrored along $v = 0$.

In polar representation $v \to |v| = s$ the corresponding speed distribution along any given angle ϕ is a symmetric superposition of particles moving forward and backward with respect to the corresponding heading direction:

$$\tilde{P}_0(s, \varphi) = \frac{1}{2}\Big(P_0(v, \phi) + P_0(-v, \phi)\Big)$$
$$= \mathcal{A}\mathcal{N}_p \, s \, \exp\Big\{-\frac{\gamma_0 \, (s - v_0)^2}{2D_v}\Big\} \left[1 + \exp\Big\{-\frac{2\gamma_0 s v_0}{D_v}\Big\}\right]. \qquad (125)$$

Please note that $\tilde{P}_0(s, \varphi)$ differs from $P_0(v, \phi)$ as it is only defined for positive speed values. The constant factor $\mathcal{A} = (2\pi)^{-1}$ is determined by the normalization with respect to the angular variable.

In analogy to $P_0(v)$ for $D/\gamma_0 \to \infty$ ($v_0 \to 0$) the distribution converges to the Rayleigh-distribution of ordinary Brownian motion (see Eq. (20)), whereas for $D/\gamma_0 \to 0$ the limiting distribution is a δ-distribution at v_0. Finally we obtain the stationary distribution in Cartesian coordinates $P_0(v_x, v_y)$ from the stationary distribution in polar coordinates $\tilde{P}_0(s, \phi) = \tilde{P}_0(s)/(2\pi)$ by corresponding coordinate transformation and we obtain Eq. (47). Examples of $P_0(v_x, v_y)$ are shown Fig. 19.

For only active fluctuations ($D = 0$) the stationary velocity probability density (122) becomes a Gaussian centered at v_0 with width D_v:

$$P_0(v|\phi) = \mathcal{N}_a \exp\Big\{-\frac{\gamma_0(v - v_0)^2}{2D_v}\Big\}, \qquad (126)$$

with $\mathcal{N}_a = \sqrt{\gamma_0/2\pi D_v}$. The normalized probability density function in polar coordinates reads

$$\tilde{P}_0(s, \varphi) = \frac{1}{(2\pi)^{3/2}} \sqrt{\frac{\gamma_0}{D_v}} \exp\Big\{-\frac{\gamma_0 \, (s - v_0)^2}{2D_v}\Big\} \left[1 + \exp\Big\{-\frac{2\gamma_0 s v_0}{D_v}\Big\}\right]. \qquad (127)$$

We emphasize the non-vanishing probability density at s and the corresponding absence of an increase of $\tilde{P}_0$ for small s as shown in Fig. 20. This atypical behavior indicates that there is no limit where $\tilde{P}_0(s)$ converges towards the Rayleigh-distribution.

The probability density in the Cartesian velocity coordinates v_x, v_y can be directly obtained through the corresponding coordinate transformation to

$$P_0(\mathbf{v}) = \frac{1}{(2\pi)^{3/2}} \sqrt{\frac{\gamma_0}{D_v}} \frac{1}{|\mathbf{v}|} \left[1 + \exp\Big\{-\frac{2\gamma_0 |\mathbf{v}| v_0}{D_v}\Big\}\right] \exp\Big\{-\frac{\gamma_0(|\mathbf{v}| - v_0)^2}{2D_v}\Big\} \qquad (128)$$

with $|\mathbf{v}| = \sqrt{v_x^2 + v_y^2}$. Please note that the velocity probability density function in Cartesian coordinates diverges for $v_x = 0$, $v_y = 0$ and as a consequence exhibits a sharp peak close to the origin as shown in Fig. 21.

3.4 Particles with Internal Motor Control

3.4.1 Propulsion of particles in arbitrary direction

Here we discuss briefly several concepts describing the two-dimensional dynamics of particles with motor, where the motor is included in the dynamical description. We
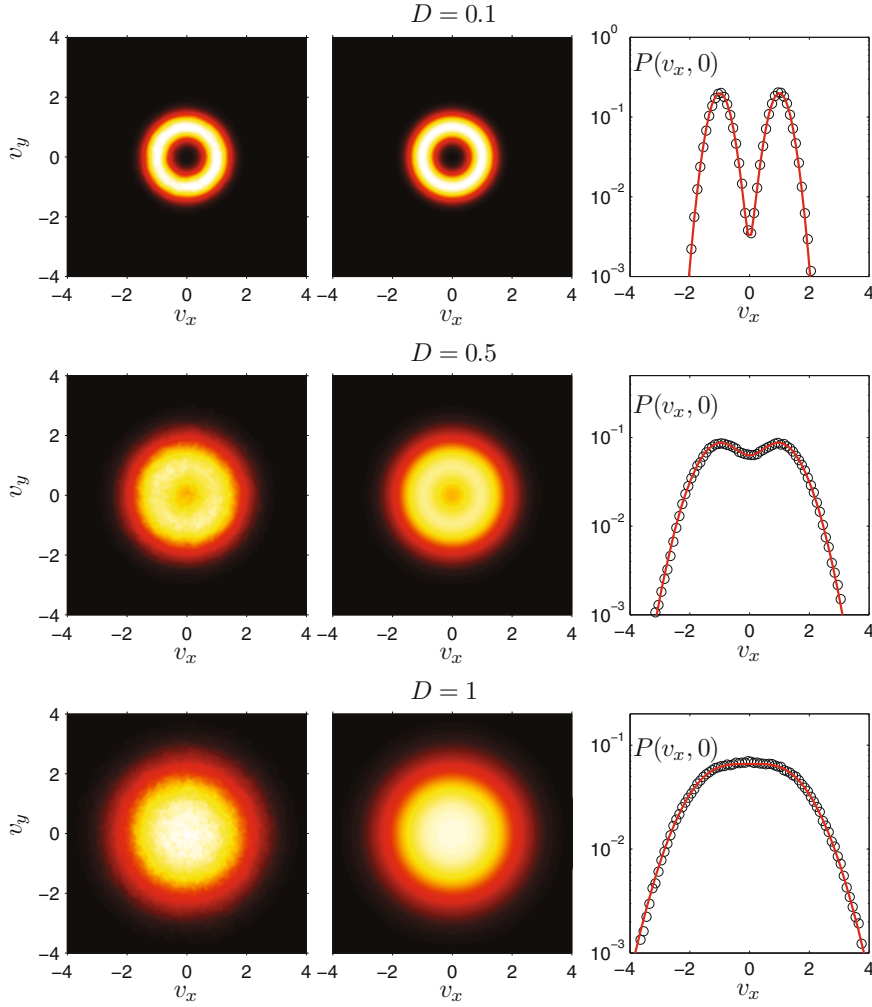
Fig. 19. Stationary velocity distributions $P_0(v_x, v_y)$ of particles with Schienbein-Gruler friction and external noise for different noise strengths: $D = 0.1$, top; $D = 0.5$, center; $D = 1.0$. Left column: results obtained from Langevin simulations; central column: analytical solution given in Eq. (47); right column: one dimensional cross-sections $P_0(v_x, 0)$ comparing analytical solutions (solid lines) with numerics (symbols). Other parameters $\gamma_0 = 1.0$, $v_0 = 1.0$ [298].

note at first that polar particles have an internal direction. It was defined in Sect. 3.1.2 by the tail-head structure expressing the spatial structure of the particle. In a similar way, one could speak about polarity in the presence of a dipole moment, magnetic moments or other features playing a role in the interaction of particles, or in the dynamical response to external forces. This may introduce a polar head-tail or left-hand asymmetry and define a distinguished direction characterizing the particle.

We have connected this polarity axis with the direction of motion $\mathbf{e}_v(t)$. It corresponds for positive velocities to the heading vector $\mathbf{e}_h(t)$, whereas for negative velocities with respect to the heading both vectors are anti-parallel. It is a situation similar to a moving ship where the positive and negative directions of velocity are parallel to the bottom of the ship from the bow to the rear, but the velocity points differently
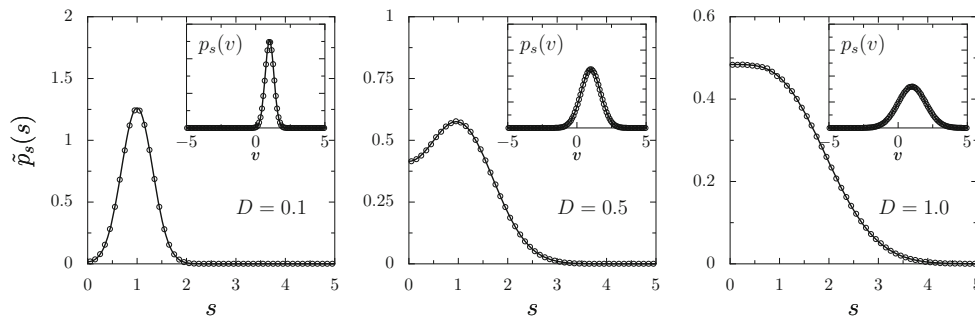
Fig. 20. Stationary speed distribution $\tilde{P}_0(s)$ of the Schienbein-Gruler model with internal noise for different noise strengths: analytical solution obtained from (127) (solid line) and numerical results (symbols). The inset shows the corresponding velocity distribution $P_0(v)$ given by a Gaussian (126). Other parameters $\gamma_0 = 1.0$, $v_0 = 1.0$ [298].

to the heading for a ship moving "backwards". Both vectors have associated angular unit vectors, we recall that $\mathbf{e}_\phi(t)$ describe rotations of the heading and $\mathbf{e}_\varphi(t)$ rotations of the velocity, respectively.

So far in most cases, we also put the non-random propulsion parallel to the velocity (Exceptions are torques which act perpendicularly). This parallelism now will be dropped, in contrast to the previous sections, we will now assume that there exist no strict and fixed relation between the velocity (or polarity) and the propulsive direction. We will explicitly allow for a propulsion mechanism that acts in a direction which is different from the direction of motion (see e.g. [113, 340]).

We define a new direction, which we will connect with the action of the propulsive motor. Let $\mathbf{a}_p(t)$ the acceleration associated to the propulsive force, which an active particle experiences from the action of an internal motor. The associated unit vector is $\mathbf{e}_p(t)$ with direction cosines $\{\cos\chi(t), \sin\chi(t)\}$. Here, $\chi(t)$ is the angle between the axis of abscissas and the considered force. We also introduce the magnitude of acceleration $a_p(t)$ by

$$\mathbf{a}_p(t) = a_p(t)\,\mathbf{e}_p(t). \tag{129}$$

An active particle with unit mass ($m = 1$) obeys the dynamical equations:

$$\frac{d\mathbf{r}}{dt} = \mathbf{v}, \quad \frac{d\mathbf{v}}{dt} = \mathbf{a}_p(t) - \gamma_0\,\mathbf{v} + \mathbf{F}_{\text{ext}} + \sqrt{2D}\,\xi(t). \tag{130}$$

Here the propulsion acts in direction of the unit vector $\mathbf{e}_p(t)$. Furthermore, the particle is driven by external forces $\mathbf{F}_{\text{ext}}$, by linear Stokes friction and by noisy agitations, which might be passive or active. The treatment of the latter was described in the previous sections.

Because propulsion and velocity vectors are not parallel anymore, the vector $\mathbf{e}_h(t)$ and its associated angle ϕ are not uniquely determined as they were in the previous sections. We define in this section that the particle starts at time $t = 0$ always with positive velocity and that in this case $\mathbf{e}_h(0) = \mathbf{e}_v(0)$ independent of the acting force. By the temporal evolution no further ambiguity occurs.

We expand the propulsive acceleration again along the $\mathbf{e}_h(t)$ and the perpendicular unit vector $\mathbf{e}_\phi(t)$. Consequently, we formulate

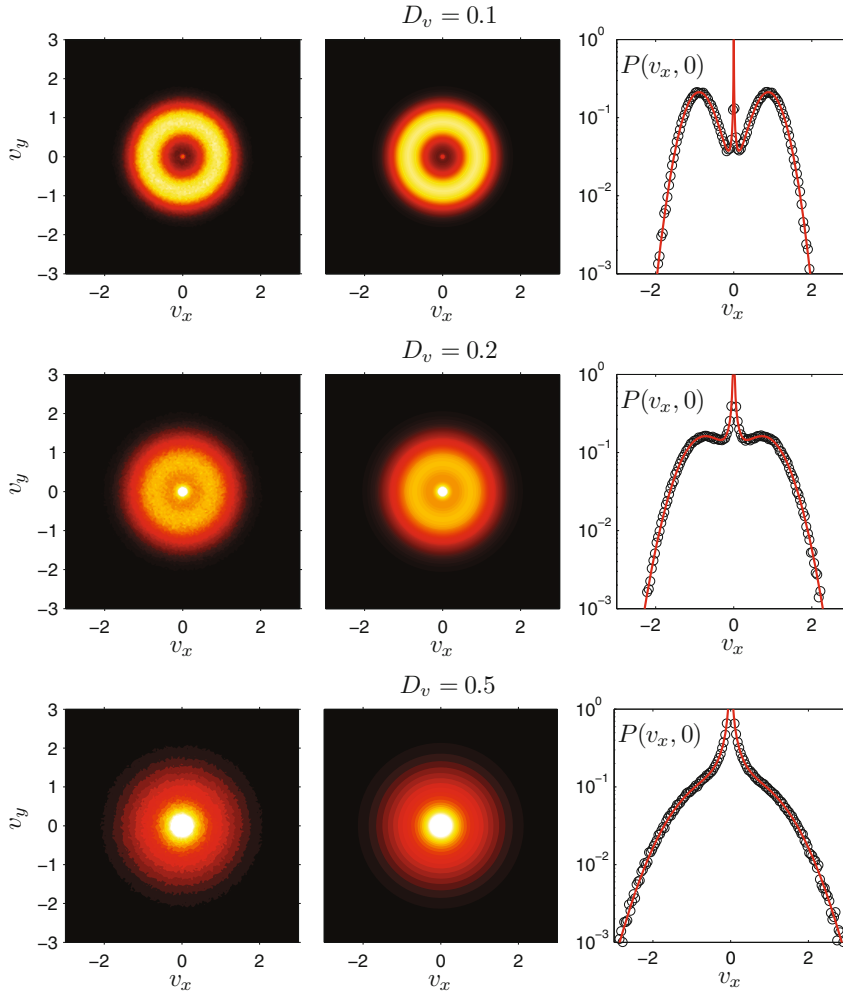$$\mathbf{a}_p(t) = a_h(t)\,\mathbf{e}_h(t) + a_\phi(t)\,\mathbf{e}_\phi(t). \tag{131}$$

Fig. 21. Stationary velocity distributions $P_0(v_x, v_y)$ of the Schienebein-Gruler model with internal noise for different noise strengths: Top: $D = 0.1$, bottom: D=0.2. Left column: results obtained from Langevin simulations; central column: analytical solution given in Eq. (128); right column: one dimensional cross-sections $P_0(v_x, 0)$ comparing analytical solutions (solid lines) with numerics (symbols); Other parameters $\gamma_0 = 1.0, v_0 = 1.0$ [298].

Then, without noise and if the external force acts along the x-axis $\mathbf{F}_{\text{ext}} = F_0 \, \mathbf{e}_x$, it follows for the dynamics of the particle

$$\frac{\mathrm{d}v}{\mathrm{d}t} = a_h(t) - \gamma_0 \, v + F_0 \cos\phi(t), \quad v\frac{\mathrm{d}\phi}{\mathrm{d}t} = a_\phi(t) - F_0 \sin\phi(t), \qquad (132)$$

where $v(t)$ is again the projection of the velocity-vector $\mathbf{v}(t)$ on the heading axis $\mathbf{e}_h(t)$, which is defined by the actual angle $\phi(t)$. If we insert explicitly the direction of the propulsion, the corresponding dynamics becomes

$$\frac{\mathrm{d}v}{\mathrm{d}t} = a_p(t)\cos(\chi - \phi) - \gamma_0 \, v + F_0 \cos\phi(t), \quad v\frac{\mathrm{d}\phi}{\mathrm{d}t} = a_p(t)\sin(\chi - \phi) - F_0 \sin\phi(t).$$
$$(133)$$

For the simplest case of a constant propulsion $\mathbf{a}_p(t) = \mathbf{a}_0$ pointing along a stationary angle χ_0 and without external force $F_0 = 0$, the angle $\phi(t)$ turns into the direction of the acceleration. Asymptotically, we get

$$\phi(t \to \infty) = \phi_0 \to \chi_0, \quad v(t \to \infty) \to a_0/\gamma_0. \tag{134}$$

Therefore, we find that the particle behaves asymptotically like it would follow a Schienbein-Gruler propulsion, i.e. the propulsion coincides with the direction of motion and in the simple case in which we obtained a stationary speed.

For a non-vanishing external force $F_0 \neq 0$, the particle is pulled in direction of the x-axis. If now the propulsion has constant magnitude a_0 and direction χ_0 the stationary solution can be found as well. The asymptotic angle of direction ϕ_0 obeys

$$\tan\phi_0 = \frac{a_p \sin\chi_0}{F_0 + a_p \cos\chi_0} \tag{135}$$

which follows also easily from a geometric construction in response to the action of two constant forces. In result, the stationary direction of motion is always sensing between the propulsive force and the x-axis. For the magnitude of the stationary speed, one obtains

$$v_0 = \frac{1}{\gamma_0} \sqrt{F_0^2 + a_p^2 + 2\,a_p\,F_0 \cos\chi_0} \tag{136}$$

which behaves as the value of a scalar product.

Within our more general framework, we briefly summarize the propulsion functions which we have used so far or will use later:

– Schienbein and Gruler [305] have found empirically the following simple "ansatz" for the cell dynamics (46)

$$a_h = \gamma_0 v_0 \quad a_\phi = 0. \tag{137}$$

The polarity axes coincide with directions of motion. In perpendicular direction normal angular noise is applied.

– In case of the Rayleigh-Helmholtz pump with $\tilde{\alpha} = \alpha - \gamma_0 \geq 0$ in (130) we defined (42)

$$a_h = (\tilde{\alpha}v - \beta v^3), \quad a_\phi = 0. \tag{138}$$

Again the pump induces an acceleration parallel to the current motion and there is no systematic torque applied and in ϕ direction we apply noise with vanishing mean.

Note that the propulsion in this case has no preferred direction along the polarity axis. It is impossible to distinguish between forward and backward motion along the polarity axes of the particle. The propulsion acts symmetrically in both positive and negative directions.

– In the frame of the the energy depot model, the stored energy $e(t)$ was transformed into kinetic energy with rate d as (see Eq. (52))

$$a_h = d\,e(t)\,v(t), \quad a_\phi = 0. \tag{139}$$

The internal motor increases kinetic energy in direction of motion.

– The case with constant speed $\mathbf{v}(t) = v_0\,\mathbf{e}_h(t)$ and random or systematic turning angle: The propulsion in directions of motion has to compensate at least the friction force. The angular dynamics can be systematic, for example, circling with

constant torque $\Omega_0 \neq 0$. It can be as well a function of the orientation if additional forces affect the motion anisotropically. Of course, random torques with Gaussian nature or shot noise and other time-dependent noise acts on the orientation. This case can be characterized with large γ_0 implying fast relaxation by

$$a_h = \gamma_0 v_0, \quad a_\phi = \Omega(v_0, \phi(t), \xi(t), t), \tag{140}$$

where $\Omega(v_0, \phi(t), \xi(t), t)$ shall describe the mentioned influences. It will be presented in more details in next sections.

3.4.2 Navigation in space following a given protocol

The human motion control of objects, say the steering of a ship or airplane or the driving of cars usually involves some moving task or protocol of navigation. There is a leader, the driver or captain, who has to follow a given optimal route in spite of stochastic forces and factors as wind, nonuniformities of space, etc. In animal mobility, the tasks are more modest but anyhow they do already exist in elementary form. An animal has to find food and shelter in a landscape with given geometry, with some distribution of food and shelter.

In order to describe such phenomena in a two-dimensional spatial set up, we have to assume at first a coordinate system in which the protocol can be defined and applied. We propose that the protocol contains the information about the current state of the propulsion mechanism or of the motor of the active particle. We will assume that this state can be characterized by a velocity-like vector $\mathbf{w}(t)$. At every instant of time, it has a direction given by the unit vector $\mathbf{e}_w$ with components $\mathbf{e}_w = \{\cos \nu(t), \sin \nu(t)\}$ in Cartesian presentation and is defined by the magnitude or by the length of the vector $w(t)$.

Both values $w(t)$ and $\nu(t)$ together make up the protocol and will define the performance of the motor over the considered time. In addition to the position and velocity, they are new variables describing the momentary state of the running motor. Changes of this motor in magnitude and direction induce a propulsive force which is exerted on the particle. The corresponding acceleration has two components

$$\mathbf{a}_p(t) = a_w(t)\, \mathbf{e}_w(t) \,+\, a_\nu(t)\, \mathbf{e}_\nu(t), \tag{141}$$

resulting either from a change of magnitude or of direction

$$a_w(t) = \frac{\mathrm{d}}{\mathrm{d}t}\, w(t), \quad a_\nu(t) = w(t)\, \frac{\mathrm{d}}{\mathrm{d}t}\, \nu(t) = w(t)\, \Omega(t), \tag{142}$$

and we have set $\dot{\nu}(t) = \Omega$. Both components of $\mathbf{a}_p$ vanish for a constant activity of the motor. The direction of the common action from the two items differs from the direction of motion $\mathbf{e}_v(t)$ and from this of the protocol $\mathbf{e}_w(t)$, in general.

The function $\mathbf{w}(t)$ would define a ideal course of the particle parameterized in time. In the absence of other forces, the performance of the particle would follow the protocol:

$$\mathbf{v}_{\mathrm{id}}(t) = \mathbf{w}(t). \tag{143}$$

With a respective initial condition, one would get the ideal course

$$\mathbf{r}_{\mathrm{id}}(t) = \mathbf{r}_0 \,+\, \int^t \mathrm{d}t'\mathbf{w}(t') \tag{144}$$

which is the wanted path in the considered coordinate system.

3.4.3 Navigation in space: The general case

In more complicated cases, the time-dependent protocol is unknown and the temporal evolution of the motor variables $w(t)$ and $\nu(t)$ has to be defined as the solution of a given dynamical problem. In general, it is reasonable to assume that the two functions obey first order differential equations

$$\frac{\mathrm{d}w}{\mathrm{d}t} = f_w(\mathbf{r}, \mathbf{v}, \mathbf{w}, t) + \sqrt{2D_w}\xi_w(t), \qquad \frac{\mathrm{d}\nu}{\mathrm{d}t} = f_\nu(\mathbf{r}, \mathbf{v}, \mathbf{w}, t) + \sqrt{2D_\nu}\xi_\nu(t). \quad (145)$$

The ξ_w and ξ_ν stand for motor noise with corresponding intensities. In particular, the solution of these equations can be also defined as a control problem, in which one has to find the correct temporal forcing in order to follow a given route under given loading.

The existence of the "internal vector" $\mathbf{w}(t)$ determining the direction of the propulsion by Eq. (143) turns the point-like particle into a Brownian particles with time-dependent propulsion. This new dynamical feature in the description of the Active Brownian particle leads to an extended state space which includes the new state variables $\mathbf{w}(t)$, respectively $w(t)$ and $\nu(t)$. The situation is similar to the case of active polar particles discussed recently by Szabó et al. [340] or Enculescu and Stark [113]. In our new frame work, the active Brownian particle is defined by the position $\mathbf{r}(t)$, by the velocity $\mathbf{v}(t)$, and by the vector $\mathbf{w}(t)$ or by the Langevin equations for position and velocity supplemented by Eqs. (145) for the motor.

The Langevin dynamics includes the acceleration exerted by the motor, linear friction, an external force $\mathbf{F}$, and noise (again we set $m = 1$, leading to $\gamma = \gamma_0$):

$$\frac{\mathrm{d}\mathbf{r}}{\mathrm{d}t} = \mathbf{v}; \quad \frac{\mathrm{d}\mathbf{v}}{\mathrm{d}t} = \dot{w}(t)\,\mathbf{e}_w(t) + w(t)\,\Omega(t)\,\mathbf{e}_\nu(t) - \gamma\,\mathbf{v} - \mathbf{F} + \sqrt{2D}\xi(t). \quad (146)$$

Here, the motor creates an acceleration with magnitude $a(t)$ acting in the direction of action $\chi(t)$.

It is instructive to first consider a simplified system. We assume that the acceleration in the direction of the motor is some constant and take for simplicity γw_0. This choice is equivalent to a Schienbein-Gruler propulsion. Furthermore, we replace in the angular acceleration the velocity in front of the angular frequency by the asymptotic constant value w_0. Doing so, the propulsion term reads

$$\mathbf{a}_p(t) = \gamma w_0 \mathbf{e}_w + w_0\,\Omega(t)\mathbf{e}_\nu. \quad (147)$$

These assumptions lead to

$$\frac{\mathrm{d}\mathbf{v}}{\mathrm{d}t} = v_0\gamma\mathbf{e}_w - \gamma\,\mathbf{v} + v_0\Omega(t)\mathbf{e}_\nu + \mathbf{F} + \sqrt{2D}\,\xi(t), \quad (148)$$

which is similar to the problem in Eq. (132). The only difference is the third term, which describes a rotation of the particle as consequence of a change of direction of the motor $\dot{\nu}(t) = \Omega \neq 0$.

Next, we consider a constant external force, which acts in x-direction $\mathbf{F} = F_0\mathbf{e}_x$. We project the Langevin equation onto the vectors $\mathbf{e}_h(t)$ being parallel to the direction of motion and the perpendicular angular direction $\mathbf{e}_\phi$. In result, we obtain

$$\frac{\mathrm{d}v}{\mathrm{d}t} = \gamma w_0 \cos(\nu - \phi) - \gamma\,v + F_0\cos\phi + w_0\,\Omega(t)\sin(\phi - \nu) + \sqrt{2D_v}\xi_v(t)$$

$$(149)$$

$$v\frac{\mathrm{d}\phi}{\mathrm{d}t} = \gamma v_0 \sin(\nu - \phi) + F_0\sin\phi + w_0\Omega(t)\cos(\nu - \phi) + \sqrt{2D_\phi}\xi_\phi(t).$$

One easily sees, that without external forces and with a constant direction of the motor ν_0 the direction ϕ of motion of the particle will asymptotically follow ν_0. Since items with Ω which is zero disappears the resulting equations are identical to the situation explained following Eq. (132).

In other cases, the angular driving $\Omega(t) = \dot{\nu}(t)$ is not defined as protocol and has to be defined. The description comprises the dynamical equations for the motor. For example, a wanted time and space dependent route $\nu_0(\mathbf{r}, t)$ may be given e.g. by the relaxation dynamics

$$\Omega(t) = \dot{\nu}(t) = -\frac{1}{\tau}(\nu(t) - \nu_0(\mathbf{r}, t)), \tag{150}$$

with some relaxation time τ. For the particular $\nu_0(\mathbf{r}, t)$ one may find from this equation $\nu(t)$ as a function of time and insert the solution into Eq. (149) in order to solve for $\phi(t)$ and for $v(t)$ and hence to obtain the complete trajectory.

As a further example, we consider a circling body. For this purpose we suppose constant motor load γw_0 and constant torque Ω_0, i.e.

$$\dot{w} = \gamma \, w_0, \quad \dot{\nu} = \Omega_0. \tag{151}$$

We simplify to the case without external force $F_0 = 0$. Then the particle follows the rotating motor with the same angular velocity $\dot{\phi} = \Omega_0$. The constant difference of the angles $\Delta = \phi - \nu$ and the stationary speed v_0 is determined by the two equations

$$\gamma \, v_0 = \gamma \, w_0 \cos \Delta + w_0 \, \Omega \sin \Delta, \quad \Omega \, v_0 = \gamma \, w_0 \sin \Delta + w_0 \, \Omega \cos \Delta, \tag{152}$$

for given motor load w_0 and Ω. They are solved by

$$\cos \Delta = \frac{v_0}{w_0}. \tag{153}$$

The stable solution should obey $\Delta = \nu - \phi > 0$. For the speed of the circling particle one obtains

$$v_0 = w_0 \frac{\Omega_0}{\sqrt{\gamma^2 + \Omega_0^2}}, \tag{154}$$

which becomes maximal if the dissipation is weak, i.e. γ is small. In this case, the velocity becomes approximately w_0 and the difference of the angle between motor and particle vanishes.

Generally, the motor works with maximal efficiency (maximal speed) if the direction of the motor agrees with the current velocity vector. Therefore, an important requirement is a minimization of the deviation between $\nu(t)$ and $\phi(t)$ also in the case when $\nu(t)$ changes permanently. One possibility to implement this requirement would be an adaptation dynamics, in which $\nu(t)$ approaches $\phi(t)$ with a positive rate $q > 0$

$$\dot{\nu}(t) = -q[\nu(t) - \phi(t)]. \tag{155}$$

More generally, the dynamics for ν may be described in terms of a potential

$$\frac{\mathrm{d}\nu}{\mathrm{d}t} \propto -\frac{\partial U(\nu - \phi)}{\partial \nu}. \tag{156}$$

With the particular choice $U(\nu - \phi) = -q \cos(\nu - \phi)$ the motor will also follow the current velocity, in case $q \to \infty$ both directions converge and the motor dynamics reduces to forces which can be interpreted as negative friction. In general, the outlined search for obtaining a maximal speed defines a problem of optimization. This problem is then similar to that of the navigation problem of a captain who selects the direction

of his ship by turning the rudder and the speed by changing the motor power. Finally, we mention that one can also assume that the direction of motion in the dynamics is delayed by a fixed period, i.e. $\phi(t - \tau)$, with $\tau > 0$.

Particularly important in our review will be the case that the motor is driven by random forces. We will discuss this point in more detail in the next Section, where we consider the diffusion of active particles. Already a first inspection of the Eqs. (149) shows that the action of isotropic random alterations of the motor will not result in a preferred direction. Nevertheless, the random action of the motor will induce a diffusional spread over the free space. The respective diffusion coefficients and distribution functions in confined geometries which quantify this behavior will be the topic of the next two Chapters (4 and 5).

4 Diffusion of active particles

In this Section, we discuss several aspects of the undirected spatial spreading of active particles in absence of external forces, i.e. diffusion of free active particles. Diffusion is not only a fundamental feature of random motion and the mean squared displacement and the corresponding effective diffusion coefficient are characteristic observables easily accessible in experiments. The properties of diffusive motion have important biological implications for animal searching behavior as they have a major impact on the ability of individual animals to exploit spatially distributed patches of nutrients (see e.g. [19,20,200,307]). As a starting point, before discussing different aspects of diffusion of active particles, we will give in this context one example for the importance of the value of the effective diffusion coefficient [200,307]. Other examples from ecology have been discussed by Okubo and Levin [252]. We intend to show that simple organisms might gather different amount of food in dependence on the value of the spatial diffusion coefficient. It will be of special importance that the food is localized, say in bounded regions which extend over a finite distance only. If then the organism has only a finite time for foraging, his strategy to locate a maximal amount of food is obviously an object of optimization as recently outlined in [77,78,133].

We assume that the density of the independent organisms $\rho(\mathbf{r}, t)$, thus the single individual probability distribution, obeys a diffusion equation with a diffusion coefficient D_r

$$\frac{\partial \rho}{\partial t} = D_r \Delta \rho. \tag{157}$$

In two dimension the resulting probability density in space is

$$\rho(\mathbf{r}, t) = \frac{1}{4\pi \, D_r \, t} \exp\left[-\frac{\mathbf{r}^2}{4 D_r t} \right]. \tag{158}$$

We assume that the particle consumes with constant rate k a food C, which is given by its density $c(\mathbf{r}, t)$, during its random motion. The food is stationary in space. Hence the consumption of food is described by

$$\frac{\partial}{\partial t} c(\mathbf{r}, t) = - k \, c(\mathbf{r}, t) \, \rho(\mathbf{r}, t). \tag{159}$$

The latter equation can be solved exactly if the solution (158) is inserted. Simple quadrature gives

$$c(\mathbf{r}, t) = c_0(\mathbf{r}) \exp\left[-\int_{t_0}^{t} k \, \rho(\mathbf{r}, t') \, \mathrm{d}t' \right]. \tag{160}$$
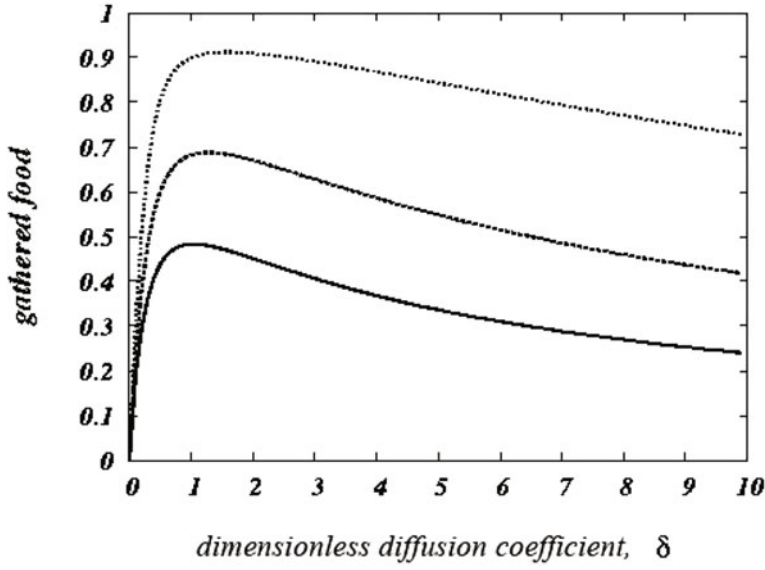
Fig. 22. Fraction of food gathered, which can be obtained using Eq. (164), as function of the dimensionless diffusion coefficient for three values of the clearance rate: $k = 1$ (solid line), $k = 1$ (dashed line), $k = 5$ dotted line. The gathered food is expressed as a fractions of the original total amount [133].

With the definition of the exponential integral [2]

$$\mathrm{Ei}(1, a) = \int_a^\infty \frac{\exp(-z)}{z} \mathrm{d}z \tag{161}$$

we obtain in compact form

$$c(\mathbf{r}, t) = c_0(\mathbf{r}) \, \exp\left[-\frac{k}{4\pi D_r} \, \mathrm{Ei}\left(1, \frac{\mathbf{r}^2}{4D_r t} \right) \right], \tag{162}$$

where we used $t_0 = 0$.

We consider now bounded distributed food patch. As a prototypical distribution we take a circular patch with radius R where C is present. Outside of the patch no food is located. For simplicity we assume the circle positioned at the origin, i.e.

$$c_0(\mathbf{r}) = c_0 = const., \quad \text{if} \quad |\mathbf{r}| < R, \tag{163}$$

and vanishing food concentration, elsewhere. Then after a fixed time T we determine the overall food which is still left. By integration we obtain [307]

$$C(T) = 2\pi \, c_0 \int_0^R \exp\left[-\frac{k}{4\pi D_r} \, \mathrm{Ei}\left(1, \frac{r^2}{4D_r T} \right) \right] r \, \mathrm{d}r. \tag{164}$$

Inspection of this expression shows that there exist a minimum with respect to the diffusion coefficient D_r. Thus the variation of the effective diffusion coefficient gives rise to a change in the overall food consumption. One might speculate that in nature the effective diffusion coefficient has been optimized for maximal foraging success [77,78,133].

The fraction of consumed food $(C(0) - C(T))/C(0)$ as a function of the diffusion coefficient is shown in Fig. 22. We have chosen the spatial diffusion coefficient D_r
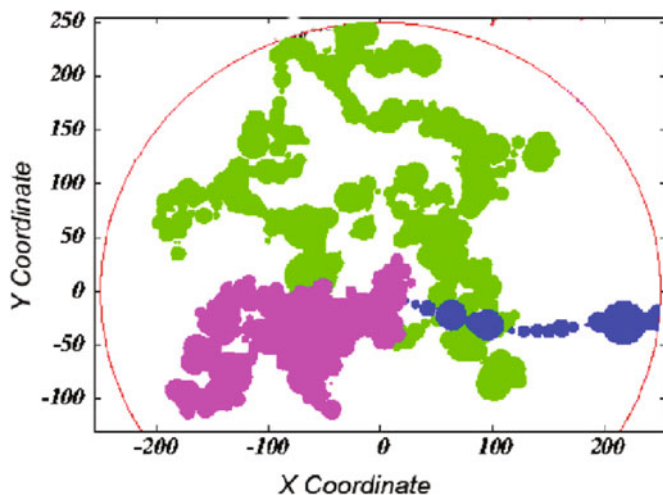
Fig. 23. Traces of food gathered by active particles for different widths of an exponentially distributed turning angle. The particles hop according to the turning angle distribution a finite step and rest a finite time in every new position gathering food; blue: $\sigma = 0.1$, green: $\sigma = 1.2$ and magenta: $\sigma = 10$, for ballistic, correlated and uncorrelated motion, respectively [133].

with respect to the normal diffusion coefficient $D_R = R^2/4T$ to cover the given sphere with radius R in time T and assigned $\delta = D_r/D_R$. A simple explanation can be given as follows. If the diffusion of particles is very large, e.g. they move almost exclusively straight forward, they will quickly leave the food patch. On the other hand, staying localized due to low diffusion coefficient, e.g. jumping permanently forwards and backwards, is also disadvantageous as the particle spends a lot of time in the region where it already consumed the food. Hence there exists an optimal diffusion coefficient, for which the particles spend the most time within the food patch and are able to consume the maximal amount of food. It does not matter whether they start at the center of the food patch or not.

This situation is illustrated in Fig. 23 where particles hop with exponentially distributed turning angles

$$P(\Delta\varphi) = \sigma \, \exp(-\sigma|\Delta\varphi|) \tag{165}$$

and a constant hop length [133]. Between two hops they rest a random time (with mean $\langle \Delta t \rangle = 0.25$) and consume food. In Fig. 23, the consumed food for three different width's σ of the turning angle distribution is shown. The large circle depicts the finite radius of the food patch. It is seen that an optimal width leads to a maximal consumption of food from the patch.

4.1 Taylor-Kubo relations for the diffusion coefficient

An interesting yet nontrivial question about the dynamics of active particles concerns their diffusive behavior in the simple situation in which there is neither interaction with other active particles nor nonlinear external fields. In these situations it is of interest whether the Active Brownian particles exhibits a mean drift with non-vanishing mean velocity $\langle \mathbf{v} \rangle$, possibly due to an asymmetry in its friction function or due to some interaction between the friction and the driving noise. Furthermore, it is not

clear *a priori* whether the active particle will execute a normal Brownian motion or whether for certain friction functions anomalous diffusion may be observable. In many cases, it turns out that active Brownian particles perform just normal Brownian motion with a linear asymptotic growth of the mean square displacement. In these cases, however, it may still be surprising how the diffusion coefficient depends on system parameters as, for instance, the noise intensity.

Generally, if the velocity dynamics obeys a stationary statistics, we may express the mean square displacement (m.s.d.) $\Delta \mathbf{r}^2(t) = (\mathbf{r}(t) - \mathbf{r}(0))^2(t)$ by the velocity auto-correlation function via the Green-Kubo relation. For convenience, we set the initial position to $\mathbf{r}(0) = \mathbf{0}$ and can thus express the position at t by the integral over the velocity vector $\int_0^t dt' \mathbf{v}(t')$. First we assume vanishing stationary mean velocity $\langle \mathbf{v} \rangle = 0$. By inserting this into the m.s.d., exchanging integration and averaging, using stationarity, and simplifying the integrals, one arrives at

$$\langle \Delta \mathbf{r}^2(t) \rangle = \langle \mathbf{r}^2(t) \rangle = \int_0^t \int_0^t dt' dt'' \langle \mathbf{v}(t') \mathbf{v}(t'') \rangle. \tag{166}$$

If the stochastic process governing the evolution of $\mathbf{v}$ is stationary, the expectation value of $\langle \mathbf{v}(t') \mathbf{v}(t'') \rangle$ depends only on the absolute value of the time difference $\tau = |t' - t''|$ and we may rewrite the above relation as an integral over the velocity-velocity correlation function $C_{\mathbf{vv}} = \langle \mathbf{v}(\tau) \mathbf{v}(0) \rangle$:

$$\langle \Delta \mathbf{r}^2(t) \rangle == 2 t \int_0^t d\tau \left(1 - \frac{\tau}{t} \right) C_{\mathbf{vv}}(\tau). \tag{167}$$

Assuming a sufficiently fast decaying $C_{\mathbf{vv}}(\tau)$ so that the integral over τ converges for $t \to \infty$ we may or large times t replace the upper limit of the integration by infinity which yields:

$$\langle \Delta \mathbf{r}^2(t) \rangle = 2 \left[\int_0^\infty d\tau C_{\mathbf{vv}}(\tau) \right] t. \tag{168}$$

Thus we define the diffusion coefficient according to the Taylor-Kubo formula in arbitrary spatial dimensions d as:

$$D_{\mathrm{eff}} = \frac{1}{d} \int_0^\infty d\tau \langle \mathbf{v}(\tau) \mathbf{v}(0) \rangle. \tag{169}$$

Note that the pre-factor with d being the spatial dimension was chosen in analogy to ordinary Brownian diffusion (Eq. (8)), and may differ from other definitions of the (effective) diffusion coefficient. All of the outlined formulas can be generalized to the case with a finite mean speed. The diffusion coefficient then describes the diffusive spread around the mean motion:

$$D_{\mathrm{eff}} = \frac{1}{d} \lim_{t \to \infty} \frac{\langle \mathbf{r}^2(t) \rangle - \langle \mathbf{r}(t) \rangle^2}{2t} = \frac{1}{d} \int_0^\infty d\tau [\langle \mathbf{v}(0) \mathbf{v}(\tau) \rangle - \langle \mathbf{v} \rangle^2]. \tag{170}$$

There exists a simple yet rather useful reformulation of this formula. Using the variance $\langle \Delta \mathbf{v}^2 \rangle$ and one particular definition of a velocity correlation time, namely the integral over the normalized auto correlation function, we can write

$$D_{\mathrm{eff}} = \frac{\langle \Delta \mathbf{v}^2 \rangle \tau_{corr}}{d}. \tag{171}$$

So, the diffusion coefficient depends not only on the variance of the velocity fluctuations but also on their typical duration which is characterized by the correlation time. We stress that this interpretation holds only for non-oscillatory correlation functions.

For the cases studied in the following, the velocity correlation function is generally not known because of the nonlinearities introduced by the friction function. In one spatial dimension, however, one can solve for the integral of the correlation function over the entire time interval $(0, \infty)$ and in this way obtain an analytical expression for the diffusion coefficient. This can be achieved not only for the dynamics of active Brownian particles with white noise but also for a nonlinear velocity dynamics driven by a specific correlated (colored) fluctuations, namely, the dichotomous noise. In higher spatial dimensions, approximations for the calculation of the diffusion coefficient may be employed which exploit the specific symmetries of the speed-dependent friction (phase dynamics in 2d and 3d, scaling behavior for friction functions obeying a power law).

In the following, we review the diffusive behavior of active particles with different friction functions, under the influence of asymmetries, and driven by white or colored noise. A particularly simple kind of nonlinear friction functions, namely those given by a power law, is treated separately because it makes certain limit cases for the diffusion of active particles more comprehensible. We then proceed with new features occurring in the diffusion in higher spatial dimensions.

4.2 Diffusion in one dimension

4.2.1 Diffusion for a symmetric friction function and white noise

Let us first consider $\gamma(-v) = \gamma(v)$ and a driving by a white Gaussian noise. In this spatially symmetric case we obtain a vanishing stationary mean velocity

$$\langle v \rangle = 0 \tag{172}$$

and the diffusion coefficient is the remaining statistics of interest. We mention that different approximations for the diffusion coefficient have been suggested for the one-dimensional case [66, 98, 218, 236]; the derivation of the exact solution will be shown in the following.

Useful for the calculation of the diffusion coefficient is the introduction of a velocity potential given by

$$\Phi(v) = \int_0^v \mathrm{d}v' \gamma(v') v'. \tag{173}$$

For a typical friction function of an active particle, this potential is bistable and thus has two metastable states with finite speed whereas the zero velocity is dynamically unstable. Specifically, for the Rayleigh-Helmholtz friction function introduced in Eq. (42), the potential reads

$$\Phi(v) = \beta \frac{v^4}{4} - \alpha \frac{v^2}{2}; \tag{174}$$

in this section, we set $\alpha = \beta = 1$. For the friction function of the depot model in Eq. (55), one obtains the potential

$$\Phi(v) = \frac{\gamma_0}{2} \left[v^2 - \frac{q}{\gamma_0} \ln(1 + v^2 d/c) \right]. \tag{175}$$

In the following, we use the numerical values $\gamma_0 = 20, d/c = 40, q = 5$.

The Fokker-Planck equation for the velocity process reads

$$\partial_t P(v,t) = \partial_v [\Phi'(v) + D\partial_v] P(v,t). \tag{176}$$

We recall [292] that (i) this equation can be easily solved in the stationary state, yielding a Boltzmann-like distribution $P_0 \sim \exp[-\Phi(v)/D]$; (ii) the transition probability $P(v,t|v_0,0)$ is governed by the FPE with the initial condition $P(v,0) = \delta(v - v_0)$; (iii) there is no general solution for $P(v,t|v_0,0)$ for a general nonlinear force $-\Phi'(v)$. If we would know $P(v,t|v_0,0)$ we could calculate the velocity correlation function by

$$\langle v(t)v(0) \rangle = \int \mathrm{d}v \int \mathrm{d}v_0 v v_0 P(v,t|v_0,0) P_0(v_0) \tag{177}$$

where the last two factors express the joint probability density $P(v,t;v_0,0)$ by means of Bayes' theorem. Inserting the correlation function into the Green-Kubo formula, we may write

$$D_{\mathrm{eff}} = \int \mathrm{d}v v \int_0^\infty \mathrm{d}t \int \mathrm{d}v_0 v_0 P(v,t|v_0,0) P_0(v_0) = \int \mathrm{d}v v G(v). \tag{178}$$

An ordinary differential equation for $G(v)$ can be obtained from the Fokker-Planck Eq. (176) by integrating over time, multiplying with the known stationary probability density in v_0, and integrating over the latter variable. The resulting equation reads:

$$-v P_0(v) = (\Phi'(v)G(v))' + D G''(v) \tag{179}$$

which can be solved in terms of quadratures. After a few simplifications (using also the symmetry of the potential), the result for the diffusion coefficient reads [219]

$$D_{\mathrm{eff}} = \frac{\int_0^\infty \mathrm{d}v_2 \, e^{\Phi(v_2)/D} \left[\int_{v_2}^\infty \mathrm{d}v_1 \, e^{-\Phi(v_1)/D} v_1 \right]^2}{D^2 \int_0^\infty \mathrm{d}v_3 \, e^{-\Phi(v_3)/D}}. \tag{180}$$

We note that the same techniques has been used by Jung and Risken [184] and in particular by Risken in the second edition of his well-known textbook [292] to obtain an analytical expression for the correlation time of a stochastic process governed by a nonlinear Langevin equation (the connection to τ_{corr} is evident in Eq. (171)).

Before coming to the case of active Brownian motion, let us first consider a simpler nonlinear speed-dependence of the friction which is given by a power law. In particular, we assume that

$$\gamma(v) = \gamma_0 v^{2\alpha}, \quad \alpha \geq 0, \tag{181}$$

(note that α has nothing to do with the parameter of the RH friction function, which we set to zero). This problem has been studied in detail in Ref. [220] where it has been shown that the diffusion coefficient in this case scales like a power law with the system's parameters:

$$D_{\mathrm{eff}} \sim \gamma^{-\frac{2}{1+\alpha}} D^{\frac{1-\alpha}{1+\alpha}}. \tag{182}$$

This result can be obtained from the exact expression by changing the integration variables appropriately (the factor of proportionality is then given by an integral that still depends on α but not on D or γ_0 anymore). It can be, however, also obtained by renormalization of the original Langevin equation (see [219]) a techniques by means of which one can show that Eq. (182) holds also true in arbitrary dimensions although of course with different pre-factor than in the one-dimensional case.

On closer inspection, Eq. (182) is a little surprising. It tells us, for instance, that for a pure cubic friction ($\alpha = 1$), the diffusion coefficient does not depend on the
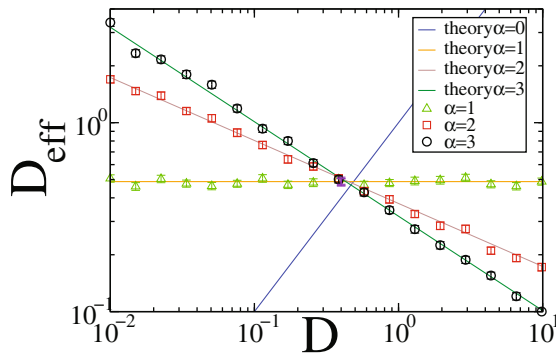
Fig. 24. Diffusion coefficient vs. noise intensity D for the one-dimensional case ($\gamma = 1$) and various values of the exponent. Theory (numerical evaluation of Eq. (180)) is compared to simulation results. Modified from [220].

noise intensity D at all. Furthermore, for stronger than cubic friction ($\alpha > 1$), the diffusion coefficient decreases monotonically with increasing D and diverges in the limit of vanishing noise intensity. In the case of normal Brownian motion ($\alpha = 0$), the diffusion coefficient is proportional to the noise intensity as expected. All of these conclusions are illustrated and confirmed by results of numerical simulations in Fig. 24.

In order to explain this behavior we have to recall that according to Eq. (171) the diffusion coefficient is given by the product of the variance and the correlation time of the velocity fluctuations. Increasing the noise intensity will in all considered cases increase the variance. The effect on the correlation time, however, is more complicated. For strong noise and a strong nonlinear friction ($\alpha \geq 1$), the velocity attains typically large values at which the dissipation term $v^{2\alpha+1}$ is stronger than in the linear case, hence the correlation time is shorter and becomes even shorter for further increasing noise. In the opposite limit of vanishing noise, the velocity is typically at values close to zero where the dissipation term is now much weaker than in the case of normal Brownian motion. For a cubic friction the tendency of increasing velocity variance and decreasing correlation time balance exactly and their product remains constant upon variations of D. For a stronger friction, the sensitivity of the correlation time with respect to changes in the noise is even stronger and dominates the dependence of the diffusion coefficient on D.

Let us now turn to the case of an active Brownian particle. First we consider the dependence of the diffusion coefficient for the depot model introduced in Sect. 3.1.3. In this case the quadrature formula has been evaluated numerically and the result is shown in Fig. 25.

We observe a nonmonotonic relation between the diffusion coefficient and the noise level: the diffusion is minimized at an intermediate noise level. We can understand the growth with D seen at large noise intensity because at large values of the velocity (typically attained at strong noise) the depot model approaches the Stokes limit of a speed-independent friction coefficient. At the level of the velocity potential this implies a parabolic potential at large speed (cf. Fig. 25(b)). In the opposite limit of weak noise the bistability of the velocity potential becomes essential. Here the velocity undergoes noise-induced transitions between the two metastable states corresponding to the minima of the potential. For such a process, the diffusion coefficient is inversely proportional to the Kramers hopping rate [98,236]

$$D_{\text{eff}} \approx \frac{v_0^2 \pi}{Q\sqrt{\Phi''(v_0)|\Phi''(0)|}} \exp\left[\frac{\Delta\Phi}{D}\right] = \frac{v_0^2}{2r_K}. \tag{183}$$
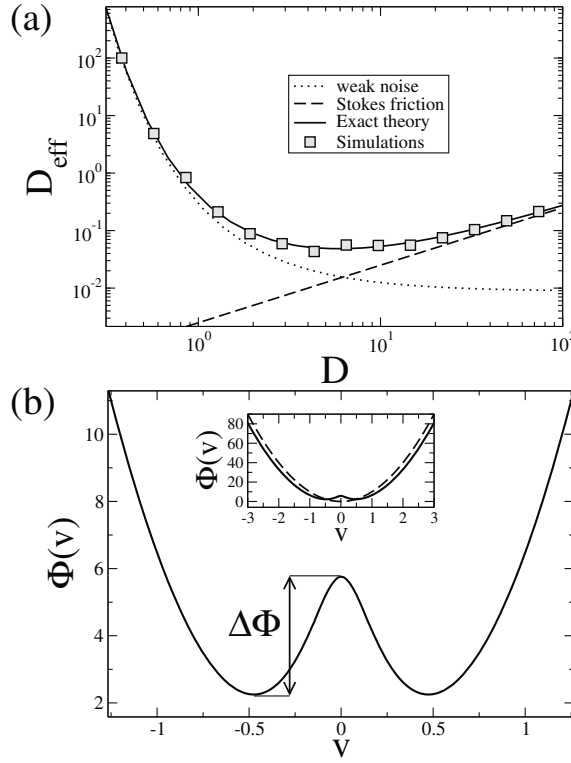
Fig. 25. Diffusion coefficient vs. noise intensity D (a) and velocity potential (b) for the friction function of the depot model. In (a), theory (numerical evaluation of Eq. (180) with the potential Eq. (175)) is compared to simulation results. The inset in (b) illustrates that the velocity potential behaves asymptotically as a parabola $\Phi(v) \sim v^2$ (dashed line). Modified from [219].

The latter relation agrees with Eq. (31) for $\lambda_\pm = r_k, |v_\pm| = v_0$; it has been derived for a velocity following a telegraph process with rate r_k in [301]. Assuming weak noise D, Eq. (183) can be also derived via a saddle-point approximation from the exact result Eq. (180).

The divergence of the diffusion coefficient can be understood by considering the spread of an ensemble of active Brownian particles. At equilibrium half of the particles are in the left well with a corresponding finite speed going to the left while the other half is situated in the right well and thus go with finite speed to the right. Without any transitions between the wells (a limit that is approached for vanishing noise), the growth of the m.s.d. would occur ballistically. Incidentally, this has to be taken into account when choosing a simulation time for an estimation of the diffusion coefficient. One has to wait at least a multiple of the correlation time of the process, in order to see a diffusive growth of the m.s.d. Very similar to the case of normal Brownian motion, there is a ballistic phase in the m.s.d. time course. The time of this t^2 growth can be estimated from the relation between diffusion coefficient, variance, and correlation time Eq. (171): $\tau_{corr} = D_{\text{eff}}/\langle \Delta v^2 \rangle$. because in our numerical example $\langle \Delta v^2 \rangle \simeq 1$ but D_{eff} is exponentially large, the correlation time is rather large. In order to get reasonable estimates for the diffusion coefficient, an ensemble of trajectories has to be simulated at least for a multiple of this large correlation time.

Turning back to the minimum, which we observed for the diffusion coefficient vs noise intensity: is such a minimum observed for all possible friction functions
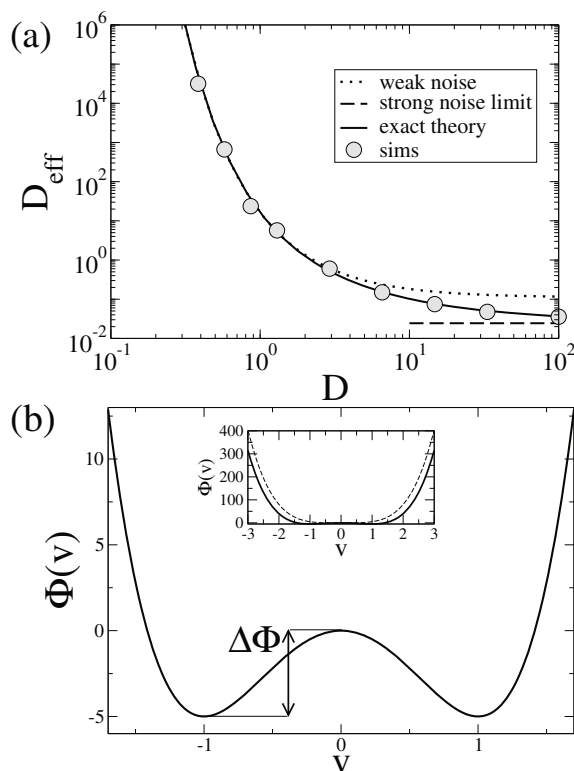
Fig. 26. Diffusion coefficient vs. noise intensity D (a) and velocity potential (b) for the RH model. In (a), theory (numerical evaluation of Eq. (180) with the potential Eq. (174)) is compared to simulation results. The inset in (b) shows the asymptotic behavior of the potential which is dominated for the RH model by the quartic term $\Phi(v) \sim v^4$ (dashed line). Modified from [224].

of active Brownian particles? The results on the power-law friction function tell us otherwise. If a friction function has a nonlinear asymptotic limit such that the friction increases like a power equal or stronger than cubic friction, the diffusion coefficient will either saturate (for cubic friction $\gamma(v)v \sim v^3$) or even decrease (for friction stronger increasing than $\gamma \sim v^2$) in the asymptotic limit of large noise D. So in these cases we cannot expect to observe a minimum. Indeed for the RH model which is at large speed dominated by the cubic term, the diffusion coefficient decreases monotonically with the noise intensity D. We note that the divergence of the diffusion coefficient in the limit $D \to 0$ is untouched by the asymptotics of the velocity potential because this divergence hinges solely upon the presence of a potential barrier.

4.2.2 Diffusion in the spatially symmetric case with colored noise

The assumptions we make on the phenomenological model of an active particle are often based on simplicity. One such assumption is the lack of correlations in the driving noise process $\xi(t)$. After we have reached some understanding of the active Brownian motion dynamics in one dimension with white noise, we may relax this condition and consider the case where the fluctuations have a finite correlation time, i.e. we consider

$$\frac{\mathrm{d}}{\mathrm{d}t}x = v, \quad \frac{\mathrm{d}}{\mathrm{d}t}v = -\gamma(v)v + \eta(t) \tag{184}$$

where $\eta(t)$ is a colored noise that we choose here to have an exponential correlation function

$$\langle \eta(t)\eta(0) \rangle = \sigma^2 e^{-2\lambda t}. \tag{185}$$

There are two simple stochastic processes with such a correlation function but different probability density. The first one is the symmetric dichotomous Markov process (DMP, also called telegraph noise) which jumps between two values $-\sigma$ and σ with transition rates λ. The other one is a Gaussian noise, the Ornstein-Uhlenbeck process (OUP) η, which can be obtained by integrating the stochastic differential equation

$$\frac{\mathrm{d}}{\mathrm{d}t}\eta = -2\lambda\eta(t) + 2\sigma\sqrt{\lambda}\xi(t) \tag{186}$$

($\xi(t)$ is as usual white Gaussian noise with $\langle \xi(t)\xi(t') \rangle = \delta(t-t')$). The unusual scaling in the OUP ensures that variance and correlation time are the same for OUP and DMP in terms of the parameters (σ, λ).

If the driving noise introduces a finite correlation time, one question of interest is how this time scale affects the diffusion coefficient. The DMP offers a simple case in which this question can be explored analytically. By a very similar approach as discussed above for the white-noise case, one can derive an exact quadrature formula for the diffusion coefficient [221].

For the velocity process driven by a dichotomous noise, we may write down evolution equations for the probability densities $P_+(v)$ and $P_-(v)$ that the velocity attains the value v and that the noise is at $\eta = \sigma$ and $\eta = -\sigma$, respectively:

$$\partial_t P_+ = \partial_v[\gamma(v)v - \sigma]P_+ - \lambda P_+ + \lambda P_- \tag{187}$$

$$\partial_t P_- = \partial_v[\gamma(v)v + \sigma]P_- + \lambda P_+ - \lambda P_-. \tag{188}$$

These two equations solved for different initial conditions with respect to the noise would yield four transition probabilities $p_{\pm,\pm}(v,t)$ ($p_{+,-}(v,t|v_0)$, for instance, is the probability to find the velocity at v and the noise at $\eta = \sigma$ if initially at $t = 0$ the velocity was at v_0 and the noise was $\eta(0) = -\sigma$) by means of which the velocity correlation function can expressed:

$$\langle v(t)v(t+\tau) \rangle = \int_{-v_m}^{v_m} \mathrm{d}v v \left[\int_{-v_m}^{v_m} \mathrm{d}v_0 \, v_0 \left\{ (P_{++} + P_{-+})P_+^0 + (P_{+-} + P_{--})P_-^0 \right\} \right]. \tag{189}$$

We can use again the fact that for the diffusion coefficient we have to know only the integral over the correlation function. By integrating Eqs. (187) we obtain a system of ordinary differential equations for two auxiliary functions (comparable to the function $G(v)$ in the previous subsection), the integral of which then yields the diffusion coefficient. Further details on the lengthy but straightforward calculation can be found in [221]; the final result reads

$$D_{\mathrm{eff}} = 2\lambda\sigma^2 \frac{\int_0^{v_m} \mathrm{d}x \frac{e^{\hat{\Phi}(x)}}{\sigma^2 - f^2(x)} \left(\int_x^{v_m} \mathrm{d}y \frac{e^{-\hat{\Phi}(y)}}{\sigma^2 - f^2(y)} y \right)^2}{\int_0^{v_m} \mathrm{d}z e^{-\hat{\Phi}(z)}[\sigma^2 - f^2(z)]^{-1}}, \quad \hat{\Phi}(v) = -2\lambda \int_0^v \mathrm{d}x \frac{f(x)}{\sigma^2 - f^2(x)}. \tag{190}$$

The value of v_m is set by the maximal speed by which the particle can go under dichotomous driving and is found from the equation $\gamma(v_m)v_m = \sigma$.

In the white-noise limit of the dichotomous fluctuations $\lambda \to \infty, \sigma \to \infty$ with $D = \sigma^2/(2\lambda) = const$, the expression approaches the result Eq. (180). Further limit cases as well as the numerical evaluation of the integrals is discussed in [221]. Here we review the dependence of the diffusion coefficient on the new time scale in the problem given by the switching rate of the DMP.
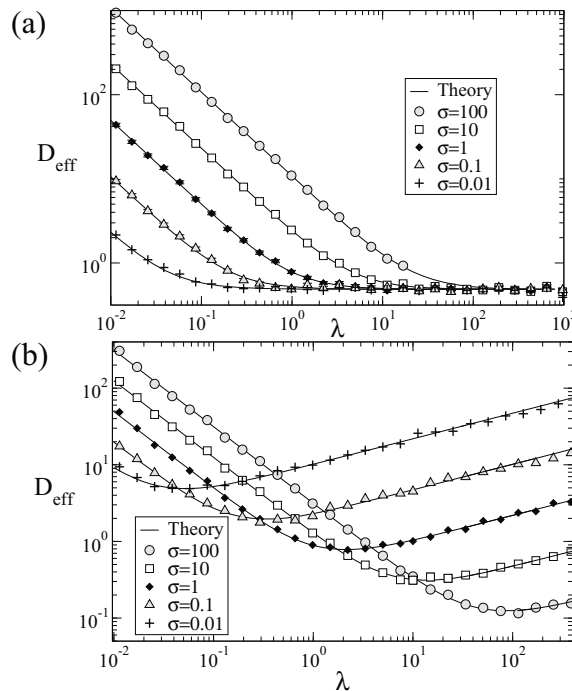
Fig. 27. Diffusion coefficient vs. switching rate of the telegraph noise for a cubic (a) and a quintic friction function (b) for different amplitudes of the driving as indicated. Theory (solid lines, Eq. (190)) is compared to simulation results. Modified from [221].

Let us first consider the simple case of a power law friction. The diffusion coefficient for a cubic friction decreases monotonically with increasing switching rate. We can understand the limits of small and large rate based on the results from the previous subsection. At small switching rate the velocity process relaxes towards the asymptotic value $\pm v_m$ – the dichotomous character of the input process carries over to the velocity with an amplitude which is determined by the nonlinear equation for v_m. We mentioned already that for a velocity following a telegraph noise, the diffusion coefficient is proportional to the inverse of the switching rate and this is exactly the behavior observed in Fig. 27 in the limit $\lambda \to 0$. In the opposite limit of a large rate, the DMP approaches white noise with a vanishing intensity because $D = \sigma^2/(2\lambda)$ (σ is constant). For a cubic friction, however, the diffusion coefficient does not depend on the noise intensity and thus D_{eff} approaches the constant value that we already obtained in the white noise case for $\gamma(v)v = \gamma_0 v^3$ (cf. in Fig. 24 the data for $\alpha = 1$).

For a friction function with stronger nonlinearity, for instance, for a quintic dependence on v, the divergence at small rate remains the same (also here we observe a dichotomous velocity process dictated by the slow driving), at strong rates, however, the diffusion coefficient also diverges in marked contrast to the cubic case (Fig. 27b). The reason for the increase at large rate is also quite plausible. With increasing rate the white-noise limit is approached with a noise intensity that decreases with rate. We saw before that for a friction function with $\alpha > 1$ the diffusion coefficient diverges for vanishing noise and it is exactly this divergence that we now observe for increasing rate. As a consequence of asymptotic behavior, the diffusion coefficient attains a minimal value at intermediate rate. The rate for the minimal diffusion coefficient depends on the amplitude and is approximately given by [221]

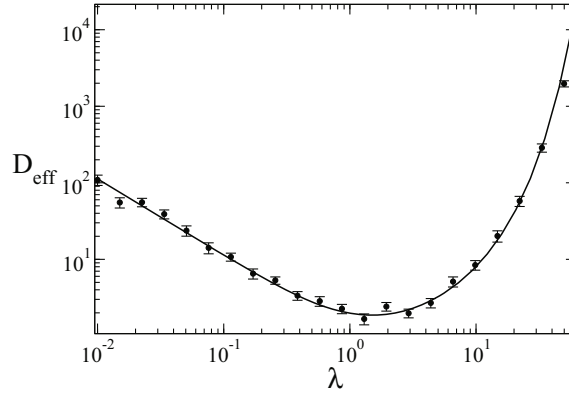$$\lambda_{min} \approx 2(A^4\gamma)^{1/5}. \tag{191}$$

Fig. 28. Diffusion coefficient vs. DMP switching rate a Rayleigh-Helmholtz friction function; amplitude of the driving is $\sigma = 1.875$. Theory (solid line, Eq. (190)) is compared to simulation results. Modified from [221].

For an active Brownian particle we also find a minimum in the diffusion coefficient vs rate (Fig. 28) because in this case we recover in the limit of large rate the weak-noise limit of the white-noise case associated with a bidirectional motion with rare reversals. Hence, here in both limits of small and large switching rate of the telegraph noise we observe a bidirectional motion although for two different physical reasons. We note that for the Rayleigh-Helmholtz friction function used in (Fig. 28), our theory is constraint to the condition of a sufficiently large amplitude ensuring that transitions between the metastable states are possible at all.

One may wonder how much the above results hinge upon the discrete support of the telegraph noise. Surprisingly, for all the cases discussed above it does not make much of a difference if we replace the colored dichotomous noise by a colored Gaussian noise, i.e. by the Ornstein-Uhlenbeck process. In this case, simulations reveal a minimum in the diffusion coefficient for a quintic friction function (Fig. 29a) and also for a for a Rayleigh-Helmoltz friction of an active particle (Fig. 29b). Even a naive comparison of the OUP simulations to the theory for dichotomous driving shows a rather good agreement (cf. solid lines in Fig. 29). At least for a sufficient amplitude of the driving, the variance and the correlation function of the driving noise (statistical features shared by DMP and OUP) seem to be essential in determining the diffusion coefficient and the exact distribution of their values (a feature that distinguishes DMP and OUP) is immaterial.

4.2.3 Particles with asymmetric friction function under white-noise driving: critical asymmetry

So far we have considered symmetric friction functions and symmetric noise sources for which the mean velocity vanishes. A perfectly symmetric friction function is not expected in the dynamics of active particles. Assemblies of molecular motors interact with filaments of a certain polarity; if the assemblies are described by an active Brownian particle dynamics then this dynamics will not be symmetric ($\gamma(-v) \neq \gamma(v)$).

A simple way to introduce an asymmetry is an external bias. Thus we may consider the Langevin dynamics

$$\frac{\mathrm{d}}{\mathrm{d}t}x = v, \quad \frac{\mathrm{d}}{\mathrm{d}t}v = -\gamma(v)v + F + \sqrt{2D}\xi(t). \tag{192}$$
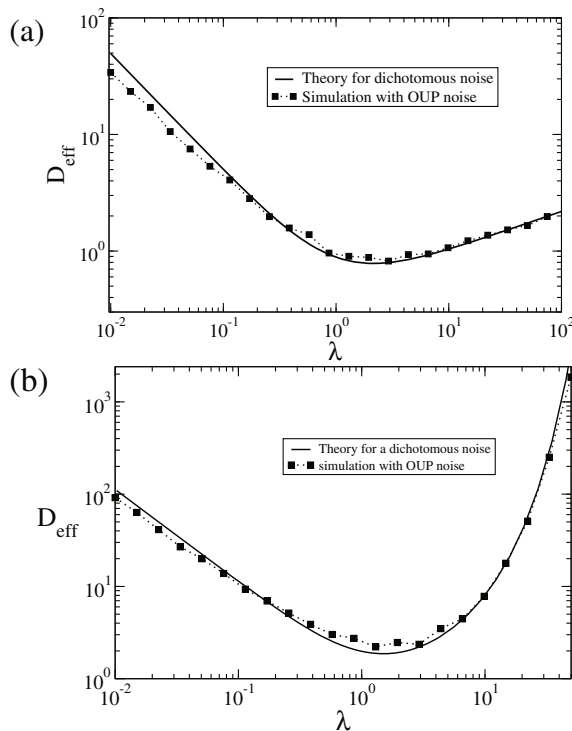
Fig. 29. Diffusion coefficient vs. switching rate of the Ornstein-Uhlenbeck noise for a quintic (a) and a Rayleigh-Helmholtz friction function (b). The theory for the dichotomous process with the same variance and rate (solid lines, Eq. (190)) is shown for comparison. Modified from [221].

We can lump both nonlinear friction ("pumping") force and the external bias into the derivative of one effective velocity potential. This potential is not symmetric anymore but tilted and for a sufficiently strong force even its bistability will be lost (see Fig. 30). In terms of this potential it is very clear that the asymmetry will have a profound effect on the diffusive properties of the particle. The strong diffusion we observed in the symmetric case and at weak noise relies on the bimodality of the velocity which will, however, vanish if the velocity potential is not bistable anymore. Thus we can expect that the diffusion coefficient becomes very small in the limit of strong force whereas it diverges for finite but small forces. It is, however, not clear what the exact value of the force is where the divergence of the diffusion coefficient vanishes. One first guess would be the force at which the potential loses its bistability. A closer inspection, however, disproves this conjecture.

First, we can repeat the previous calculation for the calculation of the diffusion coefficient based on the Fokker-Planck equation (see the related calculation for the correlation time in supplement S.9 in [292]). The more general result for the diffusion coefficient reads [223].

$$D_{\text{eff}} = \frac{\int_{-\infty}^{\infty} \mathrm{d}x \, e^{\Phi(x)/D} \Big[\int_{-\infty}^{x} \mathrm{d}y \, [y - \langle v \rangle] e^{-\Phi(y)/D} \Big]^2}{D \int_{-\infty}^{\infty} \mathrm{d}v \, e^{-\Phi(v)/D}}. \tag{193}$$

Here $\Phi(x)$ is the new effective potential which includes the bias. For weak noise and a bistable potential we can perform a saddle-point approximation of this result and
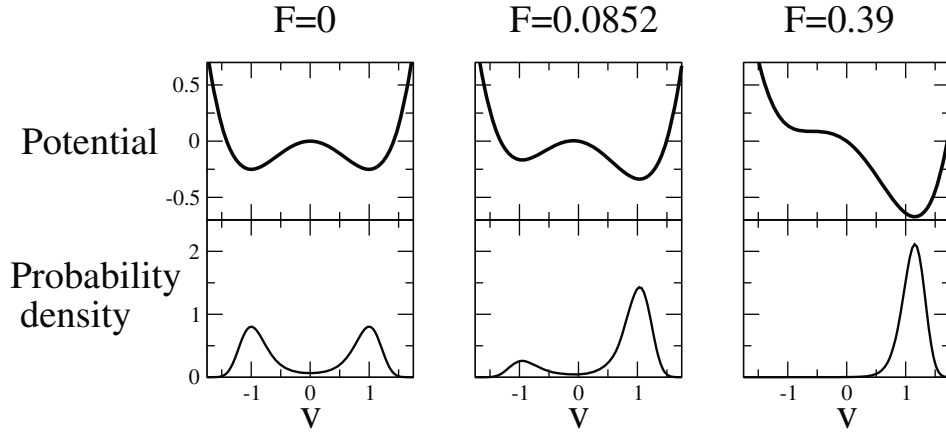
Fig. 30. Quartic velocity potentials $\Phi(v) = v^4/4 - v^2/2 - Fv$ (upper row) and the corresponding velocity probability densities $P(v) \sim \exp[-\Phi(v)/D]$ (lower row) for three different values of the external force F as indicated and a noise intensity of $D = 0.1$.
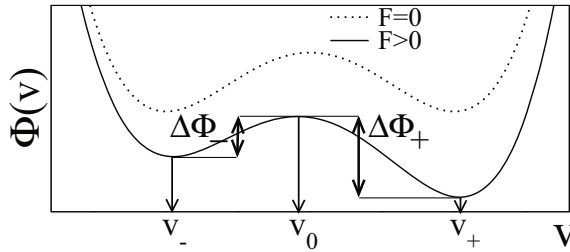

Fig. 31. Symmetric (dotted line) and asymmetric (solid line) potentials with potential barriers indicated.

obtain a much simpler formula. The latter can be alternatively derived by a two-state theory that yields a better physical insight.

In the asymmetric case, the motion of the velocity in the bistable potential is governed by two Kramers rates $r_\pm$ for the escape over the larger (smaller) barrier and the velocity obeys the statistics of a dichotomous noise. Correlation time and variance the product of which forms the diffusion coefficient are given by [135]

$$\tau_{corr} = [r_- + r_+]^{-1}, \quad \langle \Delta v^2 \rangle = \frac{(v_+ - v_-)^2 r_+ r_-}{(r_+ + r_-)^2}, \tag{194}$$

in accordance with Eq. (31). We are specifically interested in the limit of vanishing noise intensity for which both rates go to zero. In the general asymmetric case, the rates differ by an exponential pre-factor given by the difference between the two potential barriers, $r_+/r_- \sim \exp[-(\Delta\Phi_+ - \Delta\Phi_-)/D]$ and, hence, the correlation time diverges but the variance vanishes. The latter finding implies that in the limit of vanishing noise the particles dwells with probability one within the deeper well. Because the diffusion coefficient is the product of variance and correlation time, it is not clear at all when the divergence of the correlation time and when the vanishing of the variance dominates the diffusion coefficient. Inserting the Kramers formula into the product one obtains the specific formula

$$D_{\text{eff}} \approx \frac{2\pi(v_+ - v_-)\omega_+\omega_-/|\omega_0|}{[\omega_- e^{-(2\Delta\Phi_- - \Delta\Phi_+)/(3D)} + \omega_+ e^{-(2\Delta\Phi_+ - \Delta\Phi_-)/(3D)}]^3}, \tag{195}$$
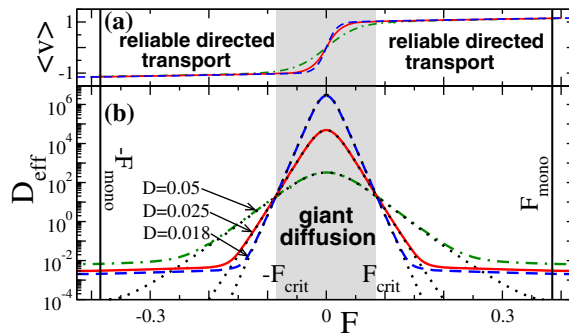
Fig. 32. Mean velocity (top) and effective diffusion coefficient (bottom) vs. external bias for three different noise intensities as indicated. Color lines give the theory from Eq. (193) while black dotted lines is the weak-noise approximation from Eq. (195). Modified from [223].

which is also obtained by a saddle-point approximation of the exact result Eq. (193). Here, $\omega_{\pm}$ are the curvatures in the extrema of the potential. This approximation is valid in the limit of weak noise and yields the most interesting result in the thermodynamic limit of vanishing noise ($D \to 0$) that we explore now. Let us assume without loss of generality that $\Delta\Phi_+$ is the *larger* barrier. Then the second exponential in the denominator of Eq. (195) will vanish rapidly for $D \to 0$. The first exponential, however, can either go to infinity (resulting in a vanishing diffusion coefficient) or to zero (yielding a divergence in the diffusion coefficient) depending on the sign of the exponent $2\Delta\Phi_- - \Delta\Phi_+$. In the case of a mild asymmetry, the larger barrier $\Delta\Phi_+$ will be still smaller than twice the smaller barrier $\Delta\Phi_-$ — in this case the diffusion coefficient diverges as in the symmetric case. A stronger asymmetry, which does not destroy the potential's bistability but makes the larger barrier greater than twice the smaller barrier, leads to a positive exponent and thus makes the diffusion coefficient vanish in the limit of zero noise. The critical force by which these two distinct diffusive behaviors are separated is clearly determined by the condition

$$\Delta\Phi_+(F_{\text{crit}}) = 2\Delta\Phi_-(F_{\text{crit}}). \tag{196}$$

The critical force (and its symmetric counter part $-F_{\text{crit}}$) form the boundary of a region of giant diffusion (shaded region in Fig. 32b). Generally, no transition is seen in the mean velocity (shown in Fig. 32a). Hence if for strong asymmetry the mean velocity is finite, we are entitled to talk about a parameter region of regular transport (outside the shaded region in Fig. 32). In Fig. 32 the comparison between the full numerical evaluation of the exact solution Eq. (193) and the weak-noise expansion Eq. (195) reveals good agreement in the region of foremost interest where both potential barriers still exist but can also significantly differ.

Note that we have not used in our arguments above that F is an additive bias. Thus all conclusions regarding the critical asymmetry apply also to the case where the asymmetry controls the barrier heights in a more complicated way; also we may generalize the line of reasoning to the case of an active Brownian particles with multiplicative noise. In all cases we will have a behavior of the diffusion coefficient similar to this shown in Fig. 32: There is a finite region of weak asymmetry, for which the diffusion coefficient diverges in the limit $D \to 0$ whereas outside this region the same limit yields a small or vanishing diffusion coefficient.

In Sect. 3.1.6 we gave some evidence that the active Brownian dynamics can reproduce the bidirectional motion of coupled molecular motors. Does this imply that
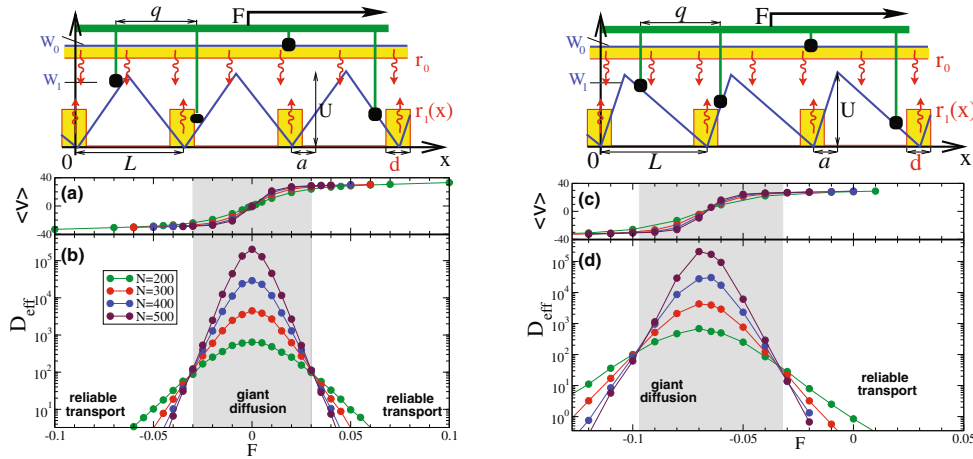
Fig. 33. Mean velocity (a,c) and diffusion coefficient (b,d) of assemblies of molecular motors as a function of the external force. (a) and (c) are for a symmetric motor-filament interaction (see the spatial potential sketched above panels) with $a = 0.5$; (b) and (d) are for the asymmetric case with $a = 0.4$. Results for various numbers of motors as indicated. Modified from [223].

for coupled molecular motors a similar critical asymmetry as found above exists? This question was studied in [223] and the result of extensive simulations is shown in Fig. 33 for a symmetric (a,b) or an asymmetric (c,d) motor-filament interaction.

For the motor system noise intensity is set by the inverse number of motors. Indeed, just as in the case of active Brownian particles, diffusion curves for different motor numbers (different noise levels) intersect at critical values of the external force. These values are the boundaries for the forcing region of giant diffusion. If the unbiased system is spatially symmetric as in Fig. 33a,b, the dependence of mean velocity and diffusion coefficient on F resemble strongly the results for the Brownian motion with Rayleigh-Helmholtz friction. Please note that the latter is also spatially symmetric and that any asymmetry in the system is due to the bias force F. If the system, however, shows a spatial asymmetry ($a = 0.4$ for the piecewise-linear ratchet potential as shown in Fig. 33), both statistics are shifted. At zero force, there is already a finite mean velocity and the motion is rather regular because the diffusion coefficient is small. Biasing the motor assembly against its preferred (ratchet-induced) direction, however, results for a finite range of forces again in a giant diffusion. Roughly speaking, the two kinds of asymmetries add up and maximal diffusion is achieved if the system is rather symmetric, i.e. both directions of motion are roughly equal. Further support for the similarity of the underlying mechanism for the critical asymmetry observed for active Brownian particles and for coupled molecular motors comes from a measure based on the velocity's probability density which can be derived from Eq. (196); for details, see [223].

4.3 Diffusion in two dimensions

4.3.1 Two dimensional random walk with correlated turning angle

In this section we consider diffusion of active particles in two dimensions. The central aim remains the calculation of the diffusion coefficient including correlations in motion, respectively, if the trajectories of the particles exhibit some persistence.

We will start with a discrete random walker in two dimensions which jumps with a fixed step length l_0. It could be modeled by a shot noise where the sequence of δ-peaks is supplied with constant weight l_0. As in Eq. (12), we restrict in the consideration to an overdamped situation. The equation of motion reads.

$$\frac{\mathrm{d}}{\mathrm{d}t}\mathbf{r} = \xi_S(t) = \sum_{i}^{n(t)} l_0 \mathbf{e}_{v_i}\, \delta(t - t_i). \tag{197}$$

This δ-kicks change the position vector by l_0 pointing in the direction of the unit vector $\mathbf{e}_{v_i}$. The t_i are generated due to the waiting time density between two strokes $w(\tau)$. The mean of this shot noise is obviously $1/\langle\tau\rangle$ where $\langle\tau\rangle$ is the mean time between two spikes. For simplicity, the jumps shall occur with a fixed time interval τ_0 [187, 252], i.e. $w(\tau) = \delta(\tau - \tau_0)$.

The mean speed is obviously $s = v_0 = l_0/\langle\tau\rangle > 0$. The unit vector of the direction $\mathbf{e_v}$ is determined by its angle respective to the x-axis which we again label by $\varphi(t)$. We assume that the two angles between two subsequent steps i and $i+1$ are not independent. The angle of the velocity vector is shifted at each jump by a turning angle η_i, for which we assume a given turning angle distribution $P(\eta)$. The existence of a structured distribution $P(\eta)$ different from a uniform one creates some persistence in the motion. We will assume that the correlations are weak and that they extend over one step, only. It implies that the sequence of turning angels $\eta_1, \eta_2, \ldots, \eta_i, \ldots$ shall be independent.

This situation was considered by Kareiva and Shigesada and is discussed in detail in the monograph by Okubo and Levin [187, 252]. The i-th displacement is given by:

$$\Delta\mathbf{r}_i = l_0\left(\mathbf{e}_x \cos\varphi_i + \mathbf{e}_y \sin\varphi_i\right), \qquad \varphi_i = \varphi_{i-1} + \eta_i, \tag{198}$$

where φ_i is the angle between the x-axis and the direction of motion. After $n = [t/\tau_0]$ steps the walker has a squared distance from the point of start of:

$$\mathbf{r}_n^2 = \sum_{i=1}^{n} \Delta\mathbf{r}_i \cdot \sum_{j=1}^{n} \Delta\mathbf{r}_j. \tag{199}$$

Averaging over an ensemble of walkers and expanding the sum yields:

$$\langle\mathbf{r}_n^2\rangle = \sum_{i=1}^{n} \langle\Delta\mathbf{r}_i^2\rangle + 2\sum_{i=1}^{n-1}\sum_{j>i}^{n} \langle\Delta\mathbf{r}_i \cdot \Delta\mathbf{r}_j\rangle$$

$$= n\, l_0^2 + 2\, l_0^2 \sum_{i=1}^{n-1}\sum_{j>i}^{n} \langle\cos(\varphi_i - \varphi_j)\rangle. \tag{200}$$

The second term on the r.h.s requires a distribution of the turning angles $P(\eta)$ which we assume to be symmetric in η. Then the mean squared displacement is expressed by the angular correlation defined as the average Γ of the cosine of the turning angle

$$\Gamma = \left\langle \cos\eta \right\rangle = \int_{-\pi}^{\pi} \mathrm{d}\eta\, \cos\eta\, P(\eta). \tag{201}$$

This expression has the physical meaning of how much on average the length of the unit vector $\mathbf{e}_v$ is reduced if projected on the direction of the previous jump. Since correlations have been considered only between successive steps we get for two jumps

$$\langle\cos(\varphi_i - \varphi_{i+2})\rangle = \int_{-\pi}^{\pi} \mathrm{d}\eta\, P(\eta) \int_{-\pi}^{\pi} \mathrm{d}\eta'\, P(\eta') \cos(\eta + \eta') = \Gamma^2. \tag{202}$$

It can be shown as well with $k > 2$ that

$$\langle \cos(\varphi_i - \varphi_{i+k}) \rangle = \Gamma^k. \tag{203}$$

So we can solve the sum in (200) and get a formula for the mean squared displacement after n steps of a 2D correlated random walk like in [252] and [173], which was derived previously by Kareiva and Shigesada [187]:

$$\langle \mathbf{r}_n^2 \rangle = l_0^2 \left(n \frac{1+\Gamma}{1-\Gamma} - 2\Gamma \frac{1-\Gamma^n}{(1-\Gamma)^2} \right) \propto l_0^2 \left(n \frac{1+\Gamma}{1-\Gamma} - \frac{2\Gamma}{(1-\Gamma)^2} \right). \tag{204}$$

In the limit $n \to \infty$ the second term on the right hand side of (204) becomes time independent for large n since $|\Gamma| < 1$.

Therefore the diffusion is anomalous at short times and converges to normal diffusion at long times with the coefficient.

$$D_{\text{eff}} = \frac{1+\Gamma}{1-\Gamma} \frac{l_0^2}{4\tau_0}. \tag{205}$$

The second term in the sum can be interpreted as the square of a characteristic length scale. If this length scale is much smaller than the length scale of the process itself, normal diffusion approximation holds.

As can be seen from Eq. (201) Γ vanishes if η is equally distributed. This corresponds to the motion of a freely diffusing particle without any directional correlations between the jumps. We see also that a persistence of the trajectory with Γ larger than zero enhances diffusion. An negative sign of the correlation parameter decreases the diffusion coefficient.

We will also have a look at the diffusion coefficient without correlations $\Gamma = 0$. One can replace the jump length by velocity divided by the duration of the jump, i.e. $l_0 = v_0 \tau_0$. Afterwards we set τ_0 equal to the relaxation time for the angular fluctuations from Eq. (67), i.e. $\tau_0 = \tau_\varphi = D/v_0^2$. With this the effective diffusion coefficients behaves as $\sim v_0^4/D$. We will encounter this result several times later on from the continuous theory of Active Brownian particles [236]. It means, surprisingly, that increasing noise decreases the value of the diffusion coefficient.

An application to particular situation of a hopping Daphnia motion was given in [133,200]. Therein specific angle distribution, like exponential and bimodal ones have been assumed in order to control the diffusion coefficient.

One has to add that the same way of calculation of the diffusion coefficient was used by R. Fürth [131] who considered persistent random walk in one dimension. He assumed the probabilities p and $1 - p$ that the particles jumps after t_0 the length l_0 preferentially in the same direction or in the opposite one, respectively. This way he formulated correlations between successive hops. In consequence, one can also find the probabilities for all longer sequences of possible jumps and also the respective correlations. By summing up all the jumps in (200) one determines the mean squared displacement in one dimension.

One limit is the case with $p = 1/2$, i.e. no preference in the angle is assumed and the diffusional motion is free and the diffusion coefficient equals $l_0^2/(2\tau_0)$. In contrast in the limit $p \to 1$ and $\tau_0 \to 0$ with $(1-p)/\tau_0 = \gamma/2 = const$ the diffusion coefficient of a Brownian particles with inertia and $m = 1$ as in (7) is obtained. The correlation time $\tau_{corr} = 1/\gamma$ quantifies the persistence length $l_{pers} = v_0 \tau$ with assumed fixed velocity $v_0 = l_0/\tau_0$.

4.3.2 Diffusion for independent velocity and heading dynamics

In higher dimensions, the diffusion of active Brownian particles becomes more complicated and is only in a few cases analytically tractable. A popular and reasonable approximation in this case is the assumption that velocity and direction of motion are independent variables; this will be presented here, following the work by Peruani and Morelli [273].

In general the motion of an active Brownian particle in arbitrary dimensions d can be described by its a unit vector describing the direction of motion (heading) $\mathbf{e}_h(t)$ at time t and the velocity with respect to the heading direction (see Sect. 2.3).

In two spatial dimensions, where $\mathbf{e}_h(t) = (\sin\phi(t), \cos\phi(t))$, assuming completely independent dynamics in v and ϕ (heading angle) the evolution of the velocity vector $\mathbf{v} = v(t)\mathbf{e}_h(t)$ is determined by the following stochastic differential equations:

$$\dot{v} = -\gamma(v)v + \eta_v(t) \tag{206}$$

$$\dot{\phi} = \eta_\phi(t). \tag{207}$$

The first term in the velocity equation is again an arbitrary velocity dependent friction function which describes the deterministic evolution of the velocity. The second term is the stochastic part with η_v being the component of random force acting on the velocity. The evolution of the heading angle is assumed to consist only of a stochastic torque acting on ϕ. In (207), it is assumed that the angular velocity (or turning rate) does not dependent on the velocity v, and we should note that it is in general not the case, in particular, if we consider turning behavior with inertia.

In general the fluctuations $\eta_{v,\phi}(t)$ can obey arbitrary distributions and temporal statistics. Here, we consider independent and uncorrelated Gaussian (white) noise terms, based on our ansatz for active fluctuations (Sect. 3.2)

$$\eta_v = \sqrt{2D_v}\xi_v, \quad \eta_\phi(t) = \sqrt{2D_\phi}\xi_\phi, \tag{208}$$

which is, based on the center limit theorem, a reasonable approximation of many random processes occurring in nature.

For independent v and ϕ-dynamics the joint probability distribution my be decomposed as $P(v,\phi,t) = P_v(v,t)P_\phi(\phi,t)$. Thus the expectation value for the displacement $\langle\mathbf{r}(t)\rangle$ reads

$$\langle\mathbf{r}(t)\rangle = \int_0^t \mathrm{d}t' \langle v(t')\mathbf{e}_h(t')\rangle = \int_0^t dt' \langle v(t')\rangle\langle\mathbf{e}_h(t')\rangle. \tag{209}$$

In the absence of a preferred direction of motion (uniform distribution of ϕ), the time average and ensemble average with respect to $\mathbf{e}_h$ vanishes and so does the mean displacement $\langle\mathbf{r}(t)\rangle = 0$.

The mean square displacement $\langle\mathbf{r}^2\rangle(t)$ in the absence of directional bias can be obtained according to Eq. (166) from the velocity-velocity correlation function. Here $C_{\mathbf{vv}}(\tau)$ decomposes into independent vv and $\mathbf{e}_h\mathbf{e}_h$-correlation functions:

$$\langle\mathbf{r}^2(t)\rangle = \int_0^t dt' \int_0^{t'} d\tau \langle\mathbf{v}(0)\mathbf{v}(\tau)\rangle = \int_0^t dt' \int_0^{t'} d\tau \langle v(0)v(\tau)\rangle\langle\mathbf{e}_h(0)\mathbf{e}_h(\tau)\rangle. \tag{210}$$

Assuming an exponential decay of the velocity correlations we may rewrite the velocity correlations in the stationary case as

$$\langle v(0)v(\tau)\rangle = \langle v^2\rangle e^{-\kappa_v\tau} + \langle v\rangle^2(1 - e^{-\kappa_v\tau}) \tag{211}$$

with $\langle v \rangle$ and $\langle v^2 \rangle$ being the first and second moment of the stationary velocity distribution $p_s(v)$ and κ_v being the relaxation rate (inverse relaxation time).

The angular dynamics in Eq. (207) results in a free diffusive motion of $\mathbf{e}_h$ on a unit circle, with an exponential decay of autocorrelations:

$$\langle \mathbf{e}_h(0)\mathbf{e}_h(\tau) \rangle = e^{-\kappa_h \tau}, \tag{212}$$

with κ_h being the correlation decay rate of the direction of motion. In the case of free diffusion of ϕ it is equal to the angular diffusion coefficient: $\kappa_h = D_\phi$.

Inserting Eqs. (211) and (212) in Eq. (210) yields finally [273]:

$$\langle \mathbf{r}^2(t) \rangle = 2\frac{\langle v \rangle^2}{\kappa_h} \left[t + \frac{1}{\kappa_h} \left(e^{-\kappa_h t} - 1 \right) \right]$$
$$+ 2\frac{\langle v^2 \rangle - \langle v \rangle^2}{\kappa_v + \kappa_h} \left[t + \frac{1}{\kappa_v + \kappa_h} \left(e^{-(\kappa_v + \kappa_h)t} - 1 \right) \right]. \tag{213}$$

The first term describes the contribution of the mean square displacement due to self-propelled motion with (constant) mean velocity $\langle v \rangle$ and a stochastic direction of motion, whereas the second term takes into account the impact of velocity fluctuations on the mean square displacement.

For particles moving with constant speed ($\langle v \rangle = v_0 = const.$) there exist two different scaling regimes of $\langle \mathbf{r}^2(t) \rangle$ with t similar to ordinary Brownian motion: The so-called ballistic regime at short times with $\langle \mathbf{r}^2(t) \rangle \propto t^2$ and the diffusive regime with $\langle \mathbf{r}^2(t) \rangle \propto t$ for $t \to \infty$. Between the two regimes there is a crossover at time $t \sim \kappa_h^{-1}$.

The introduction of an additional time-scale due to velocity fluctuations may lead to a mean square displacement with four distinct regimes and three crossovers in between. For large time scale separation: $(\kappa_h + \kappa_v)^{-1} \ll \kappa_h^{-1}$ the angular correlation decays much slower than the velocity correlations ($\kappa_h/\kappa_v \ll 1$). Thus starting from its initial position at $t = 0$ the particles perform first a quasi one-dimensional motion along their initial direction of motion. The stochastic decorrelation of the velocity in this effective one-dimensional motion leads to a first crossover from ballistic to diffusive motion. After the velocity dynamics reach a stationary state, what matters is only the average motion with the mean velocity $\langle v \rangle$. This regime corresponds to self-propelled particles with constant speed performing (still) effectively a one-dimensional motion with $\langle \mathbf{r}^2 \rangle \propto t^2$. As a consequence a second crossover can be observed from the transient diffusive regime to a second ballistic regime. Finally, in the limit of large times $t \to \infty$, the slow decorrelation of the direction of motion leads to the third and last crossover towards the final diffusive regime.

The diffusion coefficient of the limiting diffusive regime reads (Eq. 169):

$$D_{\text{eff}} = \frac{1}{d} \left(\frac{\langle v \rangle^2}{\kappa_h} + \frac{\langle v^2 \rangle - \langle v \rangle^2}{\kappa_v + \kappa_h} \right). \tag{214}$$

This results, as well as Eq. (213), holds for arbitrary dimensions $d = 1, 2, 3$ as long as the heading correlations decay exponentially and are governed by a single time scale given by κ_h^{-1}.

An additional bias (e.g. external force), may even introduce yet another time-scale and in this case even five crossovers are possible [273]. This complicated behavior of the mean squared displacement can be an explanation for experimental observations of superdiffusive motion of active particles [83,372]: several crossovers and averaging over nonidentical active particles may lead to observations of mean squared displacements, which appear to be in between ballistic and diffusive motion.

4.3.3 Diffusion of active particles with passive fluctuations

In contrast to the previous section, we consider now active particles with correlated fluctuations in the velocity and direction of motion, due to only passive (or external) fluctuations acting simultaneously on both degrees of freedom as introduced in Sect. 3.3 with $D_v, D_\phi = 0$. At low external noise intensities D the velocity distribution for an arbitrary friction function is given by a narrow peak around the stationary velocity v_0 and as a first approximation the velocity can be assumed as constant: $v = v_0 = const$. The external (passive) fluctuation act only on the direction of motion. In this limit the velocity correlation function reads

$$\langle v(0)v(\tau) \cos(\varphi(\tau) - \varphi(0)) \rangle = v_0^2 \left\langle \cos(\varphi(\tau) - \varphi(0)) \right\rangle = v_0^2 \exp\left(-\frac{D}{v_0^2} \tau \right). \quad (215)$$

Inserting Eq. (215) in Eq. (213) gives us the mean square displacement:

$$\left\langle \Delta \mathbf{r}^2(t) \right\rangle = 2 \frac{v_0^4}{D} \left[t + \frac{v_0^2}{D} \left(\exp\left\{ -\frac{D}{v_0^2} t \right\} - 1 \right) \right]. \quad (216)$$

This is a well known result obtained previously by Meinköhn and Mikhailov [236].

The corresponding long time effective spatial diffusion coefficient is inversely proportional to D and reads

$$D_{\mathrm{MM}} = \lim_{t \to \infty} \frac{\left\langle \Delta \mathbf{r}^2(t) \right\rangle}{4t} = \frac{v_0^4}{2D}. \quad (217)$$

Please note the different power-law dependence of D_{MM} on $v_0 = \langle v \rangle$ in comparison to (214) for vanishing velocity fluctuations ($\langle v^2 \rangle - \langle v \rangle^2 = 0$). This is due to the fact that we consider here active motion with inertia.

In general, the diffusion coefficient of self-propelled particles ($v \approx v_0 = const.$), decreases with increasing noise strength D in contrast to ordinary Brownian motion. In the limit $D = 0$ the fluctuations in the direction of motion vanish and the self-propelled particles moves with constant velocity along its initial direction of motion. The mean squared displacement increases as $\sim t^2$ and we observe only ballistic motion - no diffusion. Thus, for $D \to 0$ the effective diffusion coefficient diverges. On the other hand, with increasing D the fluctuations in the direction of motion increase — the particle changes its direction of motion with increasing frequency. As the velocity does not increase with D this leads effectively to a localization of the particle and decreasing diffusion. Thus, for active particles moving with a constant speed the diffusion coefficient vanishes $D_{\mathrm{MM}} \to 0$ as $D \to \infty$.

For the linear Schienbein-Gruler model (see Sect. 3.1.2) the above low-noise limit corresponds to $D/\gamma_0 \ll v_0^2$. Thus in the limit $D \to 0$ the effective diffusion coefficient will converge to Eq. (217). However, in the limit of large noise intensities $D/\gamma_0 \gg v_0^2$ we may neglect the active motion term in the Schienbein-Gruler friction and put $v_0 = 0$. The dynamics reduces to ordinary Brownian motion with the effective diffusion coefficient $D_{\mathrm{BM}} = D/\gamma_0$ which increases linearly with D.

Based on the two asymptotic limits it becomes evident that there must exist a minimum of the effective diffusion coefficient. A crude approximation for D_{eff} can be obtained by a sum of the two asymptotic diffusion coefficients:

$$D_{\mathrm{I}} = D_{\mathrm{MM}} + D_{\mathrm{BM}} = \frac{v_0^4}{2D} + \frac{D}{\gamma^2}. \quad (218)$$

This approximation has the right asymptotic behavior and reproduces qualitatively the behavior of D_{eff} at intermediate noise strengths D. But a comparison with the

numerical results reveals that this approximation underestimates the diffusion coefficient close to the minimum.

We attempt to improve the approximation of D_{eff} by considering the velocity drift term in the Fokker-Planck Equation (19) with $v_0 > 0$. The most probable velocities $\tilde{v}$, corresponding to the maxima of the velocity probability distribution, are given as roots of the drift term according to the Stratonovich interpretation:

$$-\gamma_0(\tilde{v} - v_0) + \frac{D}{\tilde{v}} = 0. \tag{219}$$

By multiplying with $\tilde{v}$ we obtain a quadratic equation for $\tilde{v}$ with the roots:

$$\tilde{v}_{+/-} = \frac{v_0}{2} \pm \sqrt{\frac{v_0^2}{4} + \frac{D}{\gamma_0}}. \tag{220}$$

The positive root corresponds to the maximum at positive velocities close to v_0 whereas the negative root corresponds to the maximum at negative velocities (backwards motion). At low D the backwards motion may be neglected and the most probable velocity is given by the positive root $\tilde{v}_+$. Inserting $v = \tilde{v}_+$ in D_{MM} (217) gives us qualitatively the right behavior of the diffusion coefficient with a minimum at intermediate D but does not reproduce the correct asymptotic for $D \to \infty$. In order to eliminate this deviation we add a correction term $D/(2\gamma_0^2)$ and obtain a second approximation as:

$$D_{\text{II}} = \frac{\left(\frac{v_0}{2} + \sqrt{\frac{v_0}{4} + \frac{D}{\gamma_0}}\right)^4}{2D} + \frac{D}{2\gamma_0^2}. \tag{221}$$

A comparison of D_{II} with numerical results shows that it offers a better approximation then the D_{I} but overestimates the diffusion coefficient close to the minimum.

The two approximations appear to provide a lower and an upper bound of the effective diffusion coefficient close to the minimum. We obtain a third approximation by taking the average of D_{I} and D_{II}. This heuristic ansatz does not yield any additional qualitative insights but results in an analytical expression for D_{eff} with a good agreement to numerical simulation:

$$D_{\text{eff}} \approx D_{\text{III}} = \frac{1}{2}(D_{\text{I}} + D_{\text{II}})$$

$$= \frac{3D}{4\gamma_0^2} + \frac{v_0^4}{4D} + \frac{1}{64D}\left(v_0 + \sqrt{v_0^4 + \frac{4D}{\gamma_0}}\right)^4. \tag{222}$$

In Fig. 34 we show a comparison of the three analytical approximations for D_{eff}. Please note that at low noise intensities all approximations seem to yield systematically larger values of D_{eff} then the numerical simulations. This can be associated with the coupling of the effective angular diffusion to the velocity dynamics, which have not been taken into account correctly.

4.3.4 Turning angles as Gaussian Ornstein-Uhlenbeck process

Another model to include correlations of the trajectories starts with equation of motion for the angle dynamics (See Eq. 69). So far in case of constant speed v_0 and a continuous angle changes we widely have used that the turning angle is a Wiener
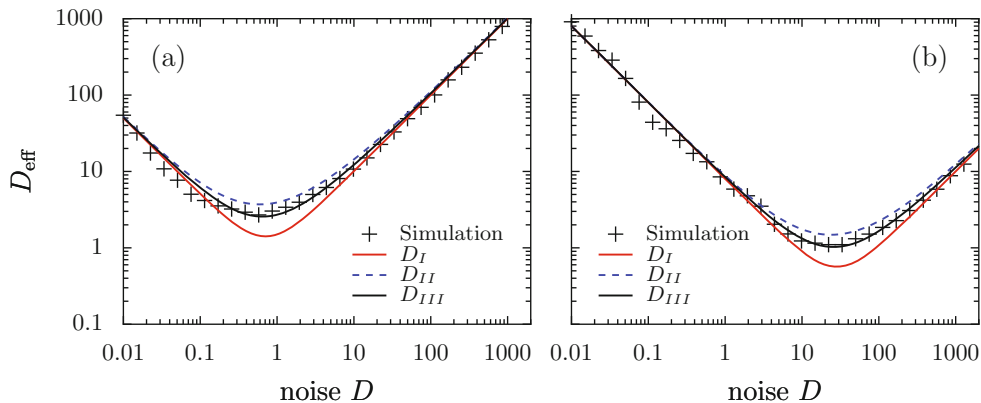
Fig. 34. Effective diffusion coefficient of Schienbein-Gruler model with external noise versus noise intensity D for two different parameter sets: (a) $\gamma_0 = 1.0$ and $v_0 = 1.0$, (b) $\gamma_0 = 10.0$ and $v_0 = 2.0$. Comparison of numerical results with the analytical approximations D_{I} (218), D_{II} (221) and D_{III} (222).

process and, respectively, its angular velocity Gaussian white noise. The corresponding solution of the FPE is simply formulated from Eq. (72) putting $\Omega = 0$ or from Eq. (66) if periodically wrapped.

The situation without preferred turning angle (see Eq. (63)) can be generalized to a correlated Ornstein-Uhlenbeck process [58,153,167,355] as a model of possible correlations. Some exemplary models of correlated dynamics are found in [214,302,310]. Here, applied to angular dynamics, the corresponding angular velocities have vanishing mean but possess Gaussian deviations correlated over a characteristic time τ_C. The corresponding dynamics for the angular velocity is defined by the system of stochastic differential equation

$$\dot{\varphi} = \frac{1}{v_0}\,\Omega(t), \quad \dot{\Omega} = -\kappa\Omega + \sqrt{2D_\Omega}\,\xi(t).$$

The coefficients κ plays the role of the inverse of the correlation time τ_C of the angular velocity.

Considering unwrapped angles with $\varphi \in [-\infty, \infty]$, the angular dynamics resemble the equations of motion of a Brownian particle with Stokes friction $\propto \kappa$ and noise intensity D_Ω (compare Eq. (5)). The solution of this Langevin equation is known since the seminal paper by Uhlenbeck and Ornstein [355] which was later generalized by Chandrasekhar to motion in a higher dimensional space [58]. From the time-dependent solution of the FPE, which is a Gaussian in the angle φ and in the angle velocity Ω, we obtain, for a given initial angular velocity Ω_0, the transition probability of the angle as [355]

$$P(\varphi_2, \tau | \varphi_1, \Omega_0, 0) = \sqrt{\frac{\kappa^3 v_0^2}{2\pi D(\tau)}} \exp\!\Big(-\frac{k^3 v_0^2}{2D(\tau)}\big(\varphi_2 - \varphi_1 - \frac{\Omega_0}{\kappa}(1 - \exp(-\kappa\tau))\big)^2\Big).$$

$$(223)$$

Therein the time dependent mean square increment of the angle reads

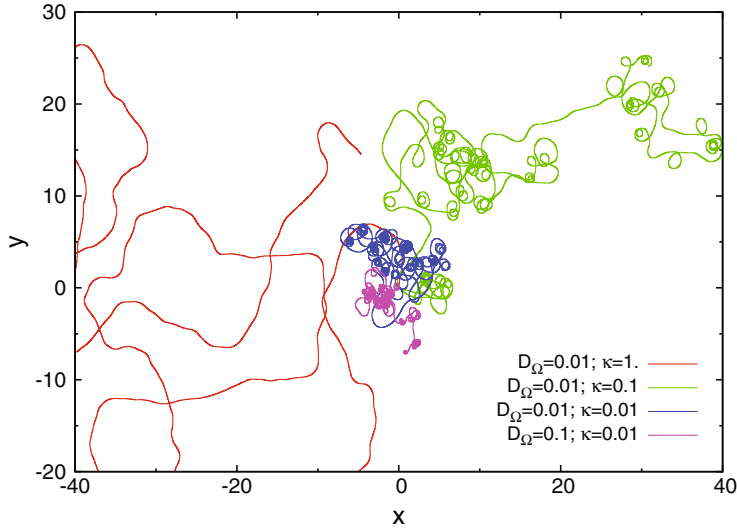$$D(\tau) = D_\Omega(2\kappa\tau - 3 + 4\exp(-\kappa\tau) - \exp(-2\kappa\tau))$$

Fig. 35. Trajectories of particles with constant speed and correlated turning angles for different values of correlation. Other parameters: $v_0 = 1$ [366].

which exactly agrees in the unwrapped approximation with the spatial diffusion coefficient calculated by Langevin for the mean squared displacement (7).

And thus the increment in the angle is a Gaussian distributed random variable. It simplifies the calculation of the mean projection along the former path according to (215) which yields

$$\langle \cos \Delta\varphi(\tau) \rangle = \exp\left(- \frac{D_\Omega}{v_0^2 \kappa^3}(\kappa\tau - 1 + \exp(-\kappa\tau)) \right) \qquad (224)$$

and results in the mean squared displacement of the particle

$$\langle \Delta\mathbf{r}^2(t) \rangle = 2\,v_0^2 \int_0^t (t - \tau)\langle \cos \Delta\varphi(\tau) \rangle \, \mathrm{d}\tau. \qquad (225)$$

The expression with double exponentials (224) can be evaluated either numerically in the general case or analytically in limiting cases [366]. We observe that it starts with a ballistic growth $\propto t^2$ and crosses over to a diffusional regime $\propto t$. One can easily verify that in the two temporal limits

$$\lim_{\tau \to 0} \frac{\mathrm{d}}{\mathrm{d}t}\langle\, \langle \Delta\mathbf{r}^2(t) \rangle = 2\,v_0^2\,\tau. \qquad (226)$$

and

$$\lim_{\tau \to \infty} \frac{\mathrm{d}}{\mathrm{d}\tau}\langle \Delta\mathbf{r}^2(t) \rangle = 2v_0^2 \int_0^\infty \exp\left[-\frac{D_\Omega}{v_0^2 \kappa^3}\left(\kappa\tau - 1 \right) \right] \mathrm{d}\tau = \mathrm{const.} \qquad (227)$$

The crossover times between both regimes depend on the coupling. Let $\tau_1 = v_0 \sqrt{\kappa/D_\Omega}$. For large correlation times $\tau = 1/\kappa \geq \tau_1$ the crossover time equals $t_{cross} = \tau_1$. In contrast, for $\tau = 1/\kappa \leq \tau_1$ the mean squared displacement becomes diffusional beyond $t_{cross} = \tau_1^2 \kappa$.

An analytically tractable limit is $\kappa \to \infty$ with $D_\Omega = \mathrm{const}$. It corresponds to a frozen angle with the variance being ballistic $\langle \Delta\mathbf{r}^2(t) \rangle = v_0^2 \tau^2$. One might return
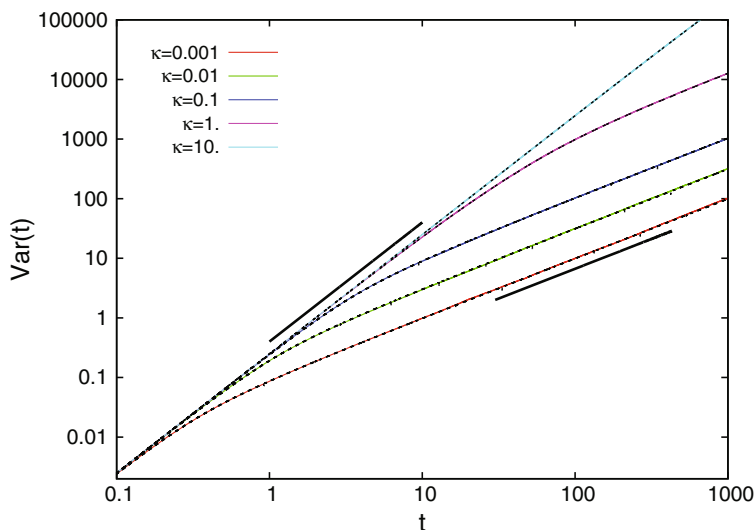
Fig. 36. Mean squared displacement of a particle with constant speed and correlated angular velocity for different inverse correlation times κ [366].

also to the case that the angular velocity is white noise in the same limit $\kappa \to \infty$. However, this time the noise intensity shall scale with κ as $D_\Omega = \kappa^2 D$. This case was studied previously in Section 4.3.3, where the mean squared displacement is given by Eq. (217) [236].

As shown before in Sect. 4.3.2 under the assumption of independent speed and angular fluctuations both contribute additively to the mean squared displacement. Assuming an energy pump of the Schienbein-Gruler type

$$\dot{v} = -\gamma(v - v_0) + \sqrt{2D_v}\,\xi(t)$$

the speed fluctuations lead to an replacement of the constant squared velocities in (225) by the time dependent autocorrelation function

$$v_0^2 \to v_0^2 + \frac{D_v}{\gamma}\exp(-\gamma\tau). \tag{228}$$

Parameters have been selected such, that the growth of the mean squared displacement versus time undergoes three crossovers [273] (see also Sect. 4.3.2). The corresponding times are given by the relations [366]

$$t_1 = \frac{1}{\gamma}, \quad t_2 = \frac{D_\Omega}{\gamma^2 v_0^2}, \quad t_3 = \frac{v_0^2 \kappa^2}{D_\Omega}. \tag{229}$$

The first time t_1 gives the crossing of the speed fluctuations, whereas the last one t_3 has its origin in the change of the angular fluctuations. At the time t_2 both the value of ballistic displacement caused by the angular noise starts to overcome the diffusional displacement created by speed fluctuations. Therefore the displacement returns to a ballistic growth.
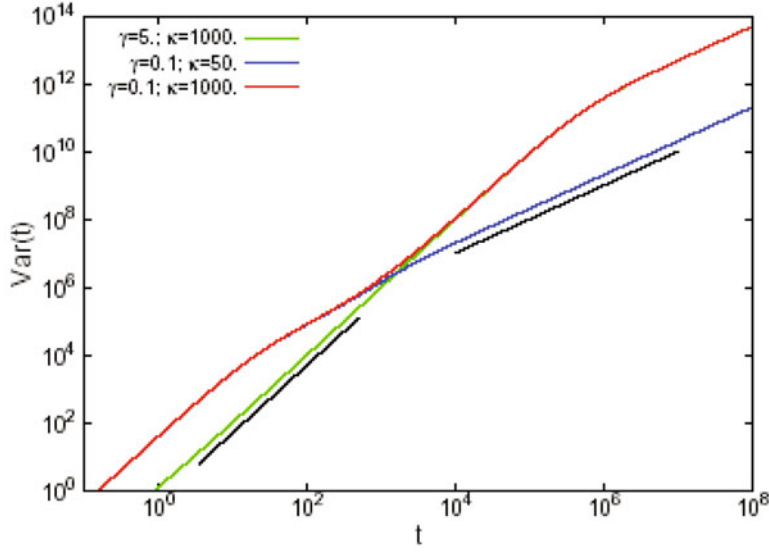
Fig. 37. Mean squared displacement of a particle with fluctuating speed and correlated angular velocities [366].

4.3.5 Stochastic, dichotomous angular dynamics

Markovian switch between two operating orientations

In the following, we consider again particles moving with constant speed $s = v_0$ and under the influence of a time-dependent torque [128,129,358]. However, this time we assume that the rotational motion switches dichotomously between leftward and rightward turning [152,200,307]. In detail, we consider as switching protocol for $\Omega(t)$ the symmetric dichotomous Markov process (see Sect. 2.4), which is another colored noise taken as the driving torque. $\Omega(t)$ may possess the two values $\pm\omega$ and switches between them with a constant rate λ. Additionally, angular white Gaussian noise with intensity $D_\varphi = D/v_0^2$ is present and perturbs the angle.

The Langevin equation for this situation is easily formulated and reads

$$\dot{\varphi} = \Omega(t) + \sqrt{2D_\varphi}\,\xi_2(t). \tag{230}$$

In Fig. 38 we show simulations of typical trajectories where the random torque $\Omega(t)$ is given by a symmetric dichotomous Markov process [366,367], as introduced in Eq. (230). We assume that the angular velocity vanishes in average, i.e. $\langle\dot{\varphi}\rangle = 0$.

We define the probability density functions for both rotational modes in analogy to Sect. 2.4 and the description reduces to angular dynamics $\varphi(t)$. The particle has the joint probability density function $P_+(\varphi, t|\varphi_0)$ to have the angle φ and angular velocity $\Omega(t) = +\omega$ at time t conditioned by the initial value φ_0 at $t = 0$. Equivalently, one defines $P_-(\varphi, t|\varphi_0)$ for the state with $\Omega = -\omega$. Both densities obey the equations [9]

$$\frac{\partial}{\partial t}P_\pm(\varphi, t) = \mp\omega\frac{\partial P_\pm(\varphi, t)}{\partial\varphi} + D_\varphi\frac{\partial^2 P_\pm(\varphi, t)}{\partial\varphi^2} - \lambda P_\pm(\varphi, t) + \lambda P_\mp(\varphi, t), \tag{231}$$

where we have omitted the initial values. The common probability density to have an angle φ at time t then follows from

$$P(\varphi, t) = P_+(\varphi, t) + P_-(\varphi, t), \tag{232}$$

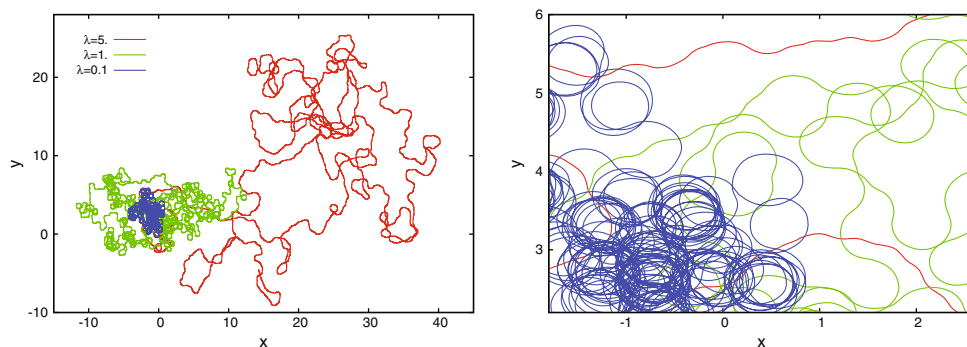which will be used for the determination of the effective spatial diffusion coefficient.

Fig. 38. Trajectories of particles with constant speed and random torque. The angular velocities switches as a symmetric DMP between $\Omega = \pm 1.5$. Different rates of transitions create different magnitude of spreading as presented in the left figure. The right figure zooms into the left one to show the different trajectories. Other parameters: $v_0 = 0.5$ [366].

We proceed to discuss the physical situation in two limiting cases. First we neglect the Gaussian fluctuations. We put $D = 0$ and subsequently $D_\varphi = 0$. Then the evolution of $P(\varphi, t)$ is given by the telegraph equation (28)

$$\frac{1}{2\lambda} \frac{\partial^2}{\partial t^2} P(\varphi, t) + \frac{\partial}{\partial t} P(\varphi, t) = \frac{\omega^2}{2\lambda} \frac{\partial^2 P(\varphi, t)}{\partial \varphi^2}. \tag{233}$$

For large times $t \gg 1/\lambda$ and $\varphi - \varphi_0 \ll \omega t$ the term with the second derivative can be neglected. One gets again a diffusion equation for the angle dynamics. As a result, again a Gaussian density is established as in Eq. (72). The effective angle diffusion coefficient follows as

$$D_\varphi = \frac{\omega^2}{2\lambda}. \tag{234}$$

In the second case we look at the governing equation for the common probability density function including the Gaussian noise. It looks complicated

$$\frac{\partial}{\partial t} P(\varphi, t) = -\frac{1}{2\lambda} \frac{\partial^2}{\partial t^2} P(\varphi, t) + \frac{D_\varphi}{\lambda} \frac{\partial^3 P(\varphi, t)}{\partial t \partial \varphi^2}$$
$$+ \left(\frac{\omega^2}{2\lambda} + D_\varphi \right) \frac{\partial^2 P(\varphi, t)}{\partial \varphi^2} - \frac{D_\varphi^2}{2\lambda} \frac{\partial^4 P(\varphi, t)}{\partial \varphi^4}, \tag{235}$$

however this equation simplifies significantly in the limit of fast switching $\lambda \to \infty$. Additionally we assume in this limit a fixed $\omega^2/\lambda = const$. Then, the evolution operator again reduces to a simple diffusion equation

$$\frac{\partial}{\partial t} P(\varphi, t) = \left(\frac{\omega^2}{2\lambda} + D_\varphi \right) \frac{\partial^2 P(\varphi, t)}{\partial \varphi^2}. \tag{236}$$

The angle dynamics becomes diffusional with the effective diffusion coefficient

$$D_\varphi^{\text{eff}} = \frac{\omega^2}{2\lambda} + D_\varphi. \tag{237}$$

In addition to the intensity of the Gaussian angle noise a second contribution arises from the switching. Again the time dependent solution has a Gaussian form (72) and

the wrapped 2π-periodic solution corresponds to Eq. (66) with (237). We mention that both limits correspond to the Gaussian white noise limits of the stochastic force $\Omega(t)$ in the Langevin equation for the angle dynamics, with fixed velocity $v = v_0$ and $g(v) = 1/v_0$. In this approximation $\Omega(t)$ was interpreted as a second Gaussian white noise in (69), which is uncorrelated with the stochastic term $\xi(t)$.

Equation (236) and its Gaussian solution are valid in the limit of large angle and long times. It turns to be out that the corresponding approximation is insufficient to obtain the correct value of the effective spatial diffusion coefficient D_{eff} describing the motion of the particle in a plane. The latter is strongly determined by the small angle behavior (long stretches without considerable turning). The largest contribution to the spatial diffusion stems from trajectories corresponding to long stretches along the same direction, i.e. is determined by the small-angle behavior.

Therefore, before turning to the calculation of the spatial diffusion coefficient, we discuss a renewal approach which allows a generalization to a non-Markovian case as well as leads us to the effective angular diffusion (237) more directly.

Renewal model for two operating orientations

The previous section dealt with a Markovian dichotomous switchings. Hence, the times spent within two states with fixed direction of rotation are distributed exponentially. Here, we generalize to arbitrary distributions of the switching times [152]. A different techniques will be applied, which is based on a continuous time generalization of a persistent random walk. In particular, our analysis applies methods developed in Ref. [152,230].

We consider the switching between the two states as an alternating renewal process. The probability density function of the sojourn time τ in each state is given by a function $w(\tau)$. In each of these states the motion rotates with the constant angular velocity $\pm\omega$. The overall process is expressed as a sequence of steps in φ_i, each of which corresponds to the sojourn in one of the rotational states.

As in Eq. (199) for the position, the angular displacement $\varphi(t)$ of the system is given by the n complete steps followed by the last $(n+1)$st incomplete step:

$$\varphi(t) = \sum_{i=1}^{n} \varphi_i + \varphi_{n+1}. \tag{238}$$

The corresponding joint probability density function (pdf) $h(\varphi, \tau)$ of the displacement φ and the duration τ of a completed step in a corresponding state can be written as

$$h_\pm(\varphi, \tau) = R_\pm(\varphi, \tau)\, w(\tau), \tag{239}$$

where $R_\pm(\varphi, t)$ is the conditional pdf of rotation for given step duration τ. It is given by Eq. (72) with $\Omega = \pm\omega$:

$$R_\pm(\varphi, \tau) = \frac{1}{\sqrt{2\pi D_\varphi \tau}} \exp\left[-\frac{(\varphi \mp \omega\tau)^2}{4 D_\varphi \tau}\right]. \tag{240}$$

As auxiliary functions in the approach of Ref. [230] we need the probability not to perform a step up to time t

$$W(\tau) = 1 - \int_0^\tau w(\tau')\mathrm{d}\tau', \tag{241}$$

which defines the two distributions

$$H_\pm(\varphi, \tau) = R_\pm(\varphi, \tau)W(\tau) \tag{242}$$

corresponding to (239).

The probabilities $Q_\pm$ to rotate over the overall angle φ just having completed a step corresponding to $+$ or $-$ state at time t read

$$Q_\pm(\varphi, t) = \frac{h_\pm(\varphi, t)}{2} + \int_{-\infty}^{\infty} \mathrm{d}\varphi \int_0^t \mathrm{d}t' h_\pm(\varphi - \varphi', t - t') Q_\mp(\varphi', t'). \qquad (243)$$

It follows from the consideration that the temporal stay in one of the states $(+/-)$, ending at time t is either the first stay, with the probability $1/2$ of being in one of the states, or the walker has already made several steps, and entered at time t', to its last $+$ $(-)$-state. The latter ends at time t and since the process is a renewal one, transition depend on the last jump only.

The probabilities $P_\pm$ still to be at φ at time t are

$$P_\pm(\varphi, t) = \frac{H_\mp(\varphi, t)}{2} + \int_{-\infty}^{\infty} \mathrm{d}\varphi' \int_0^t \mathrm{d}t' H_\mp(\varphi - \varphi', t - t') Q_\pm(\varphi', t'). \qquad (244)$$

By adding the probabilities for φ at time t in both states one finally gets the common probability $P(\varphi, t)$ for the angle distribution.

The integrals in Eq. (244) have the form of a convolution in spatial and temporal variables. Such equations transform into algebraic ones in the Fourier-Laplace domain where solutions can be easier found. In [152] the solution was given as

$$\tilde{p}(k, \tilde{s}) = \frac{\tilde{H}_+(k, \tilde{s})\big[1 + \tilde{h}_-(k, \tilde{s})\big] + \tilde{H}_-(k, \tilde{s})\big[1 + \tilde{h}_+(k, \tilde{s})\big]}{2\big[1 - \tilde{h}_-(k, \tilde{s})\tilde{h}_+(k, \tilde{s})\big]}, \qquad (245)$$

where $\tilde{p}(k, \tilde{s})$, $\tilde{p}_\pm(k, \tilde{s})$ assign the Fourier-Laplace transforms of the corresponding probability density function.

The Fourier-Laplace transforms of the densities $h_\pm$ and $H_\pm$ follow from the transformation of a Gaussian and from the shift theorem for the Laplace transform. They can be expressed as

$$\tilde{h}_\pm(k, \tilde{s}) = \tilde{w}(\tilde{s} + D_\varphi k^2 \pm i\omega k), \quad \tilde{H}_\pm(k, \tilde{s}) = \tilde{W}(\tilde{s} + D_\varphi k^2 \pm i\omega k), \qquad (246)$$

with $\tilde{W}(u) = [1 - \tilde{w}(u)]/u$.

As example we consider again that the two states of the random torque $\Omega(t)$ are due to a symmetric and Markovian protocol. In consequence, we take exponential waiting time distribution with rate λ (see Eq. (231)) $w(t) = \lambda \exp(-\lambda t)$. After corresponding Fourier Laplace transforms we obtain

$$\tilde{p}(k, \tilde{s}) = \frac{\tilde{s} + 2\lambda + D_\varphi k^2}{\tilde{s}^2 + [\omega^2 + 2\lambda D_\varphi]k^2 + D_\varphi^2 k^4 + 2\lambda\tilde{s} + 2\tilde{s}D_\varphi k^2}. \qquad (247)$$

It is interesting to underline that this solution from the renewal model solves Eq. (235) in the Fourier-Laplace domain. It will be used in the next paragraph to obtain the effective spatial diffusion coefficient which describes the asymptotic behavior of the particle.

Let us shortly return to the diffusional approximation of the angular dynamics. We let $\tilde{s} \to 0$. The first term of the denominator (quadratic in $\tilde{s}$) can be neglected. Additionally we look at the limit of large overall turning angles taking leading terms in the limit $k \to 0$, only. In this limit one re-obtains angular diffusion with the effective diffusion coefficient defined in Eq. (237). We note that one gets the same result for any waiting time density $w(t)$ if the first moment reads: $\tau = \int_0^\infty \mathrm{d}t' t' w(t') = 1/\lambda$ [152].

Spatial diffusion coefficient under two random rotation

Eventually, we aim to calculate the spatial diffusion coefficient D_{eff} on a plane for the situation with two random rotations and Gaussian angular noise. We apply again the Taylor-Kubo relation [102,307] taking $d = 2$ in Eq. (169). For a motion with constant speed v_0 the correlation function $C_{\mathbf{vv}}$ is governed by the behavior of the angular coordinate only, so that

$$C_{\mathbf{vv}}(t) = v_0^2 \langle \cos[\varphi(t)] \rangle. \tag{248}$$

Here we assumed $\varphi(0) = 0$. The diffusion coefficient reads

$$D_{\text{eff}} = \frac{v_0^2}{2} \int_0^\infty \langle \cos[\varphi(t)] \rangle \, \mathrm{d}t. \tag{249}$$

Let

$$\tilde{P}(k,t) = \left\langle e^{ik\varphi} \right\rangle = \int_{-\infty}^\infty \mathrm{d}\varphi e^{ik\varphi} P(\varphi,t) \tag{250}$$

be the characteristic function of the angular distribution at time t (its temporal Laplace transform gives us $\tilde{p}(k,\tilde{s})$). The mean value in the expression Eq. (249) is then $\langle \cos[\varphi(t)] \rangle = \operatorname{Re} \tilde{P}(1,t)$. Therefore the Laplace transform of the latter expression in its temporal variable yields

$$\int_0^\infty \mathrm{d}t e^{-\tilde{s}t} \langle \cos[\varphi(t)] \rangle = \operatorname{Re} \tilde{p}(1,\tilde{s}). \tag{251}$$

Since in our case the function $\tilde{p}(1,\tilde{s})$ is real, the Re-symbol can be omitted. From comparison of Eq. (251) and Eq. (249), we obtain the diffusion coefficient for the considered particle dynamics. It reads following Eq. (247)

$$D_{\text{eff}} = \frac{1}{2} v_0^2 \tilde{p}(1,0) = \frac{1}{2} v_0^2 \frac{2\lambda + D_\varphi}{\omega^2 + 2\lambda D_\varphi + D_\varphi^2}. \tag{252}$$

Using Eq. (65) we can rewrite the last expression as [152]

$$D_{\text{eff}} = \frac{v_0^4}{2D} \cdot \frac{1}{1 + \frac{\omega^2 v_0^4}{D(D+2\lambda v_0^2)}}. \tag{253}$$

The first factor is the already often cited diffusion coefficient of active Brownian particles [236] which appears, for example, also in Eq. (216). It defines the upper limit in the situation with two random rotations. We see that a directed turning motion decreases the diffusion process since the second multiplicand is always smaller than 1 if $\omega \neq 0$. It is the effect of the bounded motion along the circles and the precision along these curved trajectories which obviously decreases the effective diffusion. The dependence of the diffusion coefficient as function of the noise intensity D is presented in Fig. 39 for several rates of transitions λ between the two angular velocities.

Starting from Eq. (253) this behavior is also found for $\omega = 0$ or in the case of high noise $D \to \infty$. In this situation the second factor becomes unity. As $\lambda \to 0$ the particle will rotate always clockwise or counterclockwise without switching between the two turning directions. Then one obtains

$$D_{\text{eff}} = \frac{v_0^4}{2D} \cdot \frac{1}{1 + \frac{\omega^2 v_0^4}{D^2}}. \tag{254}$$
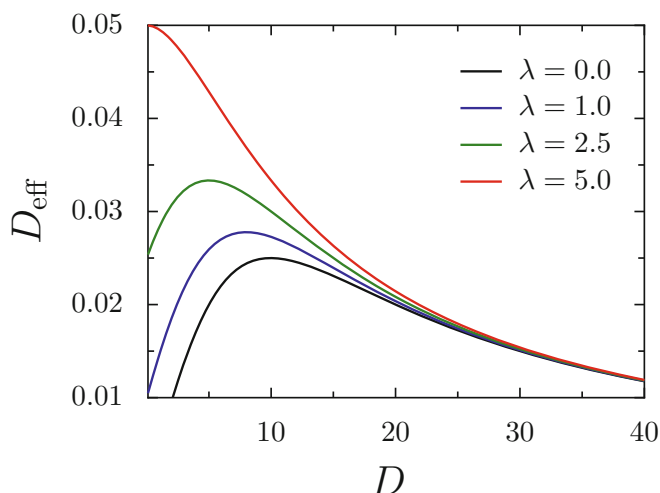
Fig. 39. Diffusion coefficient for active particle with negative and positive angular velocity $\omega = 10$ and $v_0 = 1$ vs. noise intensity D. The upper curve $\lambda = 5$ converges in good agreement with the dependence of D_{eff} for $\lambda \to \infty$. The lower curve corresponds to $\lambda = 0$ but averaged over both values of $\pm\omega$.

This result was previously derived in [307]. The effect of the switchings between the two values of ω decreases the value standing in the denominator of the second factor. Hence the diffusion coefficient decreases if switches between both turning directions are allowed.

Another interesting case is the Gaussian limit of the dichotomous phase velocities. As in the Sect. 4 we suppose the common limit $\lambda \to \infty$ and $\omega^2 \to \infty$ holding thereby fixed their ratio. Then it follows

$$D_{\text{eff}} = \frac{v_0^4}{2(D + \frac{\omega^2 v_0^2}{2\lambda})}. \tag{255}$$

It yields the result of Meinköhn and Mikhailov but with the increased noise intensity $D \to D + \omega^2 v_0^2 / 2\lambda$ coming from the fast switches of the velocity-phase φ.

5 Stochastic dynamics of active particles in confining potentials

In this section, we address the question of active motion in external confinements and analyze the typical trajectories and distribution functions. Throughout this section, we use passive fluctuation independent on the direction of motion.

Rotational motion of biological agents has been observed as a result of an external confinement [137,254,255]. Furthermore, collective rotation is a very common mode of the motion of swarms [252]. Motivated by these observations, in order to imitate the rotational mode, we will therefore consider first a single particle in an external harmonic potential

$$U_{\text{H}}(\mathbf{r}) = \frac{1}{2}\omega^2 \mathbf{r}^2. \tag{256}$$

It is well known that this system possesses a stable solution corresponding to a circular motion with radius $r_0 = v_0/\omega$ [306]. In the absence of noise, the angular momentum $\mathbf{L} = \mathbf{r} \times \mathbf{v}$ is fixed, and the direction of motion depends on the initial conditions.
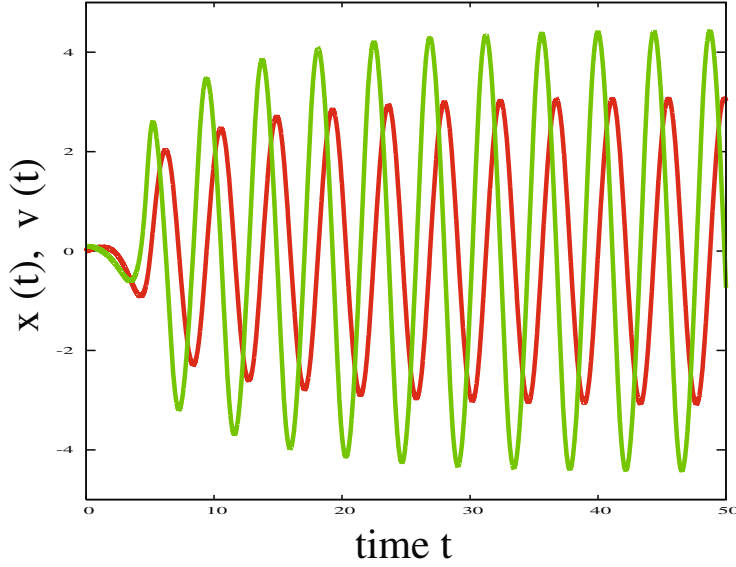
Fig. 40. The coordinate $x(t)$ and the velocity $v(t)$ for limit-cycle oscillations of a 1d driven oscillatory systems. The active particle is driven by a Rayleigh friction force. Parameters: $q = 1, d = 0.8, c = 0.1, \gamma_0 = 0.1$.

A constant force will break the isotropy of the problem. In a large system, or infinite space, the presence of dissipation will create a situation with a constant velocity and we can cross to a co-moving frame.

A more interesting situation is obtained for potentials which create a confinement. New dynamical solutions are then limit cycles in the phase space. In the following, we will restrict mainly to the discussion of the Rayleigh-Helmholtz friction. Then the problem of active Brownian motion in external attracting potentials transforms into the study of (higher dimensional) van-der-Pol oscillators with noise.

5.1 Basic solutions for the active motion in harmonic potentials

Let us first study the active motion of a 1d driven oscillator without noise, which for the Rayleigh model is described by [9]

$$\frac{\mathrm{d}x}{\mathrm{d}t} = v, \qquad \frac{\mathrm{d}v}{\mathrm{d}t} + \omega_0^2 x = v(\alpha - \beta v^2), \tag{257}$$

where $v_0^2 = \alpha/\beta$ defines the stationary velocity. Figure 40 shows the results obtained from integration of (257). The systems exhibits self-excited oscillations, so-called limit cycles - as discussed already by Rayleigh in 1894 [284]. An approximative solution for small driving (small values of α) [9] reads

$$x(t) = r_0 \sin(\omega_0 t + \Phi), \qquad v(t) = v_0 \cos(\omega_0 t + \Phi), \tag{258}$$

where the amplitude of the oscillations is $r_0 = v_0/\omega_0$. This approximate solution is valid for all active friction functions which have one zero at v_0. Any initial condition in the x, v space converges to the circle

$$H(x, v) = \frac{1}{2}v^2 + \frac{1}{2}\omega_0^2 x^2 = v_0^2. \tag{259}$$

This circle is an attracting limit cycle of our system [9]. In a next step we will study two-dimensional oscillators. We specify the potential $U(\mathbf{r})$ as a symmetric harmonic potential in two dimensions:

$$U(x_1, x_2) = \frac{1}{2}\omega_0^2 (x_1^2 + x_2^2). \tag{260}$$

First, we restrict the discussion to the deterministic case, which then is described by four coupled first-order differential equations:

$$\begin{aligned} \dot{x}_1 = v_1, \quad & \dot{v}_1 = -\gamma(v_1, v_2)v_1 - \omega_0^2 x_1 \\ \dot{x}_2 = v_2, \quad & \dot{v}_2 = -\gamma(v_1, v_2)v_2 - \omega_0^2 x_2. \end{aligned} \tag{261}$$

In the 2d case the energy pump of the r.h.s. of the velocity equation (257) is generalized to

$$\gamma(v_1, v_2) = -\alpha + \beta(v_1^2 + v_2^2). \tag{262}$$

We can show by simulation and theoretical considerations that two limit cycles in the four-dimensional phase space are created [121]. The projections of both these periodic motions to the $\{v_1, v_2\}$ plane is the circle

$$v_1^2 + v_2^2 = v_0^2 = \frac{\alpha}{\beta} = \text{const.} \tag{263}$$

The projection to the $\{x_1, x_2\}$ plane also corresponds to a circle

$$x_1^2 + x_2^2 = r_0^2 = \text{const.} \tag{264}$$

Due to the condition of equilibrium between centripetal and centrifugal forces on the limit cycle we have

$$\frac{v_0^2}{r_0} = r_0 \omega_0^2. \tag{265}$$

Therefore the radius of the limit cycle is given by

$$r_0 = \frac{v_0}{\omega_0}. \tag{266}$$

From equation (265) follows

$$\frac{1}{2}v_0^2 = \frac{\omega_0^2}{2}r_0^2. \tag{267}$$

This means we have equal distribution of potential and kinetic energy on the limit cycle [106]. As for the harmonic oscillator in 1-d, both parts of energy contribute the same amount to the total energy. Therefore the energy of motions on the limit cycle, which is asymptotically reached, is twice the kinetic energy

$$H \longrightarrow H_0 = v_0^2. \tag{268}$$

The energy is a slow (adiabatic) variable which allows a phase average with respect to the phases of the rotation [121].

Two exact stationary solutions can be easily found. The first cycle in the four-dimensional phase space reads with arbitrary initial phase Φ:

$$x_1 = r_0 \cos(\omega_0 t + \Phi) \qquad v_1 = -r_0 \omega \sin(\omega_0 t + \Phi)$$

$$x_2 = r_0 \sin(\omega_0 t + \Phi) \qquad v_2 = r_0 \omega \cos(\omega_0 t + \Phi).$$
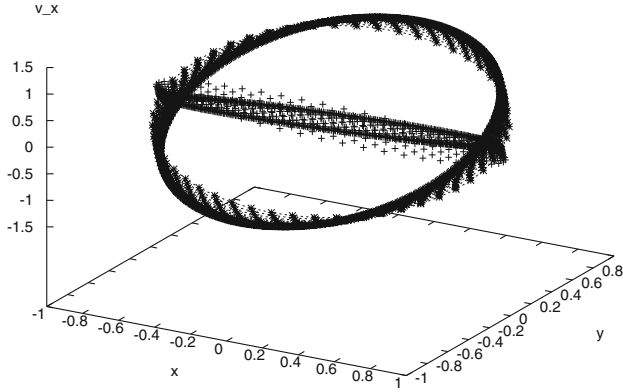
Fig. 41. Stroboscopic plot of the 2 limit cycles for driven Brownian motion. We show projections of solutions for $v_0 = 1$ to the subspace $\{x_1, x_2, v_1\}$.

This means, the particle rotates even for strong pumping with the frequency given by the linear oscillator frequency ω_0. One can check that this is indeed an exact solution of the dynamic equations. The trajectory defined by the four equations looks like a hoop in the four-dimensional phase space. Most projections to the two-dimensional subspaces are circles or ellipses however there are to subspaces namely $\{x_1, v_2\}$ and $\{x_2, v_1\}$ where the projection is like a rod.

The second limit cycle is obtained by inversion of the motion, i.e. $t \to -t, v_1(0) \to -v_1(0), v_2(0) \to -v_2(0), \omega_0 \to -\omega_0$ which yields

$$x_1 = r_0 \cos(\omega_0 t - \Phi) \qquad v_1 = -r_0 \omega \sin(\omega_0 t - \Phi)$$

$$x_2 = -r_0 \sin(\omega_0 t - \Phi) \qquad v_2 = -r_0 \omega \cos(\omega_0 t - \Phi).$$

This second cycle forms also a ring in the four-dimensional phase space which is different from the first one. However, both limit cycles have the same projections to the $\{x_1, x_2\}$ and to the $\{v_1, v_2\}$ plane. The projection to the $x_1 - x_2-$ plane has the opposite direction of rotation in comparison with the first limit cycle. The projections of the two rings on the $\{x_1, x_2\}$ plane or on the $\{v_1, v_2\}$ plane are circles (Fig. 41). The ring-like distribution intersect perpendicular the $\{x_1, v_2\}$ plane and the $\{x_2, v_1\}$ plane (see Fig. 41). The projections to these planes are rod-like and the intersection manifold with these planes consists of two ellipses located in the diagonals of the planes (see Fig. 41).

The main effect of noise is the spreading of the deterministic attractors. Thus, in the presence of noise, the two ring-like embracing limit cycles are converted into two crossing toroids with cross-sections increasing with increasing noise intensity (see Fig. 44).

We already examined that in the case of dimension $d = 2$ a very useful representation is obtained in polar coordinates [306]. Following Eq. (15) and with

$$x = r(t) \cos(\psi(t)), \quad y = r(t) \sin(\psi(t)), \tag{269}$$

we introduce polar coordinates $r(t), \psi(t), s(t), \varphi(t)$ in the four-dimensional phase space $(\mathbf{r}, \mathbf{v})$ for the case of active motion. In polar coordinates the equations of

motion read

$$\dot{r} = v\cos\theta, \quad \dot{s} = -\gamma(s)s - \omega r\cos\theta,$$

$$\dot{\theta} = \left(\frac{\omega_0^2 r}{s} - \frac{s}{r}\right)\sin\theta, \quad \dot{\psi} = \frac{s}{r}\sin\theta, \tag{270}$$

with $\theta(t) = \varphi - \psi$.

The stationary solutions (Eqs. 269, 269) can be easily found. The difference of the two angles θ approaches two values, $\theta = \pm\pi/2$. These two solution resemble the two limit cycles with $v_0 = \alpha/\beta$, $r_0 = v_0\omega_0$ and two stationary rotations (clockwise and counter clockwise) with stationary angular velocity $\dot{\psi} = \dot{\varphi} = \pm\omega_0$. The particle rotates even at strong pumping with the frequency given by the linear oscillator frequency ω_0.

In order to construct solutions for stochastic motions, we need beside $H = v_0^2$ other appropriate invariants of motion. Looking at the first solution (269) we see, that the following relation is valid

$$v_1 + \omega_0 x_2 = 0; \qquad v_2 - \omega_0 x_1 = 0. \tag{271}$$

In order to characterize the first limit cycle, we introduce the invariant

$$J_+ = H - \omega_0 L = \frac{1}{2}(v_1 + \omega_0 x_2)^2 + \frac{1}{2}(v_2 - \omega_0 x_1)^2. \tag{272}$$

where we have introduced the angular momentum $L = (x_1 v_2 - x_2 v_1)$. We see immediately that $J_+ = 0$ holds on the first limit cycle which corresponds to positive angular momentum. In order to characterize the second limit cycle from equation (269) we use the invariant

$$J_- = H + \omega_0 L = \frac{1}{2}(v_1 - \omega_0 x_2)^2 + \frac{1}{2}(v_2 + \omega_0 x_1)^2. \tag{273}$$

We see that on the second limit cycle, which corresponds to negative angular momentum, holds $J_- = 0$.

5.2 Rotational motors and efficiency

A two dimensional system in a rotational mode may be considered as a simple model of a rotating motor. We consider again the 2d oscillatory system (261) this time for the general case of a friction function having one zero $\gamma(v_0) = 0$. As shown above we are able to find even an exact solution for the limit cycle oscillations (269) for the Rayleigh-Helmholtz case. The solution (269) represents a (mathematically) positive rotation. The motion of the particle on the orbit in distance r_0 from the center proceeds with velocity v_0 and runs in time t over a path of length

$$l(t) = v_0 t + l(0) \tag{274}$$

on the orbit. On this path the motor is doing work against the friction γ_0.

Generating rotations is connected with angular momentum $\mathbf{L} = \mathbf{r} \times \mathbf{v}$ which satisfies the equation of motion

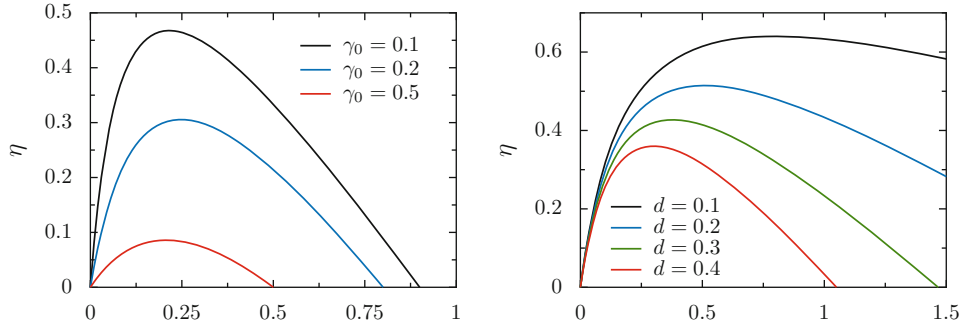$$\frac{d\mathbf{L}}{dt} = -\gamma(\mathbf{v})\mathbf{L}. \tag{275}$$

Fig. 42. Left: dependence of the power of the "motor" on the external friction Γ generated by the load force for three different values of the internal motor friction γ_0 and fixed the other parameters $c = 0.5, d = 0.5, q = 1$. Right: dependence of the power of the "motor" on the external friction Γ generated by the load force for four values of the conversion parameter d of the internal motor parameters (other parameters: $\gamma_0 = 0.2$, $c = 0.5$, $q_0 = 1.0$). We note that the efficiency decreases with increasing parameters d.

In the 2d-case the self-generated angular momentum of the stationary solution is $L = r_0 v_0$.

Let us assume some torque M_{ex} acting in opposite direction. In this case, the "motor" has to perform some additional work. For simplicity, we assume that there is some opposite force acting along the circumference of the circle with $M_{ex} = r_0 F_{ex}$. We assume this force, as some additional friction $F_{ex} = -\Gamma v_{lc}$ acting in the direction opposite to the direction of (rotational) motion. We define $v_{lc} \leq v_0$ as the velocity of the motion along the limit cycle, with $v_{lc} = v_0$ for the unperturbed limit cycle.

Let us consider the depot model (see Sect. 3.2.4). The velocity along the limit cycle without the additional torque reads

$$v_0^2 = \frac{q_0}{\gamma_0} - \frac{d_0}{c}. \tag{276}$$

If we take the additional load into account the velocity along the limit cycle changes to

$$v_{lc}^2 = \frac{q_0}{(\gamma_0 + \Gamma)} - \frac{d_0}{c}. \tag{277}$$

The power associated with the additional work is $P = F_{ex} v_{lc}$ and we define the efficiency as the relation of the generated power P to the flow of energy into the system q_0:

$$\eta = \frac{P}{q_0} = \frac{F_{ex} v_{lc}}{q_0} = \frac{\Gamma v_{lc}^2}{q_0} = \Gamma \left[\frac{1}{\gamma_0 + \Gamma} - \frac{d}{cq_0} \right] \tag{278}$$

for $F_{ex} v_{lc} \geq 0$. The corresponding dependence on the external additional friction Γ is represented in left Fig. 42. For a clear understanding we should emphasize that γ_0 is an always present internal friction, while Γ is connected with the external load and therefore connected with the work performed against the external force. The dependence of the power of the motor on the external friction for different motor parameters is represented in the right panel of Fig. 42. Depending on the internal motor parameters, we observe typically a curve with a maximum at a finite load corresponding to maximal efficiency, which in our examples is around – or less

than – 50 percent and is achieved for

$$\Gamma_{max} = (cq_0/d) - \gamma_0. \tag{279}$$

After the maximum the efficiency decreases with increasing Γ. Above a maximal value of external friction, corresponding to vanishing velocity along the limit cycle $v_{lc} = 0$, the motor stops to work and the efficiency becomes formally negative. The curves for the efficiency of rotational motors shown above may give us some idea about the efficiency of biological motors responsible for the mobility of animals, whereby the simple model model discussed here reproduces the generic behavior expected to hold for all biological motor systems. We mention in particular the measurements and discussions of the efficiency of the kinesin motor [158,378,379].

5.3 Stochastic motion in a harmonic external potential

Since the main effect of noise is the spreading of the deterministic attractors, we may expect that the two hoop-like limit cycles are converted into a distribution looking like two embracing hoops with finite size, which for strong noise converts into two embracing tires in the four-dimensional phase space. In order to get the explicit form of the distribution, we may introduce different variables, like the amplitude and phase description as used in the previous sections. Here, we introduce the energy and angular momentum as variables and derive reduced densities. We remember that throughout the Stratonovich calculus is used [9].

On the basis of the amplitude and phase representation (polar coordinates) (15) and (269), we get for the Hamiltonian

$$H(t) = \frac{1}{2}s(t)^2 + \frac{1}{2}\omega_0^2 r(t)^2. \tag{280}$$

The angular momentum is given as

$$L(t) = (x_1 v_2 - x_2 v_1) = s(t)r(t)\cos(\theta). \tag{281}$$

Values corresponding to the two limit cycles are

$$L = +L_0; \qquad L = -L_0; \qquad L_0 = v_0^2/\omega_0, \tag{282}$$

with $v_0^2 = \alpha/\beta$. Both limit cycles are located on the sphere with $H(t) = v_0^2$.

Considering harmonic oscillators and using equipartition of potential and kinetic energy (see equation (268)) we find for motions on the limit cycle $s^2(t) = H(t)$. Assuming that $s^2 \simeq H$ holds also near to the limit cycle, the dynamic system with the pump (262) is converted to a canonical dissipative system with

$$\gamma(s^2) \simeq \gamma(H) = \gamma_H(H). \tag{283}$$

This way we come for the Rayleigh-model to the energy balance

$$\frac{\mathrm{d}}{\mathrm{d}t}H = -\gamma_H(H)\,H + \sqrt{2D_H H}\xi_H(t) \tag{284}$$

where $\xi_H(t) = \xi_1(t)\cos(\phi) + \xi_2(t)\sin(\phi)$ is again Gaussian white noise and $D_H = D$. This corresponds to the Fokker-Planck equation in energy representation

$$\frac{\partial}{\partial t}P(H,t) = \frac{\partial}{\partial H}\left[(\gamma_H(H)\,H - D_H)\,P + D_H\,\frac{\partial}{\partial H}\,H\,P\right], \tag{285}$$

with the stationary solution

$$P_0(H) = \mathcal{N} \exp\left[-\frac{1}{D_H} \int \gamma_H(H) \mathrm{d}H\right]. \tag{286}$$

The most probable value of the energy is the energy on the limit cycle. In case of the Rayleigh model it is

$$\tilde{H} = H_0 = \frac{\alpha}{\beta} = v_0^2. \tag{287}$$

The stationary distribution can be given in compact form ($H \geq 0$)

$$P_0(H) = \mathcal{N} \exp\left[-\frac{\beta}{2D}(H - H_0)^2\right], \tag{288}$$

which is a Gaussian at positive energies.

This probability is in fact distributed on the surface of the four-dimensional sphere. By using equation (280) we get for the Rayleigh-model of pumping in our approximation the following distribution of the coordinate with $r^2 = x_1^2 + x_2^2$

$$P_0(x_1, x_2) \simeq \exp\left[\frac{\alpha \omega_0^2}{D} r^2 \left(1 - \frac{r^2}{2r_0^2}\right)\right]. \tag{289}$$

We see in figure 43 that the probability crater is located above the trajectory obtained from simulations of an Active Brownian particle. This way the maximal probability corresponds indeed to the deterministic limit cycle.

So far we represented only a projection on the $\{x_1, x_2\}$ plane. The full probability distribution in the four-dimensional phase space is not constant on the four-dimensional sphere $H = v_0^2$ as suggested by equation (286) but should be concentrated around the limit cycles which are closed curves on the four-dimensional sphere $H = v_0^2$. This means, only a subspace of this sphere is filled with probability. The correct stationary probability has the form of two noisy distributions in the four-dimensional phase space, which look like hula hoops. This characteristic form of the distributions was confirmed also by simulations (see Figs. 44, 45 and [121]). The projections of the distribution to the $\{x_1, x_2\}$ plane and to the $\{v_1, v_2\}$ plane are noisy tori in the four-dimensional phase space. The hula hoop distribution intersects perpendicular the $\{x_1, v_2\}$ plane and the $\{x_2, v_1\}$ plane. The projections to these planes are rod-like and the intersection manifold with these planes consists of two ellipses located in the diagonals of the planes.

In order to refine the description, we derive the distribution of the angular momenta. We start from the Langevin equation

$$\frac{\mathrm{d}}{\mathrm{d}t} L = -\gamma\left(s^2\right) L + \sqrt{2D}r\, \xi_L(t), \tag{290}$$

with $\xi_L(t) = \xi_y(t)\cos(\phi) - \xi_x(t)\sin(\phi)$ being Gaussian white noise. On the limit cycles it holds

$$L(t) = \pm r(t)s(t), \quad s(t) = \omega_0\, r(t), \tag{291}$$

with different signs for the two possible rotation directions. To find a closed description, we assume that the Eq. (291) holds and replace

$$r(t) = \sqrt{\frac{L(t)}{\omega_0}}, \quad s^2(t) = L(t)\,\omega_0, \quad \gamma\left(s^2\right) = \gamma\left(L\omega_0\right) = \gamma_L(L), \tag{292}$$
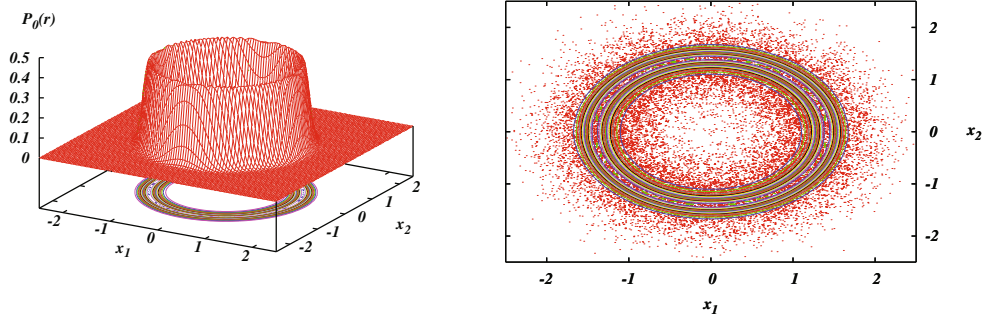
Fig. 43. Probability density for the Rayleigh-model represented over the $\{x_1, x_2\}$ plane. (a) The probability density (289). (b) Contour plot of $P_0(r)$ superimposed with data points out of simulations of the Active Brownian dynamics. Parameters: $\alpha = 2$, $D = 0.1$ and $\omega_0 = 1$.

where we have used the positive sign and hence $L > 0$. It follows

$$\frac{\mathrm{d}}{\mathrm{d}t}L = -\gamma_L(L)\,L + \sqrt{2D_L L}\,\xi_L(t) \tag{293}$$

with

$$D_L = \frac{D}{\omega_0}. \tag{294}$$

The corresponding Fokker-Planck equation is similar to the energy representation

$$\frac{\partial}{\partial t}P(L,t) = \frac{\partial}{\partial L}\left[(\gamma_L(L)\,L - D_L)\,P + D_L\,\frac{\partial}{\partial L}\,L\,P\right]. \tag{295}$$

Obviously its stationary solution reads

$$P_0(L) = \mathcal{N}\exp\left[-\frac{1}{D_L}\int \gamma_L(L)\mathrm{d}L\right], \tag{296}$$

and eventually after introducing the most probable angular momentum $L_0 = r_0 v_0 = H_0/\omega_0$ at the limit cycle the stationary solution becomes ($L > 0$)

$$P_0(L) = \mathcal{N}\exp\left[-\frac{\beta\omega_0^2}{2D}(L - L_0)^2\right]. \tag{297}$$

A corresponding solution can be found for the second cycle by replacing $L_0 \to -L_0$ for momenta with $L < 0$. Due to symmetry both values are provided with same probability one may expect a linear superposition of the two solutions

$$P_0(L) = \mathcal{N}\left(\exp\left[-\frac{\beta\omega_0^2}{2D}(L - L_0)^2\right] + \exp\left[-\frac{\beta\omega_0^2}{2D}(L + L_0)^2\right]\right). \tag{298}$$

The given method does not provide a complete solution in the four-dimensional phase space, but gives us a good idea about the projections on different planes. In order to find a distribution in the four-dimensional phase space, we combine the previously found distributions and introduce the invariants J_+, J_- which leads to the following ansatz:

$$P_0(x_1, x_2, v_1, v_2) = \mathcal{N}\exp\left[-\frac{\beta}{2D}(H - H_0)^2\right]$$
$$\times \left(\exp\left[-\frac{\beta}{2D}J_+^2\right] + \exp\left[-\frac{\beta}{2D}J_-^2\right]\right). \tag{299}$$

We may convince ourselves that this formula agrees with all projections derived above. Furthermore, it is in agreement with the general ansatz derived in earlier work from information theory [102,107]. Since our new expression for the stationary distribution does not contain any parameter characterizing the concrete potential it may be applied to arbitrary radially symmetric potentials, in particular we may use it for describing the stationary distributions for a Coulomb confinement.

5.4 Dynamics in symmetric anharmonic potentials

Here, we will discuss briefly several extensions of the theory developed in the previous section following [306]. At first, we will discuss the case of anharmonic potentials. For the general case of radially symmetric but anharmonic potentials $U(r)$, the equal distribution between potential and kinetic energy $v_0^2 = ar_0^2$, which leads to $\omega_0 = v_0/r_0 = \omega$, is no more valid. It has to be replaced by the more general condition that on the limit cycle the attracting radial forces are in equilibrium with the centrifugal forces. This condition leads to $\frac{v_0^2}{r_0} = |U'(r_0)|$. Then, if v_0 is given, the equilibrium radius may be found from the relation

$$v_0^2 = r_0\,|U'(r_0)|. \tag{300}$$

The frequency of the limit cycle oscillations follows as

$$\omega_0^2 = \frac{v_0^2}{r_0^2} = \frac{|U'(r_0)|}{r_0}. \tag{301}$$

For example, for the case of quartic oscillators with potential $U(r) = kr^4/4$ we get the limit cycle frequency

$$\omega_0 = \frac{k^{1/4}}{v_0^{1/2}}. \tag{302}$$

Alternatively for attracting Coulomb forces $U(r) = -Ze^2/r$ the stable radius reads and the limit cycle frequency, respectively,

$$r_0 = \frac{Ze^2}{v_0^2}, \quad \omega_0 = \frac{v_0^3}{Ze^2}. \tag{303}$$

Integrals of motions follow

$$H_0 = -\frac{1}{2}\,v_0^2; \qquad L_0 = \pm\frac{Ze^2}{v_0}. \tag{304}$$

We note that this expression diverges for $v_0 \to 0$ (similarly as in quantum theory the Bohr radius diverges for $h \to 0$).

If the equation (300) has several solutions, the dynamics might be much more complicated, e.g. we could find Kepler-like orbits oscillating between the solutions for r_0. In other words, we may find then beside driven rotations also driven oscillations between the multiple solutions of equation (300).

An interesting application of the theoretical results given above, is the following: Let us imagine a system of Brownian particles which are pairwise bound by a Lennard-Jones-like potential $U(r_1 - r_2)$ to dumb-bell-like configurations. Then the motion consists of two independent parts: The free motion of the center of mass, and the relative motion under the influence of the potential. The motion of the center of mass is described by the equations given in the previous section and relative motion is

described by the equations given in this section. As a consequence, the center of mass of the dumb-bell will make a driven Brownian motion but in addition the dumb-bells are driven to rotate around there center of mass. What we observe then is a system of pumped Brownian molecules which show driven translations with respect to their center of mass. On the other side the internal degrees of freedom are also excited and we observe driven rotations and in general (if Eq. (300) has several solutions) also driven oscillations. In this way we have shown that the mechanisms described here may be used also to excite the internal degrees of freedom of Brownian molecules.

5.5 Dynamics in asymmetric potentials

We will study now potential landscapes without radial symmetry and follow [117]. Problems which might be studied with these models are, for example, the synchronization between the oscillations along both axis, the existence of Arnold tongues etc. [118]. In the simplest case, we may assume that the potential is harmonic along the two axes but stretched in an asymmetric way with different elasticity constants

$$U(x,y) = \frac{1}{2}\omega_1^2 x^2 + \frac{1}{2}\omega_2^2 y^2, \tag{305}$$

denoted by $\omega_1 \neq \omega_2$. In order to give some idea about the influence of asymmetry between the modes, let us first present the result of simulations for 1000 independent active particles with the depot pump (see Sect. 3.1.3). The distribution of these particles in the phase space shows us where the probability distributions are expected to have their maxima (see Fig. 44).

We also study here a specific case of a simple relation of the frequencies $\omega_2 = 2\omega_1$. The solution of the Hamiltonian problem (e.g. no dissipation) is given by

$$\begin{aligned} x_1 &= r_1 \cos(\omega_1 t - \Phi) & v_1 &= -r_1\omega_1 \sin(\omega_1 t - \Phi), \\ x_2 &= r_2 \sin(2\omega_1 t - \Phi) & v_2 &= 2r_2\omega_1 \cos(2\omega_1 t - \Phi), \end{aligned} \tag{306}$$

where the amplitudes $r_{1,2}$ are determined by the initial conditions. In the case of active particles, $\delta = \zeta + 1 > 0$ (see Eq. 56), the dissipative forces drive the trajectories to an attractor which corresponds to $v_1^2 + v_2^2 \to v_0^2$. In a good approximation, the attractor is determined by the amplitudes

$$r_1 = \frac{v_0}{\omega_1}; \qquad r_2 = \frac{v_0}{\omega_2}. \tag{307}$$

We see that the smaller amplitude has approximately half the value of the bigger amplitude. This way, we have obtained a limit cycle shaping like a Lissajous oscillation in the form of an "8"; a second limit cycle can be found by inversion of the trajectory. The result of a stochastic simulation is shown in Fig. 44(d). We see here the projections of two stochastic trajectories (limit cycles); the projections having the form of an "8". In the case of irrational relations ω_2/ω_1, as well as for the case of nonlinear couplings between the modes, we find more complicated attractors [118]. In order to get analytical expressions for the distributions, we may introduce amplitude–phase representations [121].

5.6 Transitions bistable potentials

Let us now have a look at bistable situation in a two-dimensional landscape following [104]. In order to investigate the Kramers problem of transitions between two wells,
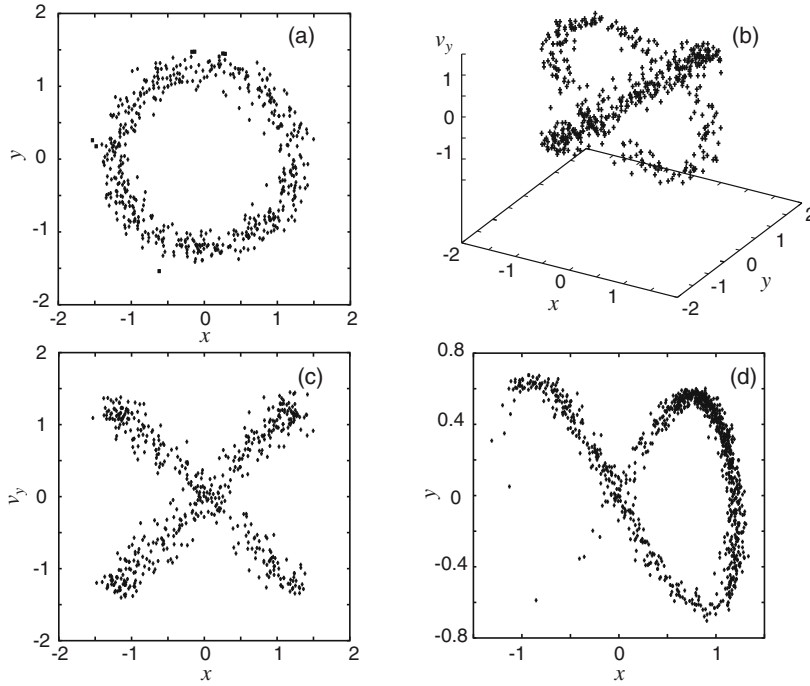
Fig. 44. Distributions according to simulations of 1000 active Brownian particles with depot pump (Sect. 3.1.3) on limit cycles in symmetric (a-c) and asymmetric (d) parabolic potentials. (a) We show projections of simulations on the $x - y-$plane. Parameters: $\zeta = 1.5, \gamma_0 = 1, D = 0.01$: (a) 2D projections on the subspace $\{x_1, x_2\}$, (b) 3D projections on the subspace $\{x_1, x_2, v_2\}$, (c) 2D projections on the subspace $\{x_1, v_2\}$, (d) 2D projections on the subspace $\{x_1, x_2\}$ for $\omega_2 = 2\omega_1$ [118].

we introduce a simple model potential with two potential minima placed on the line $x = y$. The potential is defined by

$$U(x,y) = a \left(\frac{1}{4} z^4 - \frac{1}{2} z^2 - cz \right) + \frac{1}{2}\omega^2(x - y)^2. \tag{308}$$

Here, we introduced $z = (x + y)/2$ being the reaction path, i.e. the co-ordinate along the line connecting the minima with the lowest barrier value between both. The parameter c determines the asymmetry of the wells and a determines the height of the well which is for $(c = 0)$ given by $\Delta U = a/4$. The shape of the potential is presented in Fig. 45. In the case of small excitation energy $v_0^2/2 \ll \Delta U$, and weak noise, the dynamics in each well is similar to the parabolic case. In other words, we may observe two limit cycles in each of the two wells. With increasing noise, transitions between the two wells become possible. For standard Brownian motion this is a well-studied problem [157].

Here we present numerical simulation of 10000 active particles with depot pump of energy (see Fig. 3) and provide estimates of the transition rates (Fig. 45). Initially, particles were put at $z = Z_0$ in the left potential well. In Fig. 45(b,c) the temporal evolutions of the position of the center of mass $Z(t)$ and the fraction of particle in the left well, $p(t) = n_l(t)/N$ are shown, n_l is the number of particles in the left well and $N = 10000$ is the total number of particles. As can be seen from the figure, the
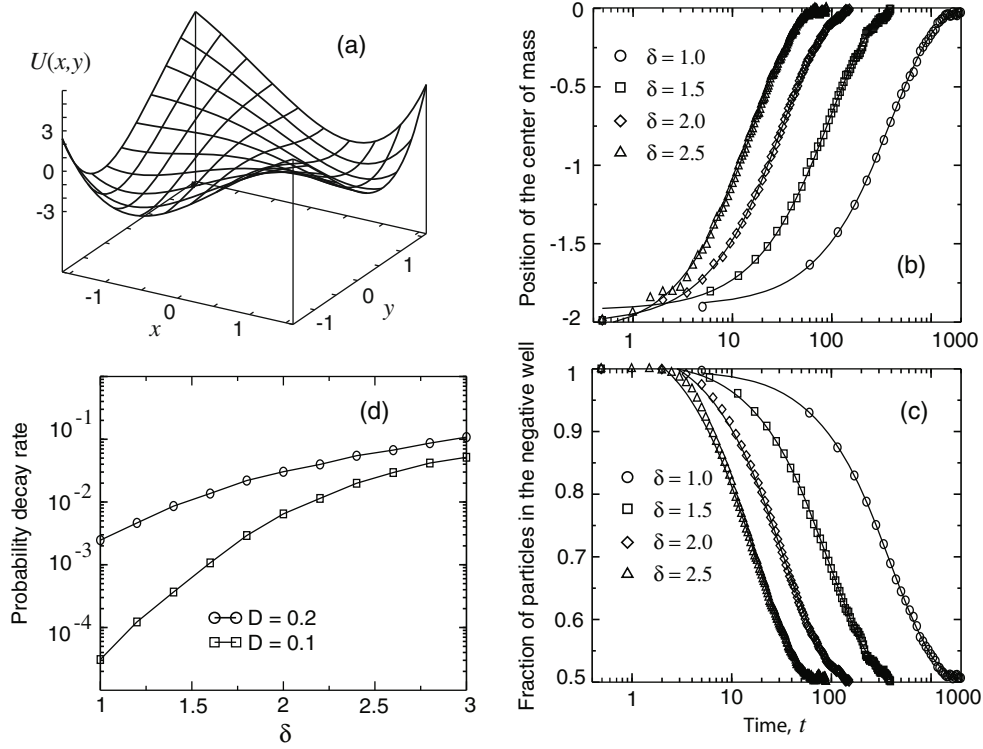
Fig. 45. Active Brownian particles in a bistable potential in 2 dimensions. (a) The shape of the potential for $\Delta U = 1 : a = 4, c = 0$, the minima are located along the diagonal. (b) The position of the center of mass of 10000 particles initially located in the left well under the influence of noise $D = 0.1$ as a function of time, for indicated values of driving parameter δ. The transitions are enhanced for larger driving. (c) The fraction of particles staying in the left well for $D = 0.1$. (d) The decay rates of the probability to stay in the left well for the noise strength for $D = 0.1$ and for $D = 0.2$. On (b) and (c) symbols shows numerical values, while the solid lines are exponential least-square fits due to Eqs. (309). Other parameters (see Fig. 3): $\gamma_0 = 1; v_d = 1$ [104].

time courses can be fitted with exponential laws:

$$Z(t) = Z_0 \exp\left(-\frac{t}{\tau}\right), \qquad p(t) = \frac{1}{2}\left[1 + \exp\left(-\frac{t}{\tau}\right)\right], \tag{309}$$

where τ is the characteristic transition time. The transition rate $1/\tau$ is shown in Fig. 45(d) as a function of $\delta = v_0^{2+1}$. A rough estimate of the transition time is

$$\tau \propto \exp\left[\frac{\Delta U - (1/2)v_0^2}{D}\right], \tag{310}$$

where $v_0^2 = (\delta - 1)$ for our model. Thus, with the increase of δ the potential barrier is effectively lowered, providing higher transition rates which agree with the result for the one-dimensional case [276].

In other words, the effect of active driving (in comparison to the passive case) may be estimated by

$$\frac{\tau_{act}}{\tau_{pas}} \propto \exp\left[-\frac{v_0^2}{2D}\right]. \tag{311}$$

Due to the nearly exponential dependence on $(\delta - 1)$ the increase of the rate with the driving strength may be rather large. We have to note, however, that the exponential "ansatz" yield just a rough estimate for moderate pumping $1 < \delta < 2$. For $\delta > 2$ we observe in Fig. 45(d) already a tendency to saturation (the particles freely penetrate the barrier) and for $\delta < 1$ (transition to the passive case) we observe a more sensitive dependence on the parameter δ.

6 Collective motion and swarming

We apply in this section the model of active Brownian dynamics to describe the collective motion in active matter systems, such as e.g. swarms of animals.

At first, we will characterize the fundamental modes of collective motion of swarms with cohesion using a quite simple model based on the idea of global coupling of the individuals in the swarm. Global coupling is not based on realistic physical interactions however it demonstrates already the most important features of "swarms". We use here the general notation of "swarms" for confined systems or clusters of particles which can perform collective motion far from equilibrium.

After the discussion on modes of collective motion induced by global coupling, we will turn to the important class of models of collective motion due to local, short-range velocity alignment between active particles. We will start with a description of active Brownian particles with nonlinear friction and velocity alignment. Further on, we proceed with the discussion of a widely used class of self-propelled particles, which correspond to limit of vanishing speed fluctuation. In this context we will focus on different interaction symmetries. Starting from the classical Vicsek model of active polar particles with polar interactions, we discuss a general classification of models that includes not only so-called active nematics, but also a second important class of models of active polar with apolar interactions. Throughout this second subsection, we will focus on the onset of collective order for increasing density or decreasing noise in various models.

Finally, in the end of this section, we will introduce alternative mechanisms for swarming and collective motion based on escape and pursuit response or chemotactic behavior of individuals.

6.1 Dynamics of swarms

6.1.1 Modes of collective motion with cohesion: translation and rotation

The model of global coupling is the most simple dynamical model of collectively moving swarms of animals. Global coupling is not based on realistic physical interactions however it demonstrates already the most important features of "swarms".

Probably the first mathematical model of swarms based on individual particles (or agents) was introduced by Suzuki and Sakai in 1973 ([339]; see also [252]). Since then, different models of swarming of animals, many of them motivated by fish schools, have been the subject of biological and ecological investigations (see e.g. [10, 41, 71, 72, 172, 252]). Here we would like to highlight the pioneering paper on swarm dynamics by Hiro-Sato Niwa published in 1994 [250]. Niwa, not only introduced a nonlinear

friction function in his model, but he is probably the first one who analyzed the stability of the different modes of swarming motion from the point of view of statistical physics. Despite the numerous biologically motivated studies, swarming dynamics is still a rather young field of physical studies. Some recent developments have been covered, for example, by Helbing [159], who discusses traffic and related self-driven many-particle systems and the comprehensive books by Vicsek [360], Mikhailov and Calenbuhr [235], and Schweitzer [311].

Based on the simulation studies of the first swarming models [339], a classification of different modes of swarming motion was performed, which can be also observed in nature (see Okubo and Levin [252]). According to these authors, three general modes of motion can be identified:

1. translational motions,
2. rotational excitations and
3. amoeba-like motions.

It is beyond the focus of this review to discuss all the swarming models, which were developed in order to account for the rich variety of observations. Instead, we will study in the following the collective modes and the distribution functions of simple models. We start here with consideration of finite systems of particles confined by global coupling which are self-propelled by active friction and parallelized by small velocity-dependent interactions. This kind of description may be considered as a simple and to large extent analytically tractable approximation of the collective dynamics of biological agents [99,105,107,116,119,237,313]. More complex models, which incorporate for example local interactions, are discussed in the forthcoming sections as well as in other publications (see e.g. Refs. [74,360–362]).

We will show here that the collective motion of swarms (large clusters) of driven Brownian particles resemble very much the typical modes of motion in swarms of living entities. The self-propulsion of the particles is modeled by active friction as introduced in Sect. 3.1.2. The analysis is restricted to two dimensional models ($d = 2$). The internal driving of the system by negative friction yields a dynamical behavior far-from equilibrium. Earlier studies have shown that such active interacting systems may have many attractors and that noise may lead to transitions between the deterministic attractors [237,313].

6.1.2 General model of swarms

We proceed with an analysis of the structure of the equations of motion of a swarm. We will characterize the motion by its attractors in the phase space and again by the stationary distribution if noise is included. First we start with the two dimensional problem and harmonic interactions. In the next section, we extend our focus to three spatial dimensions and to interaction with Morse potentials.

We consider a system on N active particles at positions $(\mathbf{r}_1(t), \ldots, \mathbf{r}_N(t))$ which are moving with velocities $\mathbf{v}_1(t), \ldots, \mathbf{v}_N(t)$. Let the particles be point-like with the mass $m = 1$. Since motion is created by forces we postulate the equations of motion for the individuals within the swarm to be given by the N (stochastic) Newtonian equations

$$\frac{\mathrm{d}}{\mathrm{d}t}\mathbf{r}_i = \mathbf{v}_i, \tag{312}$$

$$\frac{\mathrm{d}}{\mathrm{d}t}\mathbf{v}_i = -\gamma(\mathbf{v}_i)\mathbf{v}_i + \mathbf{F}_i(\mathbf{r}_1, \ldots, \mathbf{r}_N, \mathbf{v}_1, \ldots, \mathbf{v}_N) + \sqrt{2D}\xi_i(t), \tag{313}$$

where ξ_i are Gaussian white noise sources acting on every particle, independent from other particles.

The first term on the right hand side is the dissipative force, which accounts for the individual velocity dynamics (friction/energy pump). In case of the Rayleigh-Helmholtz model (Eq. (42)) these forces are read

$$-\gamma(\mathbf{v}_i)\mathbf{v}_i = (\alpha - \beta\mathbf{v}_i^2)\mathbf{v}_i. \tag{314}$$

Also the active linear dissipative force with friction coefficient (44) can be easily generalized to N particles. Eventually one can define for every particle $i = 1,\ldots,N$ an individual energy depot $e_i(t)$ which will yield a velocity-dependent friction force (54).

The second force term $\mathbf{F}_i$ accounts for the interactions between the particles, as well as possible external forces acting on individual particles. In general, it can be a function of all positions and velocities of particles forming a swarm. Here, we assume that $\mathbf{F}_i$ consists of two components: a velocity dependent (dissipative) force and a force due to potential gradients:

$$\mathbf{F}_i = \mathbf{F}_i^{\mathrm{va}}(\mathbf{v}_1,\ldots,\mathbf{v}_N) - \nabla U_N(\mathbf{r}_1,\ldots,\mathbf{r}_N). \tag{315}$$

The potential U_N is assumed to consist of an external potential $W(\mathbf{r_i})$ and a superposition of pair-wise interaction potential $U(r_{ij})$, with r_{ij} being the distance between particle i and j. Hence, the total potential reads:

$$U_N = \sum_i W(\mathbf{r_i}) + \frac{1}{2}\sum_{ij} U(r_{ij}). \tag{316}$$

We will start with a parabolic approximations of the interaction forces generated by the pair-wise potentials [105, 237, 313].

$$U(r_{ij}) = \frac{\omega^2}{2}r_{ij}^2, \tag{317}$$

which might hold if the size of the objects is small compared to the spatial scale of their motion. Harmonic interaction potentials constitute a global coupling between individual particles, which was considered in this context in various publications [237, 250, 313]. It allows to reduce the problem effectively to the motion in a well formed by harmonic forces which we considered in Sect. 5.1. With global coupling the particles are attracted by an effective spring force to the center of mass given by

$$\mathbf{r}_{c.o.m.}(t) = \frac{1}{N}\sum_j \mathbf{r}_j(t). \tag{318}$$

The effective mean field force acting on the i-th particle is defined by

$$\mathbf{K}_i = -\nabla_i U_N(\mathbf{r}_1,\ldots,\mathbf{r}_N) = -\omega_0^2[\mathbf{r}_i - \mathbf{r}_{c.o.m.}(t)]. \tag{319}$$

Several approaches to include more realistic interactions will be discussed later on. Here, we should mention that the case of constant external forces was already treated by Schienbein et al. [304, 305]. Symmetric parabolic external forces were studied in Refs. [106, 121] and the non-symmetric case is being investigated in Ref. [118]. More complicated external fields including short range repulsion were studied in detail in several publications [104, 226, 227, 306] and will also be addressed in Sect. 6.1.6.

The dissipative interaction between particles, is assumed to be a velocity-dependent interactions with the tendency to synchronize the velocities of different particles. We assume a simple alignment law [252]

$$\mathbf{F}_i^{\mathrm{va}}(\mathbf{v}_1,\ldots,\mathbf{v}_N) = -\mu\sum_j g_N(r_{ij})(\mathbf{v}_i - \mathbf{v}_j). \tag{320}$$

Here $g(r)$ is a function which accounts for possible distance dependence of the interaction, such as decay of the interaction strength with distance. This models a dissipative force which tends to parallelize the individual velocities.

In this and the next section, we will consider for simplicity a velocity coupling with an infinite range: $g_N(r) = 1/N$. Thus, in this model all particles synchronize with the total swarm velocity $\mathbf{u}(t)$ which is the velocity of the center of mass (c.o.m.) of the swarm.

$$\mathbf{u}(t) = \frac{1}{N} \sum_j \mathbf{v_j}. \tag{321}$$

In addition we will assume that the alignment strength μ is vanishingly small. Hence, in the next section our focus lies on the conservative interactions.

Other couplings with finite range $g(r)$ have been studied in numerous previous publications (see e.g. [60, 272, 360, 361]). We will discuss the (local) alignment interaction in detail in Sect. 6.2.2. There are other types of dissipative interactions, which lead to synchronization of individual velocities as, for example, hydrodynamic interactions [23, 116] or symmetry-breaking contact interactions, such as e.g. inelastic collisions [148, 258, 271, 340]. We will present and discuss different alignment interaction in detail in the forthcoming sections.

6.1.3 The model of harmonic swarms with global coupling

The concept of global coupling has proven to be very useful for the investigation of stochastic systems [9]. For the case of Rayleigh-driving, the dynamical equations for center of mass and its velocity have the form [103]

$$\frac{\mathrm{d}}{\mathrm{d}t}\mathbf{r}_{c.o.m.}(t) = \mathbf{u}(t), \tag{322}$$
$$\frac{\mathrm{d}}{\mathrm{d}t}\mathbf{u} = \left[\alpha - \beta\mathbf{u}^2\right]\mathbf{u} - \frac{\beta}{N-1}\sum_i \left((\delta\mathbf{v}_i)^2\mathbf{u} + (\mathbf{u}\cdot\delta\mathbf{v}_i)\,\delta\mathbf{v}_i\right) + \sqrt{2D}\xi_u(t).$$

Therein $\delta\mathbf{r}_i(t) = \mathbf{r}_i(t) - \mathbf{r}_{c.o.m.}(t)$ and $\delta\mathbf{v}_i(t) = \mathbf{v}_i(t) - \mathbf{u}(t)$ are the deviations of the individual objects from the center of mass, which obey

$$\frac{\mathrm{d}}{\mathrm{d}t}\delta\mathbf{r_i} = \delta\mathbf{v_i} \tag{323}$$
$$\frac{\mathrm{d}}{\mathrm{d}t}\delta\mathbf{v_i} + \omega_0^2\delta\mathbf{r_i} = \left[\alpha - \mu - \beta\delta\mathbf{v}_i^2 - \beta\mathbf{u}^2\right]\delta\mathbf{v_i} - 2\beta(\mathbf{u}\cdot\delta\mathbf{v_i})\mathbf{u} + \sqrt{2D}\delta\xi_i(t),$$

where the Gaussian white noise acting on the center of mass is defined as

$$\xi_u(t) = \frac{1}{N}\sum_i \xi_i(t), \quad \langle\xi_u(t)\rangle = 0, \quad \langle\xi_{uk}\xi_{ul}\rangle = \frac{1}{N}\delta_{kl}\delta(t-t'), \quad l,k = x,y. \tag{324}$$

The noise agitating the individual objects reads $(i,j = 1,\ldots,N)$

$$\delta\xi_i = \xi_i - \xi_u, \qquad \langle\delta\xi_i\rangle = 0, \langle\delta\xi_{ik}\delta\xi_{jl}\rangle = \delta_{ij}\delta_{kl}(1 - \frac{1}{N})\delta(t-t'), \tag{325}$$

with $k,l = x,y$. We note that these noise terms are again independent of the motion of particles.
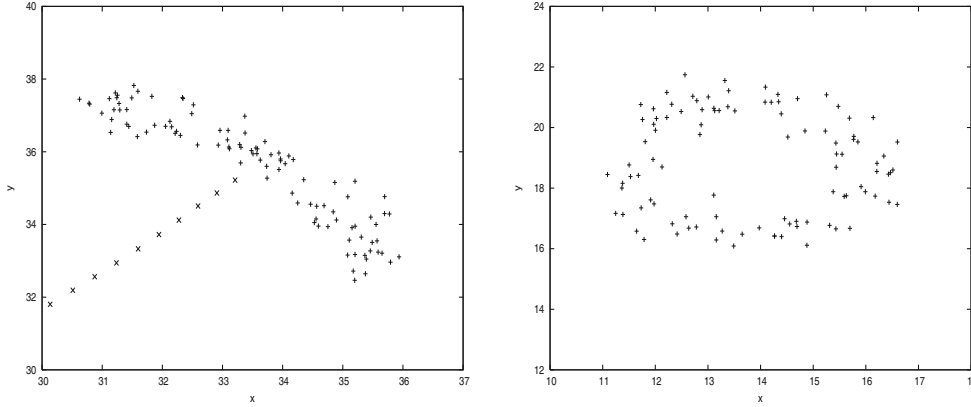
Fig. 46. The two basic configurations of a noisy system obtained by simulations of $N = 100$ globally coupled active particles. We show snapshots in the space of the two coordinates ($\omega_0^2 = 0.2, \mu = 0$). Left panel: $D = 0.001$, translational mode with a particles moving along a dumb-bell configuration perpendicularly to the translational motion of the center of mass indicated by diagonal crosses. Right panel: $D = 0.2$, rotational mode with undirected rotations around the center of mass [103].

Lets first look at dynamics of the center of mass. We start by decoupling is from the dynamics of the deviations by averaging with respect to $\delta\mathbf{v}_i$. Approximately, we get in this way

$$\frac{\mathrm{d}}{\mathrm{d}t}\mathbf{u} = (\alpha_1 - \beta\mathbf{u}^2)\mathbf{u} + \sqrt{2D}\xi_u(t). \tag{326}$$

Importantly, here $\alpha_1 < \alpha$ is determined by the positive mean quadratic dispersions of the $\delta\mathbf{v}_i$. The corresponding velocity distribution of the center of mass is

$$P^{(0)}(\mathbf{u}) = C\exp\left[N\left(\frac{\alpha_1}{2D}\mathbf{u}^2 - \frac{\beta}{4D}\mathbf{u}^4\right)\right]. \tag{327}$$

This way we find the most probable velocity as $\mathbf{u}_1 = u_1\mathbf{e}_v$ with equally distributed and diffusing directions. It yields for the average speed:

$$u_1 = \sqrt{\alpha_1/\beta}, \tag{328}$$

which is smaller than the speed of an freely moving individual object which value was $v_0 = \sqrt{\alpha/\beta}$. The shift with respect to the free mode depends on the noise strength D. The solution breaks down if the dispersion of the relative velocities $\delta\mathbf{v}_i^2$ becomes so large that the α_1 becomes negative. With increasing noise we find a bifurcation to another mode which most probable value has speed $u_2 = 0$.

This corresponds to the findings of Erdmann et al. [119] which will be discussed more detailed later on. Fig. 46 illustrates the two typical behaviors which can be observed for small noise, and for noise intensities above a critical values D^{crit}, respectively. Further on, we refer to $u_1 \neq 0$ as the translational mode, and to the second mode with vanishing center of mass speed $u_2 = 0$ as the rotational mode. We will also see that both modes can be clearly defined in three spatial dimensions.

6.1.4 Investigation of the dynamics of the relative motion of active particles

Here, we discuss the dynamics of the movement of individual particles relative to the center of mass [103]. We begin with the analysis of the deterministic case without
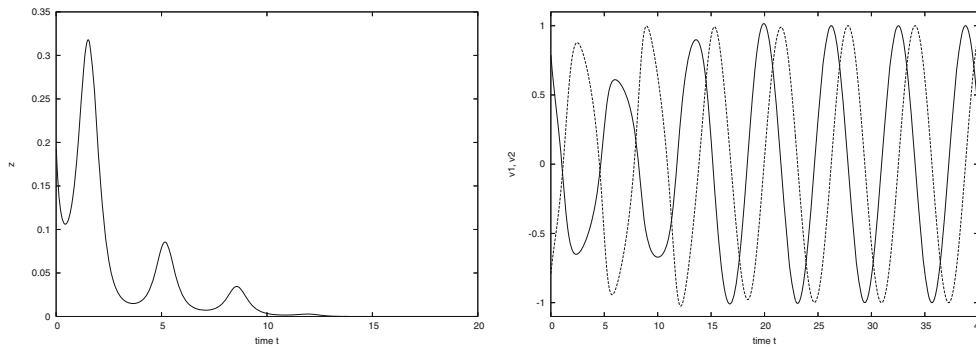
Fig. 47. Dynamics corresponding to the attractor region of the rotational motion of the pair: the left panel shows the decay of the kinetic energy of the center of mass to zero (rest state), as a function of time $z(t) = u^2(t)$. The right panel shows projections of the velocities $v_1(t), v_2(t)$ as a function of time and demonstrates the formation of sustained oscillations [103].

noise. The equations of motion are completely symmetric with respect to the particle index i. In other words, there are no cross terms including two different particles as i, j. This is an unique property of global coupling, the relative dynamics reduces completely to the binary problem, i.e., to the analysis of the (stochastic) dynamics of pairs of active Brownian particles. Therefore, we concentrate our investigation on the study of two active particles with a linear attracting force [118].

In this case, the center of mass $\mathbf{r}_{c.o.m.}$ moves with the velocity $\mathbf{u}$. The relative motion of an individual particle under the influence of the interaction force is described by the relative radius vector $\delta\mathbf{r} = \mathbf{r}_i - \mathbf{r}_{c.o.m.} = (\mathbf{r}_1 - \mathbf{r}_2)/2$ and the relative velocity $\delta\mathbf{v}$. The second particle has the same distance and velocity relatively to the center of mass but with opposite sign. We may write in Eq. (323) simply $\delta\mathbf{r}, \delta\mathbf{v}$ instead of $\delta\mathbf{r}_i, \delta\mathbf{v}_i$ and omit the sum and the denominator $1/(N-1)$ in the equation for the center of mass.

i) Let us first assume a stable rotational mode. Hence, we put $\mathbf{u} = 0$ which solves the equation of motion for the center of mass. Subsequently it follows that $\mathbf{r}_{c.o.m.} = \mathbf{r}_{c.o.m.}(0)$. In the two dimensional space the equations of motion for the $\delta\mathbf{r}$ and $\delta\mathbf{v}$ become symmetric and independent of a direction. Both assume the form of a van der Pol oscillator for system with a limit cycle

$$\frac{\mathrm{d}}{\mathrm{d}t}\delta\mathbf{r} = \delta\mathbf{v}, \quad \frac{\mathrm{d}}{\mathrm{d}t}\delta\mathbf{v} + \omega_0^2\delta\mathbf{r} = \left(\alpha - \mu - \beta\delta\mathbf{v}^2\right)\delta\mathbf{v}. \tag{329}$$

As in the case of an external field (Sect. 5) this system has two stable limit cycles, see Fig. 41. Which of them will be approached depend on the initial conditions.

The limit cycles are left in favour of the translational mode by a perturbation with an overcritical speed value. In order to understand this, we introduce a small but finite translation $u = v_1 > v_{\mathrm{crit}} > 0$. If u is sufficiently large, it leads immediately to the destruction of the rotational symmetry of the limit cycles, and to an elliptic deformation with the longer axis in the direction perpendicular to the translation. As shown by Erdmann et al. [117,118] the loss of rotational symmetry leads to leaving an Arnold tongue of stability and consequently to a destruction of the limit cycles. These authors found that the rotations are indeed stable only in and near to the plane $u = 0$ i.e. for swarms at rest or near to the resting state. This situation is presented in Fig. 47 for a subcritical initial kinetic energy of the center of mass.

ii) In case of translational mode the vector $\mathbf{u} \simeq \mathbf{e}_v$ plays a special role. We orientate the coordinate system parallel to $\mathbf{u}$. Hence, we span $\delta\mathbf{r} = (x_\parallel, x_\perp)$, $\delta\mathbf{v} = (v_\parallel, v_\perp)$ where $x_\parallel, v_\parallel$ are the components in the direction of $\mathbf{u}$ and $x_\perp, v_\perp$ perpendicular to it. Further on, we introduce the new variable $z(t) = u^2(t)$, corresponding to twice the kinetic energy of the center of mass. Then we get the following five differential equations

$$
\begin{aligned}
&\frac{\mathrm{d}}{\mathrm{d}t}x_\parallel = v_\parallel, \quad \frac{\mathrm{d}}{\mathrm{d}t}v_\parallel + \omega_0^2 x_\parallel = v_\parallel(\alpha - \mu - 3\beta z - \beta v_\parallel^2 - \beta v_\perp^2), \\
&\frac{\mathrm{d}}{\mathrm{d}t}x_\perp = v_\perp, \quad \frac{\mathrm{d}}{\mathrm{d}t}v_\perp + \omega_0^2 x_\perp = v_\perp(\alpha - \mu - \beta z - \beta v_\parallel^2 - \beta v_\perp^2), \qquad (330) \\
&\frac{\mathrm{d}}{\mathrm{d}t}z = 2z(\alpha - \beta z - 3\beta v_\parallel^2 - \beta v_\perp^2),
\end{aligned}
$$

supplemented by the definition $\dot{\mathbf{r}}_{c.o.m.} = \mathbf{u}$. The qualitative analysis of this system of nonlinear ordinary differential equations shows at first that the system possesses a stable point attractor at $z = \alpha/\beta$, $v_\parallel = v_\perp = x_\parallel = x_\perp = 0$. With parabolic attraction without hard core both particle has the same position and move with the center of mass velocity. Note that this is also solution for the N-particles.

The linear stability analysis provides the eigenvalues -2α in z-direction, in the parallel direction $\lambda_1 \pm i\sigma_1$ where $\lambda_1 = (2\alpha + \mu)/2$ and $\sigma_1 = \sqrt{\lambda_1^2 - \omega_0^2}$ and in the perpendicular direction $\lambda_2 \pm i\sigma_2$ with $\lambda_2 = \mu/2$ and $\sigma_2 = \sqrt{\lambda_2^2 - \omega_0^2}$. The point attractor is linearly stable provided $\mu > 0$. The linear stability in the direction $v_\perp$ corresponding to the motion perpendicular to the translation is given only for $\mu > 0$. However, even at $\mu = 0$ we still observe quadratic stability in this particular direction due to the terms since the $-\beta v_\perp^2$ stabilizes the motion as can be seen from the nonlinear equation of motion for $v_\perp$ around the fixed point

$$
\frac{\mathrm{d}}{\mathrm{d}t}v_\parallel = -\omega_0^2 x_\perp - v_\perp\left(\mu + \beta(v_\parallel^2 + \beta v_\perp^2)\right). \qquad (331)
$$

Now we suppose that a deviation from the fixed point exist, which is realized by some small $v_\perp^2$ and $v_\parallel^2$. Both values are not stationary, but we assume that a linear combinations of them can supplement each other to a stationary value at a longer time scale. In consequence, we require that the expression inside the brackets in the last equation of (330) vanishes, i.e. it holds

$$
\beta z = \alpha - 3\beta v_\parallel^2 - \beta v_\perp^2. \qquad (332)
$$

Since $\dot{z} = 0$, the above expression (332) represents a translational mode. The stability analysis shows that perturbations perpendicular to the motion perform harmonic oscillations around the center of mass if $v_\parallel^2$ is vanishing. Otherwise, they start to grow if there is a deviation parallel to the motion and the translational mode gets oscillating in all variables.

Indeed insertion of (332) into the dynamics of $v_\perp$ yields

$$
\frac{\mathrm{d}}{\mathrm{d}t}v_\perp + \omega_0^2 x_\perp = v_\perp(-\mu + 2\beta v_\parallel^2). \qquad (333)
$$

So if $\mu \to 0$ this state is marginally stable if the deviation of the particle points perpendicular to the center of mass, i.e. $v_\parallel = 0$. Oppositely the deviations parallel to the direction of the center of mass will be amplified in the perpendicular direction if

$$
2\beta v_\parallel^2 > \mu \geq 0. \qquad (334)
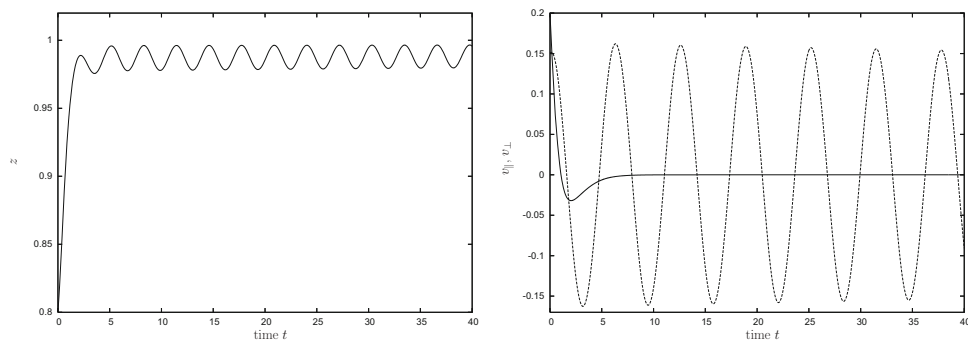$$

Fig. 48. Solutions of the Eqs. (330) as a function of time for $\mu = 0$ and initial conditions $z(0) = u^2(0) = 0.8$, corresponding to the region of the attractor of translational motion. Left panel: the translational (squared) velocity $z(t) = u^2(t)$ approaches slowly the maximal value $z = 1$. An oscillating contribution remains which is due to the neutral stability of the $v_\perp(t)$-dynamics. Right panel: the longitudinal component of the velocity $v_\parallel(t)$ goes quickly to zero and the transversal velocity $v_\perp(t)$ decays very slowly or remains constant (because of neutral stability) [103].

We see that the alignment increases the stability of parallel motion. These results illuminate the role of the velocity couplings. Without the existence of a (positive) velocity coupling, the swarms tends to show a weak instability in the transversal direction, i.e. it tends to get broader and broader, remaining concentrated around the center of mass in the longitudinal direction.

Since this mode is oscillatory with frequency ω_0, we find small oscillations of the particles perpendicularly to the direction of motion. It can be also inspected from left Fig. 46 where the particle move with a broadened distribution perpendicular to the center of mass motion.

Details about the dynamics we may obtain from explicit solutions, for the special set of parameters $\alpha = \beta = 1$. In Fig. 48 we show several solutions corresponding to initial conditions in the attractor region. We see that typically (for different initial conditions within the attractor region) the relative velocity perpendicular to the swarm translation $v_\perp(t)$ decays very slowly, and the relative velocity in the direction of the swam motion $v_\parallel(t)$ goes to zero in a very fast way. The velocity of the center of mass approaches $u_1 < v_0\alpha/\beta$ rather fast, however, the state becomes unstable and a slow oscillatory contribution appears. Including a small amount of velocity synchronization $\mu > 0$, all oscillatory components in the translational mode are damped out in the time $1/\mu$. In the limiting case $\mu = 0$, i.e. without velocity alignment, no synchronization of the velocities exist.

Note that the relative velocities $v_\parallel$ and $v_\perp$ are defined respectively to the velocity of the c.o.m.. Therefore, even if the parallel velocities vanish the oscillations of particle movement are also present in the velocities taken respectively to the origin of coordinate.

6.1.5 Influence of noise on swarms

Including noise we expect instead of the point attractor at $u = v_0$ and the two line attractors - the 2 limit cycles in the plane $u = 0$ - that the dynamic systems forms some distributions around the attractors. This will obviously lead to some permanent deviations around the center of mass (c.o.m.) and of its velocity. Here, we will find estimates of the corresponding distributions. We will use the approximation

of independent dynamics of the velocity components $v_\parallel, v_\perp$ and of u. Above we also found in Eq. (327) the velocity distribution of the center of mass with the most probable velocity given in Eq. (328) by

$$\alpha_1 = \alpha - 3\beta\langle v_\parallel^2\rangle - \beta\langle v_\perp^2\rangle. \tag{335}$$

This expression as well as Eq. (327) contains still the unknown constant α_1 which is determined by the distributions of the longitudinal and translational velocities.

For the longitudinal fluctuations around the center of mass of the swarm near to the stable attractor, we get

$$\frac{\mathrm{d}}{\mathrm{d}t}v_\parallel + \omega_0^2 x_\parallel = -2\alpha_1 v_\parallel + \sqrt{D}\xi_\parallel(t), \tag{336}$$

where the noise strength of the relative motion is reduced by factor of two. This follows from the correlators formulated above for $N = 2$. The corresponding stationary Fokker-Planck equation is solved by

$$P_0(x_\parallel, v_\parallel) = C_0 \exp\left[-\frac{1}{D}\left(2\alpha_1 v_\parallel^2 + \omega_0^2 x_\parallel^2\right)\right], \tag{337}$$

where C_0 is given by the normalization. The dispersion is given by

$$\langle v_\parallel^2\rangle \simeq \frac{D}{4\alpha_1}. \tag{338}$$

The longitudinal dispersion depends on the constant α_1 which is still to be determined.

The situation is more complicated for the fluctuations transversal with respect to the c.o.m. of the swarm due to the problems with linear stability in the $v_\perp$-direction. Neglecting the correlations with the longitudinal fluctuations $\langle v_\parallel v_\perp\rangle$, which are small, we find

$$\frac{\mathrm{d}}{\mathrm{d}t}v_\perp + \omega^2 x_\perp = v_\perp[(\alpha - \alpha_1 - \mu) - \beta(\delta v_\perp)^2] + \sqrt{D}\xi_\perp(t). \tag{339}$$

We remember that $\alpha_1 < \alpha$ for finite noise. Therefore the first term on the right hand side may be positive or negative, depending on the situation. We have to differ between two cases:

(i) For the stable solution $\mu > (\alpha - \alpha_1)$, the term with β can be neglected for small velocity deviations. We obtain the standard problem of a noisy damped oscillator with the distribution

$$P_0(x_\perp, v_\perp) = C \exp\left[-\frac{1}{D}\left(-(\mu - \alpha - \alpha_1)v_\perp^2 + \omega_0^2 x_\parallel^2\right)\right] \tag{340}$$

and the dispersion

$$\langle v_\perp^2\rangle \simeq \frac{D}{2(\mu - \alpha + \alpha_1)} \simeq \frac{D}{2\mu}. \tag{341}$$

In the present case the fluctuations of $v_\parallel$ and $v_\perp$ are rather small and the translational mode is the most favorable one.

(ii) A different situation is observed in the second case of small (or zero) contribution from parallelizing interactions. We consider now the situation $\mu < (\alpha - \alpha_1)$ in correspondence with the inequality (334). Then in Eq. (339) the term with β has to be taken into account and the system switches to the rotational mode even for such small noise values as $D = 0.001$ (see Fig. 49). However, this limit cycle is not a

standard one, since $(\alpha - \alpha_1) > \mu$ requires finite noise, i.e. the amplitude of the limit cycle is driven by noise.

We emphasize that the behavior corresponds to active motion of the center of mass supplemented by a small active oscillatory motion of individual particles relative to the center of mass (see Fig. 48).

In order to determine α_1, we need to estimate $\langle v_\perp^2 \rangle$. First we remember, that $v_\perp$ is a component of the relative velocity vector $\delta\mathbf{v} = (\mathbf{v}_1 - \mathbf{v}_2)/2$. The squared velocity-space diameter of the limit cycle in first approximation is given by $2(\alpha - \alpha_1 - \mu)/\beta$. This gives us

$$\langle v_\perp^2 \rangle \simeq \frac{\alpha - \alpha_1 - \mu}{2\beta}. \tag{342}$$

The longitudinal (338) and perpendicular dispersions (342) inserted into Eq. (335) yield: and are connected by the relations

$$\alpha_1 = \alpha - \frac{3\beta D}{2\alpha_1} + \mu. \tag{343}$$

It is a quadratic equation in α_1 and has the solution

$$\alpha_1 = \frac{1}{2}(\alpha + \mu)\left[1 - \sqrt{1 - \frac{6\beta D}{(\alpha + \mu)^2}}\right]. \tag{344}$$

We see that the dispersion of u^2, corresponding to the small oscillating motion in Fig. 48, is maximal for the critical noise strength

$$D_{cr} = \frac{(\alpha + \mu)^2}{6\beta}. \tag{345}$$

This is in good agreement with simulation results in [119].

However, we note that numeric simulations have shown that the translational mode occurs to be unstable with respect to fluctuations. We observed that the translational mode for particles with harmonic interactions in two dimensions is always a transient state. For sufficiently long simulation times, we found for $\mu = 0$ that the system switches to the rotational mode even for such small noise as $D = 0.001$ (see Figs. 49). We point out that we never observed transitions from the rotational mode back to the translational state of a moving center of mass even within extremely long simulation times.

This underlines the importance of having at least a small contribution of velocity synchronization $\mu > 0$, which stabilizes the translational mode. In the next Section we will discuss bistability between both modes which is due to a hard core potential in three dimensions. Here we show frequencies of the center of mass speed, recorded during finite simulation with translational mode as initial condition in Fig. 50, which indicate the transient bistable behavior. The amount of probability around the translation and rotational mode clearly depends on the noise intensity.

In case of simple harmonic forces the probability is distributed around two limit cycles corresponding to left or right rotations. These distributions for the rotational mode are similar to what we have found for the case of external fields. In the mean field case and with linear forces the particles do interact effectively with the resting center of mass, only. In result there is no tendency to states where all particles move synchronously along one circle. Such way the circles does not behave like attractors for the whole swarm and any decomposition of particles with right and left rotations is possible.
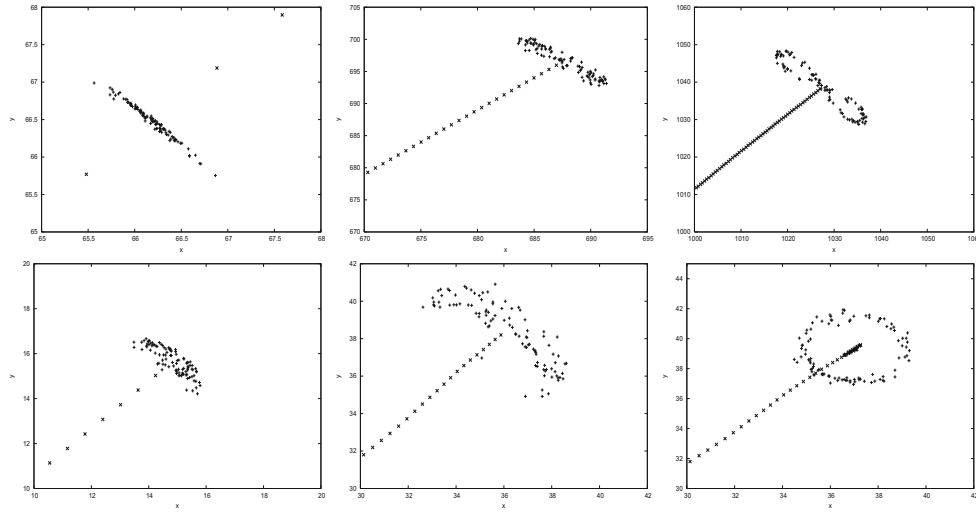
Fig. 49. Upper row: snapshots of the swarm configurations in space of coordinates in the translational mode $u = v_0$ at times $t = 100, 100, 1500$ for small noise (parameters $\omega_0^2 = 0.01; D = 0.00001; N = 100$). The straight dotted curve represents the trajectory of the center of mass. Lower row: a time sequence ($t = 20, 80, 110$) of swarm configurations in space at larger noise which end in the rotational mode (parameters $\omega_0^2 = 0.2; D = 0.001; N = 100$). The center of mass becomes eventually resting [103].
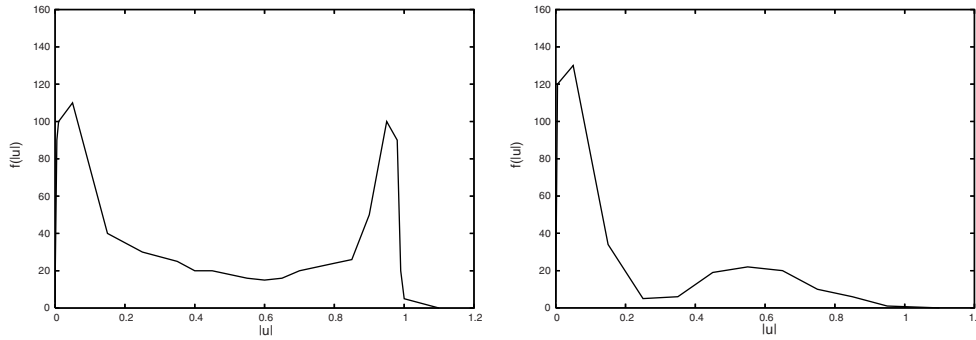

Fig. 50. Relative frequencies $f(|u|)$ of the swarm speed $|u|$ estimated from simulations along finite times which have started in the translational mode. Left panel: the translational mode produces for small noise $D = 0.00001$ a narrow maximum near to the maximal velocity of the swarm $|u| = v_0$ (here $v_0 = 1$). Right panel: at larger values of noise $D = 0.01$ the translational mode broadens and the rotational mode dominates. The latter forms forms a big maximum corresponding to more frequent rotational configurations [103].

Summarizing our findings we may state: For two interacting active particles there exist a translational and a rotational mode. In the rotational mode the center of the "dumb-bell" is at rest and the system rotates around the center of mass. Only the internal degrees of freedom are excited and we observe driven rotations. In the translational dumb-bell mode, the center of mass of the dumb-bell performs an active Brownian motion similar to a free motion of the center of mass. In this case, we may expect a distribution similar as given [306]. Larger noise leads to larger deviations from the center of mass, which finally favors transitions to the rotational state.

6.1.6 Cohesion, repulsion and bistability in 3D swarms

In this section, we present simulations of swarms and their dynamics in three spatial dimensions. We consider a set of N identical active particles interacting globally via a pair potential as outlined in the last section (Sect. 6.1). The coordinates $\mathbf{r}_i$ and velocities $\mathbf{v}_i$ have now three independent components.

We use a potential which captures fundamental properties of swarming of animals. At short range the potential has to be repulsive to avoid collisions and to prevent the agents from interpenetrating each other. An attractive force mimics the aim of the individual to stay with the group. The attraction should be of long range, but eventually approach zero to account for the limited sensing range of animals. An exponentially decaying function meets both demands.

Therefore, we consider here a generalized Morse potential, which consists of an attractive and a repulsive part. Both are exponential functions with amplitudes C_a and C_r and ranges l_a and l_r, respectively.

$$U_{\mathrm{M}}^i(\mathbf{r}_1, \ldots, \mathbf{r}_N) = \sum_{k \neq i}^{N} C_r \exp\left(\frac{-|\mathbf{r}_i - \mathbf{r}_k|}{l_r}\right) - C_a \exp\left(\frac{-|\mathbf{r}_i - \mathbf{r}_k|}{l_a}\right). \qquad (346)$$

The equilibrium distance of two particles is

$$r_0 = \frac{l_r \, l_a}{l_r - l_a} \, \ln\left(\frac{l_r \, C_a}{l_a \, C_r}\right). \qquad (347)$$

For $l_r/l_a < 1$ the potential possesses a minimum corresponding to short range repulsion and long range attraction. One can see that for $l_r/l_a < 1$ and $l_r/l_a > C_r/C_a$ the minimum would shift to negative values. Since the absolute value of the interparticle distance in Eq. (346) is positive, the potential is attractive everywhere. Therefore we will concentrate on the parameter space where $l_r/l_a < 1$ and $l_r/l_a < C_r/C_a$.

The collective behavior of active Brownian particles with Morse interaction in one spatial dimension was studied in [62,91,92,100], where it was shown, for example, that the combination of noise and active driving essentially "chooses" the eigenmodes of the Hamiltonian system. In two spatial dimensions, the self-organized rotational dynamics of a Hamiltonian system of active particles with such a pairwise Morse potential have been studied by Levine et al. [215] and d'Orsogna et al. [86]. Here, we will show that in three dimensions swarms of active Brownian particles interacting via Morse potentials with repulsion and attraction exhibit noise-induced transitions not only from translation to rotation, as in the purely attractive (harmonic) case, but also the reverse transition. These transitions occur at different noise intensities, thus leading to a hysteresis curve. This effect was not observed in two dimensions, here the rotation was stable even without noise. For comparison we also investigate the harmonic forces as introduced above in three dimensions.

To study the transition from translation to rotation, we prepare the system in the translational mode (Fig. 51, right). In this mode the particles move parallel with their stationary velocity $v_0 = \sqrt{\frac{\alpha}{\beta}}$. The spatial configuration in the center of mass system corresponds to the equilibrium configuration. Without noise, there are no fluctuations, the center of mass moves with v_0. Increasing the noise gives rise to fluctuations and leads to a decreasing velocity of the center of mass [119,237]. Above a critical noise value $D_{\mathrm{crit}}^{\mathrm{trans}}$, the translational motion breaks down and the particles start to rotate around the center of mass.

Whereas for a harmonic potential the particles rotate in any direction on the equipotential sphere, the Morse interaction leads to coherent motion in a torus shape structure, with the orientation depending on the initial conditions (Fig. 51). The
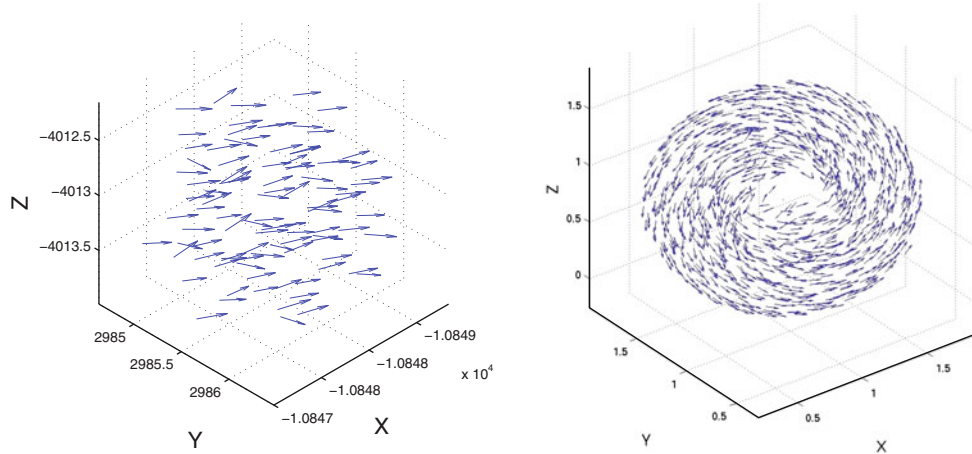
Fig. 51. Rotational (left) and translational (right) mode: particles move either coherently in a torus shape structure or parallel with the moving center of mass (c.o.m.) on a straight line. Parameter values: $N = 1000$, $\gamma_1 = 1.6$, $\gamma_2 = 0.5$, $C_r = C_s = l_r = 0.5$, $l_a = 2.0$, $D = 0$ [332].
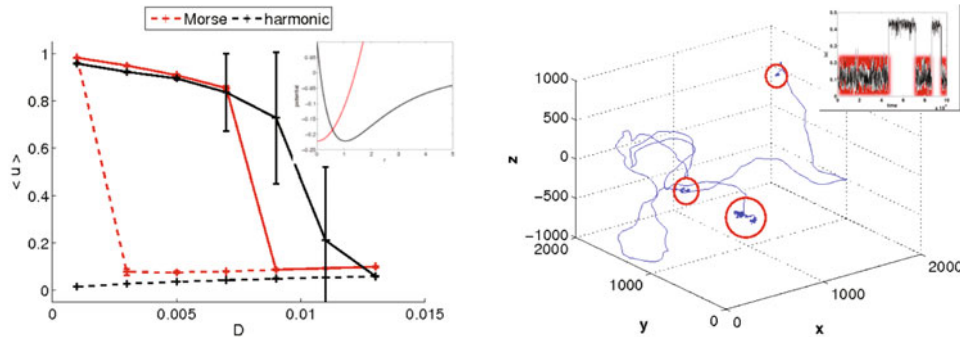

Fig. 52. Left panel: hysteresis of the center of mass speed u versus noise intensity D. Solid lines for increasing noise and dashed lines for decreasing D. The most probable values for Morse potential (red) and its harmonic approximation (not shown) are comparable and show instability of the rotational state below a critical noise intensity. For harmonic potential, or Morse potential without a minimum at finite distance, only transitions from translation to rotation can be observed. The latter is stable even without noise. Right panel: example of a trajectory of the center of mass in the bistable regime. The inlay shows the corresponding velocity. The rotational modes, where the velocity is almost zero, are highlighted red. These lead to a diffusive motion of the center of mass within the red circles. In between the system displays a stochastic trajectory in the translational mode with mean velocity $u \cong v_0 = \sqrt{\frac{\alpha}{\beta}}$ [332].

center of mass moves diffusively, therefore the absolute value of its velocity is not zero and increases with the noise intensity.

Starting from the rotational state and decreasing the noise intensity, the system exhibits a transition to the translational mode at a different critical noise value $D_{\text{crit}}^{\text{rot}}$. Surprisingly, this second transition back to translation was not observed in the two-dimensional case with harmonic attraction. In general, both transitions occur at different noise values which leads to a hysteresis curve (Fig. 52, left).

The decrease of the center of mass velocity with rising noise intensity can be shown by considering the equation of motion of the center of mass velocity. The analysis in three dimensions develops quite similar to the last Section following Eq. (322) [332]. One solution corresponds to the rotational state, the second solution to the translational state. The center of mass moves (in absence of noise) with the stationary velocity of the particles $u_0 = \sqrt{\frac{\alpha}{\beta}}$. Increasing the noise leads to higher deviations $\delta\mathbf{v}$ which decreases the center of mass velocity.

For the transition from rotation to translation the critical noise value decreases with increasing C_r/C_a. However, for $l_r/l_a < C_r/C_a < 1$ the critical noise value decreases with decreasing $\frac{C_r}{C_a}$, below $C_r/C_a = l_r/l_a$, no transition to translation takes place. In this parameter range the potential does not possess a minimum, i.e. it does not have a repulsive core and is continuously attractive for all distances. Even without noise there is no transition from rotation to translation. Otherwise the transition backwards stays unaffected. From this fact we conclude that the existence of repulsive forces induces transitions from rotation to translation.

To check this hypothesis, we approximate the Morse potential by a harmonic potential with equilibrium distance of the shape

$$U_{\mathrm{app}}(r) = a(r - r_0)^2, \tag{348}$$

with

$$a = \left(\frac{l_r C_a}{l_a C_r}\right)^{\frac{l_a}{l_a - l_r}} \frac{C_r}{2l_r} \left(\frac{1}{l_r} - \frac{1}{l_a}\right) \tag{349}$$

and r_0 given in Eq. (347). We compare it to the overall attractive harmonic potential $U_{\mathrm{H}}(r) = ar^2$ (see Fig. 52, left panel). The critical noise value for the transition from translation to rotation is equal for the Morse potential and the harmonic approximation (not shown). The translational mode of the harmonic potential U_{H} is stable for larger noise values. The main difference occurs in the transition from rotation to translation. The harmonic approximation U_{app} shows this transition, though at a different noise value than the Morse potential. In case of the harmonic potential without repulsion, the rotational mode is stable even without noise. This supports the assumption, that a short-range repulsive part of the potential is vital for the existence of the transition from rotation to translation.

We found that the critical values of the noise for both transitions decrease with growing amplitude C_r of the repulsive part in Eq. (346). Yet, the decrease is much larger for the transition from translation to rotation which leads to a parameter region where transitions in both directions occur at the same noise value.

In this region, the system alternates between the two states. The inlay of the right panel in Fig. 52 shows the center of mass velocity u which alternates between translation and rotation (red). The trajectory of the center of mass shows diffusive motion, where the system is rotating, separated by parts with stochastic translational motion (Fig. 52, right panel).

The probability distribution of u depends very sensitively on the noise intensity (Fig. 53). The region where this oscillatory behavior can be observed is very small. Changing the noise value by a few percent leads to a shift of the transition probabilities which is sufficient to destroy the oscillations. It is sketched in Fig. 53 where for both graphs the noise intensity has changed little. Nevertheless, the weights of the two states in the two distribution changes drastically.
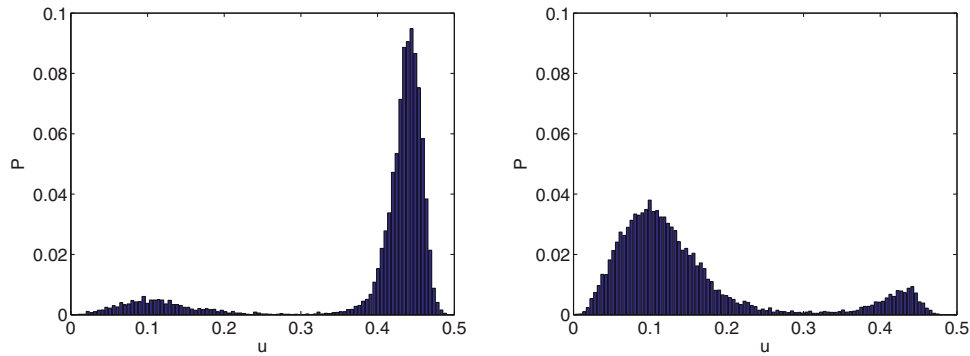
Fig. 53. Probability distribution of the speed of center of mass for different noise values of a swarm in 3D with Morse interaction [332].

6.2 Collective motion from local velocity alignment without cohesion

6.2.1 Interactions of active particles mechanisms and symmetries

Active matter may be more generally divided into in externally driven particles, e.g. shaken granular matter, and in particles which are intrinsically powered, self-propelled particles, like gliding and swarming cells, or chemically active particles, e.g. oscillating yeast cells. Self-propelled particles are almost always polar, as their propulsion mechanism determines typically their direction of motion, or, more specifically the leading and trailing edge of the particle are clearly distinguishable (see also Sect. 2.3 and 3.1). This requires an initial symmetric breaking in the internal structure of the self-propelled particle, e.g. polarization of motile biological cells or asymmetric design of manufactured granular particles under driving. Examples are driven granular particles with non-symmetric shape or mass distribution [82, 206, 207] or different chemical composition at the two ends of a particle, like chemically driven running droplets or nano-dimers (Janus particles) [265, 300, 334, 341, 352, 356]. To understand the collective dynamics of ensembles of active particles, one needs also to figure out the nature of their interactions. Swimming bacteria, flocking birds and schools of fish are often assumed to have hydrodynamic interactions that favor a joint direction of motion. Such interactions are analogous to ferromagnetic interactions of spins and try to align the vectors describing the motion of the particles; consequently, one speaks of polar interactions. In contrast, gliding bacteria or shaken rods tend to align their long axes, but still can either move in a parallel or anti-parallel fashion. Hence, such interactions are classified as apolar. Apolar interactions are analogous to nematic interactions that favor alignment, e.g. excluded volume interactions of rod-shaped particles.

The famous Vicsek model represents an example for polar particles exhibiting polar interactions [361]. Self-propelled rods with volume-exclusion interactions can be identified as polar particles with apolar interactions. The so-called *active nematics* constitute a third case, namely apolar particles with apolar interactions, that shall not be discussed here. For recent results on active nematics [350], such as the analysis of a simple Vicsek-type model [61] and experiments with externally driven elongated particles such as rice corns, see instead e.g. [13, 248, 249] and references therein.

A central question in the study of such active particles with local interactions is if and when long-range order arises. The nature of the transition between ordered and disordered types of motion has been investigated thoroughly. Below, we will discuss several mean-field theories that neglect spatial variation in the order parameter.

For the Vicsek model, the mean-field theory predict a continuous second order phase transition to long-range order. which was reported initially also in numerical simulation [75, 361]. Grégoire and Chaté later found in extensive simulations that the transition to collective motion in the Vicsek model appeared in fact in a discontinuous way provided the system size in the simulations is large enough [147]. Their result was contested by later results of Vicsek´s group [247], but recent even more extensive studies by Chaté, Ginelli et al. reaffirm the discontinuous nature of the transition at the onset of collective motion [60]. This work revealed a crossover from a second to a first order transition at sufficiently large system size, which can depend strongly on the velocity parameter used in the simulations. More importantly, their work showed that the appearance of a discontinuous transition is strongly correlated with the appearance of segregation bands, that were first reported in 2004 [147] of high particle density in a low density background that travel in the direction motion of the self-propelled particles in these bands. Such correlations between the transition behavior and spatial patterns of the particle density shall be left aside for the moment and will be treated in Section 7 that deals with pattern formation aspects of self-propelled particle systems. An important general lesson is that spatial aspects maybe crucial and need consideration. For the moment, we will however exclude them and leave their general discussion to Section 7. In the following, we proceed with the discussion of local polar (or ferromagnetic) alignment of active Brownian particles, before considering both polar and apolar alignment interactions in the framework of self-propelled particles with Vicsek-type dynamics.

6.2.2 Active Brownian particles with velocity alignment force

We consider now a system of N active Brownian particle interacting only via a local velocity alignment force $\mathbf{F}^{\text{va}}$ (see Eq. (320) [74, 252, 296, 299]), which may be written as

$$\mathbf{F}_i^{\text{va}} = \mu \left(\mathbf{u}_{i,\varepsilon} - \mathbf{v}_i \right), \tag{350}$$

with $\mathbf{u}_{i,\varepsilon}$ being the mean velocity of the particle gas within a finite distance $|\mathbf{r}_j - \mathbf{r}_i| < \varepsilon$ around the focal particle i $(i = 1, \ldots, N)$. The force aligns the velocity of the focal particle to the average local velocity with μ being the alignment strength, which corresponds in the deterministic case to the inverse relaxation time of $\mathbf{v}_i$ towards $\mathbf{u}_{i,\varepsilon}$. For solitary particles with no neighbors, or in a system in a perfectly ordered state where all particles move with equal velocity the alignment force vanishes as $\mathbf{u}_{\varepsilon,i} = \mathbf{v}_i$. On the other hand, for a large number of neighbors moving with random velocities (disordered state), the mean velocity vanishes $|\mathbf{u}_{\varepsilon,i}| = u_{\varepsilon,i} \approx 0$ and the velocity alignment force results in additional "social" friction $-\mu \mathbf{v}_i$. The alignment force may be considered as a continuous version of the Vicsek model. For self-propelled particles with constant velocity $v_i = const$ it reduces essentially to the polar alignment interaction discussed in the next section [272]. Another motivation for introduction of such an velocity alignment term comes from hydrodynamic interaction which may result in an alignment term with similar symmetry properties [23, 116].

Recently, there has been a number of publication on kinetic description of self-propelled particles with velocity alignment (see e.g. [36, 176, 213, 322, 323, 348, 349], see also Sect. 7.1). In these previous publications, the authors constructed mesoscopic equations of motion for the density and velocity fields using symmetry and conservation laws. Recently, [36] derived corresponding equations with a Boltzmann approach. Further contributions were made by C.-F. Lee [213], who studied collective dynamics due to velocity alignment by analyzing an approximated Fokker-Planck equation and by T. Ihle [176] who derived an Enskog-type kinetic theory for the Vicsek model.

Here, in contrast to the previous publications, we derive the mean field equations directly from the microscopic Langevin equations. We do not assume a constant speed and analyze the impact of the velocity-dependent friction function on the onset of collective motion. In addition to the density and velocity fields, we consider explicitly the effective temperature field of the active Brownian particle gas.

Our approach is based on the formulation of moment equations of the corresponding probability distribution. In general, far from equilibrium the probability distributions are not Gaussian and a correct description requires infinitely many moments (see for example [263,264]). Therefore approximations are necessary in order to obtain a closure of the system of moment equations.

As first example we consider a one-dimensional system with periodic boundary conditions ($d = 1$, one-dimensional ring). The n-th moments of the velocity $\langle v^n \rangle$ is defined as

$$\langle v^n \rangle = \frac{1}{\rho} \int v^n \psi(x, v, t) \mathrm{d}v, \quad n > 0, \tag{351}$$

where $\psi(x, v, t)$ is the one-particle distribution describing the probability to find a particle at time t, at position x moving with velocity v. For N identical particles it is given simply by the multiple of single particle probability density $\psi(x, v, t) = NP(x, v, t)$. The density of particles is given as

$$\rho(x, t) = \int \mathrm{d}v \, \psi(x, v, t) \mathrm{d}v = N \int \mathrm{d}v \, p(x, v, t). \tag{352}$$

Multiplying the n-th moment with the density and taking the derivative with respect to time, we obtain the dynamics of the velocity moments

$$\frac{\partial}{\partial t} (\rho \langle v^n \rangle) = \int v^n \frac{\partial \psi}{\partial t} \mathrm{d}v. \tag{353}$$

The equations of motion for active Brownian particles with Rayleigh-Helmholtz friction and velocity alignment read:

$$\dot{x}_i = v_{x,i} \tag{354}$$

$$\dot{v}_{x,i} = (\alpha - \beta v_i^2) v_{x,i} + \mu(u_{\varepsilon,i} - v_{x,i}) + \sqrt{2D} \xi_i. \tag{355}$$

The Fokker-Planck equation for a single particle in the mean velocity field u_ε reads

$$\frac{\partial \psi}{\partial t} = -v_x \frac{\partial}{\partial x} \psi - \frac{\partial}{\partial v_x} \{(\alpha - \beta v_x^2) v_x + \mu(u_\varepsilon - v_x)\} \psi + D \frac{\partial^2}{\partial v_x^2} \psi. \tag{356}$$

Here we omit the index i for simplicity. The velocity $u_\varepsilon = u_\varepsilon(x, t)$ is the mean field velocity sensed by the particle. In the continuous description we may express it as an integral over the distribution function:

$$u_\varepsilon = \frac{1}{\int_{S_\varepsilon} \rho(x', t) \mathrm{d}x'} \int_{S_\varepsilon} \mathrm{d}x' \int \mathrm{d}v' v' \psi(x', v', t). \tag{357}$$

Here S_ε represents the spatial neighborhood of the focal particle, which is defined via a metric distance: $x \in S_\varepsilon$ if $|x' - x| < \varepsilon$. For finite ε it may be seen as an approximation of the first velocity moment $\langle v \rangle$ under the assumption of a homogeneous density distributin on the corresponding length scale.

Inserting Eq. (356) in to Eq. (353) and using $\lim_{v \to \pm\infty} P(x, v, t) = 0$, the terms with partial derivatives with respect to v can be partially integrated, yielding

$$\frac{\partial}{\partial t}(\rho\langle v^n\rangle) = -\frac{\partial}{\partial x}\rho\,\langle v^{n+1}\rangle + n\,\rho\left[\alpha\,\langle v^n\rangle - \beta\,\langle v^{n+2}\rangle + \mu(u_\varepsilon\langle v^{n-1}\rangle - \langle v^n\rangle)\right]$$
$$+ n\,(n-1)\,D\,\rho\,\langle v^{n-2}\rangle. \tag{358}$$

We rewrite the velocity of the focal particle as a sum of the local velocity field $u(x, t)$ plus some deviation δv: $v = u + \delta v$. Furthermore, we assume $\langle \delta v^l \rangle = 0$ for odd exponents l ($l = 1, 3, 5, \dots$). Thus we obtain for the moments (up to $l = 4$):

$$\langle v \rangle = u, \tag{359a}$$
$$\langle v^2 \rangle = u^2 + T, \tag{359b}$$
$$\langle v^3 \rangle = u^3 + 3\,u\,T, \tag{359c}$$
$$\langle v^4 \rangle = u^4 + 6\,u^2\,T + T^2 + \theta. \tag{359d}$$

Here, T is the mean squared velocity deviation $T = \langle \delta v^2 \rangle$, which we will refer to as the "temperature" of the active particle gas, whereas θ is the average of the mean squared temperature fluctuations defined as

$$\theta = \left\langle \left((v - u)^2 - T\right)^2 \right\rangle = \langle \delta v^4 \rangle - T^2. \tag{360}$$

Now we can insert Eqs. (359) into Eq. (358). Considering the dynamics up to $n = 2$, after some calculus we arrive at a set of three coupled partial differential equations for the evolution of the density $\rho(x, t)$, the mean velocity field $u(x, t)$, and the temperature field $T(x, t)$:

$$\frac{\partial}{\partial t}\rho = -\frac{\partial}{\partial x}\left(\rho\,u\right) \tag{361a}$$
$$\frac{\partial u}{\partial t} + u\frac{\partial}{\partial x}u = \alpha\,u - \beta\,u\,\left(u^2 + 3T\right) + \mu(u_\varepsilon - u) - \frac{\partial T}{\partial x} - \frac{T}{\rho}\frac{\partial \rho}{\partial x} \tag{361b}$$
$$\frac{1}{2}\left(\frac{\partial T}{\partial t} + u\,\frac{\partial\,T}{\partial x}\right) = (\alpha - \mu)\,T - \beta\,T\left(3u^2 + T\right) - \beta\,\theta + D - T\frac{\partial u}{\partial x}. \tag{361c}$$

Let us consider for simplicity an isotropic system with vanishing gradients in mean velocity u and temperature T, which is fully analytically tractable and represents a reasonable approximation of the system dynamics at high particle densities and large ε. In this case, the local velocity in the velocity alignment force equals the constant mean velocity field across the system $u_\varepsilon = u$, and we end up with the following two ordinary differential equations for the temporal evolution of u and T:

$$\frac{du}{dt} = \alpha\,u - \beta\,u\,\left(u^2 + 3T\right), \tag{362a}$$
$$\frac{1}{2}\frac{dT}{dt} = (\alpha - \mu)\,T - \beta\,T\left(3u^2 + T\right) - \beta\theta + D. \tag{362b}$$

In order to obtain a closed system of equations, we neglect the temperature fluctuations by setting $\theta = 0$ in Eq. (360), which is a reasonable assumption at small noise intensities. Thus, the above differential equations constitute a two-dimensional dynamical system, with 6 fixed points (stationary solutions) in the (u, T) phase space, which can be analyzed by means of linear stability analysis.

The stationary solutions $(du/dt = dT/dt = 0)$ for u and T read:

$$u_{1,2} = 0, \quad T_{1,2} = \frac{\alpha - \mu \pm \sqrt{(\alpha - \mu)^2 + 4\beta D}}{2\beta}; \tag{363a}$$

$$u_{3,4} = \pm\frac{\sqrt{10\alpha - 3(\mu - \Delta)}}{4\sqrt{\beta}}, \quad T_{3,4} = \frac{2\alpha + \mu - \Delta}{16\beta}; \tag{363b}$$

$$u_{5,6} = \pm\frac{\sqrt{10\alpha - 3(\mu + \Delta)}}{4\sqrt{\beta}}, \quad T_{5,6} = \frac{2\alpha + \mu + \Delta}{16\beta}, \tag{363c}$$

with $\Delta = \sqrt{(2\alpha + \mu)^2 - 32\beta D}$.

The kinetic temperature T_j has to be positive, therefore, T_1 (positive square root) is the only physically reasonable solution for $u = 0$.

The first solution with vanishing mean velocity $u = 0$ describes a disordered phase. For $D = 0$, the temperature $T = \frac{\alpha - \mu}{\beta} = v_0^2$ equals the square of the stationary velocity of individual particles. The kinetic energy of all particles consists only of fluctuations, no systematic translational motion occurs. The second pair of solutions corresponds to translational modes which are stable below a critical noise intensity. The two solutions correspond to translational motion with positive or negative velocity u, thus, to a collective motion of the particles to the left or right. Without noise, $T_{3,4} = 0$, and the stationary mean velocity reduces to $u_{3,4} = \pm\sqrt{\alpha/\beta}$. Increasing the noise rises the kinetic temperature, and results in a decrease of the mean speed $|u|$.

The last solution pair describes unstable modes, for which the temperature decreases and the mean speed increases with increasing noise intensity D.

For low alignment strength $\mu < 2\alpha/3$, the disordered phase is always a stable solution; for $\mu > 2\alpha/3$, the linear stability analysis of the mean-field equations predicts the existence of a critical noise intensity

$$D_{d,\mathrm{crit}} = \frac{\alpha(3\mu - 2\alpha)}{9\beta}, \tag{364}$$

which determines the stability boundary of the disordered solution. Starting from large noise intensities where the disordered solution is stable and decreasing the noise below $D_{d,\mathrm{crit}}$, we observe a pitchfork-bifurcation, and the disordered phase becomes unstable. Depending on the value of μ, the pitchfork-bifurcation is either sub- or super-critical. For $\mu < 10\alpha/3$, the disordered solution becomes unstable through a collision with the two unstable translational solutions, whereas for $\mu > 10\alpha/3$ no unstable translational solutions exist and the disordered solution becomes unstable directly through the appearance of the two stable translational solutions (see Fig. 54). Thus, for $\mu > 2\alpha/3$ and $D < D_{d,\mathrm{crit}}$, only the translational solutions $u_{3,4}$ are stable.

For $\mu < 10\alpha/3$ there exists a second critical noise intensity which determines the stability of the ordered phase (translational solutions, $u \neq 0$). Above the critical noise intensity

$$D_{o,\mathrm{crit}} = \frac{(2\alpha + \mu)^2}{32\beta} \tag{365}$$

all translational solutions become unstable through a saddle-node bifurcation (Fig. 54a,b).

Due to the symmetry of the translational solutions $u_3 = -u_4$, we may distinguish the disordered phase and the ordered (translational) phase in simulations by measuring the global mean speed in our simulations:

$$\langle |u| \rangle = \left\langle \left| \frac{1}{N} \sum_{i=1}^{N} v_i \right| \right\rangle. \tag{366}$$

Here, $\langle \cdot \rangle$ denotes temporal average after the system has reached a stationary state.
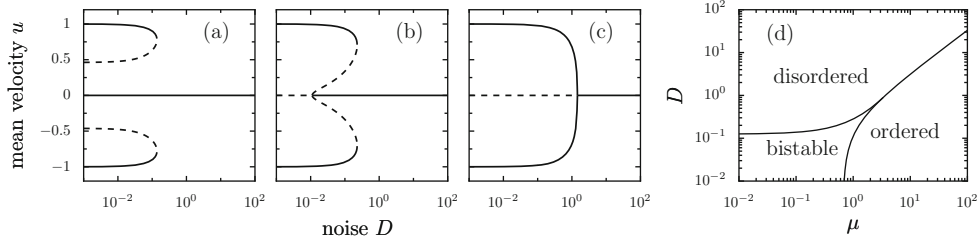
Fig. 54. Bifurcation diagram of the mean velocity u vs. noise intensity D as predicted from the mean field theory for different velocity alignment strengths ($\alpha = \beta = 1$): (a) $\mu < 2\alpha/3$ ($\mu = 0.1$), (b) $2\alpha/3 < \mu < 10\alpha/3$ ($\mu = 0.7$) and (c) $\mu > 10\alpha/3$ ($\mu = 5.0$). (d) Phase diagram with respect to velocity alignment μ and noise intensity D [296].

The stationary speed of the ordered phase versus noise intensity obtained from numerical simulations with ordered state as initial condition are in a good agreement with the theoretical predictions from the mean field theory. But simulations with disordered initial condition reveal an unexpected instability of the disordered solution. At finite μ the numerical simulations show that at intermediate D the disordered solution $u = 0$ becomes unstable via a spontaneous symmetry breaking, which is not predicted by the mean field theory.

We reproduced the instability of the disordered solution in numerical simulations for intermediate noise strengths for different particle numbers and for global coupling ($\varepsilon = L$). This suggests that it cannot be simply dismissed as a pure finite size effect or an effect of density fluctuations and should be associated with the neglected higher order fluctuations. The latter conclusion is supported by the agreement of the theoretical result and numerics at low D, where temperature fluctuations θ are negligible, as well as with deviations of the mean field temperature from the exact solution for T in the limit $\mu = 0$ [121,296]. Due to the nonlinearity of the friction function, the temperature does not increase monotonically with D as predicted by the mean field theory but exhibits a minimum at intermediate noise intensities [296]. This in turn has a destabilizing effect on the disordered state. Therefore we expect that the extension of the mean field theory to higher orders would account for this effect at the expense of the analytical tractability of the mean field solutions [115].

The same approach can be also extended to two dimensional systems where the mean field velocity is a vector: $\mathbf{u} = (u_x, u_y) = (\langle v_x \rangle, \langle v_y \rangle)$ and the temperature is given by a tensor $\hat{\mathbf{T}}$. For simplicity we assume $\hat{\mathbf{T}}$ to be a diagonal matrix with the diagonal components $(T_x, T_y) = (\langle \delta v_x^2 \rangle, \langle \delta v_y^2 \rangle)$.

$$\frac{\partial}{\partial t}\rho = -\nabla\left(\rho\mathbf{u}\right) \tag{367a}$$

$$\frac{\partial u_x}{\partial t} + \mathbf{u}\nabla_{\mathrm{r}}u_x = \alpha u_x - \beta u_x\left(\mathbf{u}^2 + 3T_x + T_y\right) + \mu(u_{\varepsilon,x} - u_x)$$
$$- \frac{\partial T_x}{\partial x} - \frac{T_x}{\rho}\frac{\partial\rho}{\partial x} \tag{367b}$$

$$\frac{1}{2}\left(\frac{\partial T_x}{\partial t} + \mathbf{u}\nabla_{\mathrm{r}}T_x\right) = (\alpha - \mu)T_x - \beta T_x\left(\mathbf{u}^2 + 2u_x^2 + T_x + T_y\right) - \beta\theta_x$$
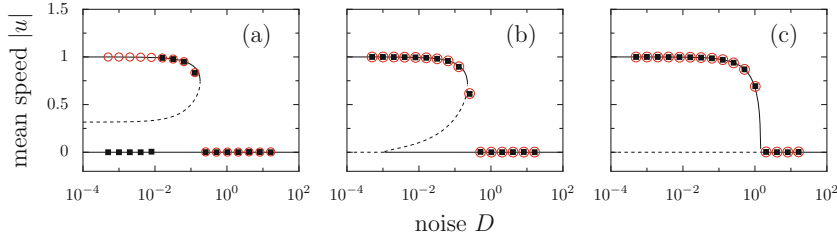$$+ D - T_x\frac{\partial u_x}{\partial x}. \tag{367c}$$

Fig. 55. (Color online) Comparison of the stationary solution obtained from simulation with theoretical prediction from the mean field theory for different velocity alignment strengths: $\mu = 0.4$ (a), $\mu = 0.67$ (b) and $\mu = 5.0$ (c). Other parameters used: particle number $N = 8192$, simulation domain $L = 500$, velocity alignment range $\epsilon = 50$ and $\alpha, \beta = 1.0$. The initial conditions were either the disordered state (black filled squares) or the ordered state (red circles). Solid (dashed) lines show the stable (unstable) stationary solutions of the mean-field equations [296].

The corresponding equations for u_y and T_y can be obtained by interchanging the indices. We can further simplify the above set of equations by choosing a reference frame, where $u_x = u_{||} = u$ corresponds to the mean field velocity and the orthogonal component vanishes $u_y = u_\perp = 0$.

Assuming again the simplest case of a spatially homogeneous system, we obtain the following set of coupled (ordinary) differential equations:

$$\frac{du}{dt} = \alpha u - \beta u \left(u^2 + 3T_{||} + T_\perp \right), \tag{368a}$$

$$\frac{1}{2}\frac{dT_{||}}{dt} = (\alpha - \mu)T_{||} - \beta T_{||} \left(3u^2 + T_{||} + T_\perp \right) + D, \tag{368b}$$

$$\frac{1}{2}\frac{dT_\perp}{dt} = (\alpha - \mu)T_\perp - \beta T_\perp \left(u^2 + T_{||} + T_\perp \right) + D, \tag{368c}$$

where $T_{||}$ and $T_\perp$ are the temperature components parallel and perpendicular to the mean field direction of motion. For $u = 0$ (disordered state) the components on $\mathbf{T}$ can be easily calculated from (368) and the corresponding solution reads:

$$u_1 = 0, \tag{369a}$$

$$T_{||,1} = T_{\perp,1} = T_1 = \frac{\alpha - \mu + \sqrt{(\alpha - \mu)^2 + 8\beta D}}{4\beta}. \tag{369b}$$

In the case of vanishing noise $D = 0$, the ordered solution can be immediately obtained as $u = \sqrt{\alpha/\beta}$ and $T_{||} = T_\perp = 0$. For $D > 0$ the temperature component parallel to the direction of motion is smaller than the perpendicular one: $T_{||} < T_\perp$.

For the general ordered state with $u > 0$ and $D > 0$ we were not able to obtain explicit stationary solution for u, $T_{||}$ and $T_\perp$ of the above ODE system (368) but the stable and unstable solutions can be determined by a numerical continuation methods as for example provided by the numerical software XPPAUT/AUTO [84,122].

A possible approach to find an explicit solution is to reduce the dimensionality of the problem. We may use the fact that at a fixed time t we always find a coordinate frame where $u_x = u_y = \tilde{u}$. In this coordinate frame due to the symmetry of the involved equations we obtain also $T_x = T_y = \tilde{T}$. Based on this observation we reduce the full problem (367) from a four dimensional system to a two dimensional system
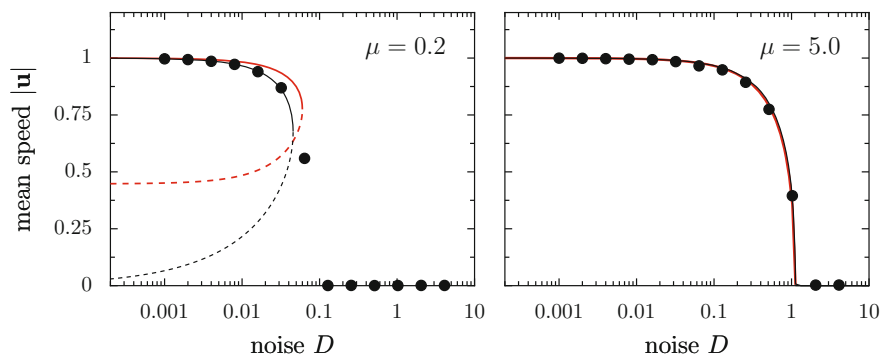
Fig. 56. Comparison of the mean field speed $|u|$ obtained from Langevin simulations (symbols) of the RH-model in two spatial dimensions at high density with the results of the mean field theory for the homogeneous case. The black lines represent the solutions obtained from the full system of mean field ODE's. The red lines represent the mean field solutions from the reduced system. The stable solutions are shown as solid lines, whereas dashed lines indicate the unstable solution. The simulations were performed with periodic boundary condition and with the disordered state as initial condition. Other parameters: $\alpha = 1$, $\beta = 1$, $L = 200$, $\varepsilon = 20$, $N = 4096$ [299].

in u and T, which in the homogeneous case simplifies to

$$\frac{d\tilde{u}}{dt} = \alpha\tilde{u} - \beta\tilde{u}\left(2\tilde{u}^2 + 4\tilde{T}\right), \tag{370a}$$

$$\frac{1}{2}\frac{d\tilde{T}}{dt} = (\alpha - \mu)\tilde{T} - \beta\tilde{T}\left(4\tilde{u}^2 + 2\tilde{T}\right) + D. \tag{370b}$$

This gives us a system of equations similar to the problem for $d = 1$, with the same structure of stationary solutions but different coefficients.

The comparison of the stationary solutions of the reduced systems with the corresponding solutions of the full systems obtained with XPPAUT/AUTO reveals a differences at low velocity alignment strengths μ (Fig. 56). The velocity of the stable ordered solution of the full system decreases stronger and exhibits an earlier breakdown with increasing D. Furthermore from the position of the disordered branch it can be deduced that the basin of attraction of the ordered state at low D for the full system is larger than for the reduced two dimensional system. But at large μ the differences between the two types of mean field solution vanish and the reduced system (370) gives a good approximation as shown in Fig. 56.

The reason for the discrepancy between the two mean field solutions at low μ is that the performed dimensional reduction throws away all informations about the asymmetry of temperature components parallel and perpendicular to the mean velocity. At large μ the evolution of the temperature coefficients is dominated by the $-\mu T_k$ term and may in a crude approximation simply be assumed as linear for both components, so that the asymmetry in the temperature components can be neglected.

In general without knowing the temperatures $T_\parallel$ and $T_\perp$ the mean speed, can be written as

$$|u| = \sqrt{v_0^2 - 3T_\parallel - T_\perp} \tag{371}$$

where $v_0^2 = \alpha/\beta$. In the limit of large μ close to the critical noise, where $\alpha, \beta \ll \mu, D$ we may approximate the temperature as $T_\parallel = T_\perp = T = D/\mu$ and obtain a simple

expression for the ordered state

$$|u| = \sqrt{v_0^2 - \frac{4D}{\mu}}. \tag{372}$$

In this limit the critical noise may be approximated as $D_{d,\text{crit}} \approx v_0^2 \mu/4 = D_{\text{crit}}$ and the above equation may be rewritten as:

$$|u| = 2\mu^{-\frac{1}{2}}(D_{\text{crit}} - D)^{\frac{1}{2}}, \tag{373}$$

which is the standard form of the order parameter for a continuous (second order) phase transition. A similar result can be also obtained for self-propelled particles with constant velocity [272], corresponding to the limit $\alpha, \beta \to \infty$ with $\alpha/\beta = v_0^2 = const.$ with $T_\parallel = 0$ and $T_\perp = D/\mu$.

The mean-field theory, suggest the possibility of a discontinuous transition from ordered to disordered state (saddle-node bifurcation) as a consequence of a nonlinear friction function at intermediate alignment strenghts. However, for limiting cases, where the nonlinear nature of the friction function is negligible, e.g. for vanishing velocity fluctuations (see next section) or strong velocity alignment, the transition in a homogeneous system is a continuous one. We should note that for very small alignment strengths μ the critical noise intensity becomes also very small. In this limit, for arbitrary friction functions, the small passive fluctuation act essentially only on the direction of motion and the speed of individual particles may be assumed as constant. Thus, in this case, the collective mean-field dynamics reduce effectively to a Kuramoto-model of coupled oscillators, which also shows a continuous transition from order (synchronized state) to disorder.

Recently, it was shown that the spatially homogeneous state is unstable in systems of interacting self-propelled particles [36,322,323]. Thus, the assumption of a spatially homogeneity should be considered only as an approximation, for sufficiently large ε. For $L \gg \varepsilon$ strong density inhomogeneities appear, such as traveling bands, which affect the global behavior of the system [38,60,239]. A detailed discussion of the spatial inhomogeneities in self-propelled particle systems will follow in Sect. 7.

In contrast to $d = 1$ no stable disordered solutions at low μ and low noise intensities D were observed in simulations (Fig. 56). A possible explanation can be the reduced basin of attraction of the disordered solution for $d = 2$ together with the already discussed instability of the disordered solution due to the neglected temperature fluctuations θ_k observed already for $d = 1$.

A more heuristic explanation for the instability of the disordered solution in two spatial dimensions for low μ and low D, in contrast to the one-dimensional case, is the absence of a velocity potential barrier between different direction of motion: In two dimensions the particles can change their direction of motion by continuous angular drift or diffusion. Thus, any small fluctuation in **u** in a finite system at vanishing noise $(D \ll 1)$ will be amplified and eventually will lead to perfect velocity alignment.

6.2.3 Mean-field theory for onset of polar and nematic order

The Vicsek-model [361] is considered the simplest model for collective motion of self-propelled particles (SPPs). It has become quite popular because it is computationally much more efficient than many other models for collective motion of active particles. In the Vicsek model, point-like particles moving with a velocity vector of constant magnitude interact by aligning their velocity direction to the local average velocity.
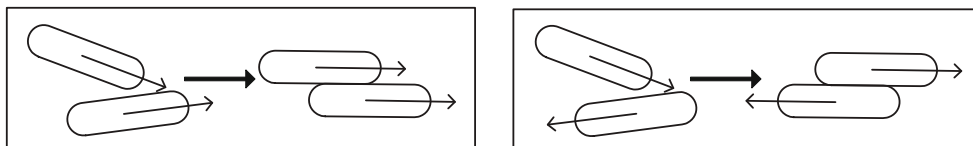
Fig. 57. Illustration of nematic LC-alignment of polar self-propelled particles illustrated by inelastic collisions of rods. Particles incoming at a small angle (left) align "polarly", but those colliding almost head-on slide past each other, maintaining their nematic alignment (right).

The Vicsek model can be considered as a model of moving spins, in which the velocity of the particles is given by the spin-vector. Extending this analogy with spin systems we denote this polar alignment mechanism as ferromagnetic (F-alignment). Initial simulations of the Vicsek model in 2D seemed to indicate a second-order phase transition which leads to long-range orientational order in collectively moving SPPs [247,361]. Later work pointed towards a first order phase transition to orientational order in sufficiently large systems [60]. Theoretical interest was stirred by the the fact that in analogous equilibrium systems of non-moving spins no long-range order is possible [201,233].

F-alignment is one possible alignment mechanism, but clearly not the only one. If a system of e.g. self-propelled rods interacts simply by volume exclusion, particles may end up moving in the same direction as well as in opposite directions. Such an apolar interaction mechanism corresponds to interactions in liquid crystals where apolar particles get locally aligned [85]. In analogy to these systems we name this mechanism hence liquid crystal alignment (LC-alignment). An graphical illustration for LC-alignment is given in Fig. 57. In a system of SPPs with LC-alignment particles align their velocity to the local average director. Orientational order observed in simulations with SPPs with LC-alignment refers to the emergence of a global director in the system, while for F-alignment orientational order refers to the appearance of a global direction of motion. In the following, two alternative continuum models for SPPs with polar, ferromagnetic resp. apolar, liquid-crystal like interaction will be introduced and compared to the Vicsek model and a recent variation [141,272] with LC-alignment interactions, the Peruani model. For the continuum version of the SPP models with local ferromagnetic resp. liquid crystal alignment a mean-field theory describing the onset of collective motion is derived and compared to simulation results obtained with the Vicsek model.

We consider point-like particles moving at constant speed in two dimensions and assume an over-damped situation such that the state of particle i at time t is given by its position $\mathbf{r}_i$ and its direction of motion φ_i. The evolution of these quantities follow:

$$\dot{\mathbf{r}}_i = v_0 \mathbf{e_v}(\varphi_i) \tag{374}$$

$$\dot{\varphi}_i = -\gamma \frac{\partial U}{\partial \varphi_i}(\mathbf{r}_i, \varphi_i) + \tilde{\eta}_i(t) \tag{375}$$

where γ is a relaxation constant, and U the interaction potential between particles, and hence $\frac{\partial U}{\partial \varphi_i}(\mathbf{r}_i, \varphi_i)$ defines the velocity alignment mechanism. Moreover, v_0 represents the active constant speed of the particles, the unit vector $\mathbf{e_v}(\varphi_i)$ is again defined as $\mathbf{e_v}(\varphi_i) = (\cos(\varphi_i), \sin(\varphi_i))$, and $\tilde{\eta}_i(t)$ is an additive white noise. In the sense of Sect. 3.2, it is an active noise acting perpendicular to the direction of motion. Eqs. (374) and (375) are expressed in terms of first derivatives. In this way, v_0 in

Eq. (374) can be considered as an active force divided by a translational friction coefficient. In analogy to spin systems, the ferromagnetic velocity alignment mechanism is given by a potential defined as:

$$U_F(\mathbf{r}_i, \varphi_i) = - \sum_{|\mathbf{r}_i - \mathbf{r}_j| \leq \varepsilon} \cos(\varphi_i - \varphi_j) \tag{376}$$

where ε is the radius of interaction of the particles. For the liquid-crystal alignment mechanism, we choose the potential originally introduced by Lebwohl and Lasher on a lattice [212] which reads:

$$U_{LC}(\mathbf{r}_i, \varphi_i) = - \sum_{|\mathbf{r}_i - \mathbf{r}_j| \leq \varepsilon} \cos^2(\varphi_i - \varphi_j). \tag{377}$$

One can add a coupling strength coefficient to the expressions (376) and (377). We assume that the coupling strength is absorbed in γ in Eq. (375). Notice that the potential given by Eq. (376) exhibits one minimum, while Eq. (377) has two minima, which correspond to particles pointing in the same direction and particles pointing in opposite directions.

In the limiting case of very fast angular relaxation we obtain from Eqs. (374) and (375) the updating rules:

$$\mathbf{r}_i^{t+\Delta t} = \mathbf{r}_i^t + v_0 \mathbf{e_v}\left(\varphi_i^t\right) \Delta t \tag{378}$$

$$\varphi_i^{t+\Delta t} = \arg\left(\sum_{|\mathbf{r}_i^t - \mathbf{r}_j^t| \leq \varepsilon} \mathbf{f}(\mathbf{e_v}(\varphi_j^t), \mathbf{e_v}(\varphi_i^t)) \right) + \eta_i(t) \tag{379}$$

where $\arg(\mathbf{b})$ indicates the angle of the vector $\mathbf{b}$ in polar coordinates, η_i^t is the random increment of the angle in the interval Δt comparable to a Wiener Process and giving rise to angular diffusion (see Sect. 3.1.4). The noise sources are statistically independent for different particles. In simulations we have used equally distributed random numbers from $\eta_i(t)\varepsilon\left[-\frac{\eta}{2}, \frac{\eta}{2}\right]^3$. The term $\mathbf{f}(\mathbf{a}, \mathbf{b})$ describes the interactions and is defined as follows. For F-alignment, $\mathbf{f}(\mathbf{a}, \mathbf{b}) = \mathbf{a}$ and Eqs. (378) and (379) correspond to the Vicsek model [361]. For LC-alignment, $\mathbf{f}$ takes the form:

$$\mathbf{f}(\mathbf{a}, \mathbf{b}) = \begin{cases} \mathbf{a} & \text{if } \mathbf{a} \cdot \mathbf{b} \geq 0 \\ -\mathbf{a} & \text{if } \mathbf{a} \cdot \mathbf{b} < 0. \end{cases} \tag{380}$$

This interaction was introduced by Peruani et al.. Hence we will refer to the corresponding model (Eqs. (378), (379), (380)) as the Peruani model. To decide if the described local alignment mechanism give rise to global order, suitable order parameters have to be defined. One such order parameter that quantifies the direction of alignment and collective motion is the modulus of the normalized total momentum (analogous to the magnetization in the XY-model [201, 233]), that we express as:

$$S^F = \left| \frac{1}{N} \sum_{i=0}^{N} \mathbf{e_v}\left(\varphi_i^t\right) \right|, \tag{381}$$

where N stands for the total number of particles in the system. The quantity S^F has the value 1 when all particle move in the same direction (perfect F-alignment).

---

[3] Variation of the temporal interval Δt implies a scaling of η with the interval. For the case of white noise in Eq. (374) the variance of $\eta_i(t)$ increases linearly Δt.
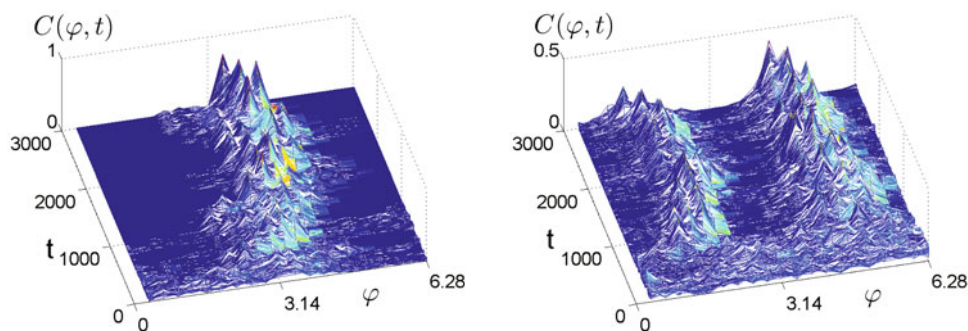
Fig. 58. Temporal evolution of the velocity direction distribution (angular distribution) in simulations of self-propelled particles with very fast angular relaxation, where (a) corresponds to the case F-alignment (Vicsek-model), while (b) shows the case of LC-alignment (Peruani model). Number of particles $N = 100$, radius of interaction $\varepsilon = 2$, linear system size $L = 42.4$, and noise amplitude $\eta = 0.25$.

In contrast, S^F is equal to 0 in the disordered case in which particles point in any direction with equal probability. An alternative measure for collective motion is the velocity direction distribution in two dimensions $C(\varphi)$. For high values of the noise, $C(\varphi)$ is flat. When the noise is decreased below a critical noise η_c, a single peak arises in $C(\varphi)$ indicating the onset of orientational order, see Fig. 58(a).

On the other hand, for perfect nematic order or LC-alignment, *i.e.* half of all particles move in one direction, and the other half in the opposite direction, S^F is identical zero. Clearly, S^F cannot distinguish between a state of LC-alignment and a disordered state. To study such LC orientational ordering, one can employ the order matrix Q of liquid crystals [85]. For two dimensions one takes the largest eigenvalue S^{LC} of Q as appropriate order parameter:

$$S^{LC} = \frac{1}{4} + \frac{3}{2}\sqrt{\frac{1}{4} - \frac{1}{N^2}\left\{\sum_{i,j}^{N} v_{xi}^2 v_{yj}^2 - v_{xi}v_{yi}v_{xj}v_{yj}\right\}} \tag{382}$$

where v_{xi} and v_{yi} are defined as $v_{xi} = \cos(\varphi_i)$ and $v_{yi} = \sin(\varphi_i)$. The order parameter S^{LC} takes the value 1 when all particles are aligned along the same director, and the value $\frac{1}{4}$ in a disordered phase without any preferred orientation. Alternatively, the velocity direction distribution $C(\varphi)$ can be considered. This function displays two peaks separated by π for simulations of the Peruani model low noise amplitudes, see Fig. 58(b).

A system of SPPs may be conveniently described through the one particle density in the phase space $\tilde{\psi}(\mathbf{r}, \mathbf{v}, t) = \psi(\mathbf{r}, \varphi, t)$ which equals the one particle probability density function $P(\mathbf{r}, \mathbf{v}, t)$ multiplied by the particles number N. Then the usual particle density at a point $\mathbf{r}$ is obtained as

$$\rho(\mathbf{r}, t) = \int_0^{2\pi} \psi(\mathbf{r}, \varphi, t)\, d\varphi. \tag{383}$$

For simplicity, we consider the angular velocity direction distribution:

$$C(\varphi, t) = \int_\Omega \psi(\mathbf{r}, \varphi, t)\, d\mathbf{r} \tag{384}$$

and neglect spatial inhomogeneities in the orientation of the particles. We recall that in the individual-based model the kinetic energy is conserved, while the momentum is

not. For F-alignment, the system tends to increase the total momentum, while for LC-alignment the tendency is to decrease it. The continuum approach has to reflect that particles always move at constant speed and that number of particles is conserved.

Consequently, the following evolution equation for $\psi(\mathbf{r}, \varphi, t)$ is obtained:

$$\partial_t \psi = D_\varphi \partial_{\varphi\varphi} \psi - \partial_\varphi [u_\varphi \psi] - \bigtriangledown_\mathbf{r} [\mathbf{u_r} \psi], \tag{385}$$

where $u_\varphi \psi$ and $\mathbf{u_r} \psi$ are deterministic fluxes, which reflect the local alignment mechanism and active motion. The quantity D_φ refers to the angular diffusion whereby we have assumed Gaussian noise in Eq. (375). It depends on the square of the noise amplitude. The term $u_\varphi(\mathbf{r}, \varphi)$ describes mean angle velocity of the alignment interactions of particles with all neighboring particles which are at a distance less than ε from their location $\mathbf{r}$. It reads

$$u_\varphi = -\gamma \int_{R(\mathbf{r})} d\mathbf{r}' \int_0^{2\pi} d\varphi' \frac{\partial U(\mathbf{r}, \varphi, \mathbf{r}', \varphi')}{\partial \varphi} \psi(\mathbf{r}', \varphi', t) \tag{386}$$

where $U(\mathbf{r}, \varphi, \mathbf{r}', \varphi')$ represents the pair potential between a particle located at $\mathbf{r}$ and pointing in direction φ with another one at $\mathbf{r}'$ and pointing in direction φ'. $R(\mathbf{r})$ denotes the interaction neighborhood. The above models have the property $U(\mathbf{r}, \varphi, \mathbf{r}', \varphi') = U(\varphi, \varphi')$, i.e. within the interaction radius the potential between particles has equal strength and is homogeneous in space. Finally, u_φ represents the "torque" felt by a particle located at $\mathbf{r}$ and pointing in direction φ. The expression for $\mathbf{u}_r$ simply reads

$$\mathbf{u}_r = v_0 \mathbf{e_v}(\varphi). \tag{387}$$

Integrating both sides of Eq. (385) over the space Ω and assuming a homogeneous spatial distribution of particles $\psi(\mathbf{r}, \varphi, t) = C(\varphi, t)\rho_0/N$, where ρ_0 is defined as $\rho_0 = N/L^2$ and L is the linear size of the system, we obtain an evolution equation for $C(\varphi, t)$:

$$\frac{\partial C(\varphi, t)}{\partial t} = D_\varphi \frac{\partial^2 C(\varphi, t)}{\partial \varphi^2} + \gamma \frac{\pi \varepsilon^2}{L^2} \partial_\varphi \left[\left\{ \int_0^{2\pi} d\varphi' \frac{\partial U(\varphi, \varphi')}{\partial \varphi} C(\varphi', t) \right\} C(\varphi, t) \right]. \tag{388}$$

The homogeneous angular distribution is a steady state of Eq. (388). The parameters for the onset of the orientational order and collective motion can be found by determining the linear instability of the disordered state. We start by analyzing the case of F-alignment. By dividing both sides of Eq. (388) by $\gamma \pi \varepsilon^2 / L^2$, and redefining time as $\tau = (\gamma \pi \varepsilon^2 / L^2)t$, and $D_\varphi' = D_\varphi / [\gamma \pi \varepsilon^2 / L^2]$ one obtains:

$$\frac{\partial C(\varphi, t)}{\partial \tau} = D_\varphi' \partial_{\varphi\varphi} C(\varphi, t) + \partial_\varphi \left[\left\{ \int d\varphi' \sin(\varphi - \varphi') C(\varphi', t) \right\} C(\varphi, t) \right]. \tag{389}$$

Next, a small perturbation of the homogeneous steady state is considered:

$$C(\varphi, t) = C^* + C_0 e^{in\varphi} e^{\lambda\tau}. \tag{390}$$

Note, that $e^{in\varphi}$ are eigenfunctions of the operators emerging from the linearization of Eq. (389) near the homogeneous steady state. By substituting into Eq. (389) and keeping only terms linear in C_0, we obtain the following eigenvalues:

$$Re(\lambda) = -D_\varphi' n^2 + \pi C^* \delta_{n,1}. \tag{391}$$

The only mode which can become unstable is $n = 1$ and the condition for the corresponding instability of the homogeneous, disordered state is

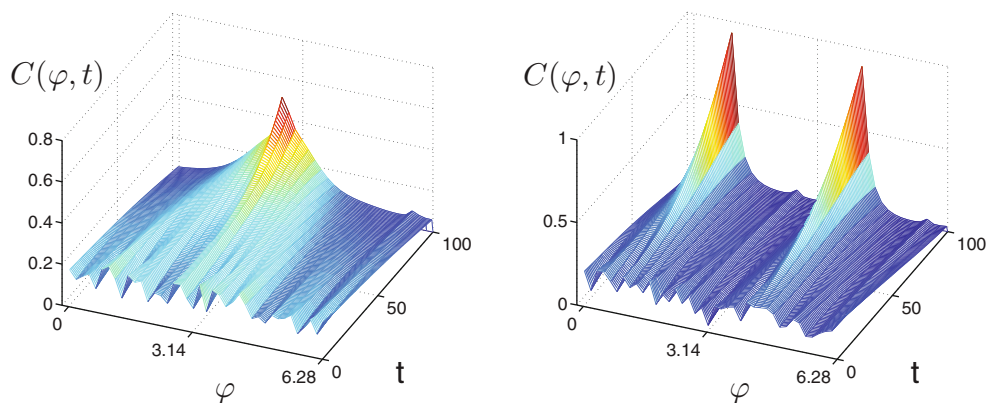$$\rho_0 > \frac{2D_\varphi}{\gamma \pi \varepsilon^2}, \tag{392}$$

Fig. 59. Temporal evolution of $C(\varphi, t)$. (top) F-alignment, numerical integration of Eq. (389) with $D_\varphi = 0.28$. (bottom) LC-alignment, numerical integration of Eq. (393) with $D_\varphi = 0.014$. For both, $C^* = 0.3183$, $\Delta t = 0.001$ and $\Delta\varphi = 0.16$. The initial condition is a random perturbation around C^*. Notice that for F-alignment a single peak emerges, while for LC-alignment the distribution develops two peaks [272].

with $\rho_0 = N/L^2$. For a given noise amplitude D_φ, there is a critical particle density above which the homogeneous solution is unstable. Fig. 59(a) shows that as a result a single peak emerges in $C(\varphi)$ from numerical integration of Eq. (389) in line with results found in simulations of the Vicsek model.

An analogous procedure for LC-alignment yields:

$$\frac{\partial C(\varphi, t)}{\partial \tau} = D'_\varphi \partial_{\varphi\varphi} C(\varphi, t) \tag{393}$$

$$+ \partial_\varphi \left[\left\{ \int d\varphi' 2\cos(\varphi - \varphi')\sin(\varphi - \varphi') C(\varphi', t) \right\} C(\varphi, t) \right].$$

As above a small perturbation to the homogeneous distribution $C(\varphi, t) = C^*$ is assumed, see Eq. (390). Again, $e^{in\varphi}$ are eigenfunctions of the linearized operator. Substituting Eq. (390) into Eq. (393) and keeping terms linear in C_0 the following expression for the eigenvalues is obtained:

$$Re(\lambda) = -D'_\varphi n^2 + 2\pi C^* \delta_{n,2}. \tag{394}$$

As for F-alignment, there is only one mode which can become unstable, but this time it is $n = 2$. The $n = 2$-mode exhibits two peaks separated by π, that correspond to two populations of particles moving in exactly the opposite direction. The homogeneous state is unstable for:

$$\rho_0 > \frac{4D_\varphi}{\gamma\pi\varepsilon^2}. \tag{395}$$

Again, this inequality defines a critical density above which the homogeneous solution is no longer stable. Fig. 58(c)–(d) shows the emergence of these two peaks for LC-alignment in individual-based simulations. Numerical integration of Eq. (393) above this critical density shows again two peaks in $C(\varphi, t)$, see Fig. 59(b). For a given density, there is a critical $D_{\varphi,c}$. Close to $D_{\varphi,c}$ we expect to observe that only one mode dominates $C(\varphi, t)$. As already mentioned, $n = 1$ is dominant for F-alignment and $n = 2$ governs LC-alignment. The steady state distribution $C_{st}(\varphi)$ near the instability has the form:

$$C_{st}(\varphi) \simeq C^* + B_1 \sqrt{D_{\varphi,c} - D_\varphi} \cos(\varphi - \varphi_0) \tag{396}$$

for F-alignment, while for LC-alignment it is:

$$C_{st}(\varphi) \simeq C^* + B_2\sqrt{D_{\varphi,c} - D_\varphi}\cos(2(\varphi - \varphi_0)) \tag{397}$$

where B_1, B_2 are constants and φ_0 is an arbitrary phase. In both cases the maximum amplitude of $C_{st}(\varphi)$ close to the $D_{\varphi,c}$ grows as $\sqrt{D_{\varphi,c} - D_\varphi}$. Inserting Eq. (396) into Eq. (381), we obtain the scaling form of the order parameter S^F:

$$S^F \simeq \tilde{B}_1\sqrt{\eta_c - \eta} \tag{398}$$

where $\tilde{B}_1$ is a constant. To obtain the scaling of the order parameter S^{LC}, Eq. (397) is inserted into Eq. (382):

$$S^{LC} \simeq \frac{1}{4} + \tilde{B}_2\sqrt{\eta_c - \eta} \tag{399}$$

where again $\tilde{B}_2$ is a constant. The above results confirm our findings for active Brownian particles from Sect. 6.2.2 in the limit of vanishing velocity fluctuations.

It is instructive to compare the results of the mean-field theory qualitatively to the results of individual-based simulations with respect to the scaling properties of the order parameters near the onset of orientational order. In addition, the prediction of the mean-field theory regarding the different critical noise amplitudes (resp. critical densities) for F- and LC-alignment can be compared with simulations of the Vicsek- and Peruani-model.

Figure 60 shows a comparison between the scaling predicted by the mean-field approach for S^{LC} (dashed curve) and the one obtained from individual-based simulations in the limit of very fast angular relaxation (symbols). One finds good agreement between the mean-field prediction and the simulations for the scaling of S near η_c that suggests that individual-based simulations with LC-alignment at high densities exhibit a mean-field type transition. Evidence seems to point towards a mean-field transition if we look at the scaling of the maximum amplitude of the angle distribution as function of the angular noise intensity η (see Fig. 60).

Finally, Fig. 60 shows that in individual-based simulations with the same parameters and different (namely LC- and F-) alignment mechanism, the limit of fast angular relaxation yields $\eta_c^{LC} < \eta_c^F$ as predicted by the mean-field theory. Note, however, that the simulations yield $2\eta_c^{LC} \approx \eta_c^F$, while the mean-field description predicts $\sqrt{2}\eta_c^{LC} = \eta_c^F$.

In summary, we have derived a mean-field theory for self-propelled particles which accounts for F- and LC-alignment. This approach predicts a continuous phase transition with the order parameter scaling with an exponent one half in both cases. In addition, the critical noise amplitude below which orientational order emerges is smaller for LC-alignment than for F-alignment, i.e., $\eta_C^{LC} < \eta_C^F$. These findings were confirmed by individual-based simulations with F- and LC-alignment.

Furthermore, we have assumed spatial homogeneous density to study the emergence of orientational order. Thus, the presented approach does not apply to situations where self-propelled particles show clustering at the onset of orientational order as will be discussed in the next section (Sect. 7). A better understanding of the problem should imply the study of the interplay between local orientational order and density fluctuations.

6.3 Alternative swarming mechanisms

6.3.1 Escape and pursuit – collective motion and group propulsion

Motivated by recent observations on cannibalistic behavior in locusts and crickets [25,324], we introduced a model of individuals (active particles) responding to others
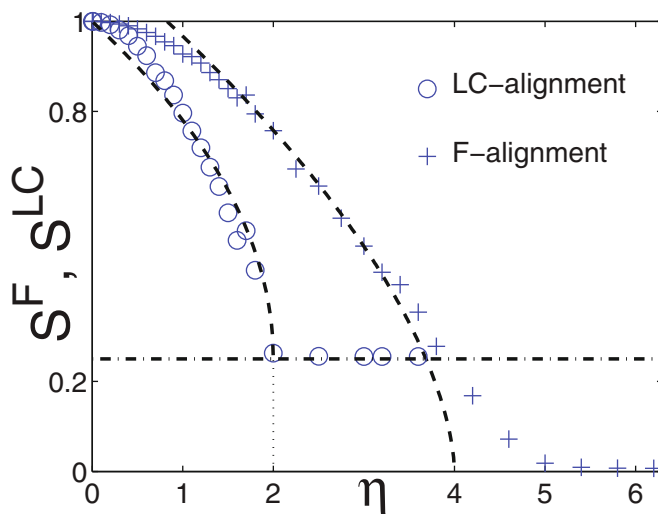
Fig. 60. Comparing simulations of particles with F-alignment (crosses) and LC-alignment (circles) in the limiting case of very fast angular relaxation. In both cases $N = 2^{14}$ and $\rho = 2.0$. Notice that the order parameter for F-alignment is S^F while for LC-alignment is S^{LC} (See text). The dashed horizontal line indicates the minimum value that S^{LC} could take. The dashed curves correspond to the best fit assuming an exponent 0.5, i.e., η_c was the fitting parameter [272].

with escape and pursuit behavior [27,294]. This biologically motivated interactions cannot be expressed simply in terms of an interaction potential as discussed in Section 6.1 and do not include a velocity alignment term as discussed in Sections 6.1 & 6.2, but constitute selective, velocity dependent attraction and repulsion interactions. Nevertheless they may lead to the onset of large scale collective motion in particular at high densities of individuals.

The behavioral response of the insects, which are particularly vulnerable to attacks from behind, was assumed in the following way:

– If approached from behind by another individual j a focal individual i increases its velocity away from it in order to prevent being attacked from behind. We refer to this behavior as *escape* (e).
– If the focal individual "sees" another individual up-front moving away, it increases its velocity in the direction of the escaping individual. We refer to this behavior as *pursuit* (p).
– No response in all other cases.

The motion of individual particles in two spatial dimension obeys the following Langevin dynamics:

$$\dot{\mathbf{r}}_i = \mathbf{v}_i, \quad \dot{\mathbf{v}}_i = -\gamma \mathrm{v}_i^{a-1} \mathbf{v}_i + \mathbf{F}_i^s + \sqrt{2D}\boldsymbol{\xi}_i. \tag{400}$$

The first term on the left hand side of the velocity equation (400) is a friction term with coefficient γ and an arbitrary power-law dependence on velocity represented by $a = 1, 2, 3, \ldots$. The social interaction of particles is described by $\mathbf{F}_i^s$. The last term is a non-correlated Gaussian random force with intensity D. A non-interacting particle ($\mathbf{F}_i^s = 0$) explores its environment by a continuous random walk, where the individual velocity statistics are determined by γ, a and D.

Furthermore we assume finite-size particles and introduce fully elastic hard-core collisions with a particle radius $R_{hc} = l_r/2$ (l_r-particle diameter) (see e.g. [45]).

The social force acting on the focal particle i is given as a sum of escape and pursuit force: $\mathbf{F}_i^s = \mathbf{f}_i^e + \mathbf{f}_i^p$ with

$$\mathbf{f}_i^e = \frac{1}{N_e} \sum_j -\hat{\mathbf{r}}_{ji} K_e(|v_{\rm rel}|)\theta(l_s - r_{ji})\theta(r_{ji} - l_r)\theta(-\mathbf{v}_i \cdot \mathbf{r}_{ji})\theta(-v_{\rm rel}), \quad \text{(401a)}$$

$$\mathbf{f}_i^p = \frac{1}{N_p} \sum_j +\hat{\mathbf{r}}_{ji} K_p(|v_{\rm rel}|)\theta(l_s - r_{ji})\theta(r_{ji} - l_r)\theta(+\mathbf{v}_i \cdot \mathbf{r}_{ji})\theta(+v_{\rm rel}), \quad \text{(401b)}$$

where $\hat{\mathbf{r}}_{ji} = (\mathbf{r}_j - \mathbf{r}_i)/|\mathbf{r}_j - \mathbf{r}_i|$ is the unit vector in the direction of the other individual j, and $v_{\rm rel} = \mathbf{v}_{ji} \cdot \hat{\mathbf{r}}_{ji} = (\mathbf{v}_j - \mathbf{v}_i)\hat{\mathbf{r}}_{ji}$ is the relative velocity of individuals j and i. The functions $K_{e,p} \geq 0$ determine the strength of the interactions. In the following we assume the response functions proportional to the relative speed: $K_{e,p} = \chi_{e,p}|v_{\rm rel}|$, where $\chi_{p,e} \geq 0$ are the corresponding interaction strengths. This choice of the response function leads to stronger response to fast approaching/escaping individuals in comparison to slowly moving ones.

The product of the θ-functions (step functions), which define the condition for the escape/pursuit interaction to take place can assume only two values: either 1 or 0. The product of the first two step functions is identical for both interaction types. It is 1 only if the individual j is within the social interaction zone defined by the hard-core distance l_r and the sensory range l_s: $l_r < r_{ji} < l_s$. The product of the last two step functions distinguishes the escape and pursuit interaction. The escape interaction takes place only if individual j is behind the focal individual i ($\mathbf{v}_i \cdot \mathbf{r}_{ji} < 0$) and is coming closer ($v_{\rm rel} < 0$), whereas the pursuit interaction takes place only if the individual j is in front of the focal individual i ($\mathbf{v}_i \cdot \mathbf{r}_{ji} > 0$) and is escaping it ($v_{\rm rel} > 0$).

The most important property of this asymmetric interactions is their anti-dissipative nature with respect to kinetic energy. Note that $\mathbf{F}_i^s$ leads only to acceleration of individuals and is analogous to the auto-catalytic mechanism proposed in [25].

Large scale numerical simulation of a N-particle system in a rectangular domain of size $L \times L$ with periodic boundary conditions show that at high density the escape and pursuit interaction leads to collective motion irrespective of the detailed parameter choice as long as the interaction is strong enough to counterbalance the individual fluctuations. Here we use for convenience a dimensionless density $\rho_s = Nl_s^2/L^2$ scaled by the interaction range.

At low ρ_s the behavior of the system depends strongly on the relative strength of escape and pursuit. This can be best understood if we consider the extreme cases of pure escape ($\chi_p = 0$) and pure pursuit ($\chi_e = 0$).

In the escape only case the particles try to keep their distance with respect to individuals approaching from behind. To the front only interactions via the short range repulsion take place. At low ρ_s an escaping particle will eventually move away from the approaching one. The probability of interaction within the characteristic time of velocity relaxation vanishes and the particles perform effectively a disordered Brownian motion. As ρ_s increases the frequency of escape interactions increases and an escaping particle will trigger escape responses from neighboring particles. We observe velocity correlation over several interaction length scales. Finally at high ρ_s a highly ordered state emerges where all particles are able to correlate their motion. At all ρ_s the density remains almost spatially homogeneous.

In the pursuit-only case the dynamics change dramatically: At low ρ_s we observe a highly inhomogeneous state initiated by formation of small particle clusters performing coherent collective motion. Without escape interaction the density of the clusters is only limited by the hard-core radius. At moderate noise intensities the clusters are sufficiently stable and a process of cluster fusion can be observed where larger clusters
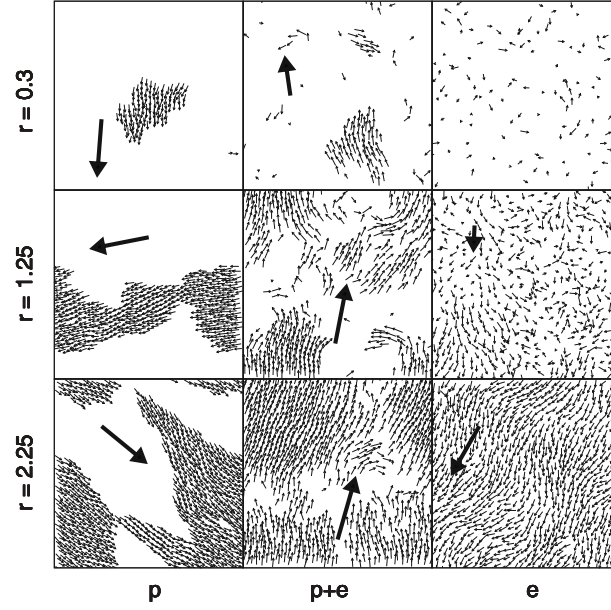
Fig. 61. Typical spatial configurations and particle velocities (small arrows) for pure pursuit (p), pursuit+escape (p+e) and pure escape (e) cases at different particle densities $\rho_s = 0.30$, 1.25, 2.25. Mean migration direction and speed U is indicated by large arrows ($U \approx 0$ for escape only and $\rho_s \ll 1$) [294].
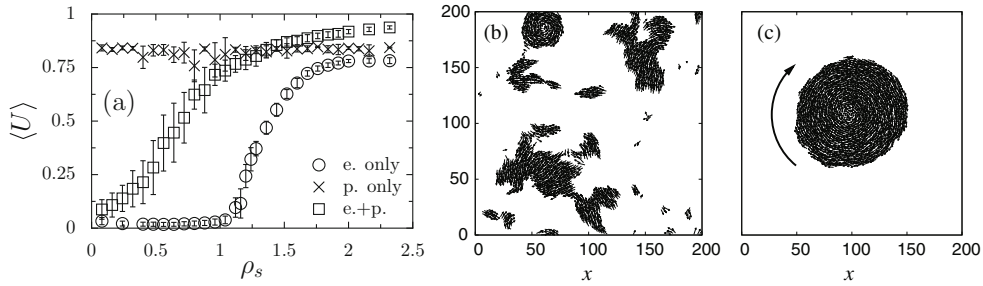

Fig. 62. (a) Mean velocity $\langle U \rangle$ for escape-only (circles) $\chi_e = 10$, $\chi_p = 0$, pursuit-only (crosses) $\chi_e = 0$, $\chi_p = 10$ and symmetric escape+pursuit (squares) $\chi_e = \chi_p = 10$ vs. ρ_s obtained from numerical simulations with periodic boundary conditions ($\gamma = 1$, $D = 0.05$, $a = 3$, $l_r = 2$, $l_s = 4$; only translational solutions were considered; error bars represent one standard deviation). Vortex formation for pursuit only: initially a rotating cluster nucleates from collision of two translational clusters at $x \approx 50$, $y \approx 180$ (b), which then grows through absorption of other translational clusters until a single rotating structure emerges (c). Figure adopted from [294].

absorb smaller clusters and solitary particles. The typical stationary configuration in a finite system with periodic boundary condition, and moderate noise, is a single cluster performing translational motion (Fig. 61). The migration speed $\langle U \rangle$ in Fig. 62(a) is given by the mean speed of a single cluster $\langle u \rangle = |\sum_{i \in \text{cluster}} \mathbf{v}_i| / N_{\text{cluster}}$. For large clusters $\langle u \rangle$ becomes independent of the cluster size and therefore independent of ρ_s. It should be emphasized that this holds only for finite systems with sufficiently strong pursuit interactions. In general there is a finite probability of a large pursuit-only

clusters to break up into smaller clusters which increases with cluster size and noise strength. The resulting different clusters will in general move in different direction which results in $\langle U \rangle \to 0$ for $L, N \to \infty$ and constant overall density $\rho_s = const. \ll 1$.

An intriguing feature of the pursuit-only interaction is the possibility of the formation of large scale vortices out of random initial conditions (Fig. 62b,c), for example via a collision of clusters moving in opposite direction. The vortices may decay either via a collision with a translational cluster or through random fluctuations. For certain parameters the vortices are very stable and may dominate the stationary configurations for the pursuit-only case. The emergence of vortex-structures is in particular remarkable because so far they have only been reported for systems of self-propelled particles with confinement, or attracting potential, respectively [74,86,363]. Here, the pursuit behavior has two functions: a propulsion mechanism and an asymmetric attraction.

Both interactions – escape and pursuit – lead to collective motion of groups but have an opposite impact on the density distribution. Whereas the escape interaction leads to a homogenization of density within the system, the pursuit interaction facilitates the formation of density inhomogeneities. Thus the combined escape+pursuit case with $\chi_p, \chi_e > 0$, is a competition of this two opposite effects. The stability of clusters is determined by the relative ratio of the interaction strengths. In general for the escape+pursuit case at low ρ_s we observe fast formation of actively moving particle clusters with complex behavior: fusion and break up of clusters due to collisions as well as spontaneous break up of clusters due to fluctuations [294].

The anti-dissipative nature of the escape and pursuit interactions leads to persistent translational motion of interacting Brownian particles. Individual clusters may be considered as self-propelled structures where the propulsion is purely due to social interactions, and constitutes an example of group-propulsion.

The scaling of the speed of individual clusters can be derived by considering the smallest possible cluster: a particle pair. We assume particle 1 is in front of particle 2 and $|\mathbf{r}_{12}| < l_s$ at all times. The transformation of Eq. (400) into polar coordinates with $\mathbf{v}_i = (v_i \cos \delta\varphi_i, v_i \sin \delta\varphi_i)$, where $\delta\varphi_i$ is defined as the angle between $\mathbf{v}_i$ and $\hat{\mathbf{r}}_{12}$, yields:

$$\frac{d}{dt}v_1 = -\gamma v_1^a + \chi_e |v_{12}|\theta(-v_{12})\cos\delta\varphi_1 + \sqrt{2D}\xi_{v,1} \tag{402a}$$

$$\frac{d}{dt}v_2 = -\gamma v_2^a + \chi_p |v_{12}|\theta(+v_{12})\cos\delta\varphi_2 + \sqrt{2D}\xi_{v,2} \tag{402b}$$

$$\frac{d}{dt}\delta\varphi_1 = \frac{1}{v_1}\left(-\chi_e |v_{12}|\theta(-v_{12})\sin\delta\varphi_1 + \sqrt{2D}\xi_{\varphi,1}\right) \tag{402c}$$

$$\frac{d}{dt}\delta\varphi_2 = \frac{1}{v_2}\left(-\chi_p |v_{12}|\theta(+v_{12})\sin\delta\varphi_2 + \sqrt{2D}\xi_{\varphi,2}\right). \tag{402d}$$

Here $v_{12} = v_1 - v_2$ is the relative velocity of the two particles and $\xi_{\varphi,i}, \xi_{v,i}$ represents the transformed noise variables. For $-\pi/2 < \varphi_1, \varphi_2 < \pi/2$ the escape and pursuit interaction leads to an increase of either v_1 or v_2 in order to harmonize the speed of the slower particle with the faster one. In addition the interaction stabilizes the translational motion along $\hat{\mathbf{r}}_{12}$, i.e. $\langle \delta\varphi_i \rangle \to 0$ (Eqs. 402c,d). After the system relaxes to a stationary state ($\hat{\mathbf{r}}_{12}$ varies slowly in time) we end up with quasi one-dimensional translational motion of the particle pair with slowly diffusing direction of motion defined by $\hat{\mathbf{r}}_{12}$. Please note that for elastic hard-core interaction the total energy and momentum of the particle pair does not change during collisions.

In order to obtain equations of motion for the particle pair in the stationary translational state, we assume that the particle velocities are given by the time averaged mean velocity u of the particle pair plus a small deviation: $v_i = u + \delta v_i$. Furthermore

the particles are assumed to have approximately the same heading so that $\delta\varphi_i \ll 1$. Assuming vanishing mean of speed deviations $\langle\delta v_i\rangle = 0$, we obtain for the time evolution of the mean pair velocity:

$$\frac{d}{dt}u = -\gamma u^a + \frac{\chi_e}{2}\langle|v_{12}|\theta(-v_{12})\rangle + \frac{\chi_p}{2}\langle|v_{12}|\theta(+v_{12})\rangle. \tag{403}$$

In the symmetric case where $\chi_e = \chi_p = \chi$ the social force terms on the right hand side can be summed up and we obtain:

$$\frac{d}{dt}u = -\gamma u^a + \frac{\chi}{2}\langle|v_{12}|\rangle. \tag{404}$$

There is permanently a social force acting on one of the particles. In order to evaluate the expectation value of the social force we assume that at all times one of the particles moves with the mean velocity u ($\delta v_{1,2} = 0$) whereas the velocity of the second particle deviates by δv as a result of the stochastic force. We approximate the expectation value $\langle|\delta v|\rangle = \langle|v_{12}|\rangle$, by considering the speed deviations as discrete increments taken from a Gaussian distribution with zero mean and variance $\sigma_1^2 = 2D\tau$ (Wiener process) with $\tau = \chi^{-1}$ being the relaxation time of the escape+pursuit interaction: $\langle|v_{12}|\rangle_{1d} = 2\sqrt{\frac{D}{\pi\chi}}$.

In the limit of quasi one-dimensional motion we obtain

$$\frac{d}{dt}u = -\gamma u^a + \sqrt{\frac{\chi D}{\pi}}, \tag{405}$$

which results in a stationary pair velocity u_{ep}^s

$$u_{ep}^s = \left(\frac{1}{\gamma}\sqrt{\frac{\chi D}{\pi}}\right)^{\frac{1}{a}}. \tag{406}$$

For symmetric escape and pursuit the particle distance increases slowly due to fluctuations which are not fully compensated by the social force, and the pairs break-up at finite times. Stable pairs, with stable particle distance are only possible for pursuit dominated dynamics and in particular for the pursuit only case $\chi_e = 0$.

In contrast to the escape and pursuit interaction for pursuit only the social force act not all the time but only if the leading (first) particle is faster then the pursuer. Thus individual velocity deviation from the mean, as well as $\langle|\delta v|\rangle_{1d}$ are larger for pursuit only, in comparison to the escape+pursuit case. We consider now both velocity deviations δv_1 and δv_2 as stochastic variables. In analogy to symmetric escape and pursuit we approximate $\langle|v_{12}|\rangle$ by considering discrete Gaussian increments with zero mean and variance $\sigma_2^2 = 2\sigma_1^2 = 4D\tau$ (difference of two independent stochastic processes with variance σ_1^2). The resulting evolution equation for the velocity in the pursuit only case reads:

$$\frac{d}{dt}u = -\gamma u^a + \sqrt{\frac{\chi_p D}{2\pi}}, \tag{407}$$

with the stationary speed

$$u_p^s = \left(\frac{1}{\gamma}\sqrt{\frac{\chi_p D}{2\pi}}\right)^{\frac{1}{a}}. \tag{408}$$

The obtained analytical expressions for the averaged pair velocity $\langle u\rangle$ are confirmed by numerical simulations for a wide parameter ranges as shown in
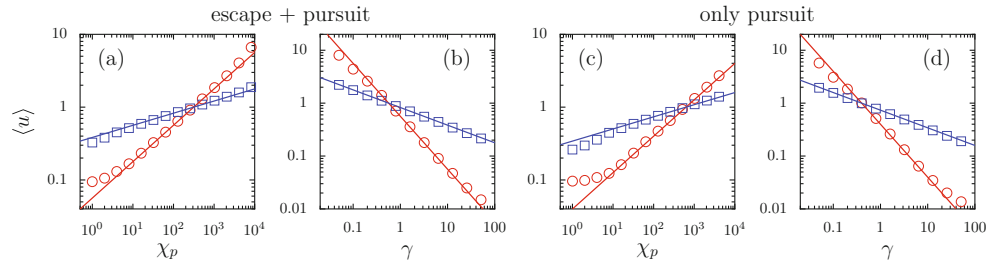
Fig. 63. (a) Mean pair velocity $\langle u \rangle$ for symmetric escape and pursuit (a,b) and pursuit only (c,d) versus interaction strength (a,c) and friction coefficient (b,d). The symbols represent the results obtained from numerical simulations of interacting particle pairs for linear friction $a = 1$ (circles) and nonlinear friction $a = 3$ (squares). The solid lines represent the corresponding analytical result Eq. (406) (a,b) and Eq. (408) (b,d).

Fig. 63 (see also [294]). Deviations become apparent where the pair dynamics deviate strongly from the effective one-dimensional situation as for example for weak coupling strengths χ.

Thus we have shown that although isolated particles perform (nonlinear) Brownian motion, the escape and pursuit interactions leads to rectifications of individual fluctuations of interacting particles leading to a collective propulsion with a non-vanishing stationary velocity. Based on Eqs. (406) and (408) we can consider a pair (or even a cluster) as a single active Brownian particle with a velocity-dependent friction function along the common heading of the form:

$$-\gamma(u)u = \alpha - \gamma u^a \tag{409}$$

with a constant pumping term α accelerating the pair and a friction term $-\gamma u^a$. For $a = 1$ this corresponds directly to the Schienbein-Gruler friction introduced in Sect. 3.1.

6.3.2 Chemotactic coupling

Another kind of coupling leading to collective dynamics is known from microbiology. Many microorganisms, as for example different bacteria strains, are able to sense various chemical agents in their environment and bias their motion along their concentration gradients. This ability is referred to as chemotaxis (see [110] for a review). Our modern understanding of bacterial chemotaxis was strongly influenced by the systematic investigations performed by J. Adler, H.C. Berg and their collaborators in the 60's and 70's of the past century [3–5,31,34,35,47]. Since then a large number of publications has appeared on various experimental and theoretical aspects of chemotaxis (see e.g. [15,29,44,76,365]).

Chemotaxis plays an important role for the survival of microorganisms in general, as it enables them to move towards beneficial environments and away from hostile environments. In the case, where individual cells bias their movement towards higher (lower) concentration of potentially beneficial (dangerous) chemical substances, the corresponding chemical agent is referred to as chemoattractant (chemorepellent). Effective coupling of individual cells comes from the ability of different microorganisms to produce the respective chemoattractant (chemorepellent) by themselves. By these means bacteria are able to exchange information about favorable or disadvantageous environmental conditions.

The auto-chemotactic interaction was identified as the mechanism responsible for complex spatio-temporal patterns of cell clusters that were observed in colonies of chemotactic bacteria such as Escherichia coli or Salmonella typhimurium [49,50,371].

Most models employed for the description of bacterial colonies with chemical cell-to-cell signaling (chemotaxis) are based on the classical Keller-Segel model (KSM) [192,193]. It is a continuous model of partial differential equations (PDEs) for the dynamics of the bacterial density $\rho(\mathbf{r},t)$ and the concentration(s) of the involved chemical agent(s) $c(\mathbf{r},t)$ (see e.g. [166,231,245,353]).

Here we discuss briefly models of (active) Brownian particles interacting via a self-generated chemoattractant, as an alternative to a pure PDEs approach [74,297,315].

We consider an ensemble of N (active) Brownian particles in two spatial dimensions, each described by individual equations of motion coupled to a self-generated chemoattractant concentration field $c(\mathbf{x},t)$:

$$\dot{\mathbf{r}}_i = \mathbf{v}_i \tag{410a}$$

$$\dot{\mathbf{v}}_i = -\gamma(\mathbf{v}_i)\mathbf{v}_i + \kappa(c)\nabla_{\mathrm{r}}\,c(\mathbf{r}_i) + \sqrt{2D}\boldsymbol{\xi}_i. \tag{410b}$$

The chemotactic force (second term in velocity equation) consists of a chemotactic sensitivity function $\kappa(c)$ which may depend on the concentration c and the gradient ∇c at the position of the individual particle (cell). Thus depending on the sign of $\kappa(c)$ the force acts either in the direction of the gradient (chemoattractant, $\kappa(c) > 0$) or in the opposite direction (chemorepellent, $\kappa(c) < 0$). Here we will restrict for simplicity to the discussion of chemotactic coupling via a single chemoattractant.

The dynamics of the chemoattractant concentration c are assumed to obey a diffusion equation:

$$\dot{c}(\mathbf{r},t) = q_0 \sum_{i=1}^{N} \delta(\mathbf{r} - \mathbf{r}_i) - d_c + D_c \Delta c. \tag{411}$$

The first term describes the production of the chemoattractant by the individual particles with rate q_0 at their respective positions $\mathbf{r}_i$. Furthermore, the chemical agent c is assumed to decay with the rate d_c and to diffuse with the diffusion coefficient D_c.

A simple model of chemotactically interacting Brownian particles with constant friction coefficient $\gamma(v) = \gamma_0 = const.$ (Stokes friction) and constant chemotactic response $\kappa(c) = \kappa_0$, was studied by Schweitzer and Schimansky-Geier [315] (SSG-Model).

Depending on the model parameters they observed formation of spike patterns of the chemoattractant field c. The spikes correspond to particle clusters aggregating at high concentration of c. The positive feedback between the spike "height" and attraction on other particles leads to a competition between spikes following an Eigen-Fisher like dynamics. After a certain relaxation time only few spikes "survive", but even if the dynamics of the system slows down, in the limiting case of $t \to \infty$ the only stationary solution is a single spike of the chemical field or cluster of particles, respectively. This process can be seen as an Ostwald-ripening process known from chemical reactions [316,376].

In the case of Stokes friction the particles within a stationary chemotactic cluster perform purely diffusive motion in an effective confining potential caused by the concentration profile of c. The introduction of active (self-propelled) motion via a velocity dependent friction function leads in general to complex rotational motion of individual particles within the cluster. In the absence of any additional interactions which may induce a symmetry breaking, no collective rotational modes are possible and the total angular momentum averages to zero.

Although bacteria are able to sense chemoattractant concentrations over several orders of magnitude via membrane receptors, it is known that at high c they lose the

ability to follow the gradient. This can be taken into account in simple form by the so-called "receptor law" [29, 245]. The resulting chemotactic force may be written as:

$$\kappa(c) = \frac{\kappa_0}{(1 + Sc)^2} \tag{412}$$

with κ_0 being the sensitivity coefficient and S being the saturation coefficient which takes into account the saturation of chemotactic receptors at high c leading to a decreasing sensitivity with increasing c.

The macroscopic behavior of the model for low S is similar to that observed in the SSG-model but with increasing S (or increasing concentrations c) the observed macroscopic patterns and microscopic dynamics within the cluster change.

The decrease of the chemotactic force at high concentrations c for $S > 0$, makes particles insensitive towards the gradient of c – the particles are able to leave the maxima of the field distribution. This behavior has significant impact on the macroscopic pattern formation. At large S any formation of clusters may be inhibited and at moderate values of S a "smoothing" of spikes in the concentration profile towards flat spots can be observed [297].

For the study of pattern formation we neglect the microscopic feature of active motion and consider the particles to behave as normal Brownian particles with a constant friction $\gamma(\mathbf{v}_i) = \gamma_0 = const$. This approach can be justified by the small stationary velocity of bacteria. With this assumption and in the overdamped limit (Smoluchowski limit) we can derive a simple PDE for the evolution of the particle density ρ. The two PDEs for ρ and c give us a reactions-diffusion system with chemotaxis which represent a variant of the Keller-Segel model. A similar system has been studied by Tyson et al. [353, 354]:

$$\dot{\rho}(\mathbf{r}, t) = \nabla \left(-\frac{\kappa_0 \rho}{\gamma_0 (1 + Sc)^2} \nabla c + D \nabla \rho \right), \tag{413a}$$

$$\dot{c} = q_0 \rho - d_c c + D_c \Delta c. \tag{413b}$$

Here, $D = D/\gamma_0^2$ is the spatial diffusion coefficient of the overdamped particles.

The simplest stationary solution of (413) is the homogeneous solution, given by the averaged particle and chemoattractant concentrations: $\bar{\rho} = N/L^2$ and $\bar{c} = q_0 \bar{\rho}/d_c$. Analyzing the linear stability of the homogenous solution with respect long wave spatial perturbations we arrive at the condition which has to be fulfilled for stable spatially homogenous solution:

$$\kappa_0 \leq \frac{D \gamma_0 d_c}{\bar{\rho} q_0} \left(1 + S \frac{q_0}{d_c} \bar{\rho} \right)^2 = \kappa_c. \tag{414}$$

For $d_c > 0$ and κ_0 smaller than the critical sensitivity κ_c all fluctuations around the homogeneous state decay exponentially. Only if $\kappa_0 \geq \kappa_c$ pattern formation on the macroscopic scale can be observed.

Although this result was derived for overdamped dynamics it can be also applied for actively moving particles with a Rayleigh-Helmholtz friction function, by taking the friction coefficient from the Stokes friction as a single fit parameter [297].

Not only the macroscopic dynamics but also the microscopic behavior of actively moving particles within a cluster depend strongly on the involved chemoattractant and chemotactic parameters. In the case of strong confinement (e.g. low S), the particles perform complex rotational motion, as discussed in Section 5. However, for large S and low diffusion of the chemoattractant we observe extended clusters where the chemoattractant concentration within a cluster is rather high but approximately constant and drops sharply at the cluster boundary leading to a steep gradient. Inside such clusters the particles perform effectively free motion
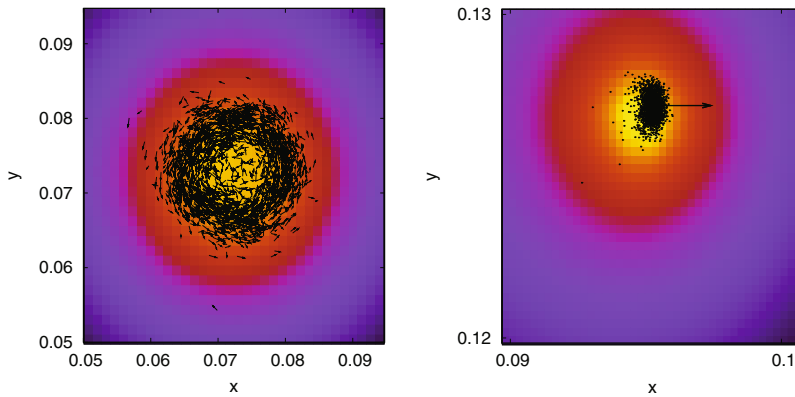
Fig. 64. Active particles with chemotactic coupling and velocity alignment. The chemoattractant concentration c is indicated by the background color with dark (bright) regions indicating low (high) c. Left: collective rotation at intermediate velocity alignment strengths. Each particle is shown by its velocity vector. Right: a moving cluster for strong velocity alignment. Only the position (symbols) and the mean velocity is shown (vector).

and are able to sense chemoattractant gradient only at the cluster boundaries which prevents them from leaving the cluster [297].

If the coupling via the self-generated chemoattractant is the only interaction between particles, no collective dynamics within a cluster take place and the center of mass of a stationary cluster performs at most slow diffusive motion. This changes dramatically if in addition to the chemotactic coupling we include the velocity alignment as introduced in Sect. 6.2.2. Increasing the alignment strengths leads first to a transition from disordered motion within a cluster to collective rotation within a stationary cluster. This situation corresponds to the dynamics in an external central field 6.2.2. A further increase in alignment strength enables the particles to escape collectively out of the stationary maximum of c. As the particles keep on producing the chemoattractant, they drag a cloud of chemoattractant around them and we observe a compact chemically bounded moving cluster of particles (see Fig. 64).

7 Pattern formation of active particles

In this section, various aspects of pattern formation in active matter systems are considered. Often pattern formation in active systems like self-propelled or driven particles refers to the formation of substantial spatial inhomogeneities in the density of the particles. Phenomena like giant number fluctuations, phase separation and clustering phenomena fall into this class and have all been observed in experiments [249, 275, 303], predicted or reproduced by theoretical analysis and numerical simulations of appropriate models [240, 271, 274, 283, 350]. Another frequent phenomenon in the collective dynamics of active particles is the formation of high-density bands in a low-density environment (segregation bands), that may travel at a constant speed (as for the classical Vicsek model) [60, 147, 247] or can be stationary (as for self-propelled rods) [141]. The high density inside such segregation bands often is associated with polar or nematic alignment order, while their low density environment typically is disordered. The precise nature of these bands (stationary or moving, polar or nematic order) is often determined by symmetries of the system, like the nature of the active particles (polar or apolar) and the specific of their interactions (ferromagnetic or nematic) [60, 141]. Finally, active particles may also exhibit classical pattern formation
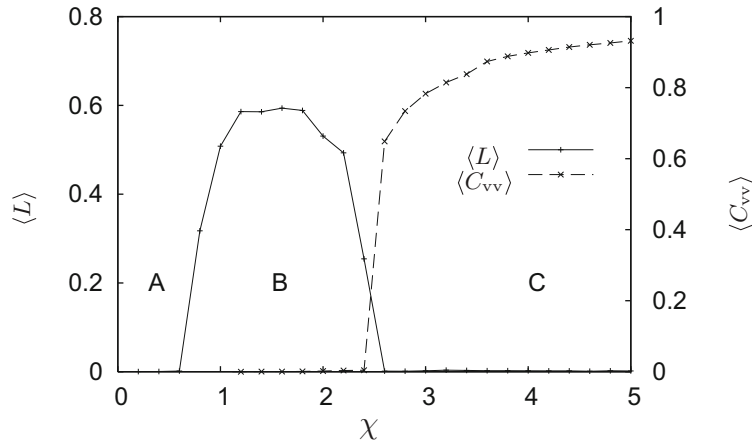
Fig. 65. The rotational motion $\langle L \rangle$ and parallel motion $\langle C_{vv} \rangle$ order parameters for an individual cluster of particles over the velocity-alignment strength χ. Depending on χ three different states can be identified: (A) no collective mode of motion; (B) collective rotation; (C) collective translation. (simulation parameters: $\kappa_0 = 1 \times 10^{-5}\,\mathrm{mm^4 s^{-2}}$, $S = 6 \times 10^{-5}\,\mathrm{mm^2}$, $d_c = 0.1\,\mathrm{s^{-1}}$, $D = 1 \times 10^{-4}\,\mathrm{mm^2 s}$, $N = 3000$ and $l_{va} = 2 \times 10^{-3}\,\mathrm{mm}$) [297].

phenomena such as Turing-type patterns respectively periodic standing and traveling waves of the density, compare e.g. [43]. In comparison to standard pattern formation systems like Rayleigh-Benard convection or chemical reaction-diffusion systems where the molecular and the pattern scale differ by many orders of magnitude, typically the length scales of pattern formation and the particle size in active matter are comparable [43]. This allows for agent-based approaches as introduced in Section 6, where the motion and dynamics of each particle is simulated. This section is structured as follows: First, we will briefly describe the results of continuum theories and their relation to findings in agent-based models. Then, work on clustering of self-propelled particles is reviewed. As an example, a simple physical model of self-propelled hard rods and simulation results therein are described. A theoretical analysis of clustering via a Smoluchowski-type kinetic approach is introduced and applied to simulations with hard rods and experiments with myxobacteria. Related phenomena in Vicsek-type models, models of colloids and granular experiments are also surveyed. Second, we describe formation of large-scale coherent structures like traveling and stationary high-density bands in simple models for self-propelled particles, namely the Vicsek model and a variation describing polar particles with apolar alignment interactions, which is illustrated with Peruani model described above, and their instabilities. Due to the rapid development of the studies in collective motion of active (Brownian) particles, we concentrate on detailed descriptions of recent developments. The review in this section is by no means exhaustive and relevant original and review papers will be cited and may be consulted. Nevertheless, the examples selected and the discussion will address the most important issues. The main message of this section is that different forms of spatial organisation like clusters and large-scale patterns, are crucial for a complete understanding of the collective dynamics of active particles. Hence, the approaches introduces in this section are necessary to complement the picture sketched in the previous section on swarming.

7.1 Continuum theories versus agent-based models

In agent-based models, one encounters often strong finite size effects. The same model may yield clustering and giant fluctuations for small and intermediate particle

numbers as well as coherent structures and large-scale patterns for big particle numbers. In addition, bands and other large-scale patterns can have instabilities against modes of a definite wavelength, that may be absent in smaller system, but highly relevant in sufficiently large systems. Such stability properties of patterns are also quite relevant for the presence of long-range order or non-zero global order parameters.

Alternatively, coarse-grained, hydrodynamic continuum models have been frequently employed to advance the understanding of collective dynamics in active matter. It would be highly desirable to establish links between the two levels of descriptions. Such efforts are, however, limited by the fact that continuum models address typically length scales that involve very large number of particles. As a result, the study of the corresponding agent-based models is often computationally extremely expensive or even prohibitive. Simulations of "microcospic" agent-based model are nevertheless very important, since they are necessary to understand the role of the noise and the fluctuations as well as the limitations of the validity of hydrodynamic descriptions. Agent-based models also allow for a simultaneous computation of coarse-grained properties like densities or alignment and of characteristic of individual particle motion. In other words, they can be used to establish a link between an Eulerian and Lagrange view of active matter systems [260]. Often, both Eulerian and Lagrangian properties of active systems are accessible to experiments. For example, fluorescence labeling allows for tracking of individual cell motion in bacterial films, while density patterns are conveniently determined by microscopy [175, 368]. This enlarges the amount of information necessary for quantitative validation of models substantially.

In contrast, continuum theories are useful to describe the large-scale behavior of active Brownian particles. Shortly after the first publication on the Vicsek model, Toner and Tu carried out pioneering work deriving a continuum theory for active systems like the Vicsek model. Their work analyzes a coarse-grained hydrodynamic description based on the velocity field $\mathbf{v}$ and the particle density ρ. These equations are of the general form:

$$\frac{\partial \mathbf{v}}{\partial t} + \lambda \mathbf{v} \cdot \nabla \mathbf{v} + \ldots = (\alpha - \beta \mathbf{v} \cdot \mathbf{v})\mathbf{v} + \Gamma \nabla \nabla \mathbf{v} - \nabla P(\rho) + \xi \tag{415}$$

$$\frac{\partial \rho}{\partial t} + \nabla \cdot \rho \mathbf{v} = 0. \tag{416}$$

Eqs. (415)–(416) capture the phase transition from the disordered state $\mathbf{v} = 0$ to the ordered state $v = \sqrt{\alpha/\beta}$. The analysis of Toner and Tu gave an explanation of the long-range order in two-dimensional systems, that is absent in equilibrium systems and had been previously observed in the simulations by Vicsek and colleagues. Moreover, it allowed the derivation of sound modes and lead to the prediction of giant number fluctuations, that shall be discussed below. A detailed discussion of the Toner-Tu field theory can be found in [282, 350]. The number fluctuations in the collective dynamics of a many particle system are often expressed as

$$\Delta N \propto N^{\phi}, \tag{417}$$

where ΔN is the standard deviation of the particle number in a given finite volume. The quantity N gives the mean number of particles in this volume. Equilibrium systems exhibit normal fluctuations with $\phi = 1/2$, whereas active systems often show $\phi > 1/2$. Such behavior out of equilibrium is consequently referred to as giant number fluctuations. The Toner-Tu field theory predicts $\phi = 7/10 + 1/5d$ for $d < 4$, where d is the spatial dimension of the system. The predicted value $\phi = 0.8$ in two dimensions has been recently confirmed in extensive numerical studies of two agent-based models, namely the original Vicsek model [60] and the Peruani model [141], in the ordered

state without segregation bands. Giant number fluctuations have also been studied for active nematics (=driven apolar particles), for which an exponent $\phi = 1/2 + 1/d$ was derived from field theory, see [282,283], where d again refers to the spatial dimension of the system. In two dimensions, the predicted value of $\phi = 1$ was recovered from extensive numerical simulations of a Vicsek-type simple agent-based model [61]. Coincidently, researchers have found in recent experiments with bacteria [275,381] similar exponents ($\phi \approx 0.8$) in two dimensions. In the latter case, the interpretation of the giant number fluctuations remains controversial because of the simultaneous observation of large coherent clusters of the investigated bacteria. Such clustering provides an alternative reason for giant number fluctuations and violates the assumptions of the Toner-Tu field theory. A similar controversy appeared in connection with experiments of shaken elongated rice corns that were devised as a realization of an active nematic and show giant number fluctuations [249]. The initial interpretation of these measurements as confirmation of the predictions of continuum theory were later contested [11] by pointing out the strong tendency of this system to form clusters. In general, the formation of clusters or large-scale patterns like segregation bands is expected to have a strong influence on the number fluctuations and goes beyond the range of validity of continuum theories.

Alternative continuum theories have recently also been investigated by Marchetti and coworkers based on symmetry consideration and expansions [23,239] as well as for a specific approach describing self-propelled hard rods [21,22]. Bertin and coworkers have pursued a continuum theory based on a kinetic approach [37] and have been able to recover qualitatively the traveling segregation bands seen in simulations of the Vicsek model [38].

Altogether, continuum theories have contributed a lot to the understanding of the collective dynamics of active Brownian particles. In recent years, large-scale agent based simulations and experiments with, e. g., driven granular particles or moving bacteria, have revealed many interesting phenomena that pose new challenges to continuum theorist. Many open questions revolve around the issue of prediction of spatial inhomogeneities, large-scale patterns and cluster formation which all have been found to play a dominant role in agent-based simulations and experiments. In the following subsections we will discuss recent developments in agent-based models and related experiments.

7.2 Clustering, segregation and band patterns – phenomena and experiments

Examples of large-scale self-organized patterns in systems of self-propelled particles with short-range interactions are found at all scales, from groups of animals [39,55,261] and human crowds [160] down to insects [51,294], bacteria [381], or actin filaments [52,303]. Such patterns are also found in non-living system like in driven granular media [82,206,207,249]. Despite the fact that the interaction mechanisms between individual elements are of a different nature, it is possible to determine some common requirement to achieve large-scale (spatial) self-organization. Particularly important for the emerging macroscopic patterns are the self-propulsion of the agents, and their velocity alignment mechanism. As described above, simple individual-based models like the Vicsek model [361] have helped to reveal the relevance of these two elements by reducing the problem to the competition between a local alignment interaction and noise [59]. Recall, that in two dimensions, self-propelled particles moving at constant speed with a ferromagnetic-like velocity alignment exhibit at low noise a phase characterized by true long-range polar order which translates into a net flux of particles [60,361]. In the previous section, we have assumed that the ordered states are spatially homogeneous. Systematic simulations and theoretical analysis based on

coarse-grained continuum models show that these ordered phases often exhibit several remarkable features of spatial organisation. For ferromagnetic alignment mechanisms, the spontaneous formation of elongated high density bands that move at roughly constant speed in the direction perpendicular to the long axis of the band, and anomalous density fluctuations for low noise levels were reported [60,239]. When the alignment is replaced by a nematic velocity alignment, self-propelled particles again display a phase characterized by true long-range nematic order at low noise intensity [141]. Interestingly, spontaneous density segregation evolves into regular bands are observed for these particles as well as anomalous density fluctuations [141]. It is noteworthy, that self-propelled particles with display large-scale high-density patterns and segregation in absence of any attracting force [60,141].

At moderate system sizes or particle numbers, self-propelled particles with ferromagnetic or nematic alignment mechanisms often do not show large-scale patterns like segregation bands. Nevertheless, collective motion in this regime is still characterized by strong density fluctuations. A phenomenon that has attracted a lot of interest recently is the formation of large polar clusters in many experiments and models, that again do not require attractive forces between the particles. It seems that the common presence of active motion and effective alignment forces of either ferromagnetic or nematic symmetry are sufficient to facilitate "condensation" of self-propelled particles into clusters. This effect has been studied extensively for alignment that results from volume exclusion interactions among self-propelled rods [270,271,375]. Related findings appeared in models for colloidal rods [369], experiments and models of driven granular particles [207] and models describing collective motion of sperms [374,375]. In many instances the appearance of polar clusters was linked to a power-law cluster size distribution [271,374,375]. Clustering effects and the emergence of steady state cluster size distributions in self-propelled particle systems were also observed in the Vicsek model [170,171] and the Peruani model [274].

In the following subsections, we will first discuss first the formation of polar clusters in a model of self-propelled rods and describe a simple kinetic theory from which the steady state cluster size distribution of self-propelled particles is obtained. This approach is a modification of the Smoluchowki kinetic equations that were developed to describe the aggregation of colloids [58,325]. Then, we will show that similar phenomena appear and a related kinetic description for the cluster size distribution applies also to models of self-propelled particles with velocity alignment as outlined before in [270,274]. In the second part of the second of the section, we review results on the formation of large-scale structures in models with velocity alignment. Finally, we give an account of results obtained in coarse-grained continuum descriptions of collective motion in active matter specifically designed to account for the phenomena observed in the simulation studies discussed before.

7.3 Clustering, phase separation and giant number fluctuations

7.3.1 Clustering of self-propelled hard rods

A recurrent question is how microorganisms such as bacteria and amobae coordinate their behavior to form groups which move collectively. Specific models for bacteria like *E. coli* as well as for amoebae like *D. discoideum* [29], have been based on chemotaxis, a long-range cell interaction mechanism according to which individual cells move in response to chemical signals produced by all other cells. However, in some bacteria there is no evidence for chemotactic cues and cells coordinate their movement by cell-to-cell signalling mechanisms in which physical contact between bacteria is needed [95,179,186]. Consequently, one may ask how such bacteria aggregate in

order to communicate. Another relevant aspect is the influence of the shape of the bacteria. The shape has been shown to be essential for individual motion of swimming bacteria [94]. In contrast, the role of the cell shape for collective motion has remained mostly unexplored. It has been demonstrated experimentally [194] that migrating elongated amoeboid cells exhibit alignment effects similar to those reported in liquid crystals [253]. A prominent example for collective behavior with no apparent long range interactions are the striking patterns observed during the life-cycle of gliding myxobacteria, see e.g. [95, 179, 186, 246]. Earlier modeling work has reproduced many of these patterns in three dimensions assuming either perfect alignment [43] or a phenomenological alignment force [6, 175]. These models have all considered patterns resulting from exchange of chemical signals, that are absent in an early stage of the myxobacterial life cycle. Nevertheless, a trend from initial independent motion towards formation of larger clusters of aligned bacteria is often observed.

Here, a model of self-propelled rods that have only repulsive excluded volume interactions in two dimensions is considered It was found that the interplay of rod geometry, self-propulsion and repulsive short-range interaction is sufficient to facilitate aggregation into clusters [271]. Consider N rod-like particles moving on a plane, for a more detailed description see [270, 271]. Each particle is equipped with a self-propelling force acting along the long axis of the particle. Velocity and angular velocity are proportional to the force and torque, correspondingly. The rod-shape of the particles requires three different friction coefficients which correspond to the resistance exerted by the medium when particles either rotate or move along their long and short axes. Inertial terms are neglected, i.e. the case of overdamped motion is considered. As a result the movement of the i-th rod is governed by the following equations for the velocity of its center of mass and angular velocity:

$$(v_\parallel^{(i)}, v_\perp^{(i)}) = \left(\frac{1}{\zeta_\parallel} \left(F - \frac{\partial U^{(i)}}{\partial x_\parallel} \right), -\frac{1}{\zeta_\perp} \frac{\partial U^{(i)}}{\partial x_\perp} \right)$$
$$\dot{\varphi}^{(i)} = -\frac{1}{\zeta_\varphi} \frac{\partial U^{(i)}}{\partial \varphi} \tag{418}$$

where $v_\parallel^{(i)}, v_\perp^{(i)}$ refer to the velocities along the long and short axis of the rods, respectively, ζ_i indicates the corresponding friction coefficients (ζ_φ is related to the friction torque), $U^{(i)}$ refers to the energy of the interaction of the i-th rod with all other rods, and F is the magnitude of the self-propelling force. The motion of the center of mass $\dot{\mathbf{r}}^{(i)} = (v_x^{(i)}, v_y^{(i)})$ of the i-th rod is given by

$$v_x^{(i)} = v_\parallel^{(i)} \cos \varphi^{(i)} + v_\perp^{(i)} \sin \varphi^{(i)}$$
$$v_y^{(i)} = v_\parallel^{(i)} \sin \varphi^{(i)} - v_\perp^{(i)} \cos \varphi^{(i)}. \tag{419}$$

Particles interact by "soft" volume exclusion, *i.e.* by a potential that penalizes particle overlaps in the following way:

$$U^{(i)}(\mathbf{r}^{(i)}, \varphi^{(i)}, \mathbf{r}^{(j)}, \varphi^{(j)}) = \mu \sum_{j=1, j\neq i}^{N} \left((\gamma - a_o^{(ij)})^{-b} - \gamma^{-b} \right) \tag{420}$$

where $a_o^{(ij)} = a_o(\mathbf{r}^{(i)}, \varphi^{(i)}, \mathbf{r}^{(j)}, \varphi^{(j)})$ is the area overlap of the rod i with rod j and μ is the interaction strength. The simulations were performed placing N identical particles initially at random inside a box of area A with periodic boundary conditions.

There are two key parameters which control the dynamics of the self-propelled rods: i) the packing fraction η, i.e., the area occupied by rods divided by the total
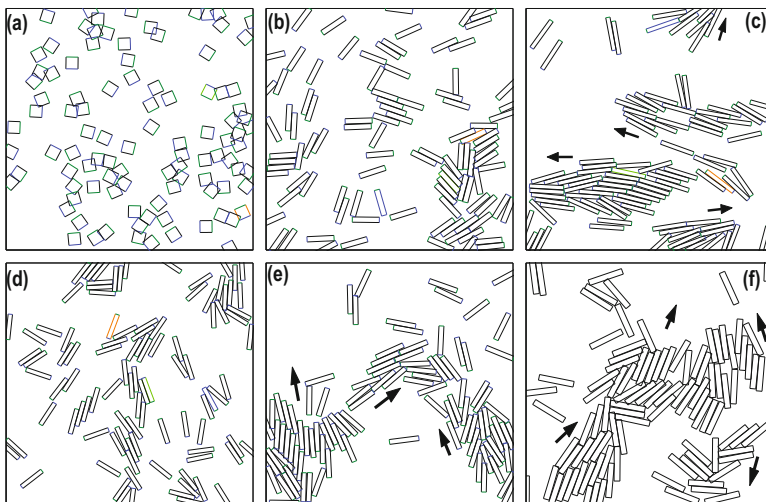
Fig. 66. Simulation snapshots of the steady states for different particle anisotropy κ and the same packing fraction η (a-c), and the same κ and different η (d-f). Fixing $\eta = 0.24$: (a) before the transition, $\kappa = 1$; (b) almost at the transition, $\kappa = 5$; (c) after the transition, $\kappa = 8$. Fixing $\kappa = 6$: (d) before the transition, $\eta = 0.18$; (e) just crossing the transition, $\eta = 0.24$; (f) after the transition, $\eta = 0.34$. In all cases, particles $N = 100$ and particle area $a = 0.2$. The arrows indicate the direction of motion of some of the clusters.

area ($\eta = Na/A$, where N is the number of particles in the system, a is the area of a single particle, and A is the total area of the box), and ii) the length-to-width aspect ratio κ ($\kappa = L/W$, where L is the length and W is the width of the rods). Simulations yield an increase of cluster formation with increasing κ or η, see Fig. 66. Clusters are defined by connected particles that have non-zero overlap area. Simulations can be characterized by the weighted cluster size distribution, $p(m)$, which indicates the probability of finding a given particle inside a cluster of mass m. Fig. 67 shows that for a given η, a critical κ_c can be defined as the value of κ for which the shape of $p(m)$ changes from unimodal to bimodal. The figure shows also typical shape of $p(m)$ before clustering, corresponding to low values of κ, and after clustering, corresponding to large values of κ. The onset of clustering is defined by the emergence of a second peak in $p(m)$. The robustness of the model against fluctuations was tested by inserting additive noise terms R_i/ζ_i in Eqs. (418), which correspond to a switch from purely active to active Brownian particles [119,121]. Clustering is still present in active Brownian rods, albeit the transition is moved to larger values of κ and η. Clustering was absent in all simulations with purely Brownian rods ($F = 0$).

Smoluchowski-type mean field approximation (MFA)

The clustering effects in simulations described so far can be analyzed by deriving kinetic equations for the number n_j of clusters of a given size j. The equations for n_j contain terms for cluster fusion and fission. For the fusion terms adopted kinetic equations originally derived by Smoluchowski for the case of coagulation of colloids [58,325] were employed, while the fission terms are empirically defined from the typical behavior seen in related simulations [271]. The numbers n_j change in time according to $\{n_j(t)\}_{j=1}^{\infty}$, where $n_j(t)$ is the number of clusters of mass j at time t.

This description allows to consider a single rate constant for all possible collision processes between clusters of mass i and j, as well as a unique disintegration constant
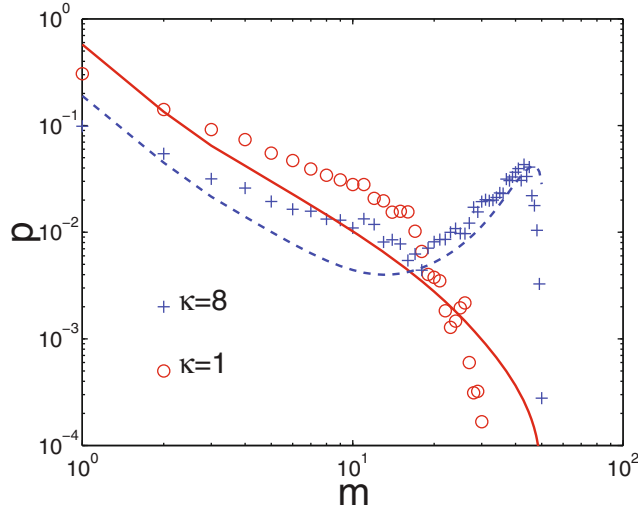
Fig. 67. $p(m)$ as function of the cluster size m for $\eta = 0.34$. Symbols show the average over eight IBM simulations for active particles with $N = 50$ and $\kappa = 1$ (circles) and $\kappa = 8$ (crosses). The lines correspond to the mean field theory for $\kappa = 1$ (solid) and $\kappa = 8$ (dashed).

for any cluster of mass i. Four additional crucial assumptions are now made: i) The total number of particles in the system, $N = \sum_{j=1}^{N} j n_j(t)$, is conserved. ii) Only binary cluster collisions are considered. Collisions between any two clusters are allowed whenever the sum of the cluster masses is less or equal to N. iii) Clusters suffer spontaneous fission only by losing individual particles at the boundary one by one, *i.e.* a cluster can only decay by a process by which a j-cluster split into a single particle plus a $(j-1)$-cluster. This is motivated by observations in the above simulations. iv) All clusters move at constant speed, $\widetilde{v} \approx F/\zeta_{\parallel}$, implying that rods in a cluster have high orientational order and interact only very weakly with their neighbors. Under all these assumptions the evolution of the n_j's is given by the following N equations:

$$\dot{n}_1 = 2B_2 n_2 + \sum_{k=3}^{N} B_k n_k - \sum_{k=1}^{N-1} A_{k,1} n_k n_1$$

$$\dot{n}_j = B_{j+1} n_{j+1} - B_j n_j - \sum_{k=1}^{N-j} A_{k,j} n_k n_j$$

$$+ \frac{1}{2} \sum_{k=1}^{j-1} A_{k,j-k} n_k n_{j-k} \quad \text{for} \quad j = 2, \ldots, N-1$$

$$\dot{n}_N = -B_N n_N + \frac{1}{2} \sum_{k=1}^{N-1} A_{k,N-k} n_k n_{N-k} \tag{421}$$

where the dot denotes time derivative, B_j represents the fission rate of a cluster of mass j, defined by $B_j = (\widetilde{v}/R)\sqrt{j}$, and $A_{j,k}$ is the collision rate between clusters of mass j and k, defined by $A_{j,k} = (\widetilde{v}\sigma_0/A)(\sqrt{j} + \sqrt{k})$. σ_0 is the scattering cross section of a single rod. R is the only free parameter and is defined the characteristic length a rod at the boundary moves with the cluster before leaving it in a typical fission event.

One sets $R = \alpha L$ taken into account that longer rods will stay attached to cluster for a longer time.

Since σ_0 can be approximated by $\sigma_0 \approx L + W = \sqrt{a}\left(\sqrt{\kappa} + \frac{1}{\sqrt{\kappa}}\right)$, the MFA depends only on the parameters κ, a, A, $\widetilde{v}$ and α. If one integrates Eqs. (421) with parameters used in IBM simulations and an initial condition $n_j(t = 0) = N\delta_{1,j}$, their solution yields steady state values n_j^0 for $t \to \infty$. From these values, we obtain a MFA for the weighted cluster size distribution $p(m) = n_m^0 m/N$ for given values of the free parameters R resp. α. The best agreement between the MFA and the IBM simulations is found for a choice of $\alpha = 1.0 \pm 0.05$ (see Fig. 67). To understand the relation between the parameters of the model and clustering effects better, one can rescale Eqs. (421) by introducing a new time variable: $\tau = t\widetilde{v}/\sqrt{a\kappa}$. The resulting equations depend only on a dimensionless parameter $P = (\kappa + 1)a/A$. Note that $\widetilde{v} \neq 0$ is scaled and does not affect the qualitative dynamics of the system. In the dimensionless model the parameter P stands for ratio between fusion and fission processes and therefore triggers the transition from a unimodal to a bimodal cluster size distribution. By numerical solving for the steady state solution of the kinetic equations, one can accurately determine a critical transition parameter P_c. Given the system area A, the rod area a and the number of rods N, this method provides a straightforward way to calculate κ_c:

$$\kappa_c = P_c(N)\frac{A}{a} - 1. \tag{422}$$

It was found that in the MFA the critical parameter value κ_c for the clustering transition does practically not depend on the number of particles as soon as $N > 50$ [271]. One proceeds by assuming that P_c is inversely proportional with N and expresses κ_c as a function of the packing fraction:

$$\kappa_c = C/\eta - 1 \tag{423}$$

where the constant was found to be $C \approx 1.46$ by comparison with simulation results [271]. So, for the range of parameters used in the IBM, the unimodal shape of the weighted cluster size distribution for small values of κ and η, and the bimodal shape for large values of the two parameters seen in the IBM was qualitatively reproduced in the MFA, see Fig. 67. A second interesting feature obtained both in the IBM and MFA is that the cluster-size distribution changes notably in shape from an function exponentially decaying with size to a function with a power-law behaviour $p(m) \propto m^{-c}$ at small cluster size and a second peak confined by a cutoff at large cluster sizes. The exponent of the power law is, however, substantially larger for the MFA ($c \approx 1.35$) than for the simulation of self-propelled rods ($c \approx 0.95$). The power-law behaviour of the cluster-size distribution characterizing self-propelled rods was also discussed extensively in recent more detailed simulations of self-propelled rods [375], where exponents of the weighted cluster-size distributions are in the range between 0.95 and 1.4. Interestingly, also recent experiments with bacteria, namely *Bacillus subtilis* [381] and a mutant of *Myxococcus xanthus* [275] report exponents c of the weighted cluster size distribution in the range of 0.85–0.9. We expect further theoretical and experimental activities, that may finally uncover universal properties in the clustering of self-propelled rods and related systems.

In summary, one finds non-equilibrium clustering for interacting self-propelled rod shaped-particles with sufficient packing density η and aspect ratio κ in simulations. The onset of clustering can be defined by a transition from a unimodal to bimodal cluster size distribution. This transition is reproduced by a mean-field description of the cluster size distribution, which yielded a simple criterion, $\kappa = C/\eta - 1$, for the onset

of clustering. It is instructive to compare these results rewritten in the form $\kappa\eta + \eta \approx$ 1.46 with the formula for the isotropic-nematic transition $\kappa\eta \approx 4.7$ found in the two-dimensional version [189] of Onsager's mean-field theory for Brownian rods [253]. This shows that actively moving rods can achieve alignment at much lower densities than Brownian rods resp. particles in equilibrium systems. The clustering phenomenon is absent in simulations with isotropic self-propelled particles as well as with Brownian rods. The model of self-propelled rods provides also an alternative explanation for collective behavior of rod-shaped objects - previous swarming models have achieved aggregation and clustering by assuming attractive long-range interactions [119,121, 147,361]. With respect to biology, the observations made for self-propelled rods offer a physical explanation for the formation of clusters in many gliding rod-shaped bacteria, that often precedes the formation of biofilms and the appearance of more complex patterns.

7.3.2 Clustering of self-propelled particles with velocity alignment

In the following, the interplay between orientation ordering by velocity alignment and clustering in self-propelled particles with ferromagnetic F- or nematic LC-alignment is analyzed and briefly discussed. Through simulations evidence was provided that at high density orientation ordering sets in before clustering [270]. In contrast, for low particle densities, the onset of orientation ordering and clustering are closely related and seem to occur at the same value of the noise [270,274] for LC-alignment. These findings indicate that the phase transition occurs rather due to mixing of particles than exclusively to the directed active motion.

In Fig. 68(a) the behavior of the orientational order parameters S^{LC} and S^{LC} vs. the noise amplitude η for high density is shown for a model with LC-alignment. A transition from a disordered (isotropic) to an orientational ordered (nematic) state is strongly suggested by the simulation data. Close to the critical noise amplitude η_c the scaling of the curve follows the scaling predicted by the mean field outlined in section 4 [272]. The departure from the mean-field prediction occurs exactly when the spatial distribution of particles can not longer be considered homogeneous, compare snapshots Fig. 68(b-d). Note, also that the ferromagnetic order parameter is zero as long as the density appears spatially homogeneous. At low density the scenario how orientational order emerges is significantly different. Fig. 69(a) shows that for $\rho = 0.25$ the dependency of the orientational order parameter S on the noise amplitude η is qualitatively different from the one observed at high density. The second remarkable difference is that the apparent onset of orientational ordering coincides with the onset of clustering. This is also confirmed by the cluster size distribution which exhibits a power-law distribution near the onset of orientational ordering [274]. Fig. 69(b) shows that for zero orientational order the spatial distribution of particle is roughly homogeneous. As soon as clustering is observed in the snapshots, see Fig. 69(c), the order parameter starts to deviate from zero. As the noise is decreased clustering effects are more pronounced, Fig. 69(d). The displayed patterns correspond to typical particle configurations in a quasi-steady steady state. In particular, the pattern of cluster does not coarsen as in a phase separation process. Here, clusters form and disintegrate in a dynamical way. The rate of growth and disintegration of the clusters is highly dependent on the value of η. Given a value of η the cluster size distribution reaches a steady distribution after an initial transient similar to the behaviour of self-propelled rods described above.

In the following, a simple theory to understand the emergence of steady state cluster size distributions in self-propelled particle systems with velocity alignment. The
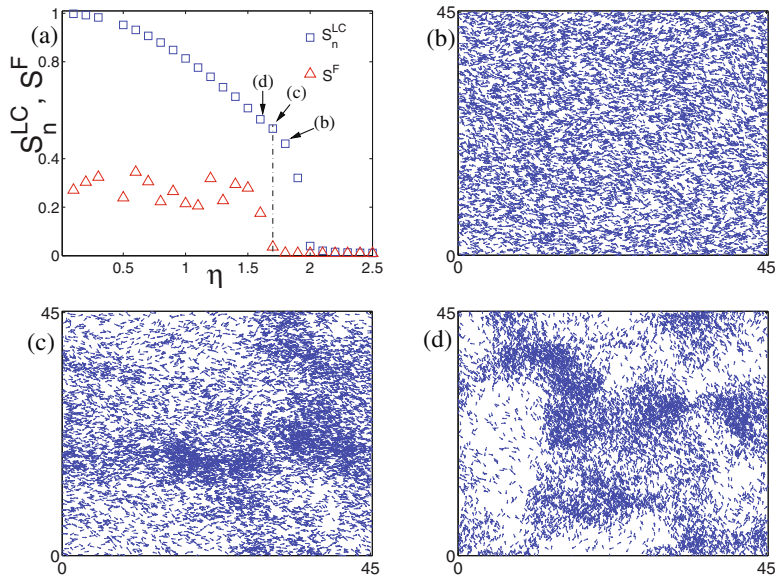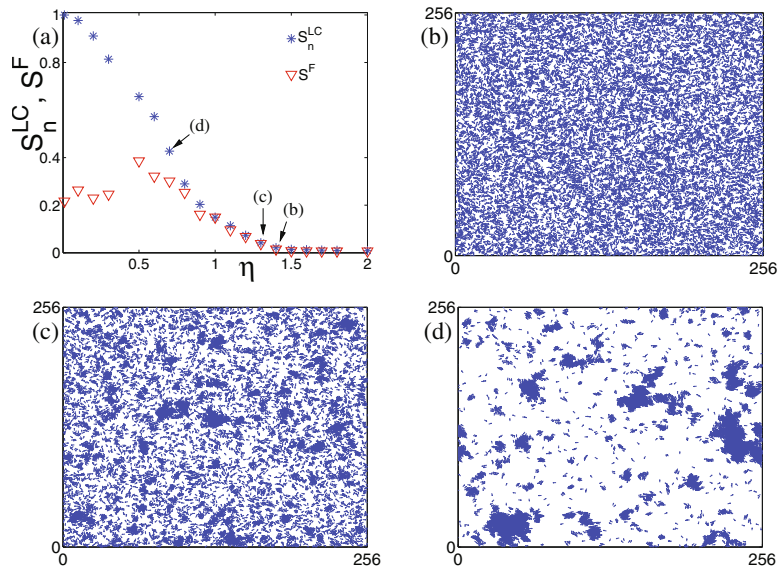
Fig. 68. Orientational dynamics and clustering at high density. Number of particles $N = 2^{14}$ and density $\rho = 4$. (a) Orientation order parameter S vs. noise amplitude η. Symbols are average over 10 realizations. The dashed curve corresponds to the scaling predicted by the mean-field while the vertical dot-dashed line indicates the onset of clustering effects. (b)-(c) Snapshots of the simulations for the values of η indicated in (a) at the steady state, time step 2.5×10^5 [270].

Fig. 69. Orientational dynamics and clustering at low density. Number of particles $N = 2^{12}$ and density $\rho = 0.25$. (a) Orientational order parameter S vs. directional noise amplitude η. Symbols are average over 10 realizations. The dashed curve corresponds to the best fit of the simulation data close to η_c. (b)-(c) Snapshots of the simulations for the values of η indicated in (a) at the steady state, time step 2.5×10^5 [270].

treatment is analogous to the one described above for the cluster-size distribution of self-propelled rods. The dynamics of the cluster-size distribution may alternatively be described by deriving a master equation for the evolution of the probability $p(\mathbf{n}(t))$, where $\mathbf{n}(t) = n_1(t), n_2(t), \ldots, n_N(t)$, with $n_1(t)$ being the number of isolated particles, $n_2(t)$ the number of two-particle clusters, $n_3(t)$ the number of three-particle clusters, etc. This kind of approach has previously been used to understand equilibrium nucleation in gases, where the transition probabilities between states are function of the associated free energy change [309,316,317]. Here, equations for the time evolution of the values of $n_1(t), n_2(t), \ldots, n_N(t)$ are derived to describe the cluster dynamics. To simplify the notation, one refer to $\langle n_1(t) \rangle$, $\langle n_2(t) \rangle$, $\ldots$, $\langle n_N(t) \rangle$ simply as $n_1(t)$, $n_2(t)$, etc. The time evolution equations for the $n_i(t)$ obey the following form:

$$\dot{n}_1 = 2B_2 n_2 + \sum_{k=3}^{N} B_k n_k - \sum_{k=1}^{N-1} A_{k,1} n_k n_1$$

$$\dot{n}_j = B_{j+1} n_{j+1} - B_j n_j - \sum_{k=1}^{N-j} A_{k,j} n_k n_j$$

$$+ \frac{1}{2} \sum_{k=1}^{j-1} A_{k,j-k} n_k n_{j-k} \quad \text{for} \quad j = 2, \ldots, N-1$$

$$\dot{n}_N = -B_N n_N + \frac{1}{2} \sum_{k=1}^{N-1} A_{k,N-k} n_k n_{N-k} \tag{424}$$

where the dot denotes the time derivative, B_j represents the rate for a cluster of mass j to loose a particle, and is defined as

$$B_j = \frac{D_{\text{eff}}(\eta)}{d^2} \sqrt{j}, \tag{425}$$

and $A_{j,k}$ is the collision rate between clusters of mass j and k, defined by

$$A_{j,k} = \frac{v_0 2\epsilon}{a} \left(\sqrt{j} + \sqrt{k} \right), \tag{426}$$

where $a = L^2$ is the area of the two-dimensional space where particles move. In Eq. (425), d denotes, the maximum distance that two particles can be separated apart to be considered as *connected* and part of the same cluster. The expression $d^2/D_{\text{eff}}(\eta)$ is an estimate for the characteristic time a particle spends at the boundary before it moves away from the cluster. The splitting rate B_j is proportional to the inverse of this characteristic time multiplied by the number of particles on the boundary, which is estimated as $\sqrt{j}$. On the other hand, the collision rate $A_{j,k}$ is derived in analogy to the collision rate in kinetic gas theory between two disk-like particles A and B [274].

Numerical integration of these equations shows that Eq. (424) produces qualitatively similar distributions as the one observed in individual-based simulations, see [274]. The different curves correspond to various values of the dimensionless parameter P, defined as $P = \frac{2\epsilon d^2 v_0}{a D_{\text{eff}}(\eta)}$. For small values of P, which correspond to large values of η, the distribution $p(m)$ monotonically decreases with m, while for large values of P, resp. small values of η, a peak at large cluster sizes emerges. A quantitative comparison between Eq. (424) and individual-based simulations is still in a very early stage [274].

Altogether, polars clusters play a fundamental role in the macroscopic dynamics of self-propelled particle systems. Orientational order and cluster dynamics are often
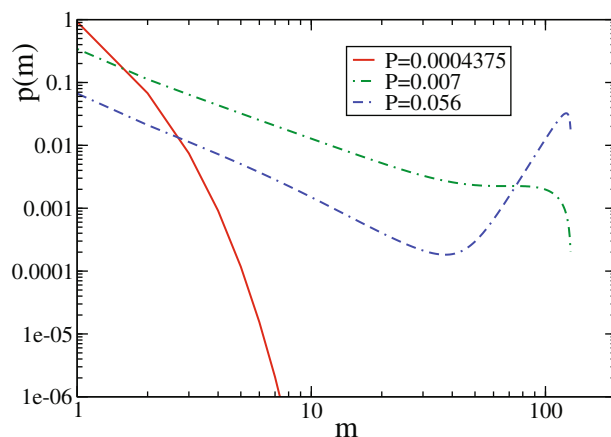
Fig. 70. Steady state cluster size distributions obtained from numerical integration of Eqs. (424) with $N = 128$ for various values of the dimensionless parameter P, where $P = \frac{2\epsilon d^2 v_0}{a D_{\text{eff}}(\eta)}$. Notice the transition from a monotonically decreasing distribution for small values of P to a non-monotonic distribution with a peak at large cluster sizes for large values of P.

closely linked. The cluster size distribution can be obtained from a set of equations of the Smoluchowski type to describe the cluster dynamics in the system. Its usefulness awaits further test by comparison to simulations and experiments in systems of self-propelled units.

7.4 Large-scale segregation bands

Segregation bands are coherent structures typically seen in large-scale simulation of self-propelled particle systems with velocity alignment [60,141,361]. These bands often represent high-density zones with a high degree of orientational order embedded in a low-density background with orientational disorder. This coupling of orientational order and density goes beyond the mean-field theories describing the onset of orientational order in systems with homogeneous density that were introduced in the previous section. Extensive simulation studies have revealed a clear correlation between the appearance of travelling segregation bands and the observation of a first-order transition to orientational order in Vicsek model [60], that was first reported in [147].

Some examples for the segregation bands in the Vicsek model are displayed in Fig. 71. The segregation bands in the Vicsek-models consist of many particles that are roughly aligned and travel mostly orthogonal to the edge of the band. Recently, improved mean-field theories were able to reproduce the simultaneous occurrence of segregation band and orientational order as well as the correct relation between the traveling [36,38,239]. An exhaustive discussion of these phenomena in the Vicsek model can be found, e.g. in [60,362].

A recent study of the Peruani model addresses the collective properties of self-propelled particles with nematic interaction (LC-alignment). Extensive simulations have revealed long-range nematic order, phase separation, and space-time chaos mediated by large-scale segregated structures, which we will describe low in greater detail [141].

The simplicity of this model allowed to deal with large numbers of particles, revealing a phenomenology previously unseen in more complicated models sharing the same symmetries [207,271,369], where mostly clustering phenomena were reported.
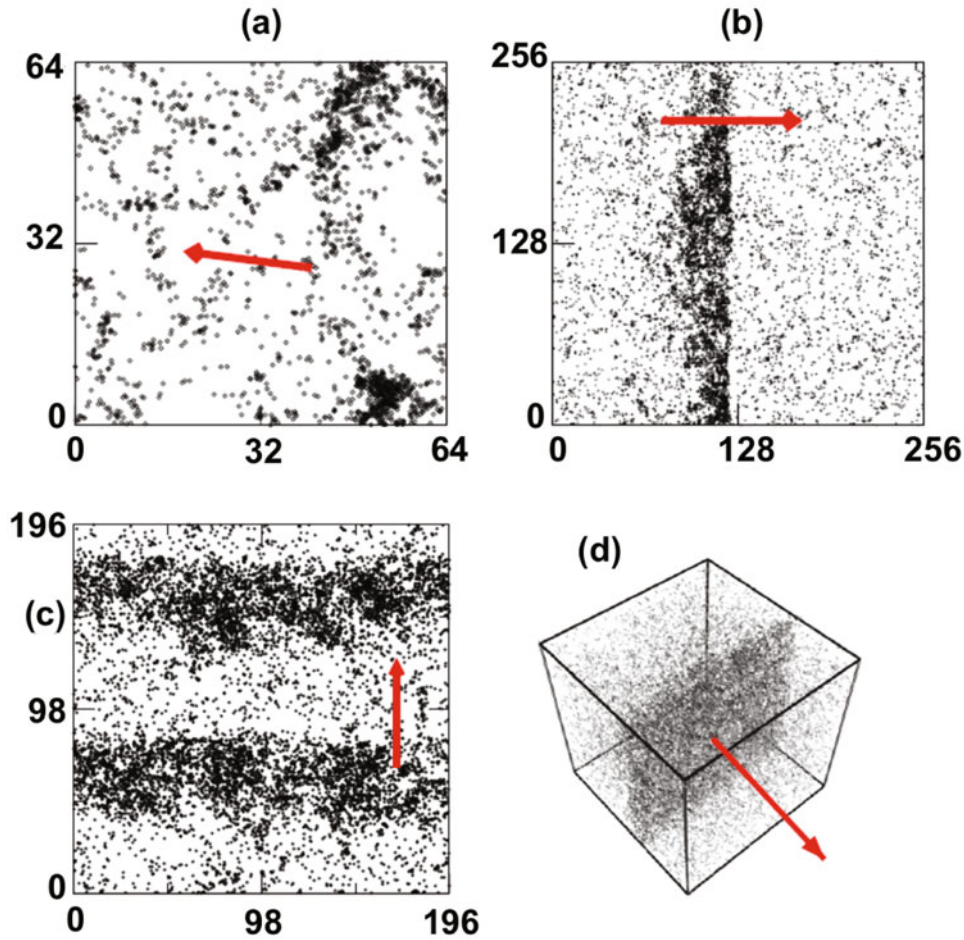
Fig. 71. Typical snapshots in the ordered phase obtained from simulations of the Vicsek-model. Points represent the position of individual particles and the red arrow points along the global direction of motion. (a,b) Vicsek model with angular noise and increasing system size. (c) Bands in simulation of Vicsek-model with angular noise, repulsive force, and periodic boundary conditions. (d) High-density sheet traveling in a three-dimensional box with periodic boundary conditions and angular noise. All figures from [60].

The two-dimensional simulation study showed large-scale segregation bands distinctively different from both those of the polar-ferromagnetic (F-alignment) case of the Vicsek model and of active nematics. Segregation appeared as a phase separation into high and low density areas: in the ordered side, a dense band occupying a fraction of space along which particles move in both directions arises when noise is strong enough. Remarkably, the instability marks the order/disorder transition. It vanishes at strong noise, splitting the disordered phase in two. The class of polar particles aligning nematically exhibits thus a total of four phases. Polar and nematic order in the model with LC-alignment can be characterized by means of the two time-dependent global scalar order parameters $P(t) = |\langle \exp(i\theta_j^t) \rangle_j|$ (polar) and $S(t) = |\langle \exp(i2\theta_j^t) \rangle_j|$ (nematic), as well as their asymptotic time averages $P = \langle P(t) \rangle_t$ and $S = \langle S(t) \rangle_t$. A brief survey of the stationary states observed in a square domain is provided in Figs. 72. Despite the polar nature of the particles, only *nematic* orientational order
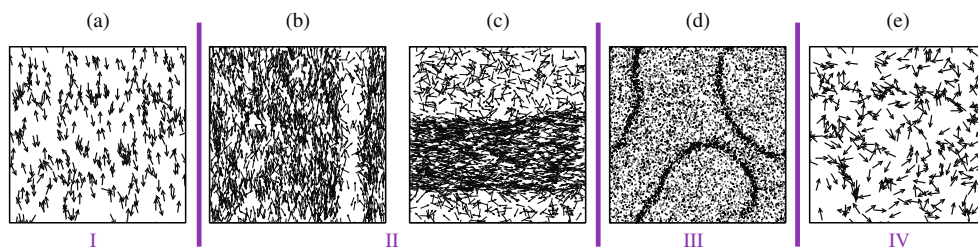
Fig. 72. (Color online) (a-c) Typical steady-state snapshots at different noise values (linear size $L = 2048$). (a) $\eta = 0.08$, (b) $\eta = 0.10$, (c) $\eta = 0.13$, (d) $\eta = 0.168$, (e) $\eta = 0.20$. Arrows indicate the polar orientation of particles (except in (d)); only a fraction of the particles are shown for clarity reasons. For a movie corresponding to (d) see suppl. material of [141].
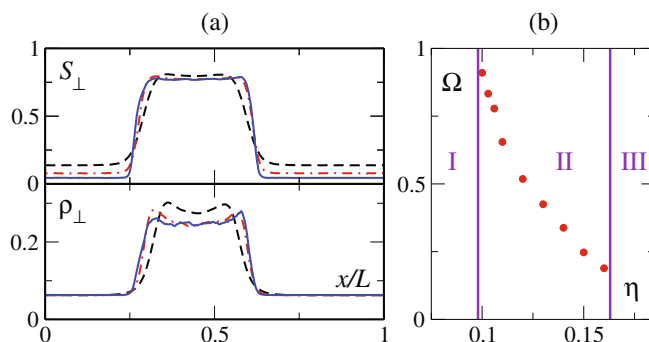

Fig. 73. (Color online) Phase II (stable bands). (a) Rescaled transverse profiles in square domains of linear size. Data averaged over the longitudinal direction and time, translated to be centered at the same location. Bottom: density profiles. Top: nematic order parameter profiles. (b) Surface fraction Ω as a function of η (defined here as the mid-height width of the rescaled S profile) [141].

arises at low noise, while P always remains near zero. Both the ordered and the disordered regimes are subdivided in two phases, one that is spatially homogeneous (Figs. 72(a,e)), and one where density segregation occurs, leading to high-density ordered bands along which the particles move back and forth (Figs. 72(b-d)). A total of four phases was observed, labeled I to IV by increasing noise strength hereafter. Phases I and II are nematically ordered, phases III and IV are disordered.

Phase I, present at the lowest η values, is ordered and spatially homogeneous (Fig. 72a). Phase II differs from phase I by the presence, in the steady-state, of a low-density disordered region. In large-enough systems, a narrow, low density channel emerges rather suddenly, like in a nucleation process (Fig. 72b). It becomes wider at larger η values, so that one can then speak of a high-density ordered band, typically oriented along one of the main axes of the box, amidst a low-density disordered background (Fig. 72c). Particles travel along the high-density band, turning around or leaving the band from time to time. Within the band, nematic order with properties similar to those of phase I is found (slow decay of S with system size, giant number fluctuations). The (rescaled) band possesses a well-defined profile with sharper and sharper edges as L increases (Fig. 73a). The fraction area Ω occupied by the band is asymptotically independent of system size and decreases continuously as the noise strength η increases (Fig. 73b).
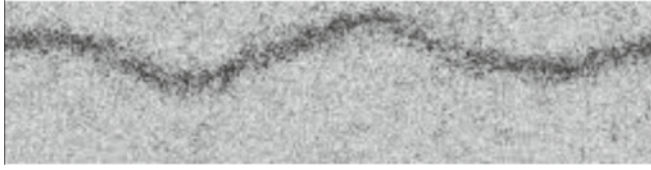
Fig. 74. Phase III (unstable bands, $\eta = 0168$). Snapshot of coarse-grained density field during the growth of the instability of an initially straight band in a 4:1 aspect ratio rectangular domain.

In phase III, spontaneous segregation into bands still occurs (for large-enough domains), however these thinner bands are unstable and constantly bend, break, reform, and merge, in an unending spectacular display of space-time chaos (Fig. 72d). Thus, the transition between phase II and III, located near $\eta_{II-III} \simeq 0.163(1)$, is the order-disorder transition of the model. It resembles a long wavelength transversal instability of the band (see for instance Fig. 74).

Increasing further the noise strength, the segregated bands vanish, leaving phase IV, an ordinary disordered phase, spatially-homogeneous, and with very short correlations in space and time (Fig. 72e). Near the transition point, at $\eta_{III-IV} \simeq 0.169(1)$, the nematic order parameter $S(t)$ exhibits bistability between a low amplitude, fast fluctuating state (typical of phase IV) and a larger amplitude, slowly fluctuating one typical of phase III [141]. This suggests a discontinuous disorder-disorder transition between phase III and IV for the Peruani model similar to the above cited results for the Vicsek-model.

Note also that the above results, and in particular the space-time chaotic motion of the spontaneously segregated bands (phase III) (see supp. material in [141]), are reminiscent of the streaming and swirling regime which characterizes the aggregation of myxobacteria [179,186,382]. The model results suggests that no adhesion or chemical signaling is needed for such behavior to emerge, LC alignment mediated by volume-exclusion interaction is sufficient to obtain complex patterns. These results may therefore be relevant for the collective dynamics of gliding bacteria, biofilms and other cells with friction and moderate adhesion.

At a more general level, the findings reveal unexpected emergent behavior among the simplest situations giving rise to collective motion. The described model of self-propelled polar objects aligning nematically stands out as a member of a universality class distinct from both that of the Vicsek model [60,349,361] and that of active nematics [61]. Thus, in the out-of-equilibrium context of self-propelled particles, the symmetries of the moving particles and of their alignment interactions must be considered separately and are both relevant ingredients. A major lesson of the discovery of large-scale separation bands of different symmetries for the models with F- and LC-alignment is that mean-field and other continuum theories have to be extended to allow for density instabilities. Improved continuum models should eventually reproduce the behaviour found in large-scale simulation, first promising steps in this direction have been provided by Bertin et al. [38] and Mishra et al. [239].

8 Discussion, outlook and conclusions

The first systematic studies of systems far from equilibrium and their surprising self-organizing capabilities date back more than half a century back and are connected to such distinguished scientists as *Alan Turing*, *Ilya Prigogine* or *Hermann Haken*. The ideas and concepts formulated and introduced by this scientific pioneers inspired

generations of statistical physicists and applied mathematicians to pursue their research on corresponding problems with applications to physics, chemistry and biology.

Recently, a subclass of such far from equilibrium systems, characterized by active motion of individuals units, received growing attention. The continuously increasing number of publications on such systems, are probably the best proof for an intense and ongoing research activity. The individual active units may be of very different type and the relevant spatial length scales may span over many orders of magnitude starting from the nanometer scale governing the motion of individual molecular motors to kilometers in the case of large collectively moving swarms of insects, such as desert locusts. Despite this apparent heterogeneity of active systems, the common fundamental properties and universal dynamical features, suggest the formulation of generic models of active motion within the framework of dynamical and stochastic systems. The mathematical description based on the concept of individual active particles, allows on the one hand the detailed understanding of the dynamics of individual units constituting an active system and on the other hand enables us in a simplified setting to derive coarse-grained equations and to study the large-scale behavior of "active matter" systems. Here, the focus lies on the rather simple models, which in the ideal case provide qualitative insights to the universal dynamics and allow often for analytical treatment at the costs of quantitative predicitive power of specific active matter realizations.

In Sections 2 and 3 we have introduced the mathematical framework for the description of self-propelled motion of individual Brownian particles and analyzed the behavior of a number of different models. We discussed the concept of active Brownian motion and its description via velocity-dependent friction functions based on the assumption of an internal degree of freedom of individual particles (energy depot) or as an effective description of ensembles of coupled active particles (molecular motors). Here, we did not restrict ourselves to the case of Gaussian fluctuations, but discussed different types of stochastic forces, such as dichotomous Markov noise or shot-noise, and their impact on the system dynamics. Based on the non-equilibrium nature of the studied dynamics, we addressed the question of the different impact of active and passive fluctuations and have shown that active fluctuations, which are correlated with the direction of motion of individual particles lead to characteristic deviations of the corresponding speed and velocity distributions, independent on model details, such as a particular choice of the friction function.

Furthermore, we analyzed the diffusive motion of free active particles (Sect. 4) and their dynamics in external confinements (Sect. 5). The detailed analysis of the individual dynamics reveals surprising features of active Brownian motion such as a giant diffusion regimes or optimal noise values, which maximize or minimize the spatial diffusion.

In the last two sections we have extended our analysis to "swarms" and "gases" of interacting active particles. In Sect. 6, we identified for example the fundamental stationary modes of collective motion of active Brownian particles with attracting interactions (swarms) and discussed novel results on the complex behavior of swarms with attraction and repulsion in three spatial dimensions.

An important class of interactions studied in the literature is the so-called velocity-alignment, which we put a particular emphasis on in Sect. 6. We have shown how, starting from microscopic Langevin equations of active Brownian particles with polar velocity alignment, we can derive systematically the corresponding mean field equations. We then focus on the onset of order in the special class of minimal models of self-propelled particles, with polar and apolar alignment interaction, motivated by the well known Vicsek-model.

Finally, we have discussed pattern formation in such minimal models, which show features such as clustering and formations of large scale density inhomogeneities in

Sect. 7. This patterns are intrinsically connected to the active motion of the inter-
acting units and the onset of large-scale collective motion, and are up to date under
intense investigation.

Despite our focus on qualitative understanding, the comparison with experimental
results of active matter systems and corresponding modelling approaches, which were
motivated by those, must not be neglected.

8.1 Individual dynamics – experiments and models

The most obvious example of autonomous self-propelled motion, which does not re-
quire external driving, is the motile behavior of biological agents. Here, the single-
celled motile organism, such as certain bacteria or eukaryotic cells (e.g. Dictyostelium
discoideum) are probably what comes closest to the concept of an "active Brownian
particle" as discussed in this review. However, being "simple" in comparison to higher
organisms, does not mean that the corresponding mechanisms of active motion is not
complex. In fact, in recent decades we witnessed a burst in scientific advances which
pushed forward our understanding of cell motility. The active translocation of cells is
driven by complex dynamics of the intracellular actin cytoskeleton (see e.g. [241]). It
is a fascinating field of interdisciplinary research already for decades, which continues
to thrive and continuously motivates theoretical investigations (see e.g [112,139,203]
and recent reviews [126,183]).

Bacteria, for example, can exhibit different motility types to propel themselves
under different environmental conditions [110,191]. Probably the best understood
bacterial motility type is swimming in a liquid medium due to the action of rotating
flagella [33,328]. The typical bacterial swimming motion consists of straight runs
interrupted by short reorientation events. This so-called "run & tumble" motion has
been successfully modelled by a random walk approach [32,64], where usually constant
speed and Poissonian distribution of reorientation events is assumed. However, a closer
look at some real trajectories reveals that in between the tumbles a bacterium does not
move in a perfect straight line with constant speed [242]. Brownian fluctuations as well
as possible fluctuation in the driving force lead to more complicated dynamics. Thus,
a more realistic model can be obtained by a combination of a Langevin description,
as discussed in this review, together with tumbling dynamics, as suggested by Condat
et al. [67]. Yet the authors considered in their model only passive fluctuations and a
consideration of active fluctuations (Sect. 3.3) will yield different results.

Swimming of bacteria, as well as other microorganisms (e.g. microalgae [89]),
takes place at extremely low Reynolds numbers ($\sim 10^{-6}$) and a large number of
theoretical studies investigated the active motility of swimmers using an overdamped
hydrodynamical description (Stokes equation) which takes into account interactions
between the active swimmer and the fluid. This approach yields some interesting
preditions on long-ranged hydrodynamical coupling between different swimmers as
well as between cells and surfaces (see e.g. [7,163,164,210,277,281], or a recent review
in [211]). However, recent experiments with *E. Coli* conducted by Drescher et al.
[88], show that in most cases the effects of long-ranged hydrodynamic interactions
are negligible in comparison to the intrinsic stochasticity in the motion of bacteria
(i.e. rotational diffusion). Thus, the authors conclude that the collective dynamics of
bacteria might be quite similar to the dynamics exhibited for example by granular
systems. Based on this surprising results, Langevin equations may be an interesting
modeling alternative, as they allow for simple implementation of various interactions
(see Section 6 and [29,74,297]).

A common objection against bacterial equations of motion of the Langevin type
are negligible inertial effects due to the extremely low Reynolds numbers at which the

dynamics takes place. However, second-order equations of motion may offer a suitable effective description in the presence of additional time scale(s) in the propulsion mechanism and the resulting bacterial response to external signals, as for example to gradients of chemical agents in their environment (chemotaxis). Furthermore, Langevin equations can provide a reasonable framework for modelling other motility types observed in bacteria, such as twitching or gliding. In particular in cases where the shortest time-scales – where the details of the specific propulsion mechanism play an important role – are not of interest.

We have only briefly discussed chemotactic behavior in the context of collective dynamics in Section 6.3.2. For a more detailed discussion on chemotaxis, we refer the interested reader to the rich literature on this fascinating topic [35, 110, 174, 228, 365].

In recent years, there has been a number of empirical studies analyzing the motion of various eukaryotic cells crawling on substrates [42, 83, 216, 217, 318, 319]. All these studies have shown that the Ornstein-Uhlenbeck model of persistent Brownian motion is not sufficient to explain the empirical observation, but differ in their conclusions. Dieterich et al. [83] suggest the description of the cell migration by a fractional Klein-Kramers equation, in order to explain the observed anomalous dynamics. However, this conclusion have been questioned as the apparent super-diffusive behavior may be a consequence of too short observation times with respect to possible long relaxation times of the direction of motion of individual cells [54, 216, 273].

The analysis of the deterministic and stochastic accelerations derived from the tracking data in [42, 216, 318, 319], show similar behavior for different cells types: 1) a negative linear drift which corresponds to constant Stokes friction, and 2) fluctuations strengths increasing with the speed of the cell, which indicates multiplicative noise in the corresponding Langevin equation.

Researchers around Henrik Flyvbjerg and Edward C. Cox, have carefully analyzed the experimental trajectories of different cell types and proposed different models of persistent motion using Langevin equations based on their empirical findings. For human epidermal cells, they formulated stochastic integro-differential equation of motion with a kernel representing a short-ranged memory of the cell [318, 319]. Hereby, they motivated their choice with the double-exponential decay of the cell velocity autocorrelation. This however can be also explained by a simper model with independent fluctuations in the velocity and direction of motion as proposed by Peruani and Morelli [273] and discussed in Sect. 4.3.2. The same group also analyzed the motion of Dictyostelium discoideum amoeba, and have shown that its motion consists of two components: a persistent stochastic motion and a fast oscillatory contribution. This oscillatory dynamics at short time-scales can be linked to the specific propulsion mechanism. The cells move forward by growing protrusions at their leading edge, so-called pseudopods, attaching them to the substrate and "pulling" themselves forward by contracting their trailing edge. A repeated right-left-right-left formation of such pseudopods leads to a zig-zag motion responsible for the oscillatory contribution [217, 318]. Similar observations have been reported previously by Shenderov and Sheetz [321], and just recently by Yang et al. [373]. In fact, oscillatory dynamics are not restricted to Dictyostelium amoeba, but have been reported also by Barnhart et al. [18] in motile fish keratocytes. The authors use a modelling approach to show, that such oscillation may be explained by the effective elastic coupling of the different parts of the cells, in particular the leading and trailing edges.

Only recently, Zaburdaev et al. [380] investigated the swimming motion of the parasite African tryponosome. Based on similar analysis of empirical data as discussed above for eukaryotes, the authors propose a Langevin model of its motion. In their model, the authors distinguish a slow velocity component, characterized by a constant speed and subject only to rotational diffusion and an additive fluctuating component with linear relaxation. Essentially, this corresponds to an active Brownian

particle, with a Schienbein-Gruler friction function as discussed in Sect. 3.3 with active and passive fluctuation terms, corresponding to the angular diffusion of the slow component and the vectorial noise in the fast component, respectively.

The Langevin models based on velocity-dependent friction function as discussed in this review, can not account for the specific details of active motion of crawling cells such as the observed oscillating dynamics on short time-scales. However, they yield a simple description at longer temporal and spatial scales, where such fast and typically small oscillatory motion can be neglected or considered as an additional quasi-stochastic contribution to the dynamical behavior.

We have introduced and discussed in Sect. 2.3 and 3.4 "internal coordinates", a co-moving coordinate system determined by the propulsion and symmetries of the active particle. Based on empirical investigation of cell trajectories, Li et al. emphasize in [216] the importance of using such a coordinate system attached to the cell instead of the laboratory reference frame.

Zooplankton species, such as Daphnia, represent another example of actively moving biological agents, which are currently investigated due their ecological importance (see e.g. [65, 78, 120, 133, 232, 255, 333]). Daphnia motion consists of straight hops interrupted by turning events with exponentially distributed turning angles [120, 133] and can be modelled as a persistent random walk (see Sect. 4 and [133, 200]). Frank Moss and coworkers advocated the theory that the specific motion pattern of Daphnia is the results of evolutionary adaptation to foraging in finite food patches. Although this hypothesis is difficult to prove, it is at least consistent with various empirical observations [79, 133].

An example of non-living active Brownian particles are the autonomously moving micro- and nanoscale particles which convert chemical energy into kinetic energy of motion (see e.g. [169, 178, 190, 199, 238, 265] or a recent reviews in [96, 140]). One general mechanism of self-propelled motion of these objects is so-called self-phoresis. In general, phoresis refers to the effective transport of colloids due to boundary layer forces induced by external fields [8]. For example, diffusiophoresis refers to a drift experienced by a colloidal particle subject to concentration gradient across its interface. Self-phoresis is thus the phenomenon, where the change in the environment, which leads to phoretic drift (e.g. formation of a concentration gradient), is induced by the particle itself. Self-propulsion can be achieved by breaking the symmetry in the ability to catalyze some "fuel" substance on its surface. For example platinum is a catalyst for the decomposition of hydrogen peroxide (H_2O_2) into oxygen and water. A particle half-coated with platinum in a fluid containing H_2O_2 will perform self-propelled motion with a speed depending on the concentration of H_2O_2 [169, 190, 356]. This was theoretically investigated using simplified models by Golestanian et al. [143, 144], as well as detailed molecular dynamics simulations by Kapral and co-workers [300, 341].

The first experimental realization of such systems, triggered a surge of research on catalytic self-propelled particles. For example, it was shown that these objects can transport cargo [337], or can be effectively controlled by external (e.g. magnetic) fields [346].

The propulsion direction set via the self-phoresis asymmetry, defines the preferred direction of motion (heading) [97, 190] as introduced in Sect. 2.3 & 3.3. Due to their small size, the particles are subject to Brownian fluctuations, but in addition we expect that non-thermal fluctuations associated with the non-equilibrium propulsion will contribute to the stochasticity in their motion. Thus, these object, as well as related autonomous swimmers appear as very good candidates for polar active particles with passive and active fluctuations as introduced in Sect. 3.3. In addition, it is possible that for non-sperical but axis-symmetric particles, a mis-alignment of the self-phoresis symetry axis with the "body axis" will introduce systematic torques into the dynamics of active particles as discussed in Sect. 4.3.5 and in [367].

Another interesting application of such chemically driven particles is the fabrication of nano-rotors by attaching the particles to a substrate [127,238], which can be described by a simple models of confined active Brownian particles discussed in Sect. 5.

Interestingly, the Cartesian velocity histograms of both, freely moving cells and artificial self-propelled particles are non-Gaussian and show increasing counts at low velocities (low speeds) [42,190,217]. In Sect. 3.2.1 and 3.3, we have shown that this behavior is generic in the presence of active fluctuations. Hereby, the deviation from a Gaussian probability distribution function at low velocities increases with increasing strength of active fluctuations. In fact, similar effect can be observed for oscillatory self-propulsion as discussed in Sect. 3.1.7 [295].

It appears that the concept of Active Brownian particles, is even better suited as a general model of such autonomously moving artificial objects than for the motion of biological agents due to the simpler propulsion mechanism. We believe it may contribute significantly to the understanding of the active diffusion of these self-propelled particles, as well as their behavior in external fields.

8.2 Collective dynamics – experiments and models

Experimental examples for collective dynamics and pattern formation of active particles are often found during the life cycles of bacteria or other microorganism like Dictyostelium discoideum (Dd) [29]. While aggregation and patterns in Dd cells are mostly driven by chemotaxis, i.e. motility responses to a chemoattractant generated by the cells itself, other organisms like myxobacteria [186] provide intriguing examples of self-organization of active, self-propelled objects. In contrast to processes controlled and influenced strongly by biochemical communication between the active agents (= cells), more recently experiments with swimming and gliding bacteria have been performed that focus on the interaction between active motion and simple physical interactions.

Swarming behavior in colonies of up to a thousand swimming bacteria *Bacillus subtilis* have been investigated by Zhang and coworkers [381]. Their setup allowed to locate the individual cells and determine their directions of motion. As a result, Zhang et al. could determine the number fluctuations as well as the cluster size statistics of the bacterial swarms. They found cluster size distributions similar to the ones reported for the self-propelled rod models for densities below the nonequilibrium clustering transition in Section 7, i.e. the identified distributions of a form $P(n) \propto n^{-b}e^{-n/n_C}$ where n denotes the cluster size and n_C a density-dependent fit parameter. The exponent b was density independent and took on a value of $b = 1.85$. In parallel, Zhang et al. report giant number fluctuations for the standard deviation of the particle numbers $\Delta_N \propto N^{\alpha}$ with an exponent α near 0.75 for small mean cell numbers N. These giant number fluctuations are presumably linked to the formation of larger clusters of cells moving in the same direction. In more recent work, Peruani et al. analyzed the collective motion of up to two thousand gliding bacteria in a two-dimensional monolayer. The organism under study was a mutant species of *Myxococcus Xanthus* that does no possess flagella and does not exchange biochemical signals relevant for the control of their motility [275]. Experiments were conducted over a large range of densities. As a result a transition to nonequilibrium clustering was found at a critical coverages of around 16 percent. The cluster size distribution at the transition became a power law with exponent $b = 1.88$ and a pronounced second maximum was found at large cluster sizes for densities above the critical value. In addition giant number fluctuations with exponent $\alpha \approx 0.8$ were found. It is striking that quite different bacterial systems (gliding myxobacteria and swimming Bacillus subtilis) exhibit similar clustering dynamics and related giant number fluctuations. If we

recall that the cluster size distribution $P(n)$ discussed here is related to the weighted cluster size distribution $p(n) = nP(n)$, we immediately get a relation $b = 1+c$, where c is the exponent of the cluster size distribution discussed in Subsection 7.3 above. The exponents $c \approx 0.9$ [271] and a c in the range of 0.9–1.3 [375]. This suggests that collective dynamics of some bacterial species may be indeed well described by self-propelled rod-shaped particles with volume exclusion interactions.

Another experimental system, wherein spectacular experimental phenomena were observed, is a motility assay with actin filament, ATP and immobilized molecular motors [303]. Below a critical density of ca. 5 filaments per square micrometre, a disordered phase with no preferred orientation is observed in these experiments. Above, the critical density different ordered patterns are observed. First moving clusters of filaments are observed similar to the observation presented for self-propelled rods. Above a second threshold of 20 filaments per square micrometre traveling density bands are observed similar to the ones found in the Vicsek model, i.e. high density traveling waves (or bands) composed of aligned filaments that travel individually in the some direction of motion as the whole wave. These bands are reminiscent of the observation in simulation presented in Fig. 71. Schaller et al. were able to reproduce their experimental findings in a cellular model that was based on similar assumptions as the simple models for collective motion discussed in Section 6 and 7 [303]. In parallel, swirling vortex-like motion states were also observed in the whole above the first critical density of ca. 5 filaments per square micrometre. In a related study with a motility assay that contained filaments, ATP, motors and crosslinking proteins, Köhler et al. report pattern formation characterized by a broad distribution of cluster sizes [198]. With time a coarsening of these clusters and a related higher percentage of large clusters was observed. A detailed quantitative analysis of the cluster sizes was not carried out. Hence, only future experiments will show if the cluster size distributions will follow similar laws as the ones reported above for similar of collective motion of active particles. A class of physical systems that realize self-propelled particles are ensembles of driven granular particles with asymmetric shape and weight distribution. Kudrolli et al. studied cylindrical rod-shaped particles with strongly asymmetric weight distribution and reported local ordering as well as a strong tendency to aggregation and persistent swirling motion in which velocities are strongly correlated with particle orientation [207]. The findings agree quite well with simulations of self-propelled system, where Wensink et al. have also reported aggregation of rods near the boundary [369].

Another experimental realization of collective motion in granular particles was designed by Deseigne *at al.* [82], who studied vibrated polar discs (= discs with asymmetric material density) in a system with a petal-shaped boundary. This particular shape avoids the aggregation of particles at the boundary and leads to more homogeneous distributions of the moving particles. The experiments then yields orientational order and giant number fluctuations with exponent $\alpha \approx 0.725$. This is again in the ballpark of the observation for the simple models discussed in Sect. 7 as well as similar to the values measured for bacterial swarms above.

Altogether, simulations of models describing the motion of active Brownian particles and their interactions are in good agreement with many recent findings for living systems such as bacteria, in-vitro biological systems like motility assays and driven granular matter. One is tempted to look for universal properties of such systems. There is however a large plethora of patterns that cannot be reproduced from the simple assumption discussed in extenso in this review. For such systems, the models analyzed and described may nevertheless provide good starting points in model developments.

Bacterial colonies and social amoeba as discussed above, are by far not the only biological systems exhibiting collective motion on large scales. In fact, colloquially

a "swarm" is typically associated with collective motion of higher organisms such as, flocks of birds, schools of fish, or the devastating mass migration of insects (e.g. desert locusts). Up to recently, experimental data on the individual behavior and collective motion patterns was rather limited [202, 252]. As a consequence most models of collective motion motivated by the different swarming phenomena relied on more or less empirically based assumptions and qualitative matching of the model behavior with empirical observations (see e.g. [10, 41, 72, 262, 286] and further references in Sect. 6). Most of these models share the following three interactions mechanisms: 1) short-ranged repulsion responsible for collision avoidance, 2) long-ranged attraction ensuring group cohesion and 3) directional alignment (typically at intermediate distances) facilitating collective motion of the group. These type of models is usually referred to as zone-models. Many of these models assume for simplicity constant speed of individuals.

However, new experimental methods, such as automated digital video recordings, allow the collection of large data sets. This enables not only the statistical analysis of collective motion in nature [51] but allows also to infer the interaction rules between individuals [17, 56, 162, 188, 225].

Based on careful analysis of experimental recordings of starling flocks and the resulting correlation functions, Ballerini et al. [17] have shown that each individual responds on average to the behavior of a fixed number of its nearest neighbors. Thus, they conclude that the interaction between individual birds is governed primarily by the topological distance and not the metric distance as assumed in most theoretical models also those discussed in Sect. 6. This feature of the interactions offers a simple explanation for large density differences observed between different flocks and may also contribute to the robustness of cohesive bird flocks with respect to external pertubations (e.g. predators). In a follow-up work, Cavagna et al. [55] report scale-free fluctuations in starling flocks, which may indicate the operation of the flock close to criticality. Being close to a critical point may be advantageous for a swarm or flock acting as a collective information processing system [243, 336, 359].

Lukeman et al. [225] have collected and analyzed data on collective behavior of surf scoters swimming on the water surface. The authors fit their data to a zone model, identify the best parameter values and argue that the standard zone model has to be complemented by an additional interaction to the front.

Very recently two studies have appeared, which infer the social interaction rules between fish [162, 188]. Both studies report that speed modulation is the primary response to close by individuals in front or in the back. This speeding up/slowing down as well as turning behavior of the fish are consistent with an attraction-repulsion behavior but show no clear evidence for directional alignment. In addition, Katz et al. [188] report that the three fish interaction is neither given by a superposition nor an averaging of pairwise-interactions, whereas Herbert-Read et al. [162] stress the importance of the interactions with the nearest neighbor.

In the light of these recent results, the active Brownian particle concept appears as a promising starting point for the development of more realistic models of collective motion as it 1) naturally accounts for a variable velocity of individuals and acceleration/deceleration due to effective forces, and 2) exhibits collective motion for simple attraction/repulsion interactions without need of alignment terms as discussed in Sect. 6.1 and 6.1.6. In this context, we should note that the escape & pursuit interaction introduced in Sect. 6.3.1, represents a special case of general position and velocity-dependent attraction/repulsion interaction [293]. Furthermore, we should mention here the fascinating experiments of Showalter and coworkers on collective motion of reaction-diffusion wave segments interacting only via attraction and repulsion [329, 347]. The non-linear motion dynamics of individual segments together with attraction and repulsion lead to an effective alignment. This is the same general

principle, reponsible also for the translational motion of active Brownian particle discussed in section 6.

As stated in Sect. 6.3.1, the escape & pursuit interactions were directly motivated by the empirical evidence for cannibalism being the driving mechanism of collective motion in certain insect species (Mormon crickets, desert locusts) [25, 26, 324]. The simple Brownian agent model [294] can be easily modified to account in more detail for movement patterns of individual insects. A parametrization of such an extended escape & pursuit model with experimental results is not only in good agreement with experimental observations, but enables us also to make specific predictions on the impact of the nutritional state of individuals on the onset of collective motion [27]. A generalized version of the model [293] can account for different types of individual interactions ranging from pure avoidance behavior, via escape & pursuit to pure attraction and allows the evolution of escape and pursuit behavior and collective motion [151].

Finally, there are important biological question in the context of collective motion of higher organisms, which go far beyond the scope of this review (see e.g. [202, 252, 335]). For example, some recent publications investigate the impact of different information available to individuals [70, 71], or the evolution of heterogeneous behavioral strategies within a group [150].

Outlook & final remarks

A major challenge for the future is the comparison of novel experimental results to predictions of the different theoretical models discussed here as well as their underlying assumptions. For example, the statistical properties of fluctuations in the dynamics of active particles can be measured and analyzed in order to refine our description of active noise terms. Furthermore, the issue of variable speed and corresponding fluctuations needs certainly to be addressed in the future. Even if the general framework of Active Brownian particles accounts for variable speed, there remain many open questions on important details. The corresponding theoretical results rely often on approximations and rather simple assumptions, which may not be justified. For example, possible non-trivial correlations between velocity fluctuations and changes in the direction may strongly influence the theoretical results.

In collective dynamics it is import to distinguish between universal and system specific properties. One would expect that minimal model systems should provide the answer. However, the unresolved connection between the giant number fluctuations and clustering in those systems reveals the conceptual difficulties which have to be addressed in the future. From the more biological perspective, in the light of the new measurement discussed above, the question arises about new models which are able to account for the observed interactions between individuals. Here, it appears that simple physically motivated pairwise "forces" might be not sufficient, and that a more biological centered ansatz, based on the sensory and cognitive capabilities of individuals, can be very promising.

In general, statistical physicists possess a large inventory of methods for describing and analysing complex systems, which is being continuously developed, on the background of a long experience in applying these methods to natural phenomena. In this spirit, the development of the mathematical description of natural active matter systems and their analysis, is essential for our understanding of the dynamical behavior of these systems, and gives us important insights into their role and function in the biological and ecological context.

In conclusion, this review gives an overview over the theoretical foundations and concepts of active (Brownian) particles systems and discusses recent developments in

the field of statistical physics applied to active particle systems far from equilibrium. We are aware that an all-encompassing review of the field is not feasible here, given the large number of publications from different disciplines and the intense ongoing research activity. Nevertheless, the focus on theoretical concepts and recent developments can be seen as complementary to other reviews on the topic [159,311,362] and we hope it will be of interest to researchers in statistical physics who would like to broaden their knowledge in this rapidly developing research field.

References

1. N. Abaid, M. Porfiri, J. R. Soc. Inter. **7**, 1441 (2010)
2. M. Abramowitz, I.A. Stegun, *Handbook of Mathematical Functions* (Dover, New York, 1970)
3. J. Adler, Cold Spring Harbor Symposia on Quantitative Biology **30**, 289 (1965)
4. J. Adler, Science **153**, 708 (1966)
5. J. Adler, Annual Rev. Biochem. **44**, 341 (1975)
6. M.S. Alber, M.A. Kiskowski, Y. Jiang, Phys. Rev. Lett. **93**, 068102 (2004)
7. G.P. Alexander, J.M. Yeomans, EPL (Europhysics Letters) **83**, 34006 (2008)
8. J.L. Anderson, Ann. Rev. Fluid Mech. **21**, 61 (1989)
9. V.S. Anishchenko, V.V. Astakhov, T.E. Vadivasova, A.B. Neiman, L. Schimansky-Geier, *Nonlinear Dynamics of Chaotic and Stochastic Systems* Springer Series in Synergetics. (Springer, Berlin Heidelberg, 2002)
10. I. Aoki, *Bulletin of the Japanese Society of Scientific Fisheries* (Japan), 1982
11. I.S. Aranson, A. Snezhko, J.S. Olafsen, J.S. Urbach, Science **320**, 612 (2008)
12. I.S. Aranson, L.S. Tsimring, Rev. Mod. Phys. **78**, 641 (2006)
13. I.S. Aranson, D. Volfson, L.S. Tsimring, Phys. Rev. E **75**, 051301 (2007)
14. M. Badoual, F. Jülicher, J. Prost, Proc. Natl. Acad. Sci. **99**, 6696 (2002)
15. M.D. Baker, P.M. Wolanin, J.B. Stock, BioEssays **28**, 9 (2006)
16. V. Balakrishnan, *Stochastic Processes Formalism and Applications* (1983), p. 96
17. M. Ballerini, N. Cabibbo, R. Candelier, A. Cavagna, E. Cisbani, I. Giardina, V. Lecomte, A. Orlandi, G. Parisi, A. Procaccini, M. Viale, V. Zdravkovic, Proc. National Acad. Sci. **105**, 1232 (2008)
18. E.L. Barnhart, G.M. Allen, F. Jülicher, J.A. Theriot, Biophys. J. **98**, 933 (2010)
19. F. Bartumeus, J. Catalan, G.M. Viswanathan, E.P. Raposo, M.G.E. da Luz, J. Theor. Biol. **252**, 43 (2008)
20. F. Bartumeus, M.G.E. da Luz, G.M. Viswanathan, J. Catalan, Ecology **86**, 3078 (2005)
21. A. Baskaran, C.M. Marchetti, J. Stat. Mech.: Theory Exper. **2010**, P04019 (2010)
22. A. Baskaran, M.C. Marchetti, Phys. Rev. E **77**, 011920 (2008)
23. A. Baskaran, M.C. Marchetti, Proc. National Acad. Sci. USA **106**, 15567 (2009)
24. A. Baule, K.V. Kumar, S. Ramaswamy, J. Stat. Mech. P11008 (2008)
25. S. Bazazi, J. Buhl, J.J. Hale, M.L. Anstey, G.A. Sword, S.J. Simpson, I.D. Couzin, Current Biology **18**, 735 (2008)

26. S. Bazazi, C.C. Ioannou, S.J. Simpson, G.A. Sword, C.J. Torney, P.D. Lorch, I.D. Couzin, PLoS ONE, **5**, e15118 (2010)
27. S. Bazazi, P. Romanczuk, S. Thomas, L. Schimansky-Geier, J.J. Hale, G.A. Miller, G.A. Sword, S.J. Simpson, I.D. Couzin, Proc. Royal Society B: Biol. Sci. (2010)
28. R. Becker, *Theory of Heat. Second Edition*, 2nd edn. (Springer, 1967)
29. E. Ben-Jacob, I. Cohen, H. Levine, Adv. Phys. **49**, 395 (2000), review ueber Bakterien u.ae
30. I. Bena, International J. Mod. Phys. B **20**, 2825 (2006)
31. H.C. Berg, Nature **254**, 389 (1975)
32. H.C. Berg, *Random Walks in Biology* (Princeton University Press, Princeton, 1993)
33. H.C. Berg, Proc. National Acad. Sci. USA **93**, 14225 (1996)
34. H.C. Berg, D.A. Brown, Nature **239**, 500 (1972)
35. H.C. Berg, E.M. Purcell, Biophys. J. **20**, 193 (1977)
36. E. Bertin, M. Droz, G. Grégoire, Phys. Rev. E **74**, 022101 (2006)
37. E. Bertin, M. Droz, G. Grégoire, Phys. Rev. E **74**, 022101 (2006)
38. E. Bertin, M. Droz, G. Grégoire, J. Phys. A: Math. Theor. **42**, 445001 (2009)
39. K. Bhattacharya, T. Vicsek, New J. Phys. **12**, 093019 (2010)
40. I.I. Blekhman, *Vibrational Mechanics: Nonlinear Dynamic Effects, General Approach, Applications* (World Scientific, 2000)
41. N.W.F. Bode, D.W. Franks, A. Jamie Wood, J. Theor. Biol. **267**, 292 (2010)
42. H.U. Bödeker, C. Beta, T.D. Frank, E. Bodenschatz, EPL (Europhysics Letters) **90**, 28005 (2010)
43. U. Börner, A. Deutsch, H. Reichenbach, M. Bär, Phys. Rev. Lett. **89**, 078101 (2002)
44. D. Bray, Proc. National Acad. Sci. USA **99**, 7 (2002)
45. N.V. Brilliantov, T. Pöschel, *Kinetic Theory of Granular Gases* (Oxford Univ. Press, 2004)
46. C. Van Den Broeck, J. Stat. Phys. **31**, 467 (1983)
47. D.A. Brown, H.C. Berg, Proc. National Acad. Sci. USA **71**, 1388 (1974)
48. R. Brown, Philosophical Mag. Ser. **4**, 161 (1828)
49. E.O. Budrene, H.C. Berg, Nature **349**, 630 (1991)
50. E.O. Budrene, H.C. Berg, Nature **376**, 49 (1995)
51. J. Buhl, D.J.T. Sumpter, I.D. Couzin, J.J. Hale, E. Despland, E.R. Miller, S.J. Simpson, Science **312**, 1402 (2006)
52. T. Butt, T. Mufti, A. Humayun, P.B. Rosenthal, S. Khan, S. Khan, J.E. Molloy, J. Biol. Chem. **285**, 4964 (2010)
53. M.O. Cáceres, A.A Budini, J. Phys. A: Math. Gen. **30**, 8427 (1997)
54. D. Campos, V. Mendez, I. Llopis, J. Theor. Biol. **267**, 526 (2010)
55. A. Cavagna, A. Cimarelli, I. Giardina, G. Parisi, R. Santagati, F. Stefanini, M. Viale, Proc. National Acad. Sci. **107**, 11865 (2010)
56. A. Cavagna, I. Giardina, A. Orlandi, G. Parisi, A. Procaccini, M. Viale, V. Zdravkovic, Animal Behaviour **76**, 217 (2008)
57. G. Cebiroglu, C. Weber, L. Schimansky-Geier, Chem. Phys. **375**, 439 (2010)
58. S. Chandrasekhar, Rev. Mod. Phys. **15**, 1 (1943)
59. H. Chaté, F. Ginelli, G. Grégoire, F. Peruani, F. Raynaud, The Euro. Phys. J. B **64**, 451 (2008)
60. H. Chaté, F. Ginelli, G. Grégoire, F. Raynaud, Phys. Rev. E **77**, 046113 (2008)
61. H. Chaté, F. Ginelli, R. Montagne, Phys. Rev. Lett. **96**, 180602 (2006)
62. A. Chetverikov, J. Dunkel, Eur. Phys. J. B **35**, 239 (2003)
63. S. Cilla, F. Falo, L.M. Floria, Phys. Rev. E **63**, 031110 (2001)
64. E.A. Codling, M.J. Plank, S. Benhamou, J. Roy. Soc. Inter. **5**, 813 (2008)
65. T.C. O'Keefe, M.C. Brewer, S.I. Dodson, J. Plankton Research **20**, 973 (1998)
66. C.A. Condat, G.J. Sibona. Phys. D **168**, 235 (2002)
67. C.A. Condat, J. Jäckle, S.A. Menchón, Phys. Rev. E **72**, 021909 (2005)
68. C.A. Condat, G.J. Sibona, Physica D: Nonlinear Phenomena **168**, 235 (2002)
69. I.D. Couzin, Trends Cognitive Sci. **13**, 36 (2009)

70. I.D. Couzin, Ch.C. Ioannou, G. Demirel, T. Gross, C.J. Torney, A. Hartnett, L. Conradt, S.A. Levin, N.E. Leonard, Science **334**, 1578 (2011)
71. I.D. Couzin, J. Krause, N.R. Franks, S.A. Levin, Nature **433**, 513 (2005)
72. I.D. Couzin, J. Krause, R. James, G.D. Ruxton, N.R. Franks, J. Theoretical Biol. **218**, 1 (2002)
73. T. Czernik, J. Luczka, Annal. Phys. **9**, 721 (2000)
74. A. Czirók, E. Ben-Jacob, I. Cohen, T. Vicsek, Phys. Rev. E **54**, 1791 (1996)
75. A. Czirók, H.E. Stanley, T. Vicsek, J. Physics A: Math. General **30**, 1375 (1997)
76. P.-G. de Gennes, European Biophys. J. **33**, 691 (2004)
77. N.D. Dees, S. Bahar, R. Garcia, F. Moss, J. Theoretical Biol. **252**, 69 (2008)
78. N.D. Dees, S. Bahar, F. Moss, Phys. Biol. **5**, 044001 (2008)
79. N.D. Dees, M. Hofmann, S. Bahar, Animal Behaviour **79**, 603 (2010)
80. C. Van den Broeck, Physica A **168**, 677 (1990)
81. S. Denisov, Phys. Lett. A **296**, 197 (2002)
82. J. Deseigne, O. Dauchot, H. Chaté, Phys. Rev. Lett. **105**, 098001 (2010)
83. P. Dieterich, R. Klages, R. Preuss, A. Schwab, Proc. National Acad. Sci. **105**, 459 (2008)
84. E.J. Doedel, Congr. Numer **30**, 265 (1981)
85. M. Doi, S.F. Edwards, *The Theory of Polymer Dynamics* (Oxford University Press, 1988)
86. M.R. D'Orsogna, Y.L. Chuang, A.L. Bertozzi, L.S. Chayes, Phys. Rev. Lett. **96**, 104302 (2006)
87. M.T. Downton, H. Stark, J. Physics: Condensed Matter **21**, 204101 (2009)
88. K. Drescher, J. Dunkel, L.H. Cisneros, S. Ganguly, R.E. Goldstein, Proc. National Acad. Sci. **108**, 10940 (2011)
89. K. Drescher, R.E. Goldstein, N. Michel, M. Polin, I. Tuval, Phys. Rev. Lett. **105**, 168101 (2010)
90. R. Dreyfus, J. Baudry, M.L. Roper, M. Fermigier, H.A. Stone, J. Bibette, Nature **437**, 862 (2005)
91. J. Dunkel, W. Ebeling, U. Erdmann, Eur. Phys. J. B **24**, 511 (2001)
92. J. Dunkel, W. Ebeling, U. Erdmann, V.A. Makarov, Int. J. Bif. Chaos **12**, 2359 (2002)
93. J. Dunkel, P. Hänggi, Physics Reports **471**, 1 (2009)
94. D.B. Dusenbery, Proc. National Acad. Sci. USA **94**, 10949 (1997)
95. M. Dworkin, D. Kaiser, *Myxobacteria II* (ASM Press, 1993)
96. S.J. Ebbens, J.R. Howse, Soft Matter **6**, 726 (2010)
97. S.J. Ebbens, J.R. Howse, Langmuir **27**, 12293 (2011)
98. W. Ebeling, Cond. Mat. Phys. **7**, 539 (2004)
99. W. Ebeling, U. Erdmann, Complexity **8**, 23 (2003)
100. W. Ebeling, U. Erdmann, J. Dunkel, M. Jenssen J. Stat. Phys. **101**, 443-457 (2000)
101. W. Ebeling, E. Gudowska-Nowak, A. Fiasconaro, Acta Phys. Polonica B **39**, 1251 (2008)
102. W. Ebeling, G. Röpke, Physica D **187**, 268 (2004)
103. W. Ebeling, L. Schimansky-Geier, The Eur. Phys. J. Special Topics **157**, 17 (2008)
104. W. Ebeling, L. Schimansky-Geier, A. Neiman, A. Scharnhorst, Fluctuation Noise Lett. **5**, 185 (2005)
105. W. Ebeling, F. Schweitzer, Theory Biosci. **120**, 207 (2001)
106. W. Ebeling, F. Schweitzer, B. Tilch, BioSystems **49**, 17 (1999)
107. W. Ebeling, I.M. Sokolov, *Statistical Thermodynamics and Stochastic Theory of Nonequilibrium Systems* (World Scientific, 2005)
108. A Einstein, Annal. Phys. **17**, 549 (1905)
109. A. Einstein, Annal. Phys. **324**, 371 (1906)
110. M. Eisenbach, *Chemotaxis* (World Scientific Publishing, 2004)
111. I. Eliazar, J. Klafter, Proc. National Acad. Sci. USA **102**, 13779 (2005)
112. M. Enculescu, M. Sabouri-Ghomi, G. Danuser, M. Falcke, Biophys. J. **98**, 1571 (2010)

113. M. Enculescu, H. Stark, Phys. Rev. Lett. **107**, 058301 (2011)
114. S.A. Endow, H. Higuchi, Nature **406**, 913 (2000)
115. U. Erdmann, *Kollektive Bewegung: Komplexe Strukturen in 2D-Systemen aktiver Brown'scher Teilchen fernab vom Gleichgewicht*, volume 10 of *Nichtlineare und Stochastische Physik* (Logos-Verlag, Berlin, 2003)
116. U. Erdmann, W. Ebeling, Fluctuation Noise Lett. **3**, 145 (2003)
117. U. Erdmann, W. Ebeling, Inter. J. Bifurcation Chaos **15**, 3623 (2005)
118. U. Erdmann, W. Ebeling, V.S. Anishchenko, Phys. Rev. E **65**, 061106 (2002)
119. U. Erdmann, W. Ebeling, A.S. Mikhailov, Phys. Rev. E **71**, 051904 (2005)
120. U. Erdmann, W. Ebeling, L. Schimansky-Geier, A. Ordemann, F. Moss (2004) http://arxiv.org/abs/q-bio.PE/0404018
121. U. Erdmann, W. Ebeling, L. Schimansky-Geier, F. Schweitzer, Eur. Phys. J. B **15**, 105 (2000)
122. B. Ermentrout, *Simulating, Analyzing, and Animating Dynamical Systems: A Guide to Xppaut for Researchers and Students (Software, Environments, Tools)*, 1st edn. (Society for Industrial Mathematics, 2002)
123. A. Fiasconaro, W. Ebeling, E. Gudowska-Nowak, Eur. Phys. J. B **65**, 403 (2008)
124. A. Fiasconaro, E. Gudowska-Nowak, W. Ebeling, J. Statistical Mech. Theory Exper. **2009**, P01029 (2009)
125. S. Flach, O. Yevtushenko, Y. Zolotaryuk, Phys. Rev. Lett. **84**, 2358 (2000)
126. B. Flaherty, J.P. McGarry, P.E. McHugh, Cell Biochem. Biophys. **49**, 14 (2007)
127. S. Fournier-Bidoz, A.C. Arsenault, I. Manners, G.A. Ozin, Chem. Comm. 441 (2005)
128. B.M. Friedrich, F. Julicher, Proc. National Acad. Sci. **104**, 13256 (2007)
129. B.M. Friedrich, F. Jülicher, New J. Phys. **10**, 123025 (2008)
130. A. Fulinski, Phys. Rev. E **50**, 2668 (1994)
131. R. Fürth, Z. Phys. **2**, 244 (1920)
132. M. Garcia, S. Berti, P. Peyla, S. Rafai, Phys. Rev. E **83**, 035301 (2011)
133. R. Garcia, F. Moss, A. Nihongi, J.R. Strickler, S. Göller, U. Erdmann, Lutz Schimansky-Geier, I.M. Sokolov, Math. Biosci. **207**, 165 (2007)
134. V. Garcia, M. Birbaumer, F. Schweitzer, Eur. Phys. J. B **82**, 235 (2011)
135. C.W. Gardiner, *Handbook of Stochastic Methods* (Springer-Verlag, Berlin, 1985)
136. C.W. Gardiner, *Handbook of Stochastic Methods for Physics, Chemistry and the Natural Sciences*, volume 13 of *Springer Series in Synergetics*, 2nd edn. (Springer, Berlin Heidelberg New York, 1985)
137. J. Gautrais, C. Jost, M. Soria, A. Campo, S. Motsch, R. Fournier, S. Blanco, G. Theraulaz, J. Math. Biol. **58**, 429 (2008)
138. S.A. Gerasimov, J. Appl. Mech. Tech. Phys. **43**, 90 (2002)
139. A. Gholami, M. Falcke, E. Frey, New J. Phys. **10**, 033022 (2008)
140. J. Gibbs, Y. Zhao, Frontiers Mater. Sci. **5**, 25 (2011)
141. F. Ginelli, F. Peruani, M. Bär, H. Chaté, Phys. Rev. Lett. **104**, 184502 (2010)
142. S. Goldstein, The Quarterly J. Mech. Appl. Math. **4**, 129 (1951)
143. R. Golestanian, T.B. Liverpool, A. Ajdari, Phys. Rev. Lett. **94**, 220801 (2005)
144. R. Golestanian, T.B. Liverpool, A. Ajdari, New J. Phys. **9**, 126 (2007)
145. M. Gouy, J. Phys. Théor. Appliquée **7**, 4 (1888)
146. I. Goychuk, P. Jung, S. Kohler, G. Schmid, P. Talkner (ed.), Chem. Phys. 375 (2010)
147. G. Grégoire, H. Chaté, Phys. Rev. Lett. **92**, 025702 (2004)
148. D. Grossman, I.S. Aranson, E.B. Jacob, New J. Phys. **10**, 023036 (2008)
149. T. Guerin, J. Prost, P. Martin, J.-F. Joanny, Curr. Opin. Cell Biol. **22**, 14 (2010)
150. V. Guttal, I.D. Couzin, Proc. National Acad. Sci. **107**, 16172 (2010)
151. V. Guttal, P. Romanczuk, I.D. Couzin, S.J. Simpson, G.A. Sword (submitted) (2012)
152. L. Haeggqwist, L. Schimansky-Geier, I.M. Sokolov, F. Moss, The Eur. Phys. J. Special Topics **157**, 33 (2008)
153. P. Hänggi, Adv. Chem. Phys. 89 (1995)
154. P. Hänggi, F. Marchesoni (ed.), Chaos 15 (2005)
155. P. Hänggi, F. Marchesoni, Rev. Mod. Phys. **81**, 387 (2009)

156. P. Hänggi, P. Talkner, M. Borkovec, Rev. Mod. Phys. **62**, 251 (1990)
157. P. Hänggi, H. Thomas, Phys. Rep. **88**, 207 (1982)
158. T. Harada, Europhys. Lett. (EPL) **70**, 49 (2005)
159. D. Helbing, Rev. Mod. Phys. **73**, 1067 (2001)
160. D. Helbing, I.J. Farkas, T. Vicsek, Phys. Rev. Lett. **84**, 1240 (2000)
161. D. Helbing, F. Schweitzer, J. Keltsch, P. Molnár, Phys. Rev. E **56**, 2527 (1997)
162. J.E. Herbert-Read, A. Perna, R.P. Mann, T.M. Schaerf, D.J.T. Sumpter, A.J.W. Ward, Proc. National Acad. Sci. (2011)
163. J.P. Hernandez-Ortiz, C.G. Stoltz, M.D. Graham, Phys. Rev. Lett. **95**, 204501 (2005)
164. J.P. Hernandez-Ortiz, P.T. Underhill, M.D. Graham, J. Phys.: Condensed Matt. **21**, 204107 (2009)
165. T. Hillen, H.G. Othmer, SIAM J. Appl. Math. **61**, 751 (2000)
166. T. Hillen, K.J. Painter, J. Math. Biol. **58**, 183 (2008)
167. W. Horsthemke, R. Lefever, *Noise-Induced Transitions: Theory and Applications in Physics, Chemistry, and Biology* (Springer Verlag, 1984)
168. J. Howard, *Mechanics of Motor Proteins and the Cytoskeleton* (Sinauer Associates, Sunderland, Mass, 2001)
169. J.R. Howse, R.A.L. Jones, A.J. Ryan, T. Gough, R. Vafabakhsh, R. Golestanian, Phys. Rev. Lett. **99**, 048102 (2007)
170. C. Huepe, M. Aldana, Phys. Rev. Lett. **92**, 168701 (2004). Copyright (C) 2008. The American Physical Society; Please report any problems to prola@aps.org
171. C. Huepe, M. Aldana, Physica A (2008)
172. A. Huth, C. Wissel, J. Theor. Biol. **156**, 365 (1992)
173. H. i Wu, B.-L. Li, T.A. Springer, W.H. Neill, Ecological Modell. **132**, 115 (2000)
174. P.A. Iglesias, P.N. Devreotes, Current Opinion Cell Biol. **20**, 35 (2008)
175. O.A. Igoshin, R. Welch, D. Kaiser, G. Oster, Proc. National Acad. Sci. USA **101**, 4256 (2004)
176. T. Ihle, Phys. Rev. E **83**, 030901 (2011)
177. J. Ingen-Housz, Verm. Schriften Physisch-Medicinischen Inhalts (1784)
178. R.F. Ismagilov, A. Schwartz, N. Bowden, G.M. Whitesides, Angewandte Chemie **114**, 674 (2002)
179. L. Jelsbak, Proc. National Acad. Sci. **99**, 2032 (2002)
180. J.-F. Joanny, F. Jülicher, J. Prost, Phys. Rev. Lett. **90**, 168102 (2003)
181. F. Jülicher, A. Ajdari, J. Prost, Rev. Mod. Phys. **69**, 1269 (1997)
182. F. Jülicher, A. Ajdari, J. Prost, Rev. Mod. Phys. **69**, 1269 (1997)
183. F. Jülicher, K. Kruse, J. Prost, J.-F. Joanny, Phys. Rep. **449**, 3 (2007)
184. P. Jung, H. Risken, Z. Phys. B **59**, 469 (1985)
185. M. Kac, Math. J **4**, 497 (1974)
186. D. Kaiser, Nat. Rev. Micro. **1**, 45 (2003)
187. P.M. Kareiva, N. Shigesada, Oecologia **56**, 234 (1983)
188. Y. Katz, K. Tunstrøm, C.C. Ioannou, C. Huepe, I.D. Couzin, Proc. National Acad. Sci. (2011)
189. R.F. Kayser, H.J. Raveché, Phys. Rev. A **17**, 2067 (1978)
190. H. Ke, S. Ye, R.L. Carroll, K. Showalter, The J. Phys. Chemistry A **114**, 5462 (2010)
191. D.B. Kearns, Nat. Rev. Micro. **8**, 634 (2010)
192. E.F. Keller, L.A. Segel, J. Theor. Biol. **30**, 225 (1971)
193. E.F. Keller, L.A. Segel, J. Theor. Biol. **30**, 235 (1971)
194. R. Kemkemer, V. Teichgräber, S. Schrank-Kaufmann, D. Kaufmann, H. Gruler, Eur. Phys. J. E **3**, 101 (2000)
195. C. Kim, E.K. Lee, P. Hänggi, P. Talkner, Phys. Rev. E **76**, 011109 (2007)
196. Y.L. Klimontovich, Physics-Uspekhi **37**, 737 (1994)
197. Yu.L. Klimontovich, *Statistical Theory of Open Systems* (Kluwer Academic Publishers, Dordrecht, Boston, London, 1995)
198. S. Köhler, V. Schaller, A.R. Bausch, Nat. Mater. **10**, 462 (2011)
199. G.V. Kolmakov, A. Schaefer, I. Aranson, A.C. Balazs, Soft Matter **8**, 180 (2011)

200. N. Komin, U. Erdmann, L. Schimansky-Geier, Fluctuation Noise Lett. **4**, L151 (2004)
201. J.M. Kosterlitz, D.J. Thouless, J. Phys. C **6**, 10 (1973)
202. J. Krause, G.D. Ruxton, *Living in groups* (Oxford University Press, 2002)
203. K. Kruse, S. Camalet, F. Jülicher, Phys. Rev. Lett. **87**, 138101 (2001)
204. K. Kruse, J.F. Joanny, F. Jülicher, J. Prost, Phys. Biol. **3**, 130 (2006)
205. R. Kubo, Rep. Prog. Phys. **29**, 255 (1966)
206. A. Kudrolli, Phys. Rev. Lett. **104**, 088001 (2010)
207. A. Kudrolli, G. Lumay, D. Volfson, L.S. Tsimring, Phys. Rev. Lett. **100**, 058001 (2008)
208. K.V. Kumar, S. Ramaswamy, M. Rao, Phys. Rev. E **77**, 020102 (2008)
209. P. Langevin, Comptes Rendus Hebdomadaires des Séances de L'Academie des Sciences **146**, 530 (1908)
210. E. Lauga, W.R. DiLuzio, G.M. Whitesides, H.A. Stone, Biophys. J. **90**, 400 (2006)
211. E. Lauga, T.R. Powers, Reports Progr. Phys. **72**, 096601 (2009)
212. P.A. Lebwohl, G. Lasher, Phys. Rev. A **6**, 426 (1972)
213. C.F. Lee, Phys. Rev. E **81**, 031125 (2010)
214. K. Lekkas, L. Schimansky-Geier, H. Engel-Herbert, Z. Phys. B Cond. Matter **70**, 517 (1988)
215. H. Levine, W.-J. Rappel, I. Cohen, Phys. Rev. E **63**, 017101 (2000)
216. L. Li, E. C. Cox, H. Flyvbjerg, Phys. Biol. **8**, 046006 (2011)
217. L. Li, S.F. Nørrelykke, Edward C. Cox, PLoS ONE **3**, e2093 (2008)
218. B. Lindner, in *Physik Irreversibler Prozesse und Selbstorganisation*, edited by T. Pöschel, H. Malchow, L. Schimansky-Geier (Logos-Verlag, Berlin, 2006)
219. B. Lindner, New J. Phys. **9**, 136 (2007)
220. B. Lindner, J. Stat. Phys. **130**, 523 (2008)
221. B. Lindner, New J. Phys. **12**, 063026 (2010)
222. B. Lindner, U. Erdmann, I. Sokolov (eds.), Eur. Phys. J. Special Topics, 187 (2010)
223. B. Lindner, E.M. Nicola, Phys. Rev. Lett. **101**, 190603 (2008)
224. B. Lindner, E.M. Nicola, Eur. Phys. J. Special Topics **157**, 43 (2008)
225. R. Lukeman, Y.-X. Li, L. Edelstein-Keshet, Proc. National Acad. Sci. **107**, 12576 (2010)
226. V.A. Makarov, E. del Río, W. Ebeling, M.G. Velarde, Phys. Rev. E **64**, 036601 (2001)
227. V.A. Makarov, W. Ebeling, M.G. Velarde, Intern. J. Bifurcation Chaos **10**, 1075 (2000)
228. M.D. Manson, Adv. Microbial Physiol. **33**, 277 (1992)
229. J. Masoliver, Phys. Rev. A **35**, 3918 (1987)
230. J. Masoliver, K. Lindenberg, G.H. Weiss, Physica A: Stat. Mech. Appl. **157**, 891 (1989)
231. M. Matsushita, J. Wakita, H. Itoh, K. Watanabe, T. Arai, T. Matsuyama, H. Sakaguchi, M. Mimura, Physica A **274**, 190 (1999), unterstreicht, dass Zellen sich aktiv bewegen
232. S. Menden-Deuer, PLoS Comput. Biol. **6**, e1000942 (2010)
233. N.D. Mermin, H. Wagner, Phys. Rev. Lett. **17**, 1133 (1966)
234. R. Metzler, J. Klafter, Phys. Rep. **339**, 1 (2000)
235. A.S. Mikhailov, V. Calenbuhr, *From Cells to Societies: Models of Complex Coherent Action* (Springer, 2002)
236. A.S. Mikhailov, D. Meinköhn, in *Stochastic Dynamics*, edited by L. Schimansky-Geier, Thorsten Pöschel, editors, vol. 484 of Lecture Notes in Physics (Springer Berlin, 1997), p. 334
237. A.S. Mikhailov, D.H. Zanette, Phys. Rev. E **60**, 4571 (1999)
238. T. Mirkovic, N.S. Zacharia, G.D. Scholes, G.A. Ozin, Small **6**, 159 (2010)
239. S. Mishra, A. Baskaran, M.C. Marchetti, Phys. Rev. E **81**, 061916 (2010)
240. S. Mishra, S. Ramaswamy, Phys. Rev. Lett. **97**, 090602 (2006)
241. T.J. Mitchison, L.P. Cramer, Cell **84**, 371 (1996)
242. N. Mittal, E.O. amd Brenner Budrene, A. van Oudenaarden, Proc. National Acad. Sci. USA **100**, 13259 (2003)
243. T. Mora, W. Bialek, J. Stat. Phys. **144**, 268 (2011)
244. H. Mori, Prog. Theor. Phys. **33**, 423 (1965)
245. J.D. Murray, *Spatial models and biomedical applications* (Springer, 2003)

246. (a) H. Reichenbach, Ber. Deutsch. Bot. Ges. **78**, 102 (1965); (b) Myxobacteriales: Schwarmentfaltung und Bildung von Protocysten, Institut für den wissenschaftlichen Film, Göttingen, 1966

247. M. Nagy, I. Daruka, T. Vicsek, Physica A: Stat. Theor. Phys. **373**, 445 (2007)

248. V. Narayan, N. Menon, S. Ramaswamy, J. Stat. Mech.: Theory Exper. **2006**, P01005 (2006)

249. V. Narayan, S. Ramaswamy, N. Menon, Science **317**, 105 (2007)

250. H.-S. Niwa, J. Theor. Biol. **171**, 123 (1994)

251. B. Nordén, Y. Zolotaryuk, P.L. Christiansen, A.V. Zolotaryuk, Phys. Rev. E **65**, 011110 (2001)

252. A. Okubo, S.A. Levin, *Diffusion and Ecological Problems: Modern Perspectives*, 2nd edn., volume 14 of Interdisciplinary Applied Mathematics (Springer, New York, 2001)

253. L. Onsager, Ann. N. Y. Acad. Sci. **51**, 627 (1949)

254. A. Ordemann, G. Balazsi, F. Moss, Physica A: Stat. Mech. Appl. **325**, 260 (2003)

255. A. Ordemann, F. Moss, G. Balazsi, in *Nonlinear Dynamics and the Spatiotemporal Principles of Biology: Leopoldina Symposium*, Vol. 88 (Deutsche Akademie der Naturforscher Leopoldina, 2003), p. 87

256. L.S. Ornstein, Proc. Ser. B Phys. Sci. **21**, 96 (1919)

257. H.G. Othmer, S.R. Dunbar, W. Alt, J. Math. Biol. **26**, 263 (1988)

258. E. Palsson, H.G. Othmer, Proc. National Acad. Sci. USA **97**, 10448 (2000)

259. A. Papoulis, *Probability, Random Variables, and Stochastic Processes*, 3rd edn. (McGraw-Hill, 1991)

260. J.K. Parrish, L. Edelstein-Keshet, Science **284**, 99 (1999)

261. J.K. Parrish, W.M. Hamner, *Animal Groups in Three Dimensions* (Cambridge University Press, 1997)

262. J.K. Parrish, S.V. Viscido, D. Grünbaum, Biol. Bull. **202**, 296 (2002)

263. R.F. Pawula, Phys. Rev. **162**, 186 (1967)

264. R.F. Pawula, Phys. Rev. A **36**, 4996 (1987)

265. W.F. Paxton, K.C. Kistler, C.C. Olmeda, A. Sen, S.K. St. Angelo, Y. Cao, T.E. Mallouk, P.E. Lammert, V.H. Crespi, J. Amer. Chem. Soc. **126**, 13424 (2004)

266. K. Pearson, Nature **72** 294 (1905)

267. K. Pearson, Nature **72** 342 (1905)

268. K. Pearson, J. Blakeman, *A Mathematical Theory of Random Migration* (Dulau and co., 1906)

269. J. Perrin, *Brownian Movement and Molecular Reality* (Dover Publications, 2005)

270. F. Peruani, *From Individual to Collective Motion of Self-Propelled Particles: the Role of Particle Shape, Orientational Ordering and Clustering*, Ph.D. thesis, Technische Universität Berlin, Berlin, 2008

271. F. Peruani, A. Deutsch, M. Bär, Phys. Rev. E **74**, 030904 (2006)

272. F. Peruani, A. Deutsch, M. Bär, Eur. Phys. J. Special Topics **157**, 111 (2008)

273. F. Peruani, L.G. Morelli, Phys. Rev. Lett. **99**, 010602 (2007)

274. F. Peruani, L. Schimansky-Geier, M. Bär, Eur. Phys. J. Special Topics **191**, 173, (2011)

275. F. Peruani, J. Starruss, V. Jakovljevic, L. Søgaard-Andersen, A. Deutsch, M. Bär, Phys. Rev. Lett. **108**, 098102 (2012)

276. L. Pohlmann, H. Tributsch, Electrochim. Acta **42**, 2737 (1997)

277. C.M. Pooley, G.P. Alexander, J.M. Yeomans, Phys. Rev. Lett. **99**, 228103 (2007)

278. K. Przibram, Pflüger, Archiv Gesammte Physiol. Mensche. Thiere **153**, 401 (1913)

279. K. Przibram, Archiv für Entwicklungsmech. Organism. **43**, 20 (1917)

280. E.M. Purcell, Am. J. Phys. **45**, 11 (1977)

281. V.B. Putz, J. Dunkel, J.M. Yeomans, Chem. Phys. **375**, 557 (2010)

282. S. Ramaswamy, Ann. Rev. Condens. Matter Phys. **1**, 323 (2010)

283. S. Ramaswamy, R.A. Simha, J. Toner, Europhysics Letters (EPL) **62**, 196 (2003)

284. J.W.S. Rayleigh, *The Theory of Sound*, Vol. I, 2nd edn. (MacMillan, London, 1894) erstmalige Erwaehnung des sog. Rayleigh-Oszillators

285. P. Reimann, Phys. Rep. **361**, 57 (2002)

286. C.W. Reynolds, Proc. 14th annual conference on Computer graphics and interactive techniques - SIGGRAPH '87, (1987), p. 25
287. M.J.E. Richardson, W. Gerstner, Neural Comput. **17**, 923 (2005)
288. M.J.E. Richardson, W. Gerstner, Chaos: Interdisciplinary J. Nonlinear Sci., **16**, 026106 (2006)
289. A.J. Ridley, M.A. Schwartz, K. Burridge, R.A. Firtel, M.H. Ginsberg, G. Borisy, J.T. Parsons, A.R. Horwitz, Science **302**, 1704 (2003)
290. I.H. Riedel, K. Kruse, J. Howard, Science **309**, 300 (2005)
291. T. Riethmüller, L. Schimansky-Geier, D. Rosenkranz, T. Pöschel, J. Stat. Phys. **86**, 421 (1997)
292. H. Risken, *The Fokker-Planck Equation: Methods of Solution and Applications* (Springer Verlag, 1996)
293. P. Romanczuk, *Active Motion and Swarming: From Individual to Collective Dynamics* (Logos Verlag, Berlin, 2011)
294. P. Romanczuk, I.D. Couzin, L. Schimansky-Geier, Phys. Rev. Lett. **102**, 010602 (2009)
295. P. Romanczuk, W. Ebeling, U. Erdmann, L. Schimansky-Geier, Chaos: Interdisciplinary J. Nonlinear Sci. **21**, 047517 (2011)
296. P. Romanczuk, U. Erdmann, Eur. Phy. J. Special Topics **187**, 127 (2010)
297. P. Romanczuk, U. Erdmann, H. Engel, L. Schimansky-Geier, Eur. Phys. J. Special Topics **157**, 61 (2008)
298. P. Romanczuk, L. Schimansky-Geier, Phys. Rev. Lett. **106**, 230601 (2011)
299. P. Romanczuk, L. Schimansky-Geier, Ecological Complexity (in press) (2011)
300. G. Ruckner, R. Kapral, Phys. Rev. Lett. **98**, 150603 (2007)
301. J.M. Sancho, J. Math. Phys. **25**, 354 (1984)
302. J.M. Sancho, M.S. Miguel, S.L. Katz, J.D. Gunton, Phys. Rev. A **26**, 1589 (1982)
303. V. Schaller, C. Weber, C. Semmrich, E. Frey, A.R. Bausch, Nature **467**, 73 (2010)
304. M. Schienbein, K. Franke, H. Gruler, Phys. Rev. E **49**, 5462 (1994)
305. M. Schienbein, H. Gruler, Bull. Math. Biol. **55**, 585 (1993)
306. L. Schimansky-Geier, W. Ebeling, U. Erdmann, Acta Phys. Polonica, **36**, 1757 (2005)
307. L. Schimansky-Geier, U. Erdmann, N. Komin, Physica A: Stat. Mech. Appl. **351**, 51 (2005)
308. L. Schimansky-Geier, M. Mieth, H. Rosè, H. Malchow, Phys. Lett. A **207**, 140 (1995)
309. L. Schimansky-Geier, F. Schweitzer, W. Ebeling, H. Ulbricht, in *Self-Organization by Nonlinear Irreversible Processes*, edited by W. Ebeling, H. Ulbricht, volume 33 of Springer Series in Synergetics (Springer, Berlin, 1986)
310. T. Schwalger, L. Schimansky-Geier, Phys. Rev. E, **77**, 031914 (2008)
311. F. Schweitzer, *Brownian Agents and Active Particles: Collective Dynamics in the Natural and Social Sciences*, 1st edn. (Springer, 2003)
312. F. Schweitzer, W. Ebeling, B. Tilch, Phys. Rev. Lett. **80**, 5044 (1998)
313. F. Schweitzer, W. Ebeling, B. Tilch, Phys. Rev. E **64**, 021110 (2001)
314. F. Schweitzer, K. Lao, F. Family, Biosystems **41**, 153 (1997)
315. F. Schweitzer, L. Schimansky-Geier, Phys. A **206**, 359 (1994)
316. F. Schweitzer, L. Schimansky-Geier, W. Ebeling, H. Ulbricht, Physica A: Stat. Mech. Appl. **150**, 261 (1988)
317. F. Schweitzer, L. Schimansky-Geier, W. Ebeling, H. Ulbricht, Physica A: Stat. Theor. Phys. **153**, 573 (1988)
318. D. Selmeczi, L. Li, L. I.I. Pedersen, S.F. Nørrelykke, P.H. Hagedorn, S. Mosler, N.B. Larsen, E.C. Cox, H. Flyvbjergm, Eur. Phys. J. Special Topics **157**, 1 (2008)
319. D. Selmeczi, S. Mosler, P.H. Hagedorn, N.B. Larsen, H. Flyvbjerg, Biophys. J. **89**, 912 (2005)
320. V.E. Shapiro, V.M. Loginov, Physica A: Stat. Theor. Phys. **91**, 563 (1978)
321. A.D. Shenderov, M.P. Sheetz, Biophys. J. **72**, 2382 (1997)
322. R.A. Simha, S. Ramaswamy, Phys. A **306**, 262 (2002)
323. R. Aditi Simha, Sriram Ramaswamy, Phys. Rev. Lett. **89**, 058101 (2002)

324. S.J. Simpson, G.A. Sword, P.D. Lorch, I.D. Couzin, PNAS **103**, 4152 (2006)
325. M. Von Smoluchowski, Z. Phys. Chem. **92**, 129 (1917)
326. A. Sokolov, I.S. Aranson, J.O. Kessler, R.E. Goldstein, Phys. Rev. Lett. **98**, 158102 (2007)
327. A. Sokolov, R.E. Goldstein, F.I. Feldchtein, I.S. Aranson, Phys. Rev. E **80**, 031903 (2009)
328. Y. Sowa, R.M. Berry, Quart. Rev. Biophys. **41**, 103 (2008)
329. A.J. Steele, M.R. Tinsley, K. Showalter, Chaos 18, 026108-1-8 (2008)
330. O. Steuernagel, W. Ebeling, V. Calenbuhr, Chaos, Solitons & Fractals **4**, 1917 (1994)
331. J. Strefler, W. Ebeling, E. Gudowska-Nowak, L. Schimansky-Geier, Eur. Phys. J. B **72**, 597 (2009)
332. J. Strefler, U. Erdmann, L. Schimansky-Geier, Phys. Rev. E **78**, 031927 (2008)
333. J.R. Strickler, Philosoph. Trans. Royal Soc. London. Series B: Biol. Sci. **353**, 671 (1998)
334. Y. Sumino, N. Magome, T. Hamada, K. Yoshikawa, Phys. Rev. Lett. **94**, 068301 (2005)
335. D.J.T. Sumpter, *Collective Animal Behavior* (Princeton University Press, 2010)
336. D.J.T. Sumpter, J. Buhl, D. Biro, I.D. Couzin, Theory Biosci. **127**, 177 (2008)
337. S. Sundararajan, P.E. Lammert, A.W. Zudans, V.H. Crespi, A. Sen, Nano Lett. **8**, 1271 (2008)
338. W. Sutherland, Philosoph. Mag. Ser. **9**, 781 (1905)
339. R. Suzuki, S. Sakai, Biophysics **13**, 281 (1973)
340. B. Szabó, G.J. Szöllösi, B. Gönci, Zs. Jurányi, D. Selmeczi, Tamás Vicsek, Phys. Rev. E **74**, 061908 (2006)
341. Y.-G. Tao, R. Kapral, J. Chem. Phys. **128**, 164518 (2008)
342. G. Taylor, Proc. Royal Soc. London. Series A. Math. Phys. Sci. **219**, 186 (1953)
343. G. Taylor, Proc. Royal Soc. London. Series A. Math. Phys. Sci. **225**, 473 (1954)
344. G. Taylor, Proc. Royal Soc. London. Series A. Math. Phys. Sci. **223**, 446 (1954)
345. G.I. Taylor, Proc. London Math. Soc. **20**, 196 (1921)
346. P. Tierno, R. Albalat, F. Sagués, Small **6**, 1749 (2010)
347. M.R. Tinsley, A.J. Steele, K. Showalter, Eur. Phys. J. Special Topics **165**, 161 (2008)
348. J. Toner, Y. Tu, Phys. Rev. Lett. **75**, 4326 (1995)
349. J. Toner, Y. Tu, Phys. Rev. E **58**, 4828 (1998)
350. J. Toner, Y. Tu, S. Ramaswamy, Ann. Phys. **318**, 170 (2005)
351. C. Touya, T. Schwalger, B. Lindner, Phys. Rev. E **83**, 051913 (2011)
352. T. Toyota, N. Maru, M.M. Hanczyc, T. Ikegami, T. Sugawara, J. Amer. Chem. Soc. **131**, 5012 (2009)
353. R. Tyson, S.R. Lubkin, J.D. Murray, Proc. Royal Soc. London B **266**, 299 (1999) hat Bilder wie meine selbstkons. Feld-Simulationen
354. R. Tyson, S.R Lubkin, J.D. Murray, J. Math. Biol. **38**, 359 (1999)
355. G.E. Uhlenbeck, L.S. Ornstein, Phys. Rev. **36**, 823 (1930)
356. L.F. Valadares, Y.G. Tao, N.S. Zacharia, V. Kitaev, F. Galembeck, R. Kapral, G.A. Ozin, Small **6**, 565 (2010)
357. N.G. van Kampen, *Stochastic Processes in Physics and Chemistry*, 2nd edn. (North-Holland, Amsterdam, 1992)
358. S. van Teeffelen, H. Löwen, Phys. Rev. E **78**, 020101 (2008)
359. F. Vanni, M. Luković, P. Grigolini. Phys. Rev. Lett. **107**, 078103 (2011)
360. T. Vicsek, *Fluctuations and Scaling in Biology* (Oxford University Press, 2001)
361. T. Vicsek, A. Czirok, E. Ben-Jacob, I. Cohen, O. Shochet, Phys. Rev. Lett. **75**, 1226 (1995)
362. T. Vicsek, A. Zafiris, Arxiv preprint [`arXiv:1010.5017`], (2010)
363. J. Vollmer, A.G. Vegh, C. Lange, B. Eckhardt, Phys. Rev. E **73**, 061924 (2006)
364. M. von Smoluchowski, Annal. Phys. **326**, 756 (1906)
365. G.H. Wadhams, J.P. Armitage, Nat. Rev. Mol. Cell. Biol. **5**, 1024 (2004)
366. C. Weber, *Diffusion of Active Particles in 2D* (Master-Thesis, Humboldt Universität zu Berlin, 2010)
367. C. Weber, P.K. Radtke, L. Schimansky-Geier, P. Hnggi, Phys. Rev. E **84**, 011132 (2011)

368. R. Welch, D. Kaiser, Proc. National Acad. Sci. USA **98**, 14907 (2001)
369. H.H. Wensink, H. Löwen, Phys. Rev. E **78**, 031409 (2008)
370. C. Wiener, Poggendorffs Annal. **118**, 79 (1863)
371. D.E. Woodward, R. Tyson, M.R. Myerscough, J.D. Murray, E.O. Budrene, H.C. Berg, Biophys. J. **68**, 2181 (1995), mathematisches Modell
372. X.-L. Wu, A. Libchaber, Phys. Rev. Lett. **84**, 3017 (2000)
373. T.D. Yang, J.-S. Park, Y. Choi, W. Choi, T.-W. Ko, K.J. Lee, PLoS ONE **6**, e20255 (2011)
374. Y. Yang, J. Elgeti, G. Gompper, Phys. Rev. E **78**, 061903 (2008)
375. Y. Yang, V. Marceau, G. Gompper, Phys. Rev. E **82**, 31904 (2010)
376. J.H. Yao, K.R Elder, H. Guo, M. Grant, Phys. Rev. B **47**, 14110 (1993)
377. C.A. Yates, R. Erban, C. Escudero, I.D. Couzin, J. Buhl, I.G. Kevrekidis, P.K. Maini, D.J.T. Sumpter, Proc. Natl. Acad. Sci. USA **106**, 5464 (2009)
378. M. Zabicki, W. Ebeling, E. Gudowska-Nowak, Chem. Phys. (2010)
379. M. Zabicki, E. Gudowska-Nowak, W. Ebeling, Acta Phys. Polonica B **41**, 1181 (2010)
380. V. Zaburdaev, S. Uppaluri, T. Pfohl, M. Engstler, R. Friedrich, H. Stark, Phys. Rev. Lett. **106**, 208103 (2011)
381. H.P. Zhang, A. Be'er, E.-L. Florin, H.L. Swinney, Proc. National Acad. Sci. **107**, 13626 (2010)
382. D.R. Zusman, A.E. Scott, Z. Yang, J.R. Kirby, Nat. Rev. Micro. **5**, 862 (2007)
383. R. Zwanzig, J. Stat. Phys. (1973)
384. R. Zygadlo, Phys. Rev. E **47**, 4067 (1993)